CLASSIFICATION CHANGE
To UNCLASSIFIED
By authority of GDS-GP-4 Date 10-75
Changed by L. Shirley
Classified Document Master Control Station, NASA
Scientific and Technical Information Facility

Copy No. 1

SID 63-1416-8

PROJECT APOLLO
FLIGHT-TEST REPORT
BOILERPLATE 23A
(U)
NAS9-150

September 1965

Apollo

(NASA-CR-97018) PROJECT APOLLO FLIGHT-TEST REPORT BOILERPLATE 23A (North American Aviation, Inc.) 229 p

N79-76141

Unclas
00/12 11093

[redacted]

C68-2333

Accession No. 09608-65

Copy No. 1 SID 63-1416-8

PROJECT APOLLO
FLIGHT-TEST REPORT
BOILERPLATE 23A
(U)
NAS9-150

September 1965

Exhibit I, Paragraph 5.11

GROUP 4
Downgraded at 3 year intervals; declassified after 12 years.

This document contains information affecting the national defense of the United States within the meaning of the Espionage Laws. Title 18 U.S.C. Section 793 and 794. Its transmission or revelation of its contents in any manner to an unauthorized person is prohibited by law.

NORTH AMERICAN AVIATION, INC.
SPACE and INFORMATION SYSTEMS DIVISION

[redacted]

[redacted]

NORTH AMERICAN AVIATION, INC. SPACE and INFORMATION SYSTEMS DIVISION

TECHNICAL REPORT INDEX/ABSTRACT

ACCESSION NUMBER						DOCUMENT SECURITY CLASSIFICATION Unclassified	

TITLE OF DOCUMENT	LIBRARY USE ONLY
Project Apollo Flight-Test Report, Boilerplate 23A	
AUTHOR(S) NAA/S&ID Apollo Engineering	

CODE	ORIGINATING AGENCY AND OTHER SOURCES	DOCUMENT NUMBER
	NAA/S&ID Apollo Engineering, Development Control, Test Evaluation Unit, D/692-405	SID 63-1416-8

PUBLICATION DATE	CONTRACT NUMBER
September 1965	NAS9-150

DESCRIPTIVE TERMS

Test
Flight Test
Apollo Test
Boilerplate 23A
Apollo Mission PA-2

ABSTRACT

The purpose of Apollo Mission PA-2 (BP-23A) was to demonstrate capability of the Apollo launch escape vehicle with a canard subsystem, boost protective cover, and Block I control weight to abort from the launch pad and recover. Boilerplate 23A test vehicle was successfully launched from Launch Complex 36 at WSMR on June 29, 1965. All test objectives were accomplished.

This report presents the NAA/S&ID evaluation of the test for NAA internal distribution.

FORM 131-V REV 11-64
PUBLICATIONS USE ONLY

FOREWORD

This report contains postflight engineering analyses of the data obtained from the Boilerplate 23A flight test and is intended for distribution primarily within NAA-S&ID.

The only distribution of this report outside NAA will be to the ASPO Test Evaluation Branch of NASA-MSC as reference material for use in preparation of the NASA-MSC Supplement to the Postlaunch Report for Apollo Mission PA-2 (BP-23A).

The definitive evaluations of the BP-23A flight test are contained in the NASA-MSC Postlaunch Report for Apollo Mission PA-2 (BP-23A) (MSC-A-R-65-3) and supplements thereto which have general distribution.

[redacted]

CONTENTS

Section		Page
	ABSTRACT	iii
	FOREWORD	v
	TABLE OF CONTENTS	vii
	LIST OF ILLUSTRATIONS	ix
	ABBREVIATIONS AND SYMBOLS	xv
1.0	SUMMARY	1-1
2.0	INTRODUCTION	2-1
3.0	TEST OBJECTIVES	3-1
4.0	CONCLUSIONS	4-1
5.0	TEST VEHICLE CONFIGURATION	5-1
6.0	LAUNCH OPERATIONS	6-1
7.0	TEST EVALUATION	7-1
	7.1 FLIGHT DYNAMICS AND AERODYNAMICS	7.1-1
	7.2 EARTH LANDING SUBSYSTEM	7.2-1
	7.3 STRUCTURES	7.3-1
	7.4 STRUCTURAL DYNAMICS	7.4-1
	7.5 MASS CHARACTERISTICS	7.5-1
	7.6 LAUNCH ESCAPE SEQUENCER SUBSYSTEM	7.6-1
	7.7 ORDNANCE EQUIPMENT	7.7-1
	7.8 LAUNCH ESCAPE PROPULSION SUBSYSTEM	7.8-1
	7.9 ELECTRICAL POWER SUBSYSTEM	7.9-1
	7.10 INSTRUMENTATION SUBSYSTEM	7.10-1
	7.11 COMMUNICATIONS SUBSYSTEM	7.11-1
	7.12 ELECTROMAGNETIC COMPATIBILITY	7.12-1

[redacted]

Section		Page
	7.13 DATA COVERAGE AND AVAILABILITY	7.13-1
	7.14 GROUND SUPPORT EQUIPMENT	7.14-1
	7.15 WINDOW SAMPLE ANALYSIS	7.15-1
	7.16 ALTITUDE INDICATOR TEST	7.16-1
8.0	SUMMARY OF MALFUNCTIONS AND DEVIATIONS	8-1
9.0	PREFLIGHT HISTORY	9-1
10.0	PROGRAM SUMMARY	10-1
11.0	REFERENCES	11-1

ILLUSTRATIONS

Figure		Page
2-1	Boilerplate 23A After Liftoff	2-4
5-1	Launch Escape Vehicle Motor Configuration, Mission PA-2	5-6
5-2	Table Comparing Configurations of BP-23 and BP-23A	5-7
5-3	Launch Escape Motor Paint Pattern, Mission PA-2	5-11
5-4	Boost Protective Cover and CM Paint Pattern, Mission PA-2	5-12
6-1	Boilerplate 23A on Launch Pad, Ready for Launch; Tiki Hut Removed	6-2
7.1-1	Table of Nominal Trajectory Parameters	7.1-21
7.1-2	Boilerplate 23A Mission Profile	7.1-22
7.1-3	Orientation of Command Module Body Axis System to Range Axis System ($\theta_{LEV} = 90°$, $\phi_{LEV} = 180°$) at Launch	7.1-23
7.1-4	Orientation of Euler Axis System to Range Axis System	7.1-24
7.1-5	Euler Attitude Angles, Relative to Range Axis System (ZYX Order of Rotation).	7.1-25
7.1-6	Trajectory Angles	7.1-26
7.1-7	Command Module Axis System, Showing Sense of Angular Displacements and Rates	7.1-27
7.1-8	Thrust-Vector Alignment Angles	7.1-28
7.1-9	Downrange Flight Profile	7.1-29
7.1-10	Crossrange Flight Profile	7.1-30
7.1-11	Altitude Time History	7.1-31
7.1-12	Mach Number Time History	7.1-32
7.1-13	Dynamic Pressure Time History	7.1-33
7.1-14	Component Wind Velocities	7.1-34
7.1-15	Ambient Pressure Time History	7.1-35
7.1-16	Variation of Atmospheric Pressure Ratio and Speed of Sound With Altitude	7.1-36
7.1-17	Flight Path Angle Time History	7.1-37
7.1-18	Angles of Attack and Sideslip Time Histories	7.1-38
7.1-19	Body Pitch, Yaw, and Roll Rate Time Histories	7.1-39

[redacted]

Figure		Page
7.1-20	Axial Acceleration Time History	7.1-40
7.1-21	Y and Z Axes Acceleration Time Histories	7.1-41
7.1-22	Table of Aerodynamic Configurations of Apollo Launch Escape Vehicles	7.1-42
7.1-23	LEV Flight Displacement Time History Comparisons	7.1-43
7.1-24	LEV Mach Number and Dynamic Pressure Time History Comparisons	7.1-44
7.1-25	LEV With Canards Deployed Flight Displacement Time History Comparisons	7.1-45
7.1-26	LEV With Canards Deployed Mach Number and Dynamic Pressure Time History Comparisons	7.1-46
7.1-27	LEV Body Rate Time History Comparisons	7.1-47
7.1-28	LEV Acceleration Time History Comparisons	7.1-48
7.1-29	LEV Angles of Attack and Sideslip Time History Comparisons	7.1-49
7.1-30	Table of Averaged Effects on LEV Roll Rate Due to System Perturbations	7.1-50
7.1-31	Effect of Perturbated Aerodynamics on LEV Body Rate Time History Comparisons	7.1-51
7.1-32	Effect of Perturbated Aerodynamics on LEV Angles of Attack and Sideslip Time History Comparisons	7.1-52
7.1-33	LEV With Canards Deployed Body Rate Time History Comparisons	7.1-53
7.1-34	LEV With Canards Deployed Acceleration Time History Comparisons	7.1-54
7.1-35	LEV With Canards Deployed Angles of Attack and Sideslip Time History Comparisons	7.1-55
7.1-36	LES-CM Vertical and Downrange Separation	7.1-56
7.1-37	LES-CM Crossrange and Downrange Separation	7.1-57
7.1-38	LES-CM Total Separation Distance Time History	7.1-58
7.1-39	LES Range Time History Comparisons	7.1-59
7.1-40	LES Altitude Time History Comparison	7.1-60
7.1-41	LES Flight Path Angle Time History Comparisons	7.1-61
7.1-42	LES Resultant Velocity Time History Comparisons	7.1-62
7.1-43	LES Pitch Plane Oscillations	7.1-63
7.1-44	Forward Heatshield Separation History	7.1-64
7.1-45	Variation of Forward Heatshield Separation Distance With Initial Angle of Attack and Pitch Rate	7.1-65
7.1-46	Variation of Forward Heatshield Relative Pitch Attitude With Initial Angle of Attack and Pitch Rate	7.1-66

[redacted]

Figure		Page
7.1-47	BP-23A Base Pressure Time Histories Compared to Wind Tunnel Data and BP-6 Flight Test Data	7.1-67
7.1-48	LEV Base Pressure Distribution During Abort	7.1-68
7.1-49	Pressure Time History Underneath the Boost Protective Cover	7.1-69
7.1-50	Pressure Differential Across the Boost Protective Cover	7.1-70
7.1-51	Boost Protective Cover Pullaway	7.1-71
7.1-52	Comparison of Vehicle Roll Attitude Time History From Attitude and Integrated Rate Gyro Data	7.1-72
7.1-53	Comparison of Vehicle Yaw Attitude Time History From Attitude and Integrated Rate Gyro Data	7.1-73
7.1-54	Comparison of Vehicle Pitch Attitude Time History From Attitude and Integrated Rate Gyro Data	7.1-74
7.1-55	Q-Ball Derived Angles of Attack and Sideslip Time Histories	7.1-75
7.1-56	Comparison of Angle of Attack Time Histories From Q-Ball Attitude and Integrated Rate Gyro Data.	7.1-76
7.1-57	Comparison of Angle of Sideslip Time Histories From Q-Ball Attitude and Integrated Rate Gyro Data	7.1-77
7.1-58	Comparison of Measured and Computed ΔPq	7.1-78
7.1-59	Comparison of Dynamic Pressure From Corrected and Uncorrected Q-Ball Data and Tracking Data	7.1-79
7.1-60	Effect of Q-Ball Bias on Q-Ball-Derived Angles of Attack	7.1-80
7.1-61	Effect of Q-Ball Bias on Q-Ball-Derived Angles of Sideslip	7.1-81
7.1-62	Comparison of Ground Recorded and Onboard-Recorded Barostatic Pressures Data Sources	7.1-82
7.1-63	Comparison of Ground Recorded and Onboard-Recorded Base Pressure Data Sources	7.1-83
7.1-64	Comparison of Ground-Recorded and Onboard Recorded Conical Surface Pressure Data Sources	7.1-84
7.1-65	Comparison of Ground Recorded and Onboard Recorded Q-Ball Differential ΔP_β and $\Delta P\alpha$ Data Sources	7.1-85
7.1-66	Comparison of Ground-Recorded and Onboard-Recorded Q-Ball Differential ΔPq Data Sources	7.1-86
7.1-67	Comparison of Ground-Recorded and Onboard X High, Y, and Z Acceleration Data Sources	7.1-87

[redacted]

Figure		Page
7.1-68	Comparison of Ground Recorded and Onboard Recorded Pitch Attitude Data Sources	7.1-88
7.1-69	Comparison of Ground Recorded and Onboard Recorded Yaw Attitude Data Sources	7.1-89
7.1-70	Comparison of Ground Recorded and Onboard Recorded Roll Attitude Data Sources	7.1-90
7.1-71	Comparison of Ground Recorded and Onboard Recorded Rate Gyro Data Sources	7.1-91
7.2-1	ELS Command Module Recovery	7.2-8
7.2-2	Recovered Command Module and Main Parachute on Ground	7.2-9
7.2-3	ELS Sequencer Block Diagram	7.2-10
7.2-4	Boilerplate 23A Parachute Configuration	7.2-11
7.2-5	Command Module Altitude Time History	7.2-12
7.2-6	Command Module Dynamic Pressure Time History	7.2-13
7.2-7	Command Module Flight Path Angle Time History	7.2-14
7.2-8	Command Module Final Descent Velocity Time History	7.2-15
7.2-9	Drogue Disconnect, Single-Point Attachment Shear Plate, Mission PA-2	7.2-16
7.2-10	Pilot Parachute Kinked Riser, Mission PA-2	7.2-17
7.2-11	Mortars and Parachute Deck After Landing	7.2-18
7.2-12	Harness and Parachute Deck After Landing	7.2-19
7.3-1	Main Heat Shield Shifted From Landing Impact, Mission PA-2	7.3-6
7.3-2	Main Heat Shield Cracked From Landing Impact	7.3-7
7.5-1	Table of Mass Characteristics, Mission PA-2	7.5-2
7.5-2	Table of Weights and Centers of Gravity, Comparing Apollo Mission PA-2 Test Vehicle With PA-1 Test Vehicle and Block I Spacecraft	7.5-3
7.5-3	Table of Weight and Balance Data for Launch Escape Vehicle Abort Phase, Mission PA-2	7.5-4
7.5-4	Table of Weight and Balance Data for Launch Escape Subsystem Jettison Phase, Mission PA-2	7.5-5
7.6-1	Boilerplate 23A Sequencer Subsystem Locations	7.6-3
7.6-2	LES Sequencer Schematic	7.6-4
7.6-3	LES Sequencer Events	7.6-5

Figure		Page
7.7-1	Table of BP-23A Ordnance Devices	7.7-5
7.8-1	Table of Boilerplate 23A LES Motor Characteristics	7.8-5
7.8-2	Table of Boilerplate 23A Launch Escape Motor and Pitch Control Motor Performance	7.8-6
7.8-3	BP-23A Ballistic Definitions	7.8-7
7.8-4	BP-23A Tower Jettison Motor With Nozzle Plug Insulation	7.8-8
7.8-5	Launch Escape Motor Pressure-Time History	7.8-9
7.8-6	Launch Escape Motor Thrust-Time History	7.8-10
7.8-7	Pitch Control Motor Pressure-Time History	7.8-11
7.8-8	Pitch Control Motor Thrust-Time History	7.8-12
7.8-9	Tower Jettison Motor Predicted Thrust-Time History	7.8-13
7.10-1	Boilerplate 23A Instrumentation Diagram	7.10-4
7.10-2	Boilerplate 23A Onboard Camera Locations	7.10-5
7.13-1	Telemetry and Meteorological Station Locations for Mission PA-2	7.13-3
7.13-2	Camera Locations for Mission PA-2	7.13-4
7.15-1	Window Sample Locations for Mission PA-2	7.15-3
7.16-1	Locations of Transducers and Pressure Ports, Altitude Indicator Test, Mission PA-2	7.16-3
7.16-2	Smoothed Baro-Reference Pressure Time History	7.16-4
7.16-3	Command Module Base Pressure Coefficient During Drogue Descent	7.16-5
7.16-4	Command Module Altitude Indicated by the Baro-Reference Pressure	7.16-6

ABBREVIATIONS AND SYMBOLS

ABBREVIATIONS

BME	Bench Maintenance Equipment
BP	Boilerplate
CM	Command Module
C/O	Checkout
CSM	Mated Command and Service Modules
ECS	Environmental Control Subsystem
EMI	Electromagnetic Interference
FP	Fluctuating Pressure
GMT	Greenwich Mean Time
KSC	John F. Kennedy Space Center
LE	Launch Escape
LES	Launch Escape Subsystem
LET	Launch Escape Tower
LEV	Launch Escape Vehicle
LJ-II	Little Joe II
LV	Launch Vehicle
MSC	Manned Spacecraft Center
MSL	Mean Sea Level
MST	Mountain Standard Time

NAA	North American Aviation, Inc.
NASA	National Aeronautics and Space Administration
R	Range
R and Z	Range and Zero
RCS	Reaction Control Subsystem
SM	Service Module
SMR	Small Missile Range
VCO	Voltage-Controlled Oscillator
WSMR	White Sands Missile Range
WT	Wind Tunnel

LETTER SYMBOLS

Symbols for Primary Concepts

a	Linear acceleration
A	Cross-sectional area
C	Coefficient
dB	Decibel
D_o	Nominal parachute canopy diameter
F	Thrust
g	Unit of graviational acceleration
h	Altitude
I	Moment of inertia
M	Mach Number
p	Body roll rate

P	Pressure
q	Dynamic pressure
q	Body pitch rate
r	Body yaw rate
S_π	Reference area, CM base area 129 feet^2
S_o	Total parachute canopy cloth area
t	Time
T	Time at liftoff
V	Velocity
X	Longitudinal axis
Y	Lateral axis
Z	Transverse axis
α	Angle of attack
β	Angle of sideslip
γ	Flight path angle
ϵ	Thrust vector alignment angle
η	Load factor
θ	Pitch angle
ϕ	Roll angle
ψ	Yaw angle
$\bar{\omega}$	Vector sum of body rotational rates

Symbols for Subscripts

a	Action time
A	Vehicle X-axis reference system

[redacted]

b	Burning time
B	Body axis system
C	Command module axis system
cg	Center of gravity
G	Ground axis system
i	Ignition
L	Local conditions
max	Maximum
o	Standard sea level condition or initial condition
P	Pressure
S	Service module coordinate system
t	Total
T	Thrust
TAIL	Tailoff
X	Referred to X axis
Y	Referred to Y axis
Z	Referred to Z axis
∞	Freestream conditions
REF	Aerodynamic reference point, (center of lift referenced to cg)

1.0 SUMMARY

The objectives of Apollo Mission PA-2, the second pad abort, were successfully accomplished with the unmanned test vehicle, Boilerplate 23A, equipped with the Block I type launch escape subsystem (LES). The primary purpose of the mission was to verify vehicle performance in a pad abort when the vehicle configuration included Block I control weight, a canard subsystem, a boost protective cover, and an apex-cover jettison subsystem.

The Boilerplate 23A test vehicle, refurbished Boilerplate 23, was successfully launched on schedule, without checkout or countdown holds, from Launch Complex 36 at White Sands Missile Range with liftoff at 06.00:01.448 MST June 29, 1965.

Liftoff, trajectory, vehicle turnaround following canard deploy, and subsystem performance were satisfactory. All events were performed in correct sequence, and miss distances for both the LES and the apex cover were satisfactory. The sequence of events is given in Figure 7.1-1, and the mission flight profile is given in Figure 7.1-2. A moderate roll rate, typical for a vehicle configuration without the reaction control subsystem, resulted in vehicle turnaround, after canard deploy, principally in the horizontal rather than the vertical plane and in jettison of the LES in an easterly rather than a northerly direction; however, the roll or resulting flight effects were not detrimental to any vehicle subsystem performance.

Postflight simulations based on LEV data and abort conditions showed good agreement with flight tracking data, exhibiting a deviation of only 1 percent. The actual trajectory in general was slightly higher and of greater range than planned. This resulted from LES thrust which was greater than planned, principally because of a high motor grain temperature corresponding to a high ground environmental temperature.

The higher trajectory together with southerly winds resulted in the longer-than-planned range and flight time. The increase in flight time appeared predominantly in a longer-than-planned time on the main parachutes.

The earth landing subsystem safely recovered the command module and performed as planned. The longer time on the main parachutes is discussed above. Only a minor abnormality occurred. As with the Boilerplate 22 flight, one pilot-parachute steel cable was kinked and slightly flattened during deployment. In neither flight was there any adverse effect.

[redacted]

The boost protective cover (BPC), having served its purpose in protecting the command module conical surface, broke up during its removal by LES jettison. No significant sooting was evident on the window samples located on the CM conical surface. The vehicle turnaround, in this flight, placed the command module out of the motor plume at BPC breakup; however, the sooting would not have been significant in any case, as the LE motor essentially was spent at tower jettison and BPC breakup.

The test results from the altitude indicators installed in the command module indicate that an aerodynamic effect resulted in an error 250 feet greater than the true altitude during the time on the drogue parachutes and at the time of main-parachute deployment. Similar spacecraft installations could be calibrated to offset the error, as discussed in section 7. 16.

The instrumentation and communications subsystems performed satisfactorily and, within design limits, provided usable data throughout the flight.

Based on an analysis of the flight data, the NAA test evaluation results indicate that the objectives of the test were accomplished, that the subsystems performed satisfactorily, and that no difficulties affecting future flights were encountered.

2.0. INTRODUCTION

This report describes Apollo Mission PA-2, the flight test of Boilerplate 23A, and presents a test evaluation by NAA based on analysis of the data gathered during the flight. The report is designed for in-house distribution only, but the test evaluation sections provide the basis for the NAA input to a supplement to the NASA-MSC postlaunch report on the flight test of Boilerplate 23A. Definitive reports on Apollo flight tests and supplements thereto will be published by NASA-MSC and will have wide distribution.

The Boilerplate 23A test vehicle, refurbished Boilerplate 23, consisting of a boilerplate command module and a Block I launch escape subsystem, was successfully launched from Launch Complex 36 at White Sands Missile Range, New Mexico, on June 29, 1965, at 06:00:01.448 MST. A photograph of the test vehicle after liftoff is shown in Figure 2-1.

Mission PA-2 was the second pad (low-altitude) abort, and the fifth abort test in a series of seven scheduled flight tests of the Apollo vehicle launch escape configuration. This second pad abort was conducted to verify performance of a vehicle which included, additional to the Boilerplate 6 configuration, a boost protective cover with proturberances, a canard subsystem, an apex-cover jettison subsystem, and a Block I control weight. A further difference consisted in the Block I type dual drogue and main parachutes of Boilerplate 23A, as compared to the interim parachutes including a single drogue for Boilerplate 6.

Two more abort tests, Spacecraft 002 and 010 with the Little Joe II launch vehicle, are scheduled to be conducted at White Sands Missile Range. Block I spacecraft suborbital, orbital, and lunar flights will be initiated at Kennedy Space Center, Florida, and will be conducted with Saturn launch vehicles.

The following boilerplate vehicles have been flight-tested:

Vehicle	Configuration	Mission
Boilerplate 6 (WSMR)	Command module and launch escape subsystem	First pad abort
Boilerplate 12 (WSMR)	Command and service modules and launch escape subsystem. Little Joe II	Transonic abort

Vehicle	Configuration	Mission
Boilerplate 13 (KSC)	Command and service modules, adapter, and launch escape subsystem. Saturn I	Determination of launch and exit environmental parameters and demonstration of primary mode of jettison of the LES
Boilerplate 15 (KSC)	Command and service modules, adapter, and launch escape subsystem. Saturn I	Determination of launch and exit environmental parameters and demonstration of the alternate mode of LES jettison
Boilerplate 16 (KSC)	Command and service modules and launch escape subsystem. Little Joe II	Launch vehicle developmental test and insertion of Pegasus I into earth orbit
Boilerplate 22 (WSMR)	Command and service modules and launch escape subsystem. Little Joe II	Low-altitude abort (planned high-altitude abort)
Boilerplate 23 (WSMR)	Command and service modules and launch escape subsystem. Little Joe II	High-q abort
Boilerplate 23A (WSMR)	Command module and launch escape subsystem	Second pad abort
Boilerplate 26 (KSC)	Command and service modules, adapter, and launch escape subsystem. Saturn I.	Launch vehicle developmental test and insertion of Pegasus II into earth orbit
Boilerplate 9A (KSC)	Command and service modules, adapter, and launch escape subsystem. Saturn I	Launch vehicle developmental flight and insertion of Pegasus III into earth orbit

The first four spacecraft to be flight-tested are:

Vehicle	Configuration	Mission
Spacecraft 002 (WSMR)	Command and service modules and launch escape subsystem. Little Joe II	Power-on tumbling boundary abort
Spacecraft 009 (KSC)	Complete spacecraft, with partial subsystems. Saturn IB	Unmanned supercircular reentry. High heat-rate
Spacecraft 010 (WSMR)	Command and service modules and launch escape subsystem. Little Joe II	Flight abort and backup for Spacecraft 002
Spacecraft 011 (KSC)	Complete spacecraft. Saturn IB	Unmanned supercircular reentry. High heat-load

[redacted]

Figure 2-1. Boilerplate 23A After Liftoff

[redacted]

3.0 TEST OBJECTIVES

The test objectives and test results are discussed below.

3.1 FIRST ORDER TEST OBJECTIVE

Demonstrate the capability of the launch-escape vehicle, equipped with a canard subsystem and a boost protective cover, to abort from the launch pad and recover.

Results: The test objective was accomplished. The command module was propelled to an apogee 960 feet higher in altitude and 790 further in range than the planned minimum requirements for a pad abort under WSMR conditions. The minimum mission requirements currently are under consideration. The canard deployed satisfactorily and provided turnaround of the LEV. The LES, the boost protective cover, and the forward heat shield were jettisoned properly, and subsequent ELS operation yielded a safe landing of the command module. Refer to section 7.1.

3.2 SECOND ORDER TEST OBJECTIVES

(a) Determine the performance and stability characteristics of the launch-escape vehicle with boost protective cover and control weight command module.

Results: The test objective was accomplished. The launch-escape vehicle performance and stability were determined for the power-on and coast phases of the flight with a six-degrees-of-freedom computer program. The dynamic characteristics were determined and found to be within the tolerances. Maximum deviations in altitude and Mach number simulations prior to canard deployment were less than 1 percent. Dynamic pressure varied by 5 percent. Simulation of the initial peak angles of attack and sideslip was within 1.5 degrees of flight-test data. Refer to Section 7.1.

(b) Determine the turnaround dynamics of the launch-escape vehicle following canard deployment.

Results: The test objective was accomplished. Using data obtained from the flight, the turnaround dynamics of the launch escape vehicle were determined for the period following canard deployment. Computer simulations showed acceptable agreement with the flight-test data on altitude, Mach number, dynamic pressure, and the angles of attack and sideslip. Refer to Section 7.1.

(c) Demonstrate satisfactory separation of the launch-escape subsystem and boost protective cover from the command module.

Results: The test objective was accomplished. Satisfactory separation of the LES plus BPC from the CM was demonstrated. Clean separation was verified by analysis of the motion-picture film, tracking data, and data from conical-surface pressure taps mounted under the BPC. Refer to Section 7.1.

(d) Demonstrate proper event sequencing during abort from the launch pad and recovery.

Results: The test objective was accomplished. The events occurred as programmed, and the timing of the programmed events was such that safe command module recovery was accomplished. Refer to sections 7.1 and 7.2.

3.3 THIRD ORDER TEST OBJECTIVE

Determine the base pressure of the launch-escape vehicle with boost protective cover during all phases of the mission.

Results: The test objective was accomplished. Using data obtained from the flight, the Boilerplate 23A aft heat shield base-pressure time history was defined for the period through tower jettison. Refer to Section 7.1.

4.0 CONCLUSIONS

The flight of Boilerplate 23A demonstrated that the performance and the stability of the launch escape vehicle were adequate to assure a successful pad abort from a Saturn launch vehicle in event of an emergency. Sufficient aerodynamic and stability data were obtained to permit simulation of an abort trajectory in good agreement with the actual trajectory. Data from wind-tunnel tests and previous flight tests were verified, and the methods of analysis were validated by the close agreement between actual and simulated trajectories. On the strength of the flight-test results, confidence may be placed in the capability of the launch escape vehicle equipped with a canard subsystem and boost protective cover to abort from the launch pad, with subsequent safe recovery of the command module.

The design of the canard subsystem was shown to be satisfactory. The subsystem operated as planned and provided the necessary aerodynamic forces required to orient the launch escape vehicle with Block I control weight in a main-heat-shield-forward attitude.

The launch escape vehicle structural performance was satisfactory, and the flight loads were less than designed. The boost protective cover breakup occurred during LE tower jettison but after the boost protective cover had protected the CM from LE motor exhaust.

The launch escape propulsion subsystem performed its function as required. All pyrotechnic devices operated properly. The launch escape and the earth landing subsystem sequencers operated as planned, initiating all events at their proper times. The LE tower and apex cover were jettisoned satisfactorily. Safe miss distances from the CM and drogue parachutes were established and maintained.

The earth landing subsystem functioned properly, damping vehicle oscillations almost completely and lowering the command module safely to the ground. The dual-drogue configuration was used for the third time, and the Block I type main parachutes were used for the second time. Again performance was satisfactory.

No design or development problems were encountered which might preclude continuation of the Apollo program along lines currently planned.

5.0 TEST VEHICLE CONFIGURATION

5.1 VEHICLE SUBSYSTEM DESCRIPTION

The Boilerplate 23A test vehicle, refurbished Boilerplate 23, is shown in the vehicle configuration diagram, Figure 5-1, with principal subsystems located. Detailed subsystems descriptions are given in section 7.0 and in reference 7. The Boilerplate 23A subsystems are summarized below. (Definitions of configuration terms are included in reference 9, appendix A.)

Spacecraft Subsystem	Configuration	Drawing No.
Structure (General Assembly)		B14-000023
Launch escape subsystem	Complete (no ablative material)	B15-000002-241
Command module	Interim	B16-000023
Launch Escape Subsystem		
Tower	Complete	V15-300100
Q-ball	Interim	ME901-0014-00032
Pitch control motor	Complete	ME467-0005-0007
Tower jettison motor	Complete	ME467-0004-1003
Launch escape motor	Complete	ME467-0003-1000
Canard subsystem	Complete	V15-300801
Boost protective cover	Interim	V15-300600
Separation Subsystems		
Command module - tower	Interim	F01-596007
Command module - forward heat shield	Interim	B16-596223 (F01-596121)
Environmental Control Subsystem (included but empty and inactive)	Interim	B16-610101
Electrical Power Subsystem	Interim	B15-450053 B16-540010

[redacted]

Spacecraft Subsystem	Configuration	Drawing No.
Communications and Instrumentation Subsystems		
Telemetry and antenna subsystem	Interim	B16-750422
Onboard recorders	Interim	B16-754009
End instruments and signal conditioners	Interim	B16-750012
C-band transponder	Not included	
Cameras		
Launch escape subsystem	Interim	B15-750375
Command module	Interim	B16-750350
Sequencer Subsystem		B16-451301
Tower sequencer	Interim	V15-452550-21
Mission sequencer	Interim	B16-540044-101
Earth landing sequencer	Interim	ME901-0400-0009
Backup abort timer (function not used)	Interim	B16-540027-101
Pyrotechnic Subsystem	Partial	F01-596007
Earth Landing Subsystem		B16-576008
Mortars (exclusive of pyrotechnics	Complete	B16-576008
Parachute subsystem	Complete	B16-576008

5.2 CONFIGURATION DIFFERENCES

The significant configuration differences between Boilerplate 23A and Boilerplate 6 consisted of the following additions and changes:

Block I control weight
Canard subsystem
Boost protective cover with protuberances
Apex-cover jettison subsystem
Block I main parachutes and dual drogues

Significant configuration differences between Boilerplate 23A and Boilerplate 23, and identification of Block I type subsystems, are given in Figure 5.2 and are discussed below.

[redacted]

Command Module Structure

The command module structure was essentially the same as the Boilerplate 23 structure with the following exceptions.

An interim forward heat shield thruster subsystem was included in Boilerplate 23A. Spacecraft 002 is to have a Block I type thruster subsystem. Boilerplates 6, 12, and 23 were not equipped with thruster subsystems.

Additional ballast of 1000 pounds was added to Boilerplate 23A to simulate Block I control weight. Previous boilerplate flight vehicles did not have Block I control weight. Spacecraft 002 will have the control weight.

In addition, dummy scimitar antennas, simulated steam and air vents, and a CM-SM simulated umbilical fairing were added to the Boilerplate 23A command module exterior. While no basic change in configuration resulted, the damaged Boilerplate 23 interim aft heat shield was replaced with the heat shield from Boilerplate 6.

Launch Escape Subsystem

The Block I LES had the same configuration as Boilerplate 23 and Boilerplate 22 except for the deletion of CM pressure ports and the addition of eight 1-inch vent holes in the soft boost cover (for hard-cover venting); the ablative material was deleted from the tower structure, since it was not needed for this flight.

The command-module/tower separation bolts were the improved single-mode type used on Boilerplate 22. Dual-mode bolts are under development for the Block I spacecraft.

As a safety measure, shear wires were added to the ELS tower umbilical interim-type electrical connectors.

Sequencer Subsystem

Mission (LES) Sequencer

The mission sequencer was of the type flown on Boilerplate 22, which included the additional apex-cover jettison function and the required 0.4-second time delay. The one-package configuration used is to be replaced in Block I with two Master Events Sequence Control (MESC) packages.

Tower Sequencer

The two tower sequencers were of the same configuration as the Boilerplate 23 sequencers, which included motor switches. One sequencer was a spare for the BP-23 flight and one was a unit designated for BP-12 which was used only for breadboard pyro firing.

For Block I spacecraft, the tower sequencer functions are to be included in each of the two MESC packages. Motor switches will be replaced with relays as in Boilerplate 22.

Earth Landing Sequencer

The one-package earth landing sequencer used was similar to the one flown on Boilerplate 23. The Block I type will be in two packages but will be essentially the same except for qualified potting.

Abort Backup Timer

The abort backup timer normal function was not required in this flight in that abort was initiated directly by land line from the blockhouse. The timer, however, served as a GSE abort lockout, hence was left on board. The timer is not used with Block I spacecraft.

Pyrotechnic Subsystem

Details of the pyrotechnic subsystem are given in section 7.7. The most significant change involved the addition of the apex-cover thruster in the Boilerplate 23A configuration.

Earth Landing Subsystem

The Boilerplate 23A earth landing subsystem included Block I parachutes; interim parachutes were used with Boilerplate 23. Additional configuration details are included in section 7.2.

Electrical Power Subsystem

The EPS of Boilerplate 23A employed two pyro batteries of a new interim type as indicated in Figure 5-2. Four pyro batteries of standard NASA R&D type were used in Boilerplate 23. Block I pyro batteries are to be NAA-furnished.

Communications and Instrumentation Subsystems

Details of the R&D instrumentation subsystem are given in section 7.10. The deletion of the C-band transponders was the only significant communications difference from the Boilerplate 23 configuration.

5.3 PAINT PATTERN ATTITUDE IDENTIFICATION

The paint patterns used for vehicle attitude identification are given in Figures 5-3 and 5-4.

~~CONFIDENTIAL~~

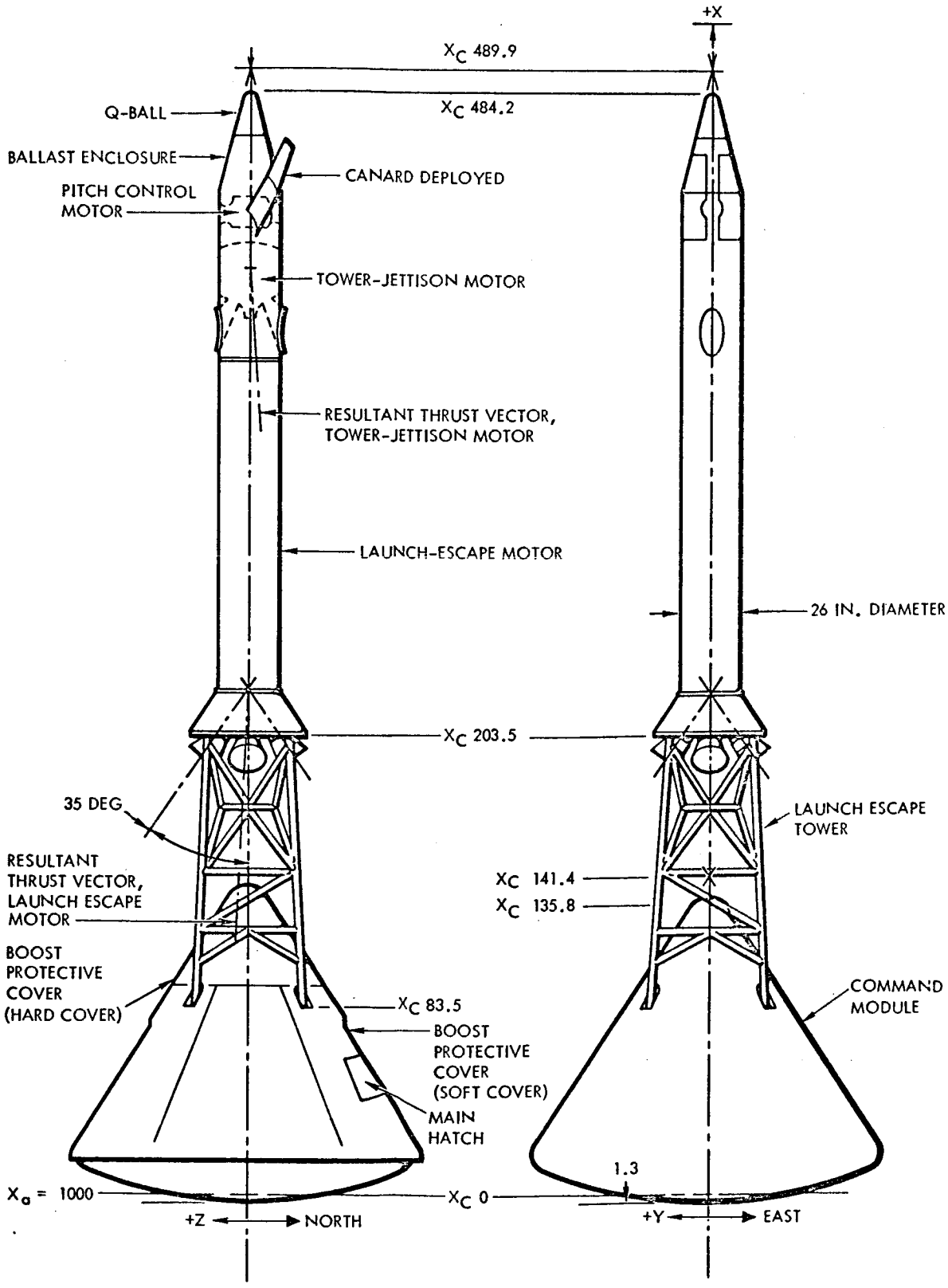

Figure 5-1. Launch Escape Vehicle Motor Configuration, Mission PA-2

~~CONFIDENTIAL~~

[redacted]

Component or Function	Mission A-002 (BP-23)	Mission PA-2 (BP-23A)
Launch Escape Subsystem		
Tower attachment	Interim Single-mode bolts	Interim Improved single-mode bolts (same type as BP-22)
Launch escape tower	Block I Thermal protection	Block I No thermal protection
CM-LES umbilical	Interim	Interim (safety-wired)
Canard	Block I	Block I
Q-Ball	Interim	Interim
Motors		
Pitch	Block I	Block I
Tower	Block I	Block I
Launch escape	Block I	Block I
Boost protective cover	Interim No protuberances	Interim (different from Block I only in stress design and vent holes) Protuberances to enclose CM exterior protuberances
	No vent holes for hard cover Instrumentation ports	Vent holes for hard cover No instrumentation ports
Sequencers		
Tower	Interim Two separate packages (Motor switches)	Interim Two separate packages (Motor switches)

Figure 5-2. Table Comparing Configurations of BP-23 and BP-23A (Sheet 1 of 4)

[redacted]

[redacted]

Component or Function	Mission A-002 (BP-23)	Mission PA-2 (BP-23A)
Mission (LES)	Interim One package and no apex-cover jettison	Interim One package, apex-cover jettison (same type as BP-22)
Backup abort timer	Interim Backup function not used	Interim Backup function not used
(Tower and mission (LES) sequencer functions are combined in the master events sequence control (MESC) for Block I)		
Command Module		
Structure	Simulated	Simulated (BP-19 apex cover and BP-6 main heat shield)
Weight	9,977 pounds	Block I 10,891 pounds, 1,000 pounds ballast added
Protuberances	None	Simulated vents, hatches, scimitar antennas, and CM-SM external umbilical
Apex cover jettison	Apex cover jettisoned with tower	Interim Thruster subsystem developed with BP-12 at El Centro
CM-SM umbilical	Interim One only	Interim Used two with lanyards to pad adapter
Earth Landing Subsystem		
Parachute Subsystem	Interim	Same as Block I and BP-22 except as noted

Figure 5-2. Table Comparing Configurations of BP-23 and BP-23A (Sheet 2 of 4)

[redacted]

[redacted]

Component or Function	Mission A-002 (BP-23)	Mission PA-2 (BP-23A)
Drogue parachutes	Dual Reefed to 40% for 6 sec, disreefed to 57%; nylon risers	Dual Reefed to 41% for 8 sec, disreefed to 64%; lower 15 feet steel risers, remainder Dacron
Pilot parachutes	10 feet dia., all nylon risers	7.2 feet dia. lower 9 feet steel risers, remainder Dacron
Main parachutes	88.1 feet dia., four-strap harness and four-point CM attachment, 5° hang angle. Ringsail, reefed 11% for 6 sec, then fully deployed. No parachute disconnect	83.5 feet dia., four-strap harness (different from Block I and BP-22 with two-point CM attachment) 5° hang angle. Open-slot Ringsail, reefed 9% for 8 sec, then fully deployed. Low-density bag pack, not Block I. No parachute disconnect
Mortars		
Pilot parachute	Interim 15-inch can length	Block I Can length reduced from BP-23
Main parachute	Block I	Block I
Sequencer	Interim One package, Block I same except two packages, and different potting and fuse modules	Interim Same as BP-23 (BP-22 had two packages similar to Block I)
Reefing-line cutters	Interim	Interim

Figure 5-2. Table Comparing Configurations of BP-23 and BP-23A (Sheet 3 of 4)

[redacted]

Component or Function	Mission A-002 (BP-23)	Mission PA-2 (BP-23A)
Environmental Control Subsystem	Interim Used on ground only	Interim Not activated
Electrical Power Subsystem	Interim Silver-zinc batteries	Interim Silver-zinc batteries
Instrumentation battery	One, MAP 4095-3 120 amp-hr at 12 amp	One, MAP 4095-3 Same as BP-23
Logic batteries	Two, MAR 4090-11 6 amp-hr at 1 amp 18 cells	Two, MAR 4090-11 Same as BP-23
Pyrotechnic batteries	Four MAR 4090-11 6 amp-hr at 1 amp, 18 cells	Two MAR 4249-1 5 amp-hr at 10 amp (BP-23 type increased to 20 cells)
Camera Batteries	Three MAR 4090-11	Two MAR 4090-11
Communications and Instrumentation	R&D	R&D
T/M link	One PAM FM/FM	Same as BP-23
Onboard data acquisition	One commutator (90 x 10) One tape recorder Three cameras	Same as BP-23 except two cameras
Radar	Transponders, two C-band	None
Service Module	Included	None
Booster	Little Joe II	No booster, CM-to-pad adapter used

Figure 5-2. Table Comparing Configurations of BP-23 and BP-23A (Sheet 4 of 4)

[redacted]

[redacted]

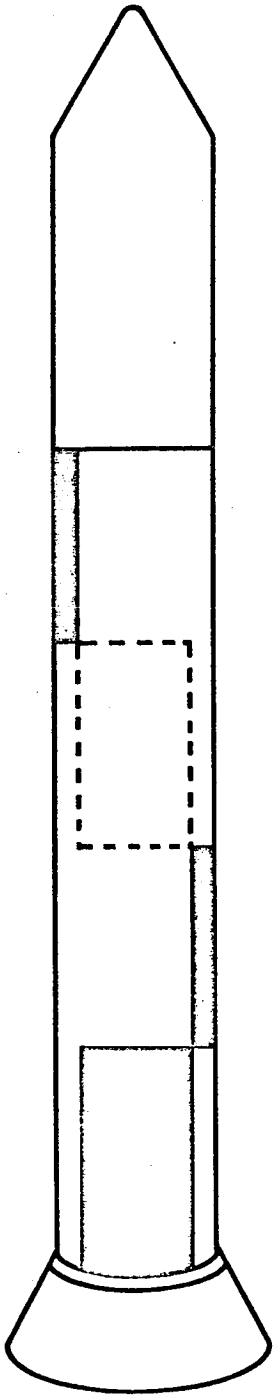

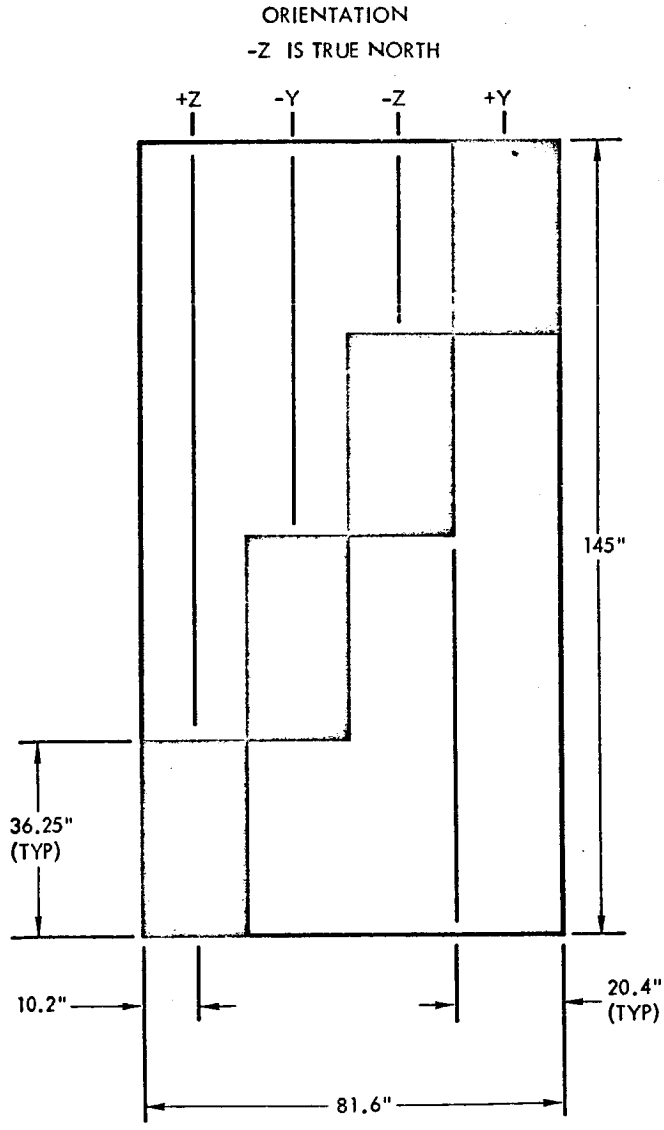

Figure 5-3. Launch Escape Motor Paint Pattern, Mission PA-2

[redacted]

[redacted]

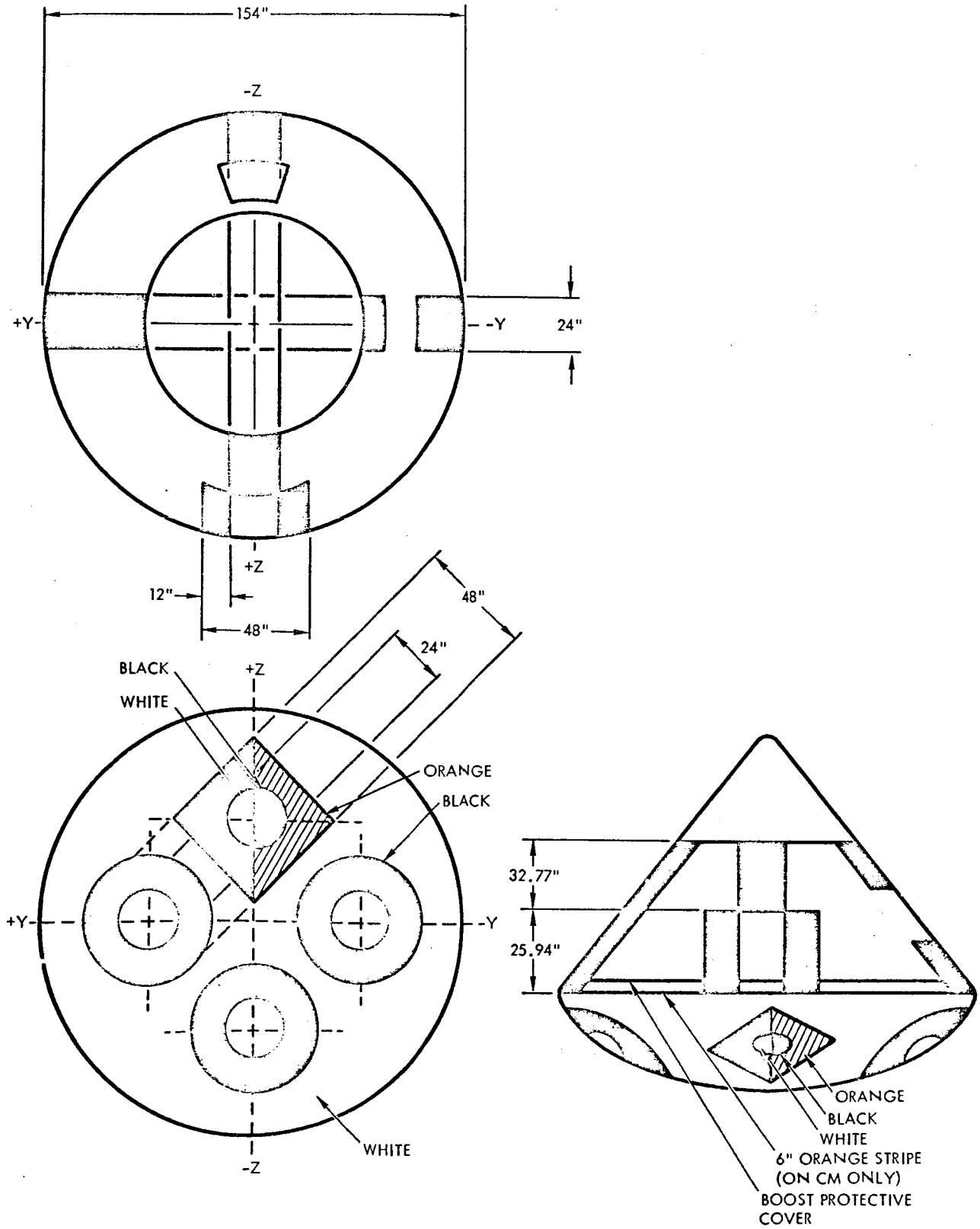

Figure 5-4. Boost Protective Cover and CM Paint Pattern, Mission PA-2

[redacted]

6.0 LAUNCH OPERATIONS

6.1 SIMULATED COUNTDOWN

A simulated countdown was performed on June 23, 1965, in order to verify the flight readiness of the Boilerplate 23A test vehicle. Deviation sheets were written to adapt the countdown procedure (OTP-A-0010) to the simulated countdown. The test vehicle was in flight configuration for this countdown except for installation of pyrotechnics. The ECS was not installed for this mission.

Only one problem was encountered: the pitch gyro cage light failed to turn off when the pitch gyro was uncaged. According to the vendor, this false indication had occurred in other installations because of faulty soldering affecting a gyro microswitch. In no instance was the attitude gyro performance affected; hence, it was decided to proceed with the launch without delay and not to consider the false indication during the final countdown.

The Flight Readiness Review was held on June 25, at which time the GSE, the facility, and the test vehicle were considered ready for the launch countdown. The vehicle is shown in ready condition in Figure 6-1.

6.2 COUNTDOWN

The countdown procedure, based on OTP-A-10 with fifteen major sections, was performed in two parts, the precountdown on June 28 and the final countdown on June 29. No problems were encountered and no holds were required in the countdown, which was concluded with a successful launch on schedule at 0600 MST June 29, 1965.

[redacted]

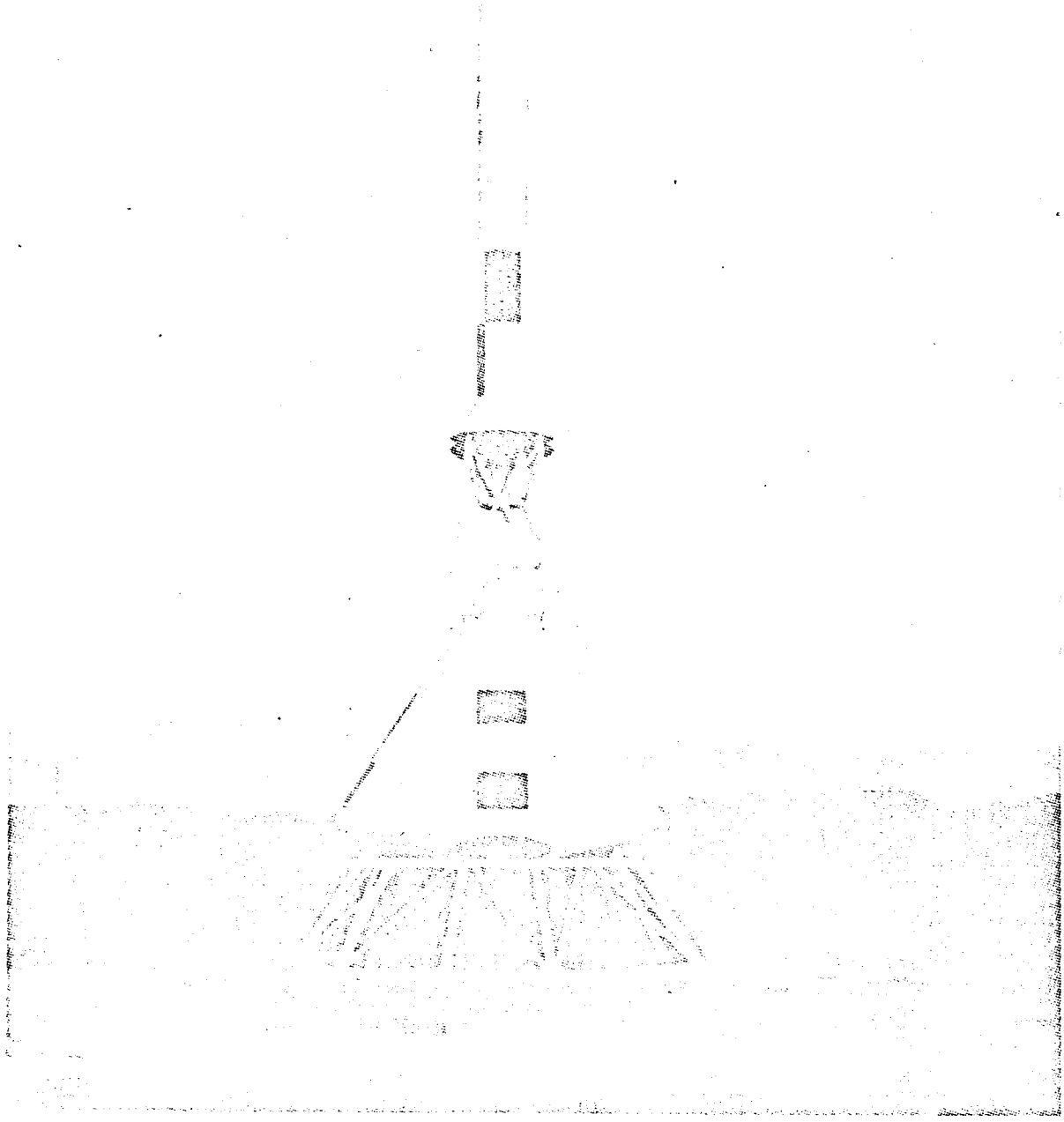

Figure 6-1. Boilerplate 23A on Launch Pad, Ready for Launch; Tiki Hut Removed

[redacted]

7.0 TEST EVALUATION

This section covers the following topics:

7.1 Flight Dynamics and Aerodynamics
7.2 Earth Landing Subsystem
7.3 Structures
7.4 Structural Dynamics
7.5 Mass Characteristics
7.6 Launch Escape Sequencer Subsystem
7.7 Ordnance Equipment
7.8 Launch Escape Propulsion Subsystem
7.9 Electrical Power Subsystem
7.10 Instrumentation Subsystem
7.11 Communications Subsystem
7.12 Electromagnetic Compatibility
7.13 Data Coverage and Availability
7.14 Ground Support Equipment
7.15 Window Sample Analysis
7.16 Altitude Indicator Test

7.1 FLIGHT DYNAMICS AND AERODYNAMICS

Summary

Boilerplate 23A was launched at WSMR from Launch Complex 36 with azimuth and elevation angles of zero (true north) and 90 degrees (up) respectively. The flight was initiated by a landline signal to the mission sequencer. Signals from the mission sequencer simultaneously ignited the launch escape motor and the pitch control motor. Both motor ignition and vehicle liftoff occurred as planned. A maximum Mach number of 0.587 and maximum dynamic pressure of 420 psf were attained 3.7 seconds after liftoff. As the vehicle was climbing, a positive roll rate developed. A maximum rate of 40 deg/sec was recorded at T + 9.5 seconds. The roll rate was probably due to a combination of thrust-vector misalignment and the influence of vehicle protuberances on the vehicle aerodynamics.

At canard deployment the vehicle had rolled approximately 270 degrees so that when the canard-induced pitch maneuver was accomplished, the vehicle pitched primarily in the horizontal rather than in the vertical plane. Altitude, Mach number, and dynamic pressure at canard deployment were 8490 feet msl, 0.293, and 95 psf, respectively.

Jettison of the launch escape subsystem (LES) occurred as programmed 3 seconds after canard deployment at an altitude of 9000 feet, a Mach number of 0.195, and a dynamic pressure of 40 psf. Simulations made using the initial conditions at LES jettison show excellent agreement between simulated and actual LES trajectory. The boost protective cover (BPC) remained intact during vehicle turnaround and did not break up until after LES jettison.

Forward heat shield separation occurred as programmed 0.4 second after LES jettison. Separation was clean with the forward heat shield being approximately 40 feet below and 30 feet behind the command module at drogue parachute deployment (T + 15.8 seconds). An apogee attitude of 9240 feet was attained 17.5 seconds after liftoff. Mach number and dynamic pressure at apogee were 0.157 and 25 psf, respectively.

Operation of the earth landing subsystem (ELS) was as programmed with command module touchdown occurring at T + 112.8 seconds, 7620 feet downrange and 370 feet crossrange (east).

The nominal trajectory parameters are tabulated in Figure 7.1-1 for significant event times. The mission profile showing flight altitude as a function of ground range is presented in Figure 7.1-2, with Mach number and dynamic pressure listed at significant times during the flight.

Definitions of body-axis, range-axis, and Euler-axis systems, together with trajectory angles, Euler angles, aerodynamic angles, and thrust-vector angles, are given in Figures 7.1-3 through 7.1-8. Trajectory parameters (i.e., range, altitude, Mach number, etc.), as well as dynamic flight parameters such as attitude, aerodynamic angles, and body rates, are presented with pertinent meteorological data in Figures 7.1-9 through 7.1-21. These figures were used as reference curves for the analyses.

Aerodynamic Configuration

Externally the BP-23A command module was configured to represent a Block I spacecraft in that the scimitar antennas, the umbilical housing, and the vents were simulated. The CM also was fitted with a boost protective cover. This BPC was different from others flown to date, since no cutouts were made to accommodate pressure taps or telemetry windows. This test represents the first time the low Mach number aerodynamic effects of the protuberances on LEV performance could be experimentally determined.

The external or aerodynamic configuration of the LES was the same as all other boilerplate vehicles flown to date with canard surfaces. Canard surfaces were also incorporated on BP-22 and BP-23, but not on Boilerplates 6, 12, 13, or 15.

The BP-23A flight was conducted to establish the effect of changes to the Block I spacecraft since the first pad abort test using the BP-6 vehicle. Major differences in vehicle configuration between the two tests were:

1. The vehicle was ballasted to the current representative Block I control weight and center of gravity.

2. The canard subsystem was incorporated.

3. A boost protective cover with simulated scimitar antennas, CM-SM umbilical fairing, and steam and air vents was incorporated.

4. Forward heatshield jettison was accomplished by means of thrusters.

5. Dual drogue parachutes (actively reefed for 8 seconds) were incorporated.

A summary of the aerodynamic configurations of Apollo launch escape vehicles (LEV) is presented in Figure 7.1-22.

Analysis of LEV Trajectory and Dynamics

The flight of Boilerplate 23A was simulated by means of a six-degrees-of-freedom digital-computer program, and the results were compared with flight data. Parameters used in the simulation, i.e., weight, inertia, atmospheric data, thrust, etc., were based on conditions at launch and/or in flight which are discussed in sections 7.5, 7.8, and 7.13. Where applicable, perturbations from the nominal values of certain parameters were made to determine their effect on matching flight data. Results of the analyses are presented below.

Trajectory of LEV Prior to Canard Deployment

A postflight simulation of the LEV flight prior to canard deployment (T + 11.0 seconds), using aerodynamic data obtained from reference 13, showed good correlation with the flight trajectory parameters. Figure 7.1-23 presents a comparison of the simulated and the flight-test altitude, X range, and Y range as functions of time from abort. The flight-test displacement parameters are within the simulation envelope obtained from the uncertainties in thrust-vector alignment ($\Delta\epsilon_{XX} = \pm 0.3°$, $\Delta\epsilon_{YZ} = \pm 7°$). Figure 7.1-24 presents plots comparing simulated and test Mach number (M) and dynamic pressure as functions of time from abort. The M and q test parameters lie outside the envelope of dispersions during the first 4 seconds of flight because of alignment tolerances. A 3% increase in LEV thrust level during this time interval was then used, yielding good correlation in M and q as shown. A similar effect on M and q can be obtained by a reduction of the LEV power-on axial drag force, a trend which has generally evolved from previous boilerplate tests in transonic flight regions. However, a combined error of 3% on thrust level and/or vehicle drag is within the expected deviation. The LE motor thrust accuracy is discussed in section 7.8.

Based upon the previous results, simulation was made using the indicated change in thrust level with a thrust-vector alignment of $\epsilon_{XX} = 2.0°$, $\epsilon_{YZ} = 89.2°$ ($\epsilon_{XX} = 2.1°$ and $\epsilon_{YZ} = 92.58°$ preflight nominal alignment). The results of this simulation are compared to BP-23A flight performance data at canard deployment (T + 11 seconds) in the following tabulation:

Parameter	Boilerplate 23A Flight Data	Simulation	Percent Deviation*
Altitude, msl, ft	8490	8450	-0.9
X range, ft (+, north)	2600	2620	0.8
Y range, ft (+, west)	-169	-165	2.4
Mach number	0.293	0.296	1.0
Dynamic pressure, psf	95	100	5.0
Flight path angle, deg	45	42	-6.7

*The altitude percent deviations above are referred to the launch site elevation.

[redacted]

Trajectory of LEV With Canard Deployed

A postflight simulation of the trajectory of the LEV with canard deployed (T + 11 seconds to T + 13.9 seconds) showed good correlation with the flight-test trajectory parameters. Deployment conditions were obtained from available optical tracking and telemetry data and are identical to the tabulated data given above. Figures 7.1-25 and 7.1-26 contain plots comparing simulated and test values of altitude, X range, Y range, M, and q for the canard-deployed phase as a function of time from abort. Good agreement is seen to exist between the test and the simulation data. In the following table, simulated-trajectory parameters are compared to flight data at LES jettison (T + 13.9 seconds) with canard deploy (T + 11 seconds) used as a reference.

Parameter	Flight Data: Canard Deploy, T + 11 sec	Flight Data: Tower Jettison, T + 13.9 sec	Values from Simulation, T + 13.9 sec	Percent Deviation
Altitude, MSL, ft	8490	9000	9040	7.3
X range, ft (+, north)	2600	3210	3236	4.3
Y range, ft (+, west)	-167	-218	-214	-8.2
Mach number	0.293	0.195	0.202	7.1
Dynamic pressure, psf	95	40	43	5.4
Flight path angle, deg	45	30.5	31.1	4.1

Inspection of the optical tracking data just prior to LES jettison showed a significant dip in M and q over a time interval of 0.8 second. The physical nature of the system and the inconsistency with previous flight data preclude these data from being realistic. The data were therefore faired through this region and the faired data are used for comparison in this report.

Dynamics of LEV Prior to Canard Deployment

Initial postflight simulation of the LEV flight dynamics prior to canard deployment showed considerable discrepancies in comparison to the flight-test dynamic data; simulation of vehicle flight dynamics was based on the dispersions associated with alignment tolerances. Data thus obtained are presented in Figures 7.1-27 through 7.1-29. Good agreement between the simulated and the test data is seen to exist in the pitch plane (pitch rate, X-acceleration, and angle of attack), whereas the greatest discrepancy in the data correlation occurs in the yaw and roll planes. In general, the magnitudes of these simulated-flight parameters correlate with the test data although a noticeable phase shift is evident.

[redacted]

[redacted]

Since BP-23A experienced moderate roll rates (30 to 40 degrees per second) a more detailed analysis was made in an attempt to simulate the roll rates. Perturbations in LEV thrust level, center of gravity (Y_A), initial roll rate (p_o), and initial yaw rate (r_o), as well as changes to the aerodynamic data, were analyzed for their effects. Initial roll and yaw rates could have been imparted to the vehicle during vehicle separation from the launch pad adapter. The effects are tabulated in Figure 7.1-30. As noted, perturbations in thrust level (5% increase), cg Y_A distance (+0.083 inch) and p_o (3°/sec) alter the average roll rate for the LE motor thrust period by ±3°/sec. The effect of -3°/sec initial yaw rate (negative value used to conform with initial yaw rate sign) is to decrease the average positive roll rate by 0.5° to 3°/sec due to inertia cross-coupling. Changes to the aerodynamic data were also made based on aerodynamic data used to simulate the BP-6 flight with resulting negligible roll effects. It is apparent that in the use of these perturbations no combination of positive or negative tolerances in thrust-vector alignment would bring about the roll rate encountered. An additional conclusion resulting from the use of these perturbations was that in trying to improve the roll rate simulation increased deviation resulted in the yaw rate simulation.

As previously indicated, BP-23A had a boost protective cover with protuberances simulating covers for the scimitar antennas, air and steam vents, and umbilical. Furthermore, BP-23A is the first test on which these protuberances have been simulated for a regime combining low Mach number and high thrust. During the initial thrust buildup, but before vehicle liftoff, aerodynamic forces are generated on the surface of the command module by the flow field of the jet plumes. An order-of-magnitude analysis was made to determine what roll accelerations could be obtained from interaction between the protuberances and the jet plumes. Results of the analysis indicated that roll accelerations of approximately 20 deg/sec^2 could be obtained. A roll acceleration of this magnitude is sufficient to cause the roll rate exhibited during the flight. Since only symmetric jet-on aerodynamic data are available for flight simulations, an alternate approach was used to account for the asymmetric aerodynamics. A shift of 3 inches was made in the Y_{REF} and Z_{REF} center of pressure location (aerodynamic reference point, referenced to cg) which in effect introduced asymmetric aerodynamics into the simulation. This shift is considered reasonable, since the longitudinal reference point for pitch-plane aerodynamics is considered to have a tolerance of ±3 inches. A simulation therefore was made using the thrust alignment angles recommended from the analysis of the trajectory parameters with a Y_{REF} = -3 inches and a Z_{REF} = +3 inches. The effects of this simulation on body rates and angles of attack and sideslip are shown in Figures 7.1-31 and 7.1-32. Good correlation is shown in both magnitude and phasing of the data for the first 6 seconds of flight. After 6 seconds the curves tend to become mismatched. This is to

be expected, since the aerodynamic data (or in this case aerodynamic reference point) are a function of thrust coefficient, and the thrust coefficient is approaching zero at this time. Results of simulations for other combinations of aerodynamic reference-point shifts with variations in thrust alignment are tabulated in Figure 7.1-30.

Results of the foregoing analysis indicate that the discrepancies noted in roll and yaw plane simulations can be attributed to propulsion-aerodynamic interaction with the protuberances and that LEV dynamics can be correctly predicted in this Mach number and dynamic pressure region with some modification to the currently available aerodynamic data to account for vehicle protuberances.

Dynamics of LEV With Canard Deployed

Postflight simulation of the dynamics of the LEV with canard deployed (T + 11 seconds to T + 13.9 seconds) showed good agreement with flight dynamic parameters. Deployment conditions were obtained from available optical tracking and telemetry data as previously mentioned. Figures 7.1-33 through 7.1-35 present comparisons of simulated and flight-test body rates, acceleration, and angles of attack and sideslip as functions of time from liftoff. Good agreement is shown in both phasing and magnitude for vehicle accelerations, angles of attack and sideslip, and pitch and yaw rates. However, the simulated roll rate, Figure 7.1-33, shows a greater decay with time than do the test data. This discrepancy is attributed to unknowns in the aerodynamic damping and rolling moment data used for the canard turnaround simulation.

Analysis of LES Trajectory and Dynamics

LES-CM Separation

The LES with canard deployed and with the boost protective cover attached was successfully jettisoned from the BP-23A command module 13.9 seconds after liftoff. The soft (aft) portion of the boost protective cover broke up soon after LES separation (see Analysis of BPC Loads, below); the hard portion of the cover remained with the LES to impact. Separation parameters are shown in Figures 7.1-36 through 7.1-38. The initial conditions at LES jettison are listed below:

Time from liftoff	13.9 seconds
Dynamic pressure	40.0 psf
Altitude	9000 ft (msl)
Flight path angle	30.5 deg
Heading angle	6.0 deg

[redacted]

Roll rate	9.4 deg/sec
Pitch rate	50.4 deg/sec
Yaw rate	-20.4 deg/sec
Euler angles (ZYX)	
Roll (ϕ)	170.5 deg
Pitch (θ)	-20.5 deg
Yaw (ψ)	94.9 deg

With the exception of body attitude angles and angular rates, these quantities were derived from optical tracking data. The rate gyros were used in determining the body attitudes and initial angular rates. A discussion of the derivation of the attitude angles is given in the following paragraphs.

LES Trajectory

Trajectory parameters of the BP-23A launch escape system, both actual and simulated, are shown in Figures 7.1-39 through 7.1-42. These figures present range, altitude, flight path angle, and resultant velocity histories from jettison to impact.

A knowledge of LES dynamics and the ability to simulate its trajectory is required in order to predict the miss-distance between the LES and the CM or the launch vehicle, as well as to predict the LES impact point. Simulations of the LES trajectory were accomplished by means of a six-degrees-of-freedom digital program and are shown in Figures 7.1-30 through 7.1-42. The initial conditions at jettison used in the simulations were those noted in the previous table. A simulation discussed below with $\theta = -5.5$ degrees is included additionally in Figure 7.1-40. The aerodynamic data used in the simulations were obtained from the latest revision to the Aerodynamic Data Manual (reference 13). Mass and inertia data used were for the LES without the soft portion of the boost protective cover (reference section 7.5). Meteorological data were taken from range data.

The primary factors affecting the LES trajectory, particularly the early portion of the trajectory, are the initial velocity, the flight path angle, body attitude angles, and angular rates. For the BP-23A flight, the velocity and flight path angle from optical tracking data were known with a high degree of confidence, as were body angular rates derived from the rate-gyro instrumentation. The confidence level in the body attitude angles derived from integrated rate gyro data, however, was not as high.

The pitch angle (θ) derived from integrated rate-gyro data indicated a pitch attitude of minus 5.5 degrees (nose below the horizon) at LES jettison. A simulation using this initial negative 5.5-degrees pitch attitude is included

in Figure 7.1-40. This initial pitch attitude gave a trajectory considerably higher than the actual LES flight trajectory. An additional 15 degrees of negative pitch gave the much closer simulation shown in Figure 7.1-40, and the conclusion was therefore drawn that the initial pitch attitude at LES jettison was approximately -20.5 degrees rather than the -5.5 degrees indicated by integrated rate-gyro data. Range simulations, both crossrange and downrange components, agreed well and indicated that the 94.9-degrees Euler yaw angle was approximately correct.

Flight path angle and resultant velocity histories are shown for the BP-23A LES in Figures 7.1-41 and 7.1-42, showing that the LES velocity vector was adequately simulated in both direction and magnitude. The flight path angle was simulated within 5 degrees and the resultant velocity was simulated within 10 feet per second throughout the LES trajectory.

As seen in motion pictures tracking the LES, there were pronounced oscillations in pitch and yaw for the first few seconds of LES flight. After 10 seconds these oscillations had damped to unobservable levels. There was no instrumentation available to measure LES angle of attack (α) after separation from the command module; however, the approximate times at which the peak oscillations occurred were determined from the tracking films. These times are shown in Figure 7.1-43, which presents α time histories for two LES simulations, one with pitch damping. As seen in the plot, the times corresponding to peak values in the α simulations compare favorably with those observed of the flight vehicle, and the phasing indicates that the magnitude of the actual vehicle damping is within the values used in the two simulations.

Analysis of Forward Heat Shield Separation

Separation distance data used in analyzing the separation of the forward heat shield (FHS) were obtained from the onboard camera mounted in the egress tunnel and from analysis of tracking-camera film. Range tracking data of the forward heat shield (apex cover) were not available for this analysis. The FHS trajectory provided by the onboard camera data is shown in Figure 7.1-44.

Attitude and rate values for the CM at FHS jettison, obtained from reduced tracking and telemetry gyro data, were questionable; therefore a parametric study was made to establish the effect of CM attitude and pitch rate on the CM-FHS separation characteristics. The analysis was conducted in three degrees of freedom, where the parameters varied were total angle of attack and pitch rate. For the analysis, pitch rate was assumed to be the root sum square of vehicle pitch rate and yaw rate. In the following discussion, the results of the parametric study are compared with the available flight data.

A point in the trajectory, 0.5 second after jettison initiation, which showed significant separation between the forward heat shield and the command module, and for which there were sufficient photographic data available, was used for comparison between actual and simulated jettison. Variations of the measured values with the simulated values are presented in Figures 7.1-45 and 7.1-46. The effect on separation distance due to tolerances in vehicle angle of attack and pitch rate also is shown. As deduced from the trends of the curves, the values of the parameters at apex-cover jettison giving the best simulation of the flight are an angle of attack of 100 degrees and a pitch rate of 45 degrees per second. These values are within the dispersions of the values measured by the data acquisition subsystem and therefore are considered reasonable. It also can be seen that as both angle of attack and pitch rate decrease or increase from the prescribed values, the simulation of separation distance becomes poor. Initial conditions used for the simulation are listed below:

Time from liftoff	14.3 seconds
Altitude (msl)	9060 feet
Mach number	0.187
Dynamic pressure	36 psf
Total angle of attack	100 degrees
Pitch rate	45 deg/sec

A comparison of the simulated with the actual forward heat shield separation distance time history is made in Figure 7.1-44. Good agreement is shown between the simulated and the actual separation distance, with a maximum deviation of 0.7 foot at 0.5 second after forward heat shield jettison.

After initial separation, the forward heat shield began drifting behind the command module. At drogue deployment it was sufficiently below and behind the command module so that there was no possibility of contact with the drogue chutes. From films showing both the forward heat shield and the command module at this instant, it was estimated that the apex cover (forward heat shield) was approximately 40 feet below and 30 feet behind the command module. Examination of the tracking film (T - 108, T - 173, and T - 191) and egress-tunnel camera film showed that adequate separation between the command module and the forward heat shield was maintained through forward heat shield freefall.

Analysis of LEV Base Pressures

Since prediction of vehicle performance is based on an accurate knowledge of base drag (base pressure), a comprehensive analysis of the

correlation between flight test data and wind-tunnel test data was made. BP-23A instrumention included twelve pressure transducers, covering a range of zero to 15 psia, located on the base of the command module. Telemetry data were used here in preference to the onboard recorder tape data because the scatter band was smaller. The data were biased to agree with the measured ambient conditions at liftoff.

The pressure time histories of three pressure taps in the pitch plane are shown in Figure 7.1-47. Base pressures from wind-tunnel tests (reference 14) and a previous flight test, BP-6 (reference 3), adjusted to BP-23A flight conditions, also are shown for comparison. The excellent agreement indicates that the boost protective cover has no measurable effect on base pressures and that M = 0.5 wind-tunnel data are valid for all Mach numbers below M = 0.5. This is also in agreement with the BP-6 flight-test results, which showed excellent base-pressure correlation.

The pressure was essentially constant across the base with only small variations due to excursions in the angle of attack. The pressure distribution across the base at T + 2 seconds, at which time the maximum angle of attack occurred, is presented in Figure 7.1-48. It should be noted that the data for S/R = ±1.06 correspond to pressure taps located at the command module maximum diameter and underneath the BPC. The measured base pressures were in agreement with wind-tunnel data. The pressure distribution at T + 10 seconds also is presented to further show the agreement between the M = 0.5 jet-off wind-tunnel data and the jet-off flight data below M = 0.5.

Analysis of BPC Loads

Since there are no wind-tunnel test data available that give BPC loads in the presence of the command module, design BPC loads were estimated from conical-surface pressure data and the assumption that the pressure under the BPC was equal to the base pressure. Six pressure taps were installed underneath the BPC to measure this cavity pressure and to determine whether this analytic technique was valid. Conical-surface pressure values used for the analysis were obtained from wind-tunnel test data, since results of the BP-6 pressure analysis showed that excellent correlation existed between flight test and wind-tunnel test conical-surface pressure data. The pressure time histories at two locations underneath the cover are presented in Figure 7.1-49. The measurement at X_C 79, CA0027P, was omitted because it was located above the BPC seal and indicated values higher than base pressure. BPC loads calculated from these pressures and wind-tunnel predictions for the surface pressures are presented in Figure 7.1-50. Also shown for comparison are the same curves predicted from wind-tunnel test data alone. The maximum BPC

load history for the flight obtained from wind-tunnel test data also is presented to show the worst-case condition. Comparison of the predicted curves with the curves obtained from a combination of wind-tunnel and flight-test data shows that in all cases the predicted values are larger than the values obtained from the FT/WTT data. This confirms that the design philosophy of assuming base-pressure values underneath the entire cover is valid and only slightly conservative.

The boost protective cover did not fail during LEV turnaround nor was there any increase in the pressures underneath the cover. At boost protective cover pullaway the four pressure taps nearest the shoulder, station X_C 30, all showed a downward spike in the pressures. However, the pressures at stations X_C 50.5 and X_C 79 (above the seal) did not indicate this drop in pressure. Figure 7.1-51 is a sequence of pictures from one of the tracking films showing the BPC during pullaway. The pictures show that the cover held its shape for a finite time during pullaway. This indicates that if there was a vacuum effect due to pulling the BPC away from the CM, it did not hold the BPC on the CM or exceed the structural load limit.

Venting

The venting area was large enough so that the pressure in the parachute compartment should have followed the CM pressure at station X_C 80 with no appreciable lag.

The venting for the parachute compartment was provided by a gap formed by the apex cover and the command module with an average gap size between 0.015 and 0.040 inch. The space between the apex cover and the hard boost cover was vented in turn through eight 1-inch diameter holes in the transition section between the hard and the soft portions of the BPC at station X_C 80.

The pressure history in the parachute compartment obtained from CE0035P and CE0036P is compared in Figure 7.16-2 with the predicted pressure at X_C 80 for a smooth CM and with the pressure data at X_C 79 obtained from CA0027P which is located under the transition step in the BPC. Since the vent holes are located in this step, the local pressure, approximately equal to CA0027P data, should be less than that predicted for a smooth CM module, as is indicated by the data. Further, the data from the two pressure measurements CE0035P and CE0036P closely follow the data at X_C 79 after T + 3 seconds.

This agreement, as well as the pressure history in the parachute compartment, indicates that the vent area in the BPC and the apex cover was adequate.

The venting technique used here will not be used on spacecraft command modules. Venting for spacecraft will be through spaces between the longerons and the air vents at the base of the CM. Boilerplate 22 used a 1-inch tube through the longeron spaces, but the tube is not used with spacecraft.

Analysis of Euler Angles, Aerodynamic Angles, and Dynamic Pressures

Euler Angles

Three attitude gyros and three rate gyros were utilized to determine vehicle attitude angles throughout the flight. Vehicle roll attitude angle (ϕ), yaw attitude angle (ψ), and pitch attitude angle (θ) in the YZX Euler system (+X axis up) are presented in Figures 7.1-52 through 7.1-54 for data obtained from telemetered attitude-gyro and integrated rate-gyro outputs. These data are presented for flight times between liftoff and T + 15.3 seconds. All attitude gyro data are valid between liftoff and T + 5.7 seconds. At T + 5.7 seconds, the pitch and yaw attitude gyros (Figures 7.1-53 and 7.1-54) began to give erroneous angles due to roll greater than 85°. The angles, however, did follow the general trend of the attitudes derived from the integrated rate-gyro data. The roll attitude gyro was unaffected by other attitudes until T + 12.5 seconds. At T + 15.3 seconds, the yaw rate gyro exceeded its calibration limits, and the derived attitude data are invalid beyond that time. The levels of the curves presented in Figures 7.1-52 through 7.1-54 are questionable because of errors introduced through instrument inaccuracy, data scatter, and data reduction (data smoothing, debiasing, etc.). Additional details concerning the validity of the data are presented under Onboard Data Acquisition, below, and in section 7.10.

Roll attitude angle (Figure 7.1-52) from the attitude gyro increases at a greater rate than roll angle from integration of rate-gyro data between liftoff and T + 12.5 seconds. At T+ 12.5 seconds, the integrated rate-gyro data show the vehicle to have rolled approximately 30 degrees more than shown by the attitude gyro data. Beyond T + 12.5 seconds, correlation between the two sources of data is completely lost.

Figure 7.1-53, comparing the two yaw attitudes, shows a maximum variation of approximately 10 degrees between ψ from integrated rate-gyro data and attitude-gyro data for flight times between liftoff and T + 14.2 seconds. A sharp deviation in yaw attitude at approximately T + 6 seconds corresponds to yaw gyro reference loss caused by 85 degrees of vehicle roll. Beyond this time the attitude gyro data are invalid as indicated by the discontinuities in the data. At T + 15.3 seconds, the yaw rate gyro exceeded the calibration range and invalidated the derived attitude data beyond that point.

Pitch attitude angle comparison, presented in Figure 7.1-54, shows correlation within 8 degrees for flight times up to T + 5.7 seconds between the integrated rate-gyro data and the attitude gyro data. Beyond T + 5.7 seconds, θ from the integrated rate-gyro data follows a smooth curve while θ from the attitude gyro data shows many discontinuities and erroneous attitude angles due to roll greater than 85 degrees. However, the general level of the attitude gyro data does follow the integrated rate gyro data.

Aerodynamic Angles

Angles of attack (α) and sideslip (β) time histories for the first 15.2 seconds of the flight are presented in Figure 7.1-18. These angles were obtained from Q-ball data (T + 0.7 to T + 11 seconds) and from integrated rate-gyro data (T + 11 to T + 15.2 seconds) adjusted to account for shifts in the level of the data. Correct levels of the data from T + 11 to T + 15.2 seconds were established, based on the results of the LES and FHS trajectory analyses. Angles of attack and sideslip derived from the integrated rate-gyro data were compared to the simulated α and β at the jettison times and were found to be within the limitations of the flight-test data. The level of the α and β curves then were adjusted to pass through the points obtained from the simulation at T + 13.9 and T + 14.3 seconds. The α and β time histories established by means of this technique are considered as a best estimate until more complete information is made available. (Refer to Onboard Data Acquisition, below.)

Figure 7.1-55 presents vehicle angle of attack and angle of sideslip for flight times between T + 0.7 second and T + 13.1 seconds derived from Q-ball differential pressures. These data were selected as the primary source of aerodynamic angles from T + 0.7 to T + 11 seconds.

Figures 7.1-56 and 7.1-57 are comparison plots of α and β from three sources. Q-ball data are shown between liftoff and the time when vehicle attitudes exceeded the limit of the Q-ball calibration range (T + 13.1 seconds). Aerodynamic angles from the combination of rate-gyro-derived Euler angles and tracking data (flight path and heading angles) are shown between T + 0.7 and T + 15.3 seconds when the yaw rate gyro exceeded its calibration limit. Aerodynamic angles from the combination of attitude-gyro-derived Euler angles and tracking data are shown between T + 0.7 and T + 5.7 seconds, when the Euler angles became invalid.

Figure 7.1-56 shows a level shift between α from Q-ball and α derived from the rate gyros of from 4 to 6 degrees during the LE motor thrust period. However, the peak angles of attack occur at approximately the same flight times. The amplitudes of the Q-ball α for the first two cycles

are approximately 11 degrees, while the gyro-derived α (both rate and attitude) shows amplitudes of 5 and 7 degrees for the first two cycles. At canard deployment the angle of attack is shown by Q-ball data to be -1 degree and that shown by the rate gyros is 7.7 degrees.

Figure 7.1-57 shows agreement within 2 degrees between rate-gyro-derived β and attitude-gyro-derived β for flight times up to T + 5.7 seconds, after which the attitude-gyro-derived β becomes invalid. Q-ball-derived angle of sideslip varies from 6 degrees below to 4 degrees above rate-gyro-derived β during the first 12 seconds of flight, although the peak angles of sideslip generally occur at the same flight times for both sets of data. At canard deployment, angles of sideslip shown by the Q-ball-derived data and the integrated rate-gyro-derived data are 2.2 degrees and 6.3 degrees, respectively. Thereafter, angle of sideslip increases. At T + 13.8 seconds, when α passes through 90 degrees, β jumps from 47 degrees to 132 degrees.

Dynamic Pressures

Dynamic pressure (q) derived from optical tracking and meteorological data was used for flight-test analysis, rather than q from Q-ball differential-pressure data. Q-ball-derived dynamic pressure prior to T + 1.0 second and after T + 13.9 seconds is omitted because of scatter in the q-port differential-pressure readings (ΔPq) which are within the noise level of the instrumentation, or because of vehicle attitudes which exceed the wind-tunnel calibration range for determining q.

Analysis of the Q-ball differential-pressure data has resulted in an empirical method of obtaining Q-ball dynamic pressures which are in close agreement with tracking q. The results of this analysis also provide aerodynamic angles which agree for both theoretical and wind-tunnel calibrations of the Q-ball. This agreement could not be obtained by using uncorrected flight-test data.

Figure 7.1-58 shows a comparison of the differential pressure across the Q-ball q-ports (ΔPq) obtained from BP-23A flight-test data with two empirical calculations for ΔPq. The purpose of these calculations was to match the Q-ball-derived dynamic pressure with tracking q. Figure 7.1-59, containing a plot of q from tracking, a plot of q derived from Q-ball flight-test ΔPq, and a plot of q derived from corrected Q-ball ΔPq, shows that close agreement was obtained between the first and last q sources.

Use of flight-test data biased for initial conditions resulted in the dynamic pressure curve shown in Figure 7.1-59, which is between 14 and 40 percent below tracking q throughout the entire Q-ball operating regime.

Smooth curves of Q-ball-derived α and β were not obtained because discontinuities resulted when the vehicle attitude exceeded the Q-ball wind-tunnel calibration limits and necessitated the use of theoretical calibration. Figure 7.1-60 and 7.1-61 include plots of α and β based on flight-test Q-ball differential pressures between T + 5.0 seconds and T + 10.0 seconds, which are representative of typical discontinuities. Similar discontinuities also have been experienced in previous flight tests.

To improve the results, the Q-ball data-reduction program was modified. The theoretical Q-ball calibration and the flight-test ΔPq were used to obtain α and β, which in turn were used to determine a new ΔPq required to match the optical tracking q. This calculated ΔPq is shown in Figure 7.1-58. The calculated ΔPq, when compared to flight-test ΔPq, was found to be approximately 25% greater for the entire Q-ball regime. Accordingly all biased flight-test ΔPq values were multiplied by 1.25. These calculated values of ΔPq and Q-ball wind-tunnel calibration, and, where necessary, the theoretical calibration, then were used to obtain final values of α, β, and q.

The improved results of this empirical data-reduction process are presented in Figures 7.1-55 and 7.1-59, which show α and β curves having no discontinuities, and which show a Q-ball-derived q closely matching tracking q. The small variations shown between tracking q and q obtained by the above-described method are primarily due to the Q-ball data-reduction program, which does not provide for interpolation between Mach number tables when determining q.

Onboard Data Acquisition

Data from instrumentation on board the command module and the launch escape subsystem were recorded on an onboard tape recorder and also were telemetered to ground recording stations. The telemetry data showed the least scatter and the fewest extraneous data points for the greatest number of parameters, and were used for data-reduction and analysis. Recording of instrument readings was initiated approximately 15 seconds before liftoff in order to determine bias values to be used in data reduction.

Comparison plots of onboard tape-recorded data and telemetered data are presented in Figures 7.1-62 through 7.1-71 for selected flight-time increments. These plots show that in general the onboard tape data exhibit greater scatter and have more extraneous data points than the telemetered data. Also, no commutated data were recorded on board the vehicle between T + 0 and T + 1.3 seconds. Telemetry data were available

for data reduction approximately two weeks before onboard data. These circumstances resulted in the use of telemetry data as the primary source for data reduction. Discussion of the pertinent features of each comparison plot will be included with the discussion of each instrument when applicable.

Onboard Cameras

A tower camera and an egress-tunnel camera were mounted on the vehicle for close-up observation of LES motor burning, LES and FHS jettison, and parachute events. The tower camera lens was covered with soot from the LES motor during motor tailoff and therefore did not provide useful information on LES jettison. The egress-tunnel camera was useful in providing FHS separation data from which separation distances, velocities, and accelerations of the command module and the forward heat shield were obtained.

Pressure Transducers

All barostatic (parachute compartment), base, and surface pressure transducers were operative throughout the flight. Comparisons of ground-recorded and onboard-recorded barostatic, base, and conical-surface pressures are shown in Figures 7.1-62, 7.1-63, and 7.1-64, respectively. In all cases, ground-recorded pressures contained fewer extraneous data points and smaller amplitude of scatter than onboard-recorded data, and were therefore used for analysis.

Ground-recorded (telemetry) pressure data were received with biases ranging between 0.2 psi above and 0.7 psi below the correct pressure level. The amplitude of the scatter in the data was approximately 0.4 psi throughout the flight with amplitudes as large as 1.4 at a few flight times.

Q-Ball

Commutated Q-ball differential-pressure data (ΔP_α, ΔP_β, ΔPq) were obtained between abort initiation and LES jettison. Data obtained prior to T + 1 second are invalid because of low dynamic pressure. Data at flight times after T + 11 seconds are questionable because of low dynamic pressure and after T + 13 seconds are invalid since the vehicle aerodynamic angles exceeded the limits of the Q-ball calibration.

Comparison of onboard-recorded and ground-recorded differential pressures in Figures 7.1-65 and 7.1-66 shows greater scatter and more extraneous data points inherent in the onboard recordings of $\Delta P\alpha$, $\Delta P\beta$, and ΔPq than in the ground-recorded differential pressures. As a result, ground-recorded data were selected as the primary source for Q-ball data reduction.

Differential pressures were smoothed by means of a five-point least squares digital smoothing routine. As received, the ΔP_α, ΔP_β, and ΔP_q data had biases of -65.4 psf, -72.7 psf, and -0.4 psf respectively. Analysis of the differential-pressure data has indicated that ΔPq values, after correction for bias, were approximately 20 percent below those which would be required to match dynamic pressure derived from Q-ball data and q derived from optical tracking. Discussion and presentation of the results of this analysis are included under Dynamic Pressures, above.

Accelerometers

Continuous X, Y, and Z axis accelerations were obtained throughout the flight. Fifteen-point smoothing was applied to these data before conversion to acceleration angles. Bias values applied to the X high, X low, Y, and Z command module accelerometers were 0.1948 g, 0.0112 g, -0.0571 g, and 0.1059 g, respectively. Figure 7.1-67 is a comparison plot of the X, Y, and Z acceleration data obtained from onboard and ground-recorded sources for one second of flight time. The onboard data generally contain smaller-amplitude oscillations and fewer extraneous data points throughout the flight; however, because the telemetry data were available when required, they were used in the analysis.

Attitude Gyros

Three attitude gyros were utilized to obtain vehicle attitude data relative to the vehicle axes at time of launch. These data were obtained throughout the entire flight on telemetry commutated channels. Because of the design limits of the gyros discussed in section 7.10, the data were valid only for portions of the flight. The data as received had biases of 0.42, 0.80, and -0.78 in roll, yaw, and pitch, respectively. The biases were removed, and an 11-point smoothing routine was applied to the data. Euler attitude angles of the YZX set, the Euler angle direction cosine matrix, and aerodynamic angles were formulated from the data.

Euler attitude angles of the YZX set, presented in Figures 7.1-53 through 7.1-55, include an error in that they were not biased to zero at time of liftoff. The error in bias resulted from inclusion of an extraneous preflight calibration data point in the automatic bias calculation. The magnitude of the error in the Euler angles, the direction cosine matrix, and aerodynamic angles caused by the bias error has not been determined at this time.

Comparison plots of the onboard and ground-recorded data for 5 seconds of flight time are presented in Figures 7.1-68 through 7.1-70. These plots show large-amplitude oscillations in the onboard data compared

to the ground-recorded data. As a result, the ground-recorded data were used for data reduction. Vehicle attitudes presented on these curves are all in different Euler angle reference systems. The systems are: pitch (θ) order, ZXY; roll (ϕ) order, YZX; and yaw (ψ) order, YXZ.

Rate Gyros

Continuous rate-gyro data were recorded throughout the flight. These data were valid at all flight times with the exception of short intervals during which the vehicle rates exceeded the rate-gyro calibration range (reference section 7.10). The first of these excessive rates was experienced at approximately T + 15.3 seconds when the yaw rate gyro exceeded its calibration limit.

Reduction of rate-gyro data was therefore not carried beyond this time. Raw rate-gyro data were thinned from 100 samples per second (S/S) to 20 S/S by using every fifth data point. The bias values of -0.174, -0.192, and -0.358 degree per second in roll, yaw, and pitch rates, respectively, were then removed from the 20 S/S data and an 11-point smoothing routine was applied to the data.

Comparison plots of data recorded on board and at ground stations are shown in Figure 7.1-71. These data show large-amplitude oscillations in the ground-recorded data relative to the onboard-recorded data. However, since onboard data were not immediately available, all data reduction was based on the ground-recorded data.

Euler angles of the YZX order of rotation, the Euler angle direction cosine matrix, aerodynamic angles, and angular accelerations were formulated by integration and differentiation of the rate-gyro data. To obtain the Euler angles from which the direction cosine matrix and the aerodynamic angles were derived, all angles were initialized at zero degrees and the smoothed rates were then integrated from this point. The error inherent in using every fifth data point for bias determination and data smoothing may have resulted in erroneous attitude and aerodynamic angles. The validity of the Euler angles cannot be determined, since no additional source of valid YZX Euler attitude angles is available beyond T + 5.7 seconds and the attitude gyro angles also contain the erroneous bias previously discussed. Up to T + 5.7 seconds, however, rate-gyro and attitude-gyro angles are generally in agreement.

[redacted]

Conclusions

Study of the data obtained from the BP-23A flight, and of the simulations prepared therefrom, has led to the following conclusions:

1. Simulation of the BP-23A flight was accomplished within known system limitations. The best simulation obtained was based on a thrust-vector alignment of $\epsilon_{XX} = 2.0$ deg and $\epsilon_{YZ} = 89.2$ deg with an aerodynamic reference point shift of $Y_{REF} = -3$ inches and $Z_{REF} = +3$ inches.

2. Performance of the LEV can be predicted accurately in the Mach number and dynamic pressure regime of a pad-abort mission.

3. Accurate vehicle dynamics can be predicted if the asymmetric effects of protuberances are accounted for in the simulations.

4. Satisfactory LES jettison capability was demonstrated for a typical pad abort of the Apollo vehicle with no separation problems evidenced by the flight.

5. The ability to simulate the LES trajectory closely was demonstrated.

6. Satisfactory forward heat shield jettison capability was demonstrated for a typical pad-abort mission with no separation problems evidenced by the flight.

7. The ability to closely simulate the short-term separation characteristics of the forward heat shield was demonstrated.

8. At drogue parachute deployment the forward heat shield was sufficiently below and behind the command module so that there was no possibility of the forward heat shield contacting the drogue parachutes.

9. The BPC had no effect on BP-23A base pressures.

10. Agreement of BP-23A base-pressure data, wind-tunnel test data, and BP-6 flight-test data was excellent during LE motor thrust and coast flight.

11. The design philosophy of assuming base-pressure values underneath the entire BPC for loads analysis was confirmed.

[redacted]

12. Boost protective cover breakup occurred after LES jettison was initiated, and after a finite separation distance was attained.

13. Euler attitude angles and aerodynamic angles from both rate and attitude gyros are questionable because of instrument application limits and data-reduction system accuracy.

14. Aerodynamic angles α and β obtained from Q-ball data exhibit a higher degree of accuracy than other data in the period T + 1 to T + 13.9 seconds.

15. Accuracy of the Q-ball data can be increased by implementation of one of the following methods, listed in order of accuracy obtainable:

    a. Perform a wind-tunnel calibration on each Q-ball before its installation on a flight vehicle.

    b. Use the empirical method described under Dynamic Pressures, herein, to correct the flight-test ΔPq.

16. Telemetry data showed generally less data scatter and fewer extraneous data points than onboard-recorded data. Only the availability of the telemetry data warranted its use in a few instances.

17. Pressure-data scatter was approximately ±0.4 psi throughout the flight with maximum amplitudes as large as 1.4 psi.

18. Gyro data were obtained for only portions of the flight because of the gyro application limits discussed in section 7.10.

Event	Time From Liftoff, Seconds *	Mach Number	Dynamic Pressure, PSF	Flight Path Angle, Deg	Altitude, MSL, Ft	Downrange (+, North), Ft	Crossrange (+, West), Ft
Abort Initiation	-0.2	0	0	$\theta = 90^{\circ}$ Launch	4036	0	0
Liftoff	0	0	0		4036*	0	0
Maximum LEV main motor thrust after T + 0.2	1.4	0.290	105.0	74.0	4270	60	-10
Maximum Mach number attained	3.7	0.587	420.0	62.2	5400	500	-50
LEV main motor burnout	8.7	0.373	157.0	52.2	7850	2030	-145
Canard deployment	11.0	0.293	95.0	45.0	8490	2600	-169
LES jettison	13.9	0.195	40.0	30.5	9000	3210	-218
Forward heat shield jettison	14.3	0.187	36.0	28.0	9060	3320	-228
Drogue deployment	15.8	0.172	30.0	16.2	9190	3650	-260
Apogee	17.5	0.157	25.0	0	9260	4015	-320
Drogue - disconnect/main-parachute deployment	28.6	0.187	39.5	-69.0	7871	5450	-610
Main-parachute disreef	38.5	—	8.5	-70.0	6290	5940	-720
Terminal descent conditions attained	44.0	—	1.2	-61.0	5940	6120	-720
CM landing	112.8	—	0	-50.0	4050	7620	-370

*Liftoff is time of umbilical disconnect, when vehicle is approximately 4 inches off pad.

Figure 7.1-1. Table of Nominal Trajectory Parameters

[redacted]

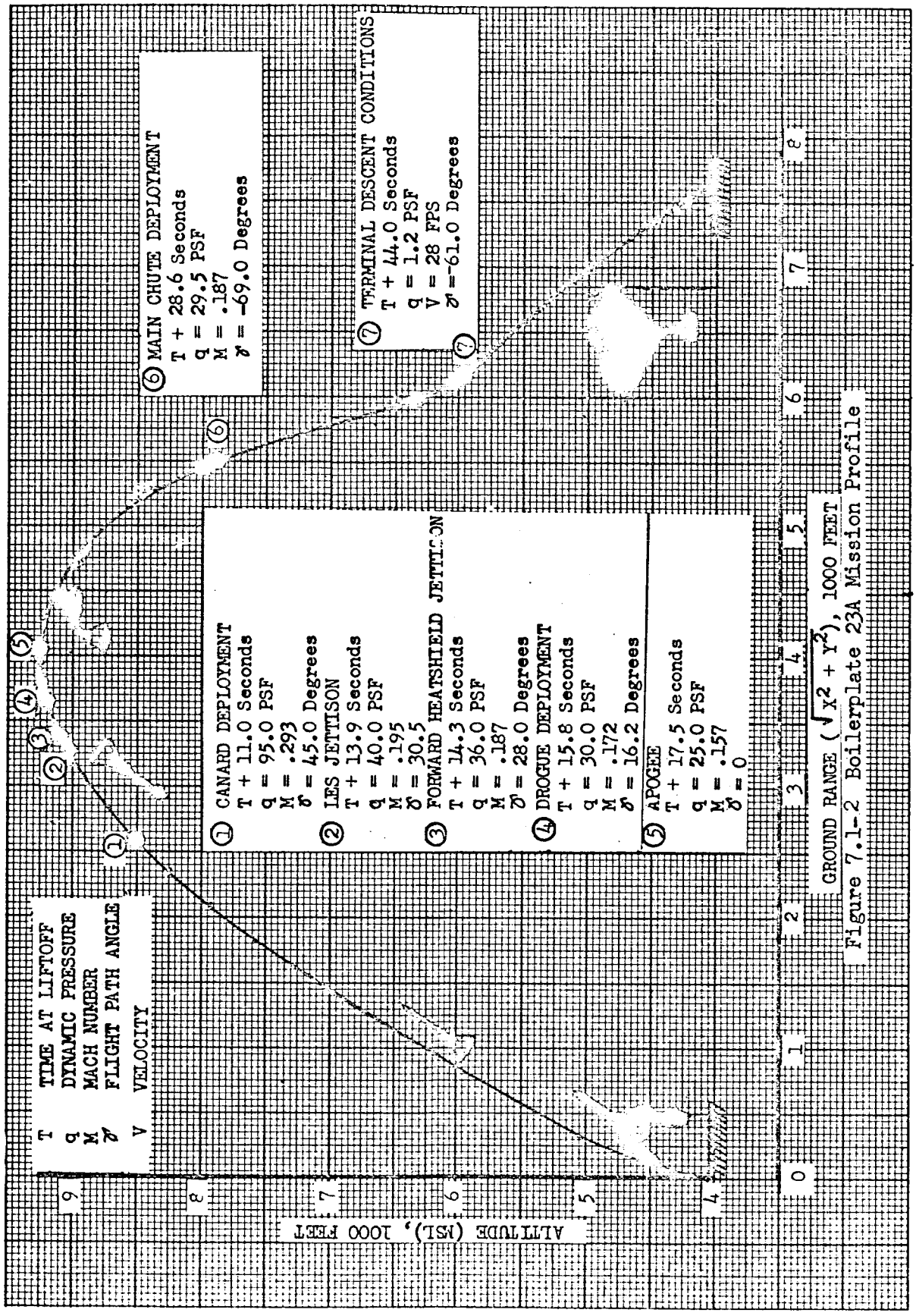

Figure 7.1-2 Boilerplate 23A Mission Profile

[redacted]

~~CONFIDENTIAL~~

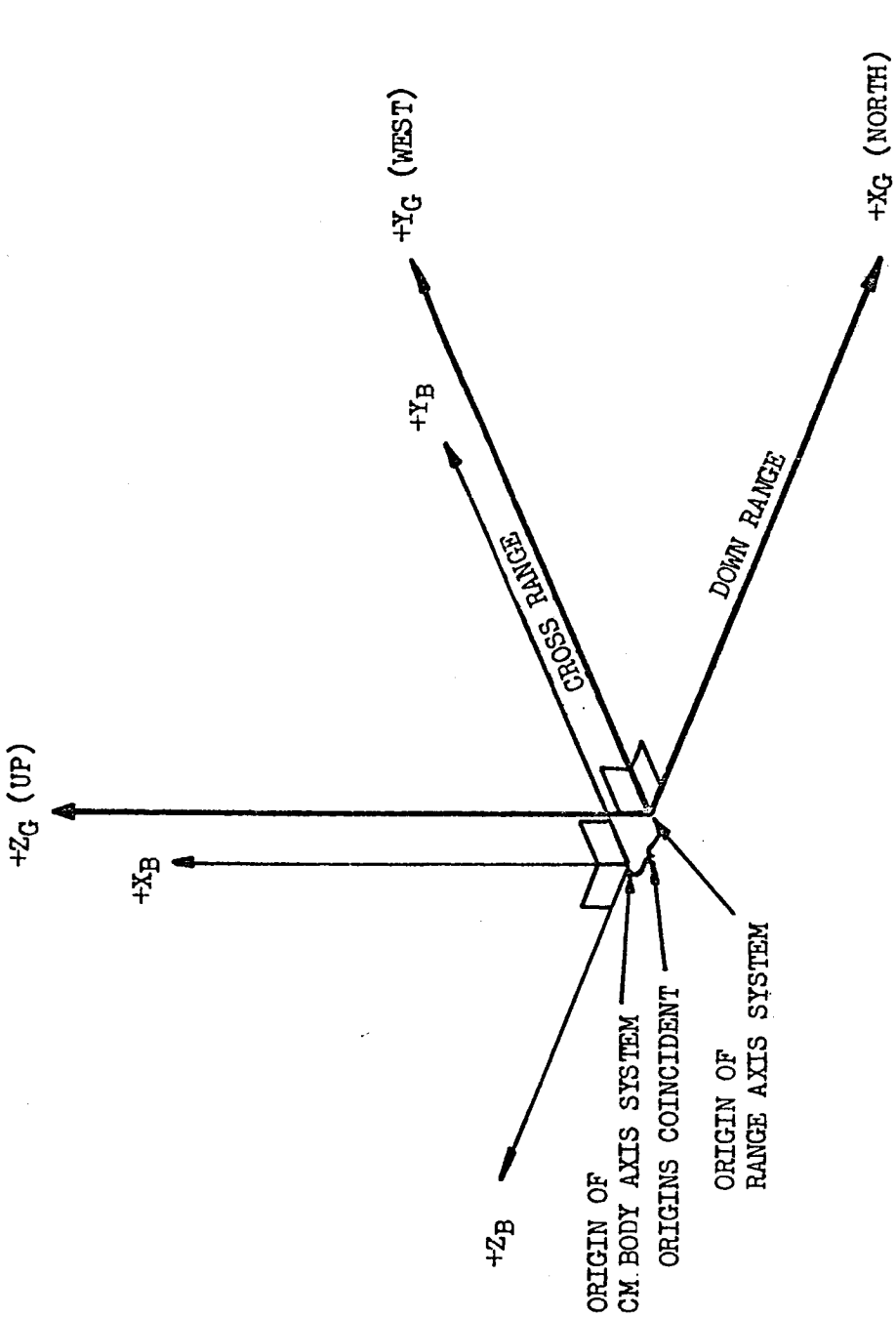

Figure 7.1-3 Orientation of Command Module Body Axis System to Range Axis System ($\theta_{LEV} = 90°$, $\phi_{LEV} = 180°$) at Launch

~~CONFIDENTIAL~~

[redacted]

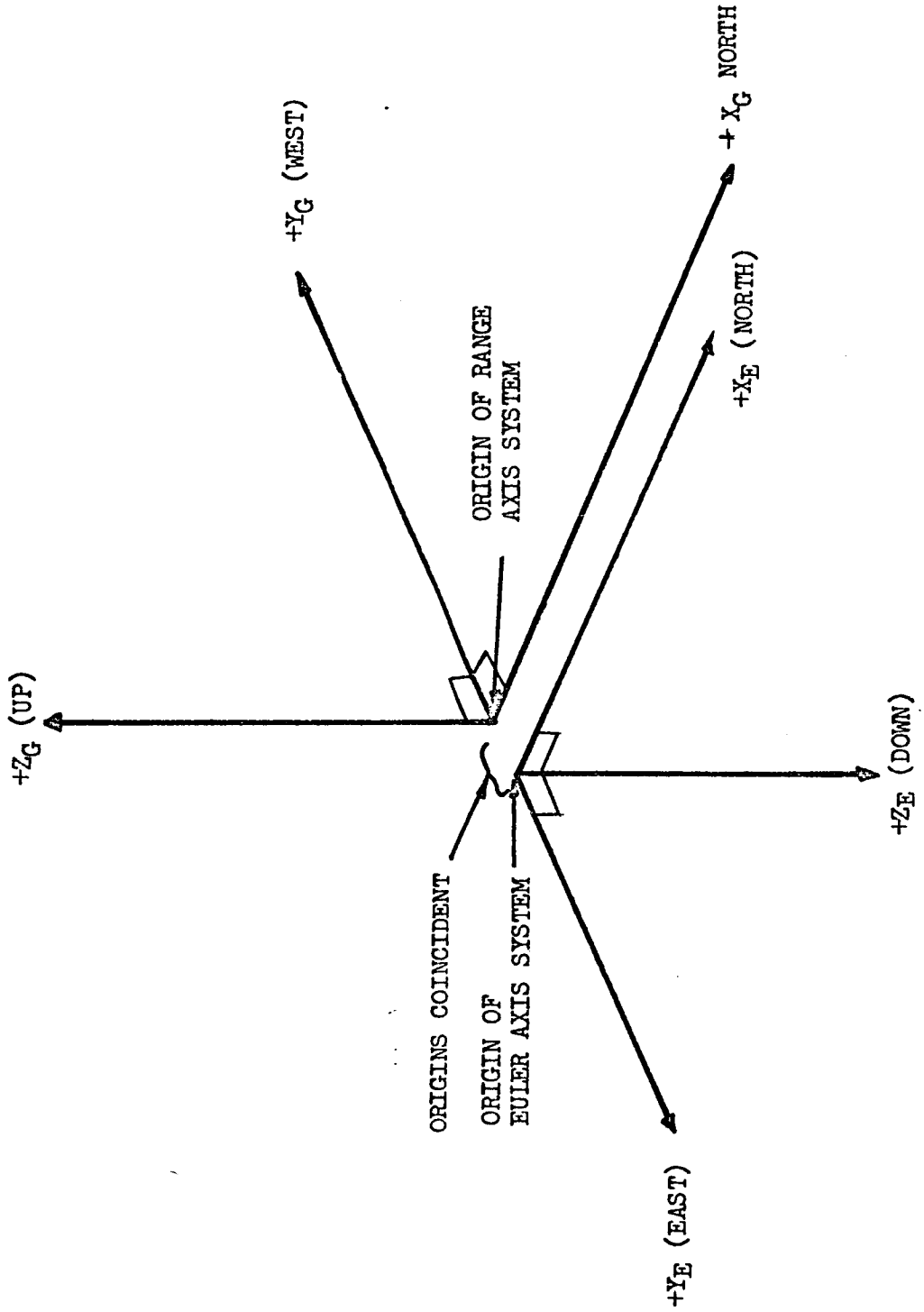

Figure 7.1-4 Orientation of Euler Axis System to Range Axis System

~~CONFIDENTIAL~~

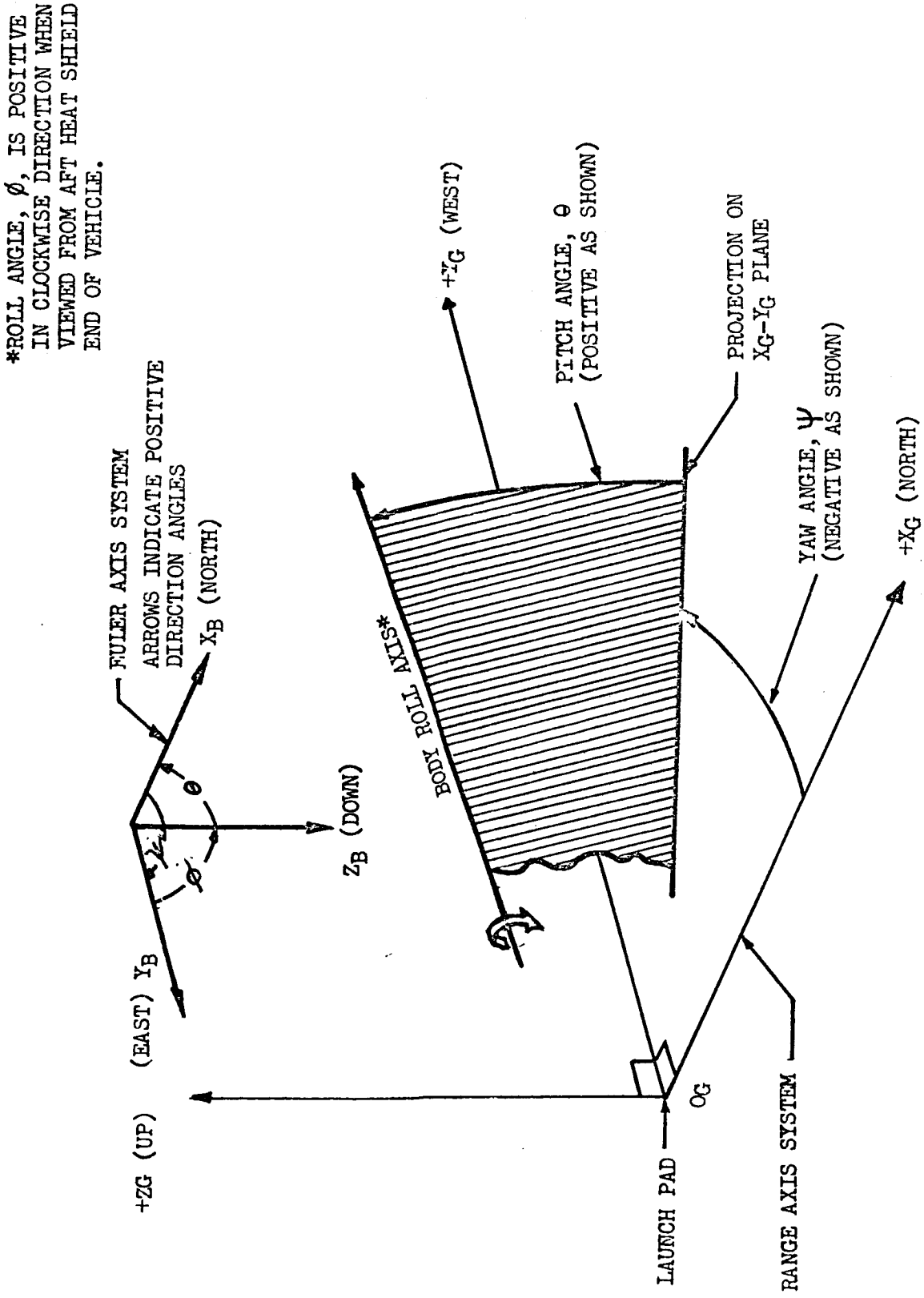

Figure 7.1-5 Euler Attitude Angles, Relative to Range Axis System (ZYX Order of Rotation)

~~CONFIDENTIAL~~

[redacted]

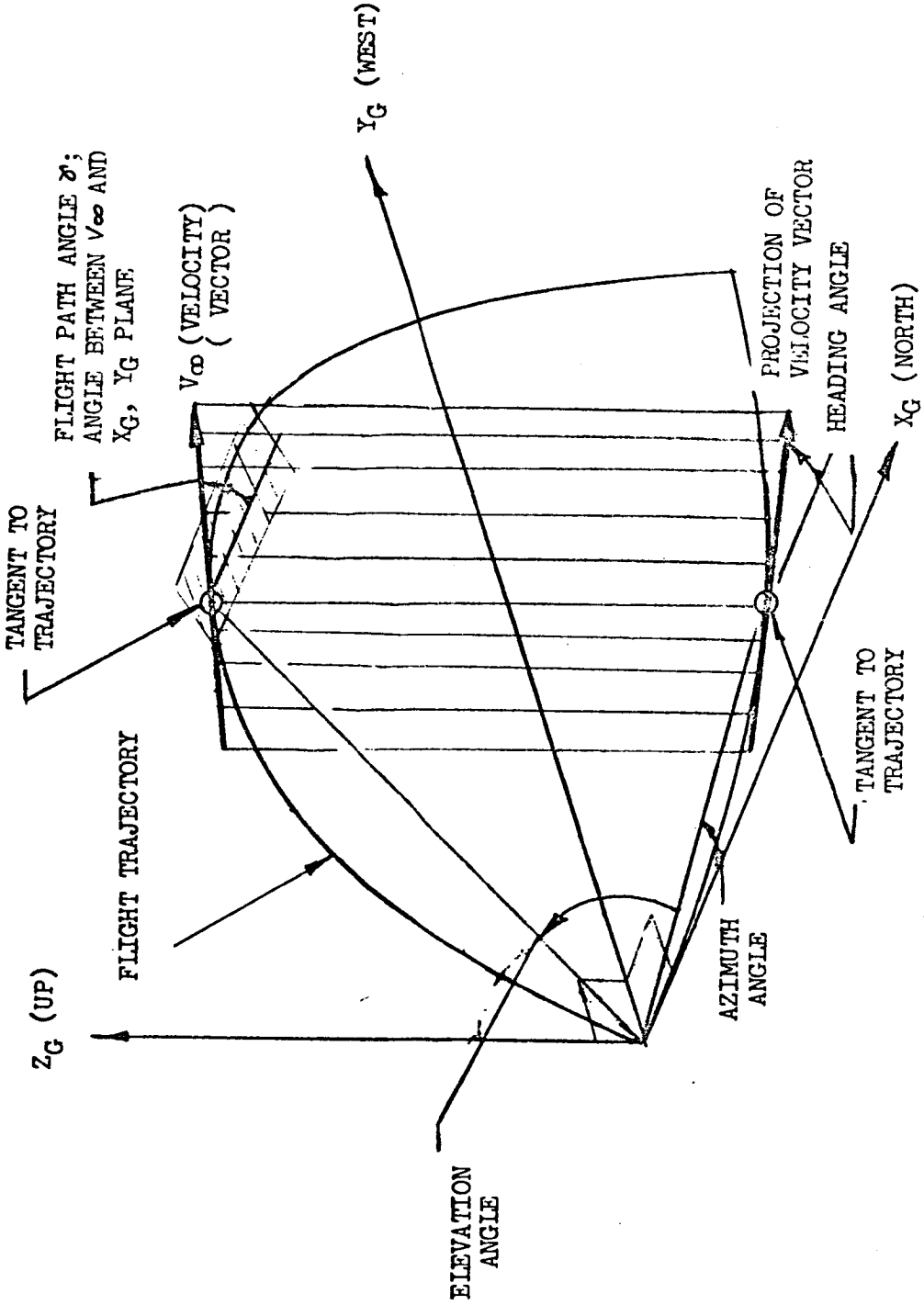

Figure 7.1-6 Trajectory Angles

[redacted]

[redacted].

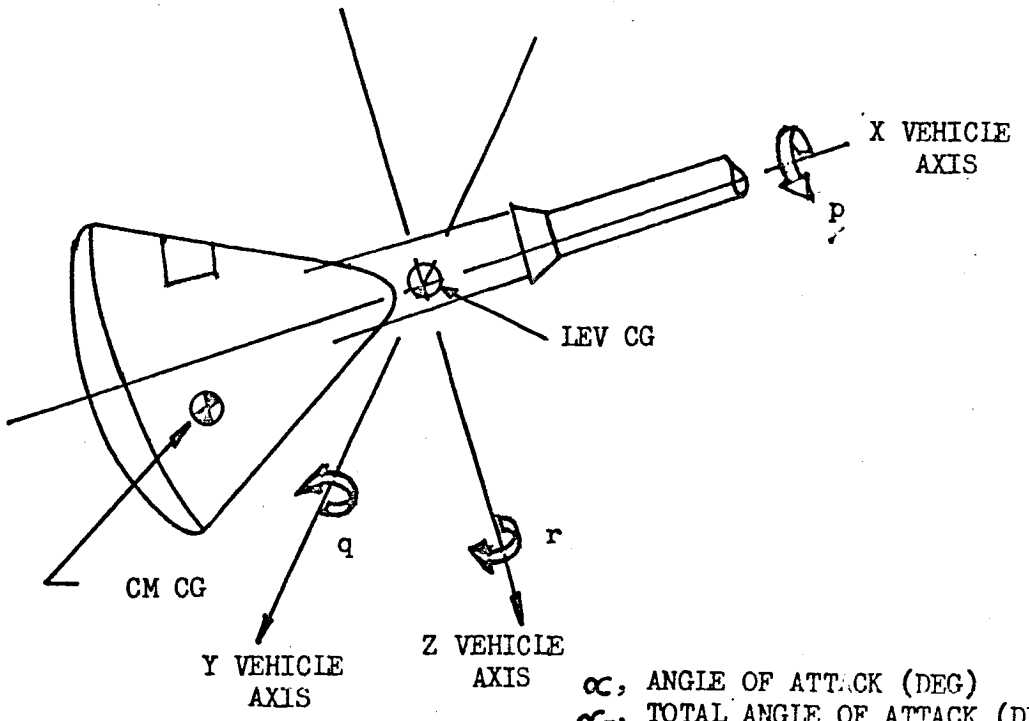

α, ANGLE OF ATTACK (DEG)
α_T, TOTAL ANGLE OF ATTACK (DEG)
β, ANGLE OF SIDESLIP (DEG)
ϕ_A, AERODYNAMIC ROLL ANGLE (DEG)
u, VELOCITY ALONG X AXIS (FT/SEC)
v, VELOCITY ALONG Y AXIS (FT/SEC)
w, VELOCITY ALONG Z AXIS (FT/SEC)
p, ROLL ABOUT X, AXIS (DEG/SEC)
q, ROLL ABOUT Y, AXIS (DEG/SEC)
r, ROLL ABOUT Z, AXIS (DEG/SEC)

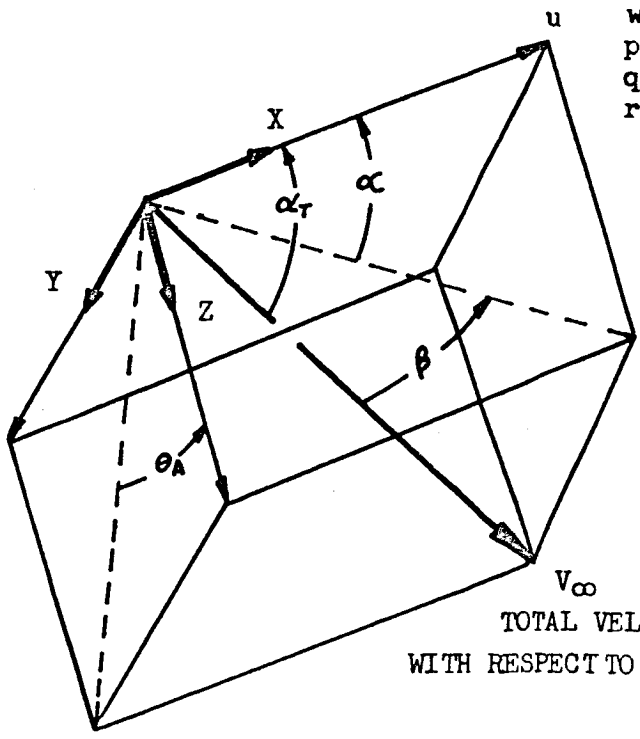

NOTE: ALL ANGLES SHOWN AS POSITIVE

Figure 7.1-7 Command Module Axis System, Showing Sense of Angular Displacements and Rates

[redacted]

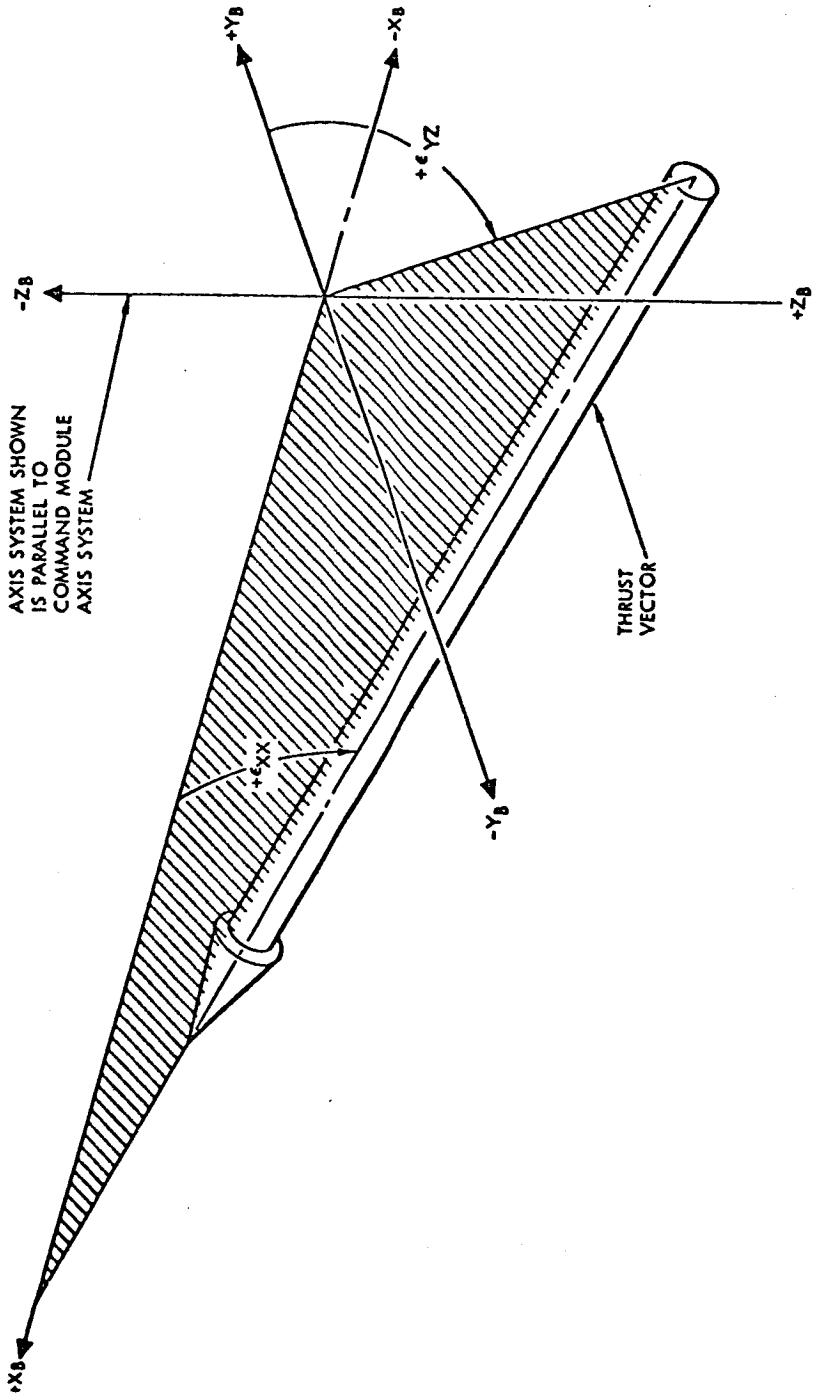

Figure 7.1-8 Thrust Vector Alignment Angles

[redacted]

~~CONFIDENTIAL~~

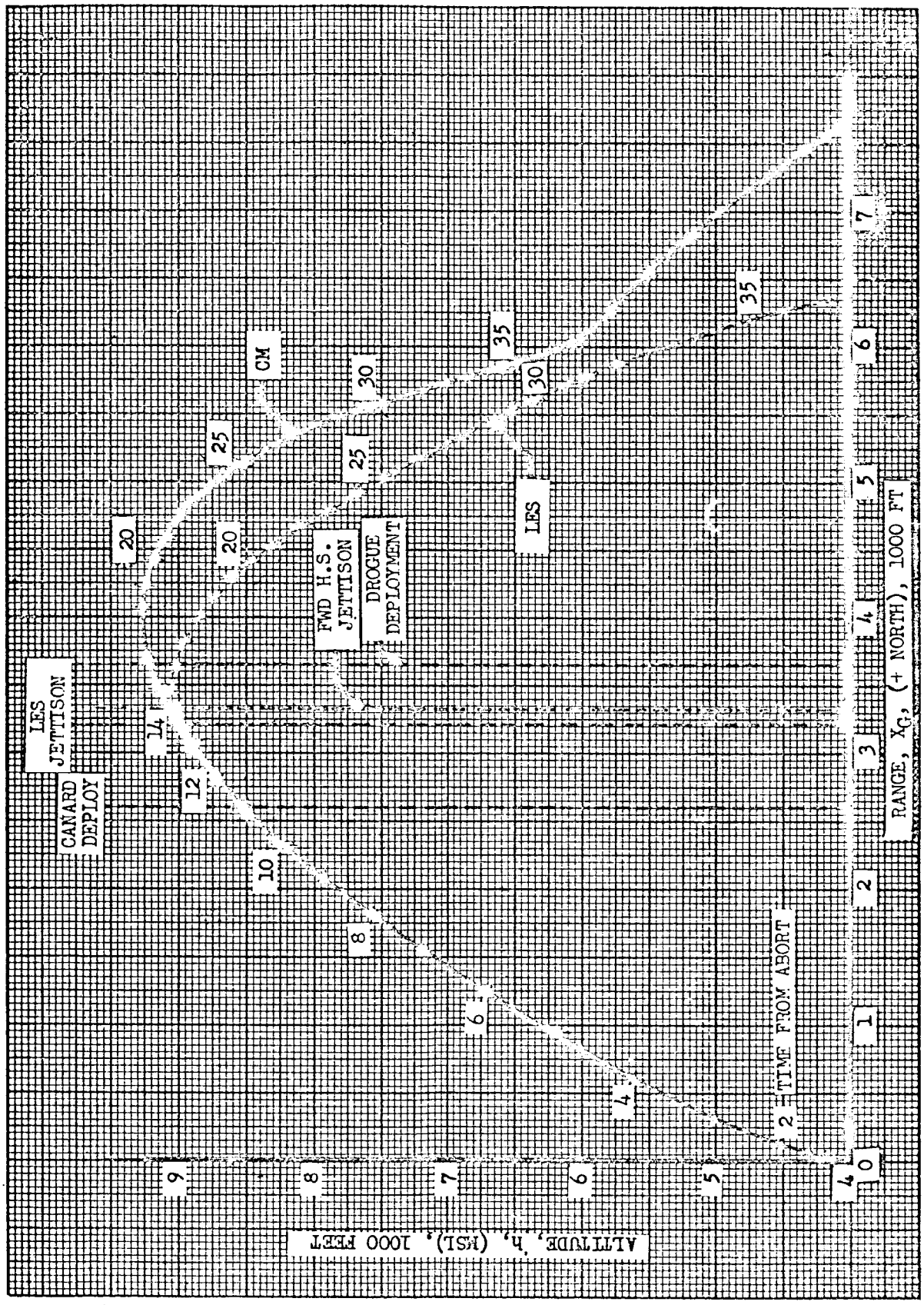

Figure 7.1-9 Downrange Flight Profile

~~CONFIDENTIAL~~

[redacted]

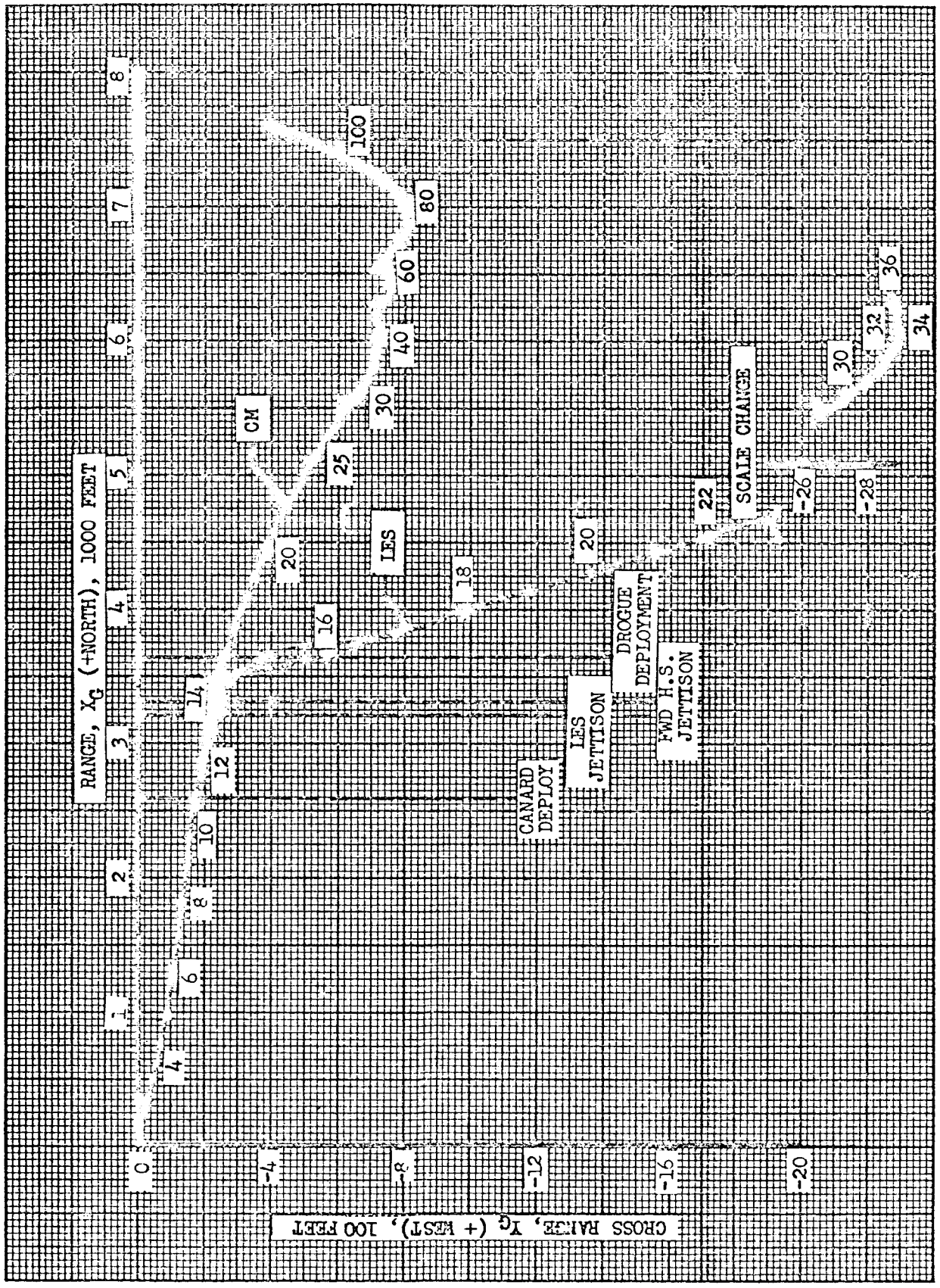

Figure 7.1-10 Crossrange Flight Profile

[redacted]

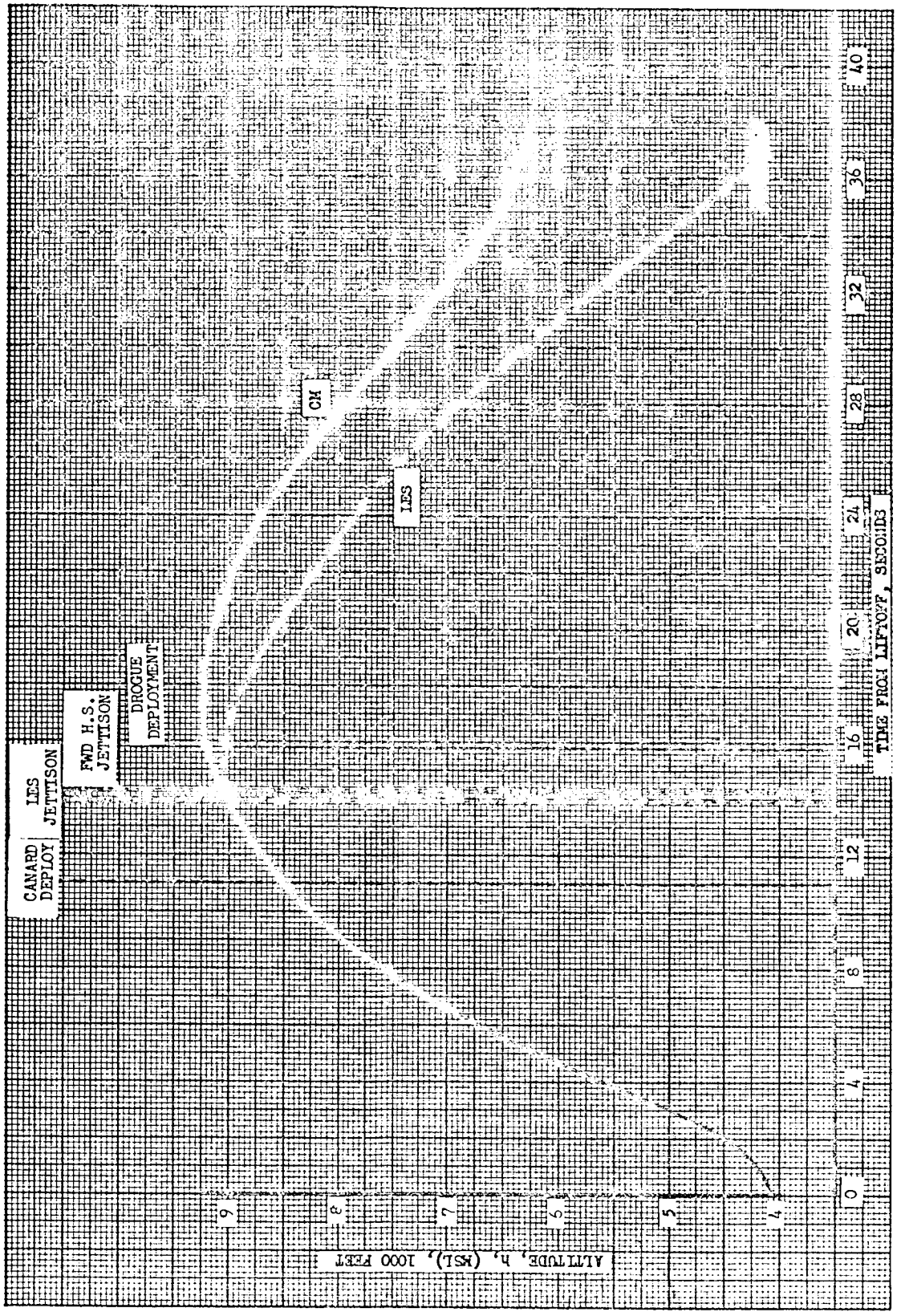

Figure 7.1-11 Altitude Time History

[redacted]

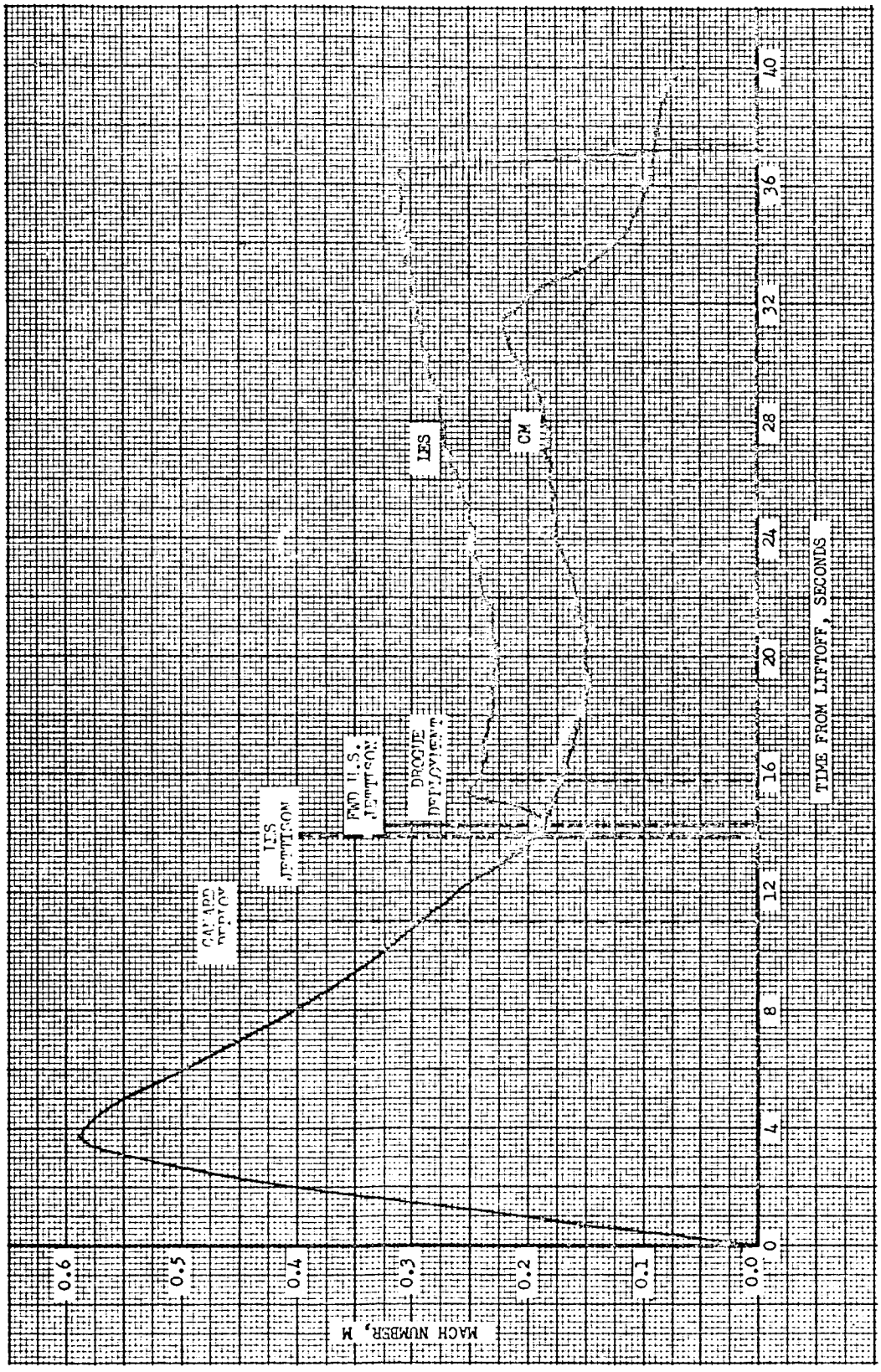

Figure 7.1-12 Mach Number Time History

[redacted]

[redacted].

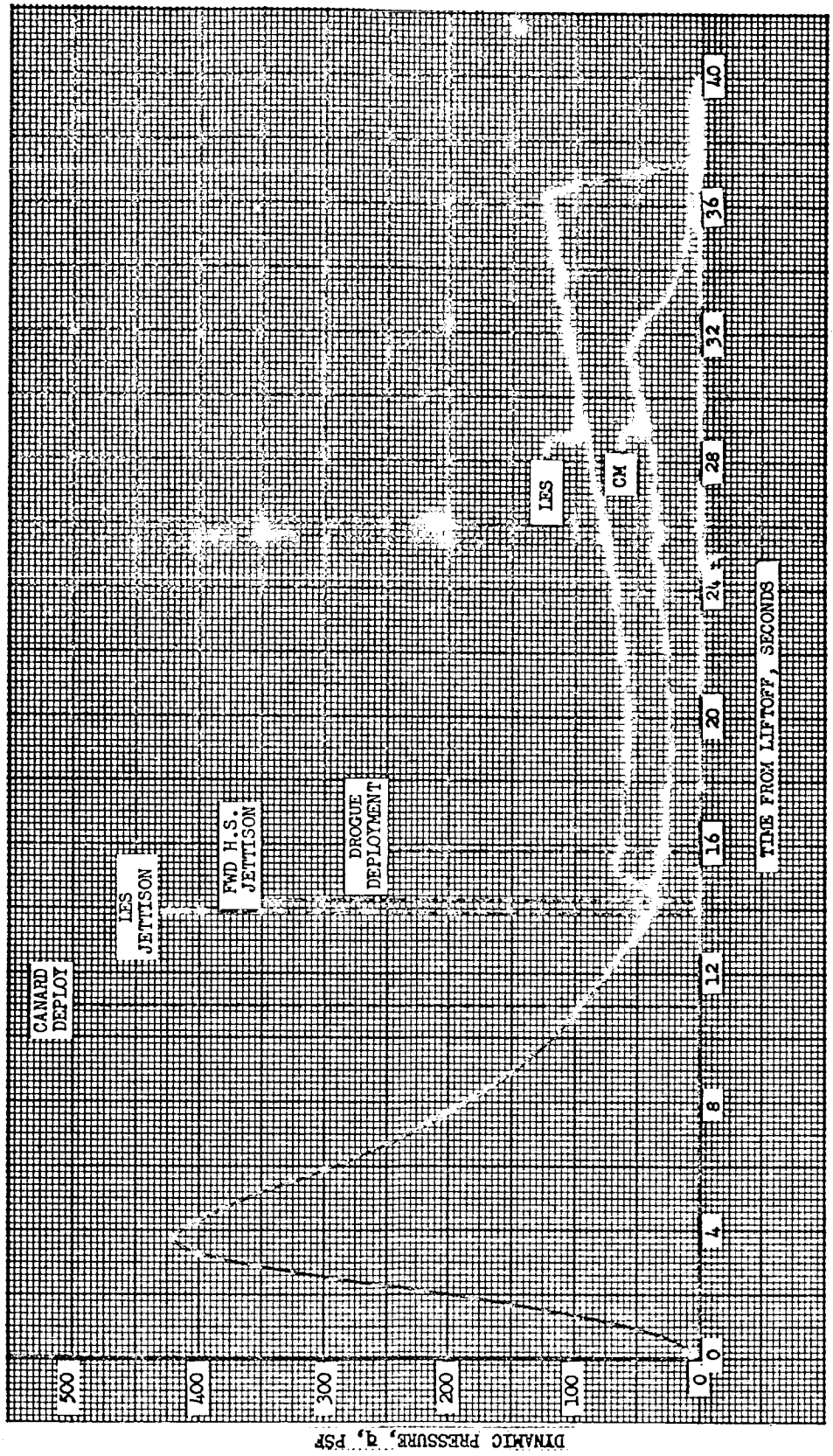

Figure 7.1-13 Dynamic Pressure Time History

[redacted]

[redacted]

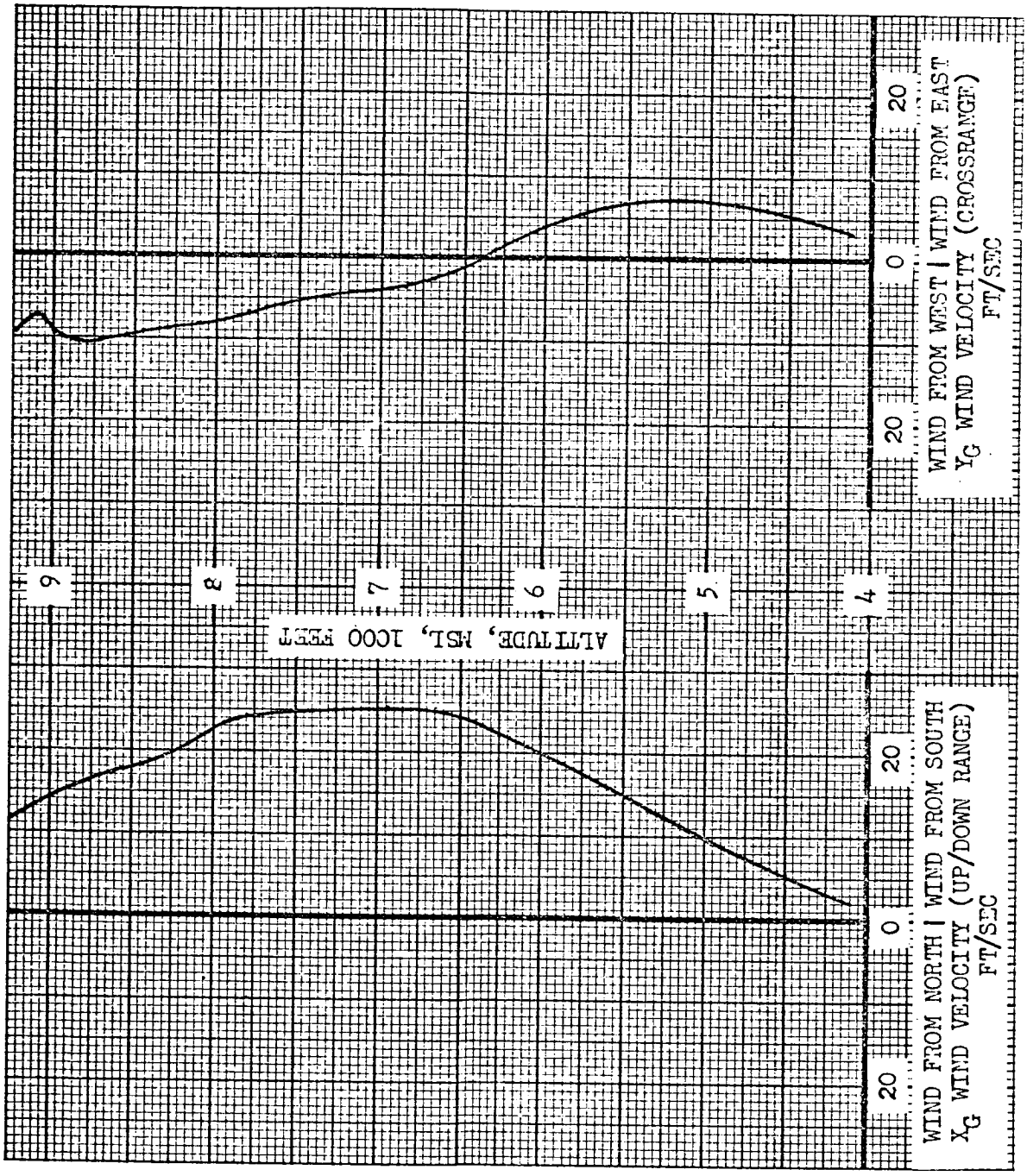

Figure 7.1-14 Component Wind Velocities

[redacted]

[redacted]

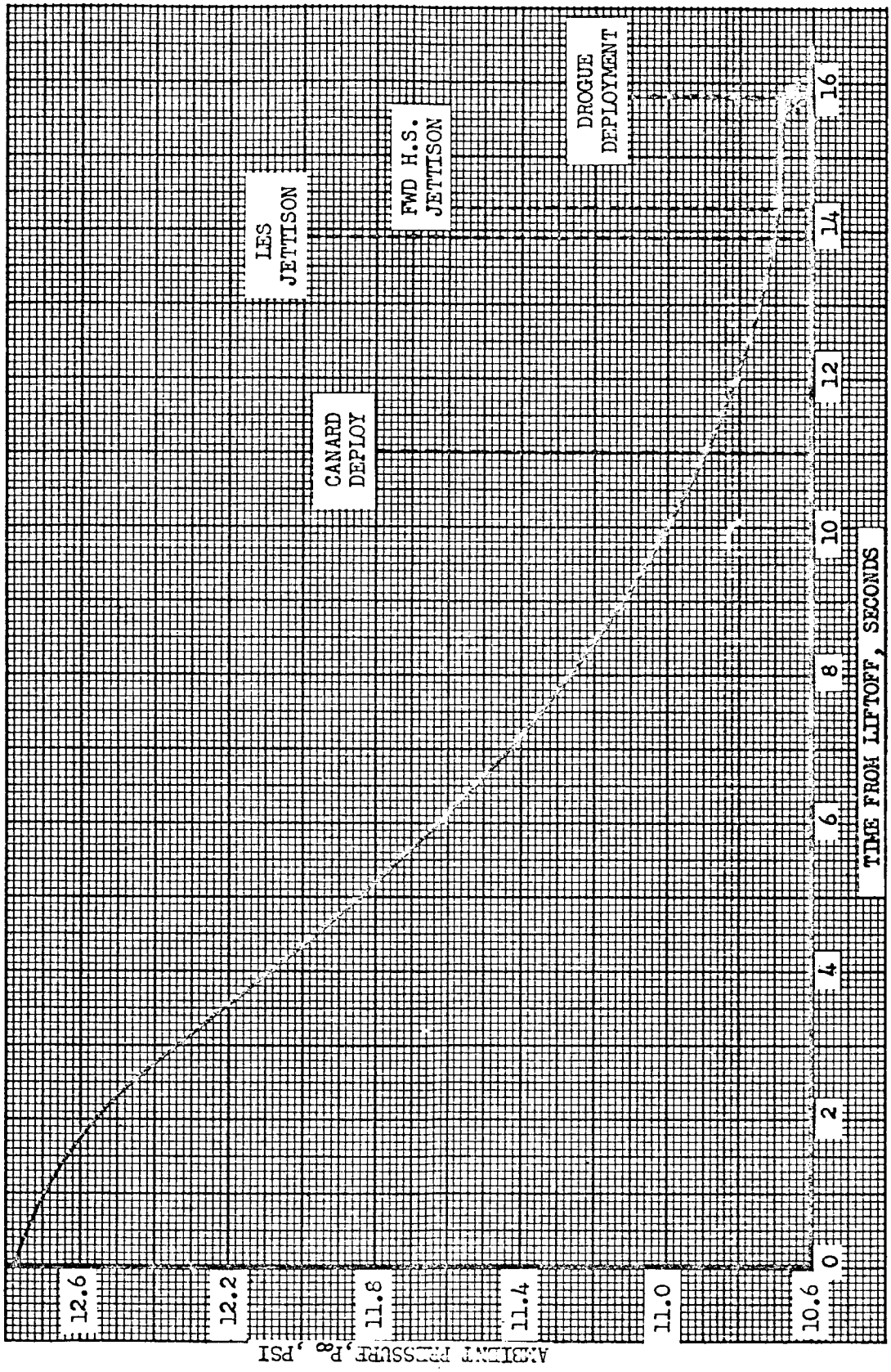

Figure 7.1-15 Ambient Pressure Time History

[redacted]

[redacted]

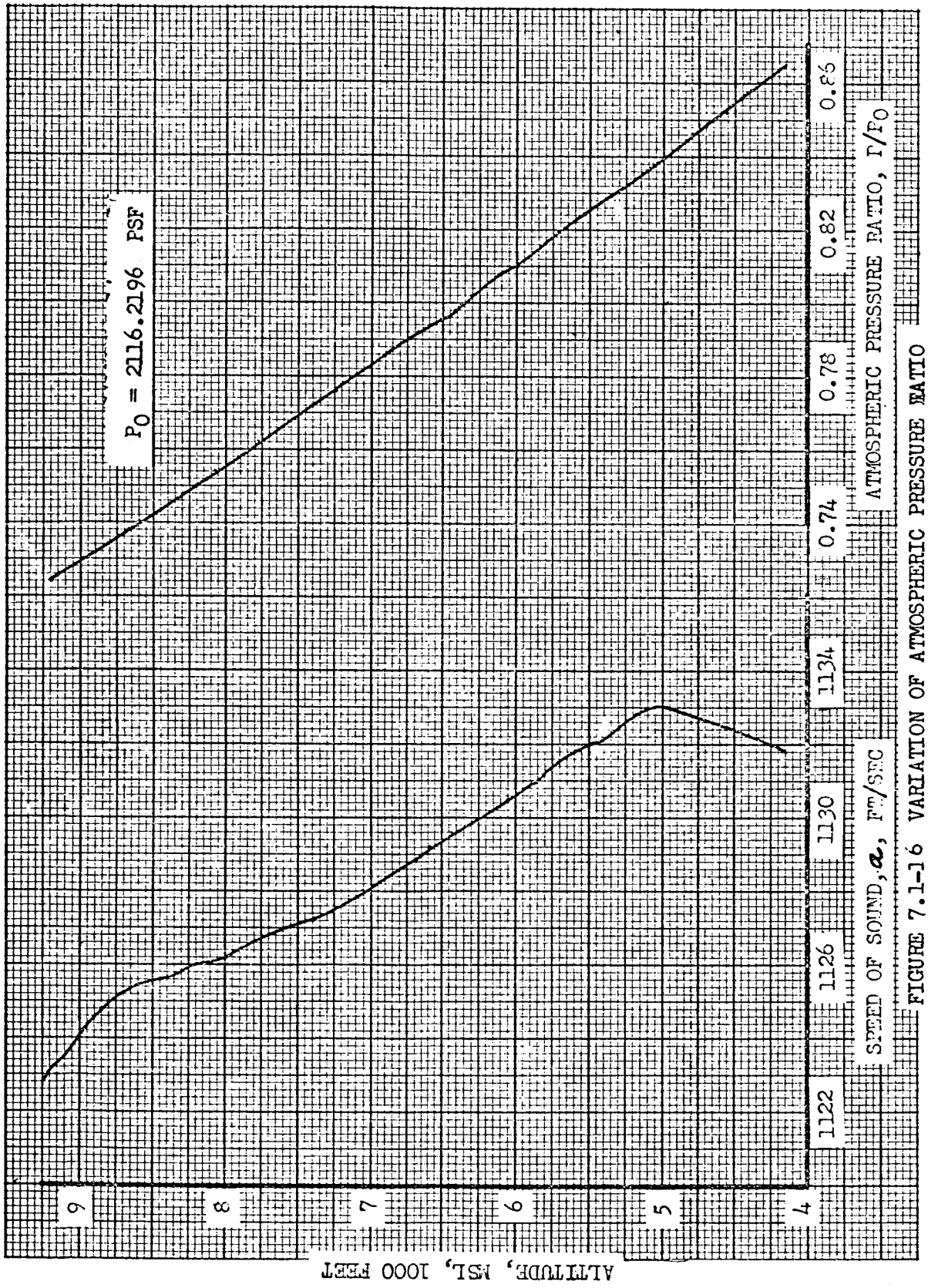

FIGURE 7.1-16 VARIATION OF ATMOSPHERIC PRESSURE RATIO AND SPEED OF SOUND WITH ALTITUDE

[redacted]

[redacted]

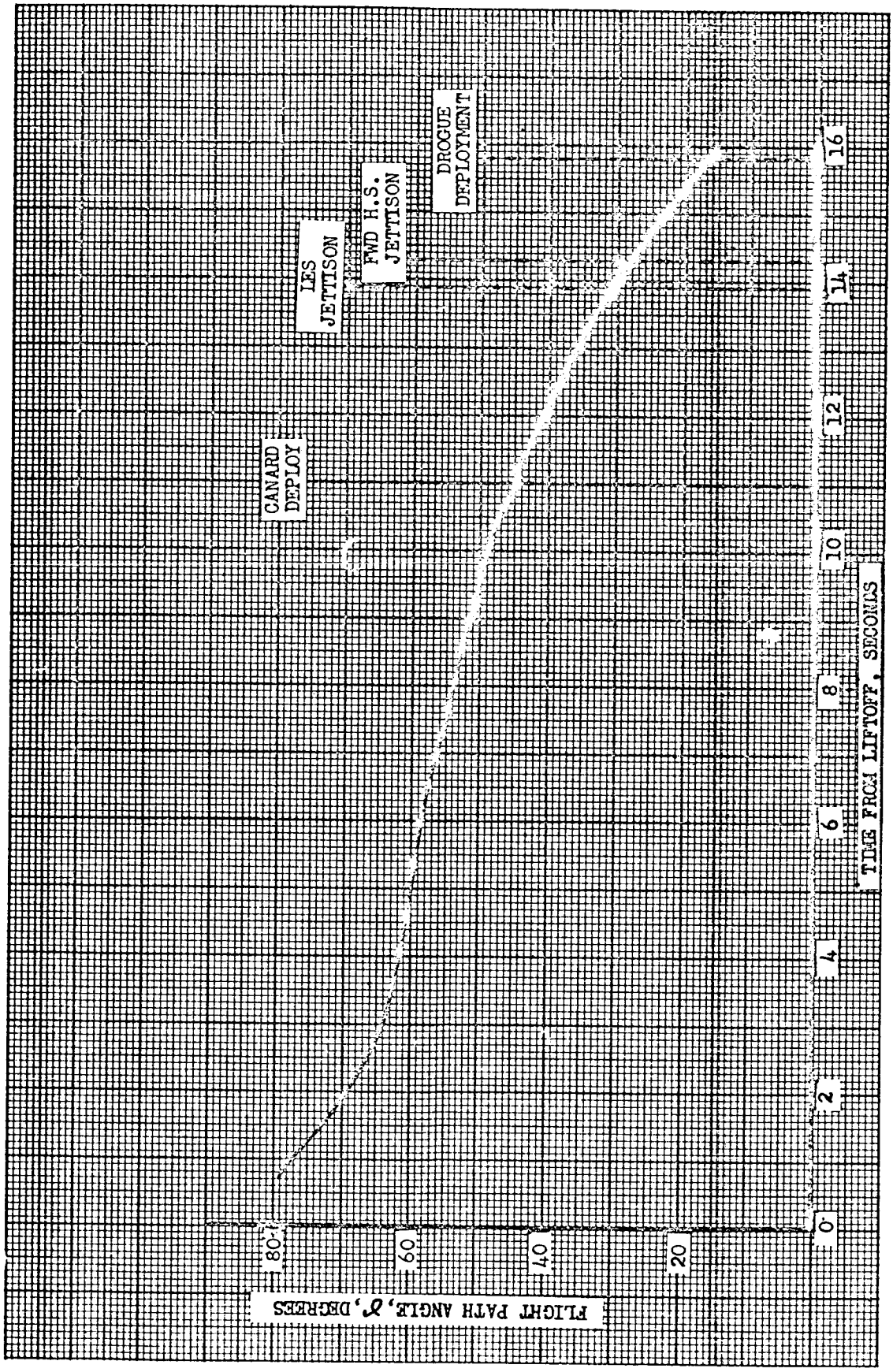

Figure 7.1-17 Flight Path Angle Time History

[redacted]

[redacted]

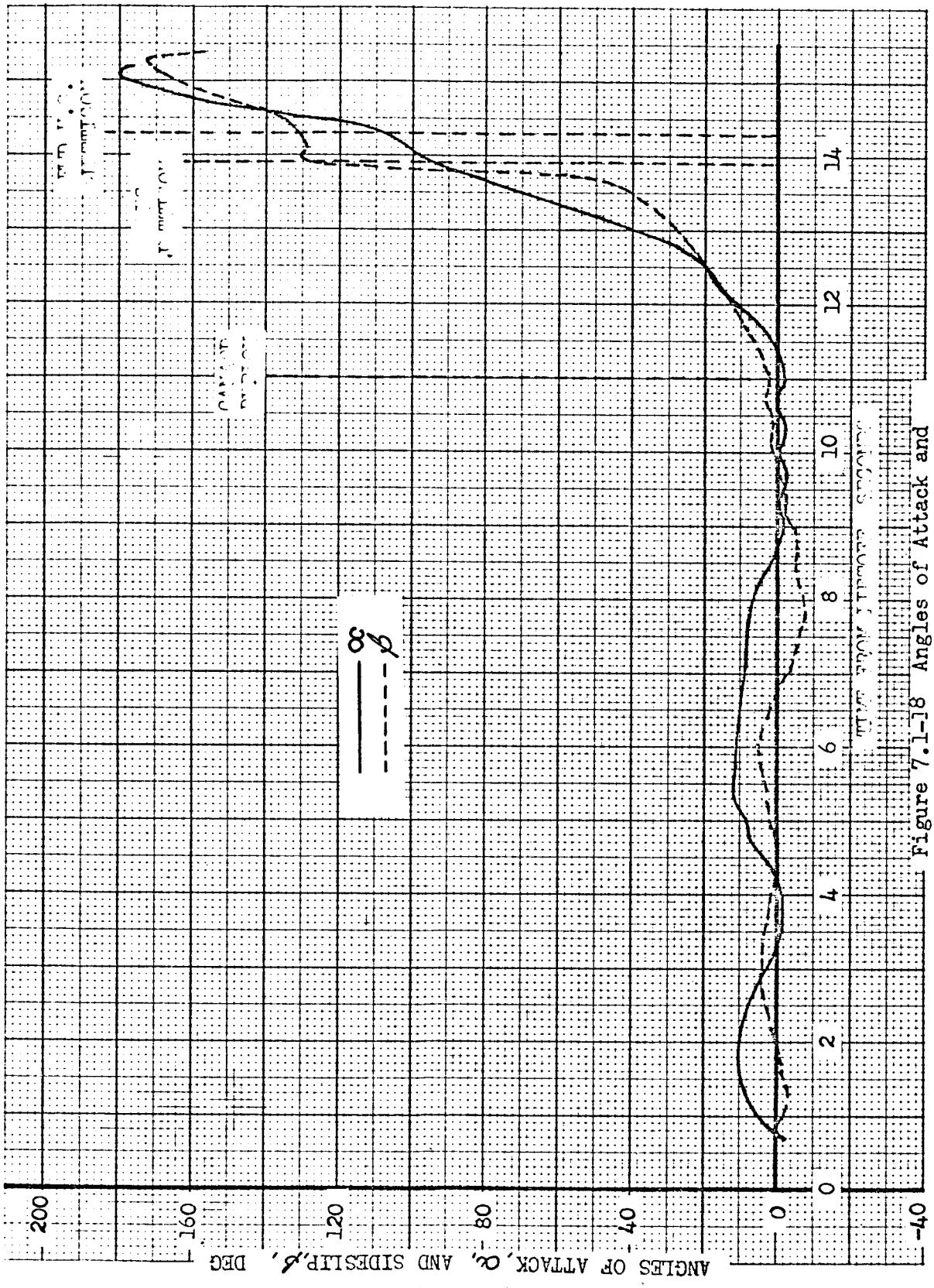

Figure 7.1-18 Angles of Attack and Sideslip Time Histories

[redacted]

[redacted]

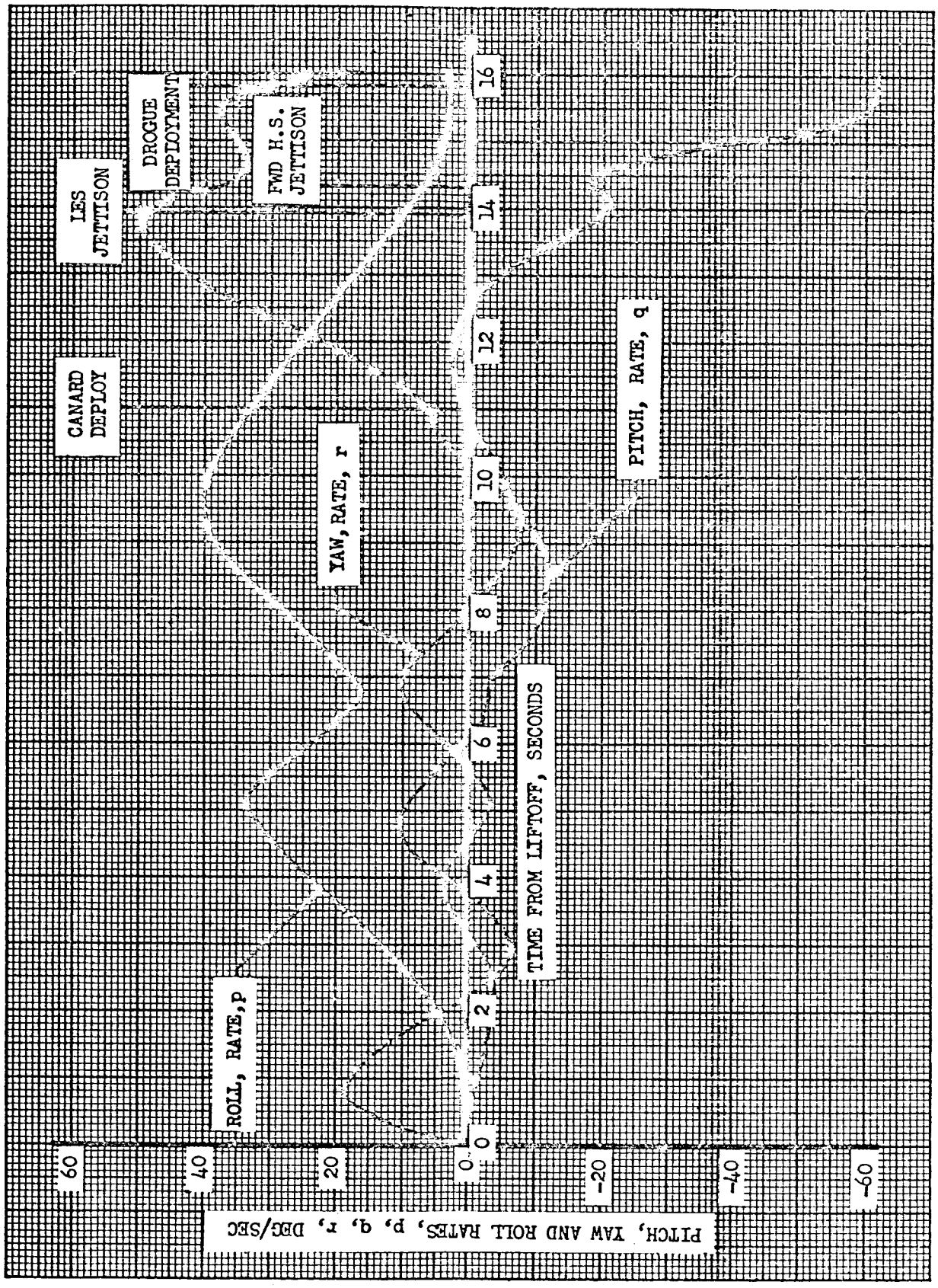

Figure 7.1-19 Body Pitch, Yaw, and Roll Rate Time Histories

[redacted]

[redacted]

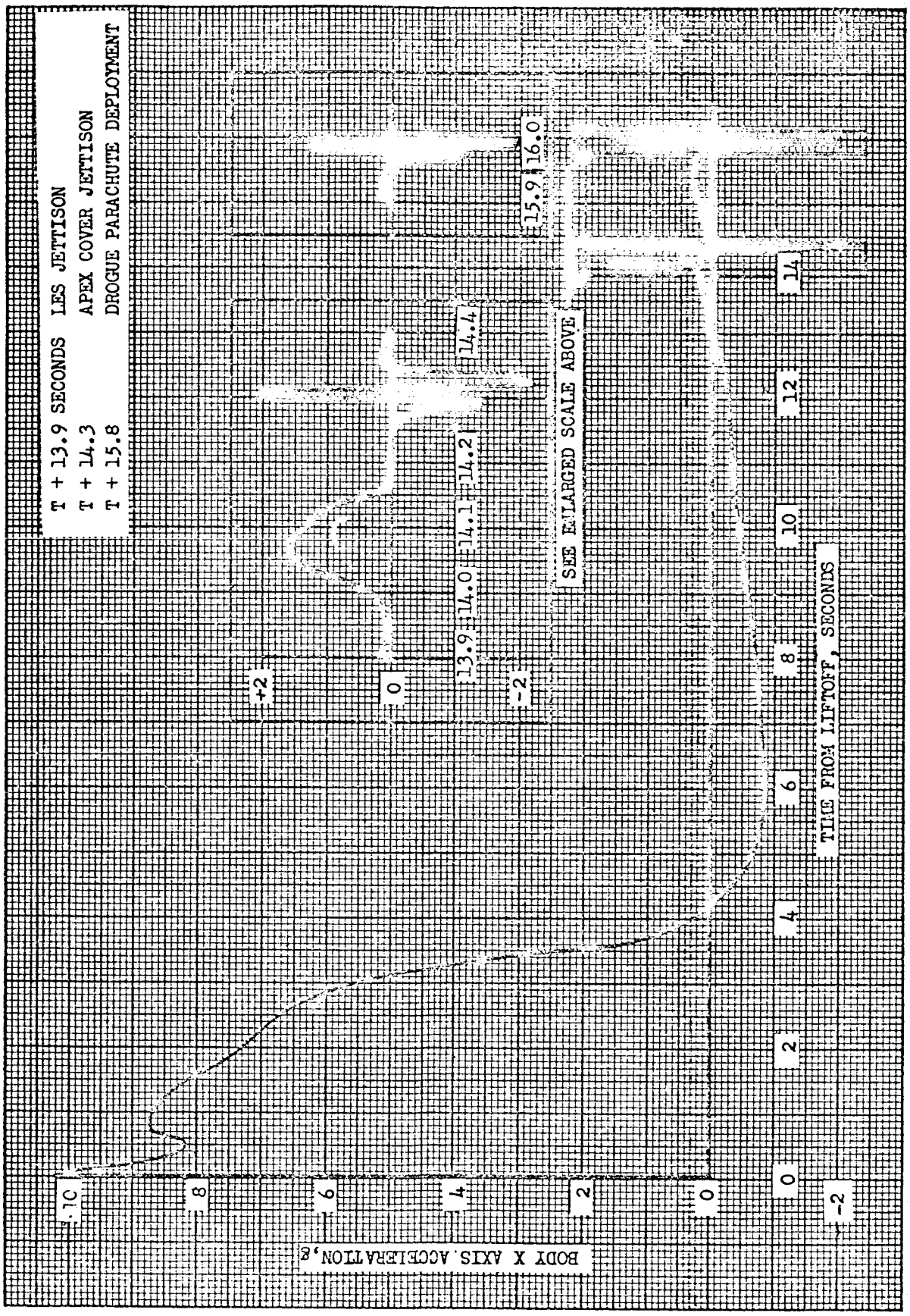

Figure 7.1-20 Axial Acceleration Time History

[redacted]

[redacted]

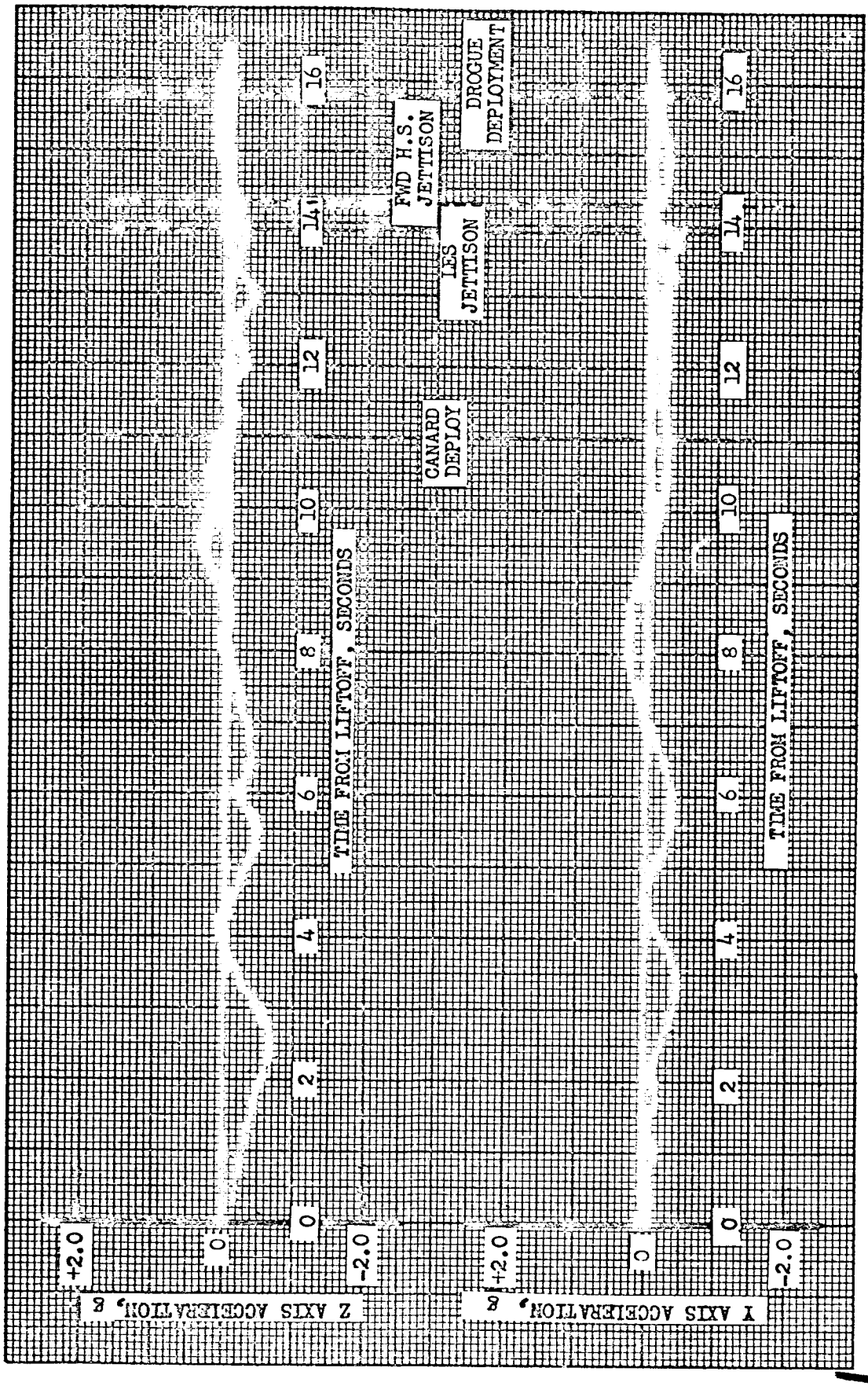

Figure 7.1-21 Y and Z Axes Acceleration Time Histories

[redacted]

[redacted]

Vehicle	BP-6	BP-12	BP-13	BP-15	BP-23	BP-22	BP-23A
Mission	Abort	Abort	Orbit	Orbit	Abort	Abort	Abort
Launch Escape Subsystem							
Canard Subsystem	No	No	No	No	Yes	Yes	Yes
Tower Camera	No	Yes	No	No	Yes	Yes	Yes
Jettison Motor Thrust Vector Offset	2.5°	2.5°	2.5°	2.5°	3.8°	3.8°	3.8°
Buna-N on tower legs	No	No	Yes	Yes	Yes	Yes	No
Boost Protective Cover							
Protuberances (Simulated)	N/A	N/A	N/A	N/A	No	Yes	Yes
Windows (Simulated)	N/A	N/A	N/A	N/A	No	Yes	No
Command Module							
Protuberances (Simulated)	No	No	Yes	Yes	No	Yes	Yes
Window Samples	Yes	Yes	No	No	Yes	Yes	Yes
Service Module							
Length, with adapter, inches	N/A	161.75	295.75	295.75	161.75	161.75	N/A
Dummy RCS Quads	N/A	No	Yes	Yes	No	Yes	N/A

N/A: Not applicable

Figure 7.1-22 Table of Aerodynamic Configurations of Apollo Launch Escape Vehicles

[redacted]

[redacted]

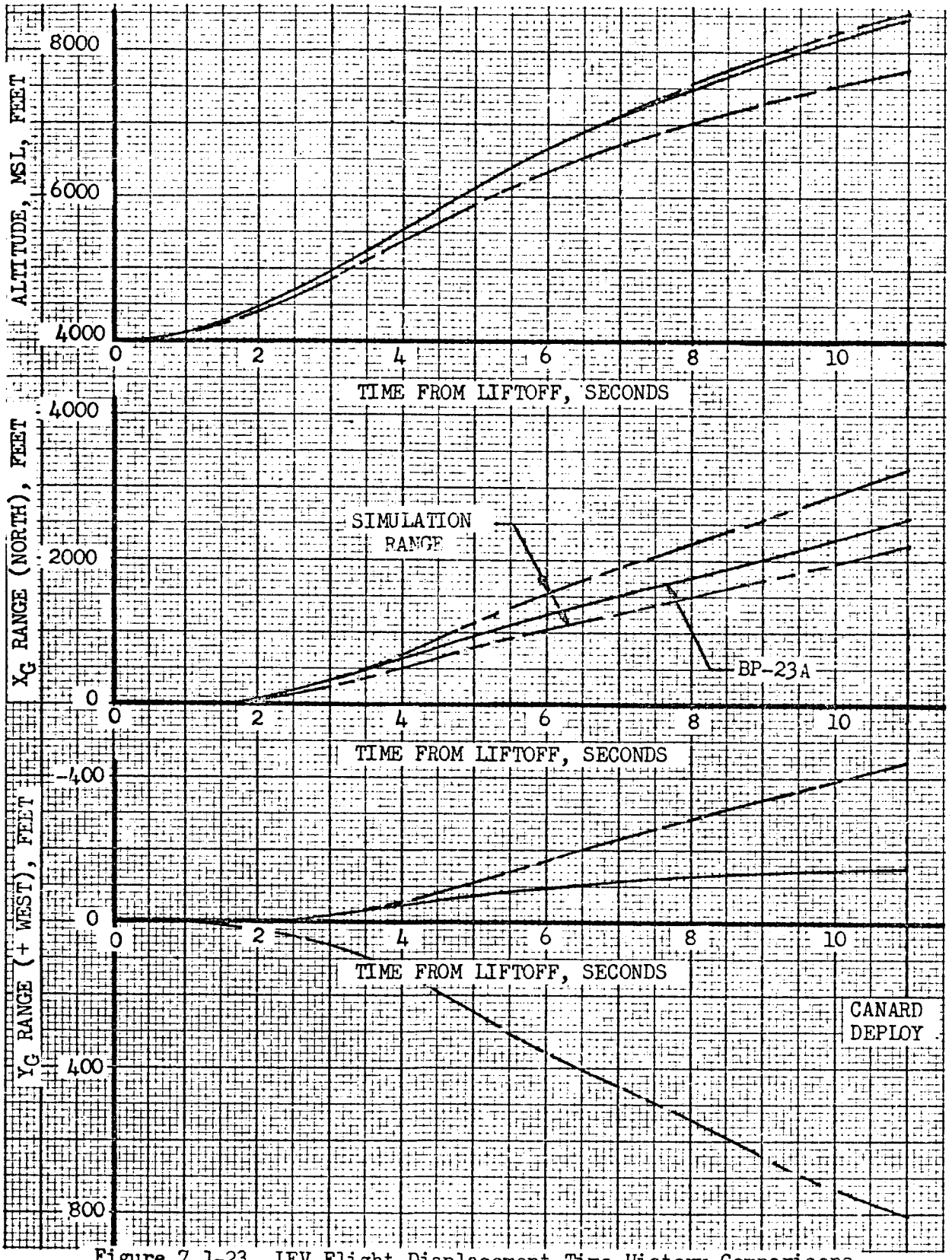

Figure 7.1-23 LEV Flight Displacement Time History Comparisons

[redacted]

[redacted]

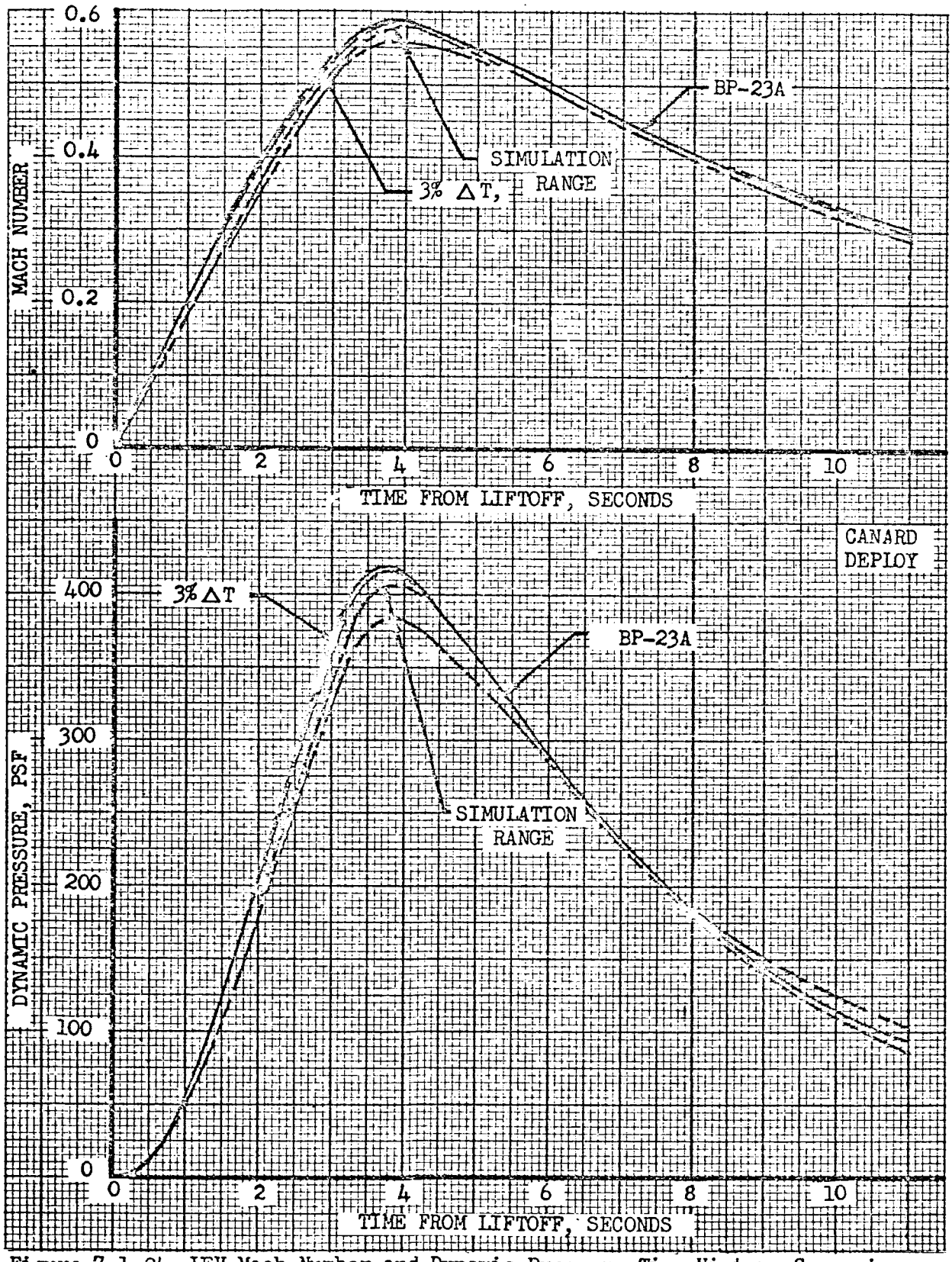

Figure 7.1-24 LEV Mach Number and Dynamic Pressure Time History Comparisons

[redacted]

[redacted]

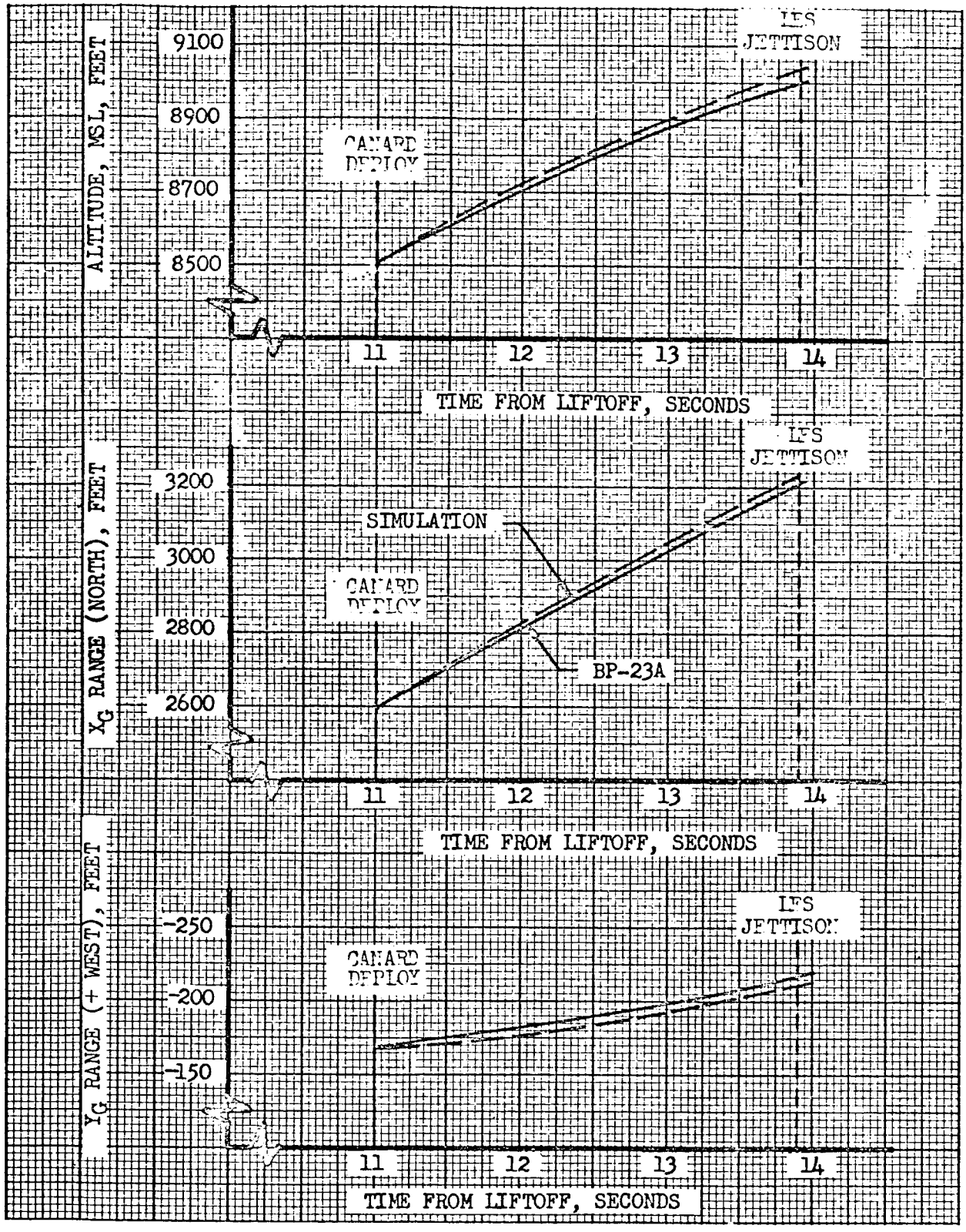

Figure 7.1-25 LEV with Canards Deployed
Flight Displacement Time History Comparisons

[redacted]

[redacted]

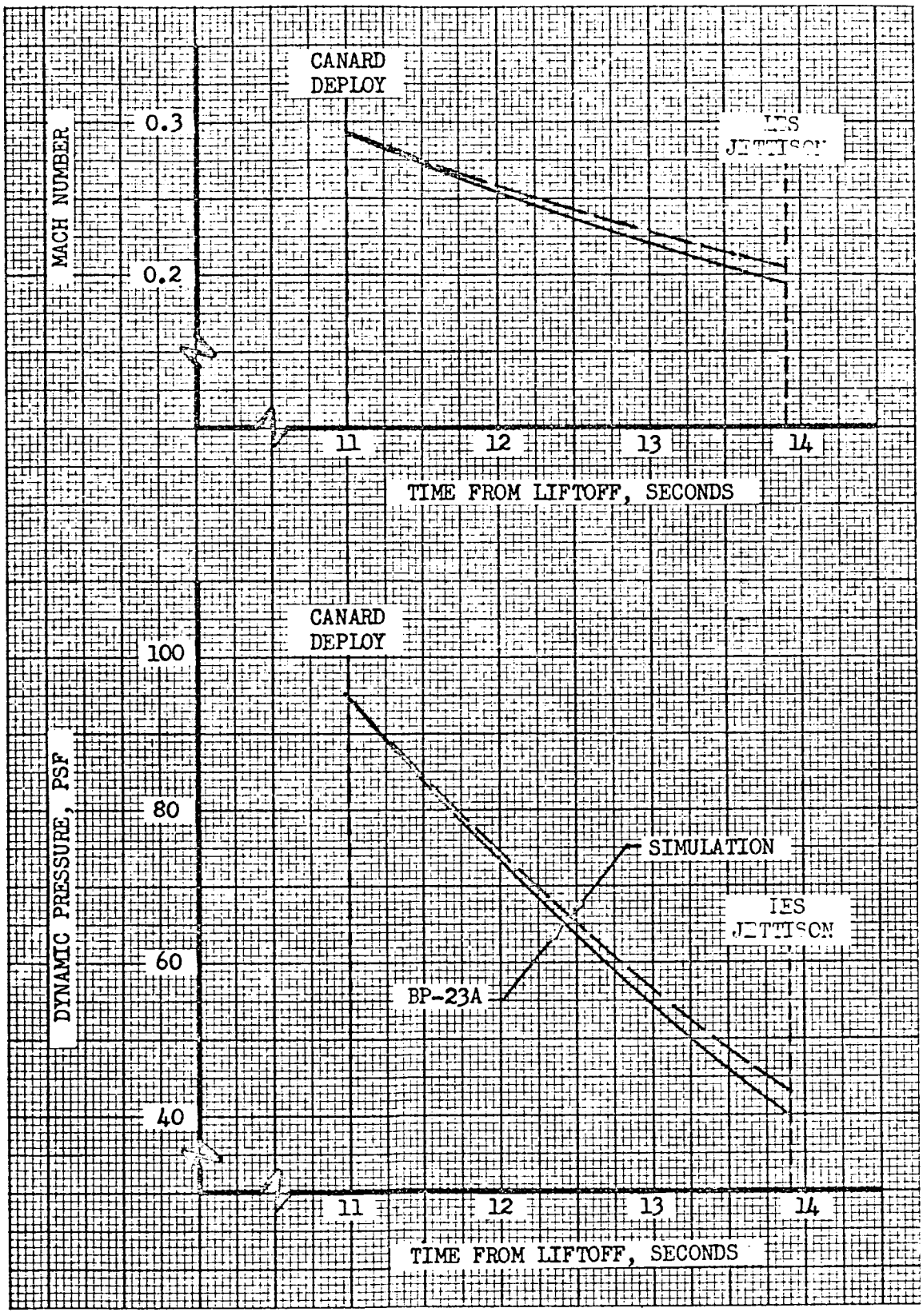

Figure 7.1-26 LEV with Canards Deployed Mach Number and Dynamic Pressure Time History Comparisons

[redacted]

[redacted]

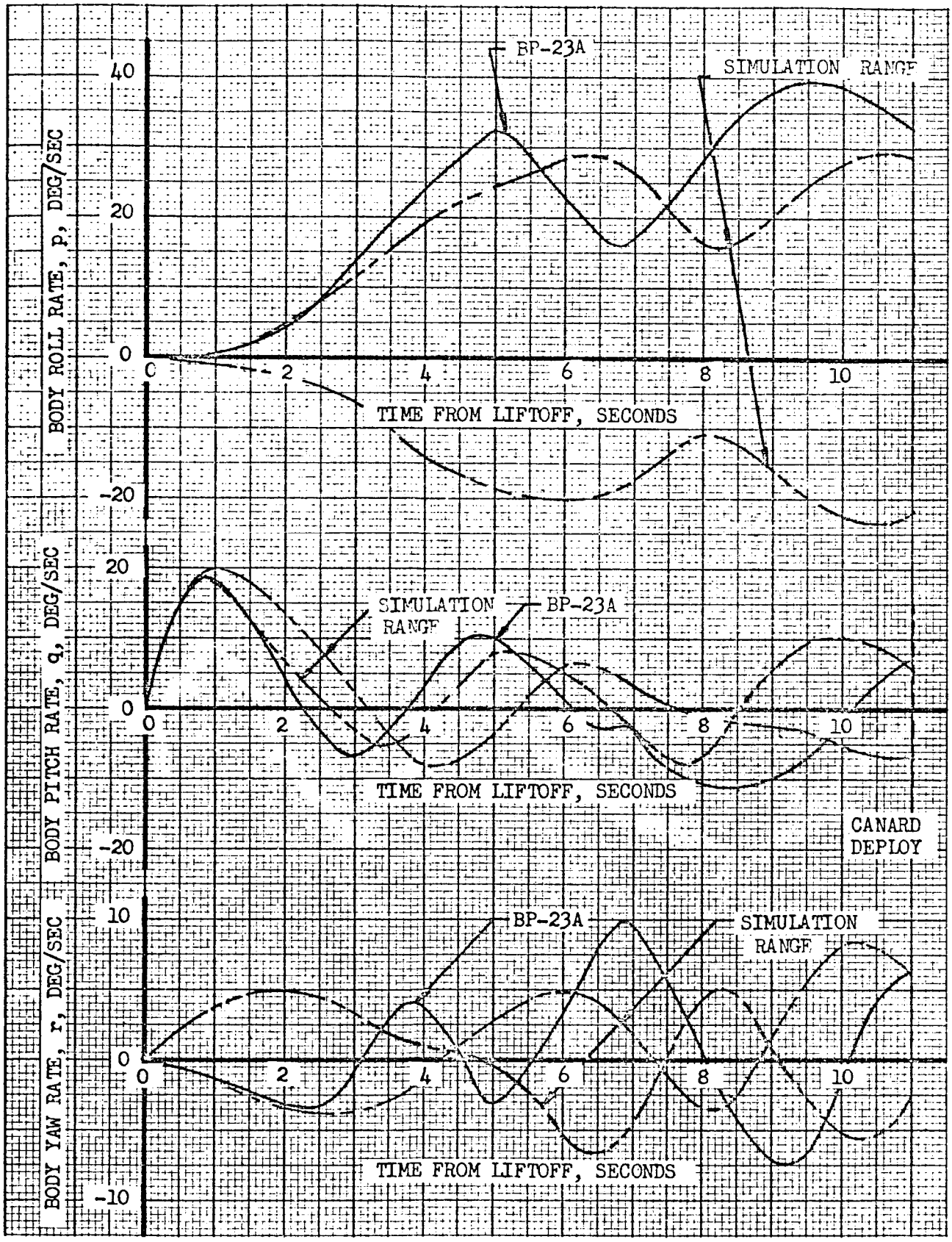

Figure 7.1-27 LEV Body Rate Time History Comparisons

 [redacted]

[redacted]

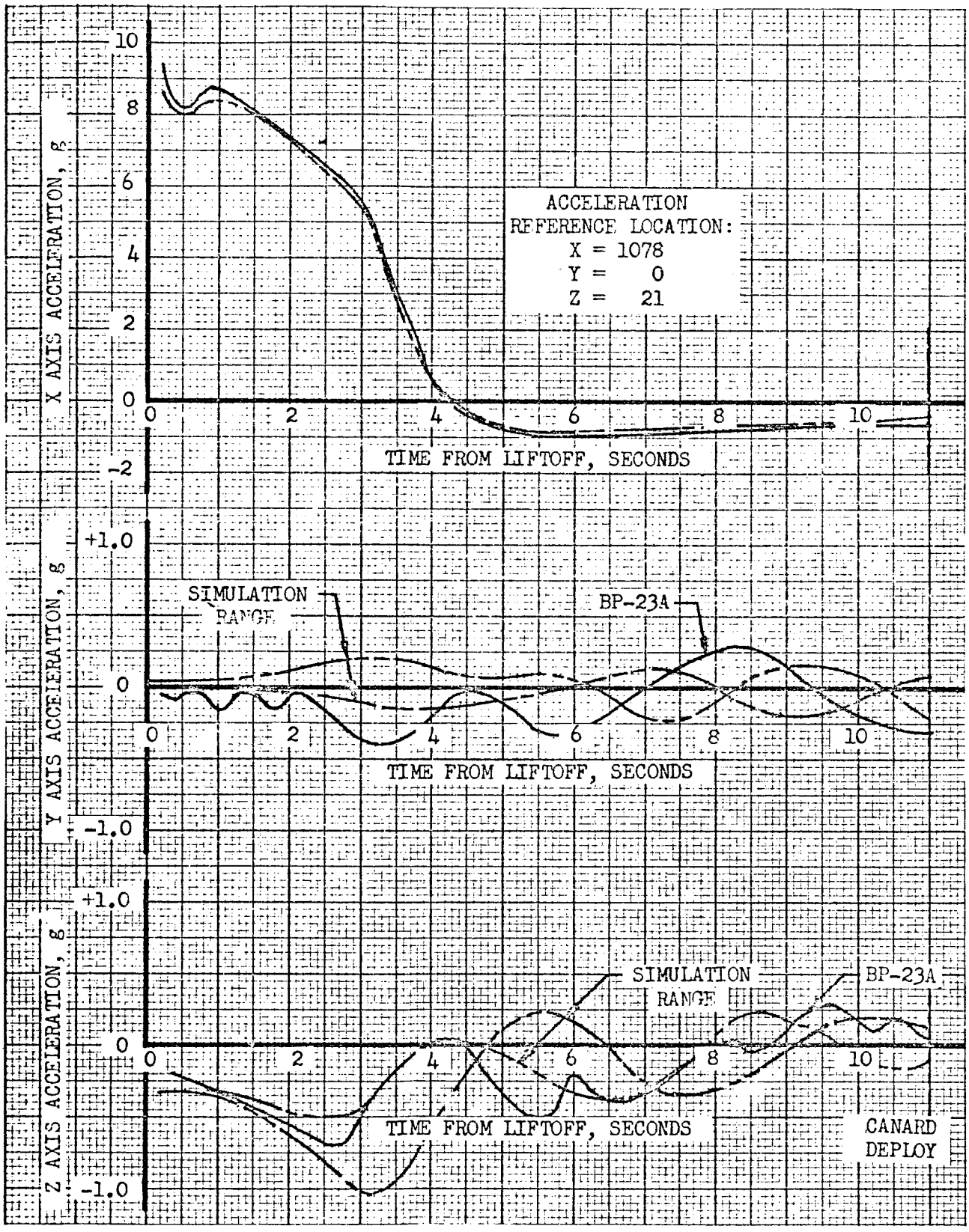

Figure 7.1-28 LEV Acceleration Time History Comparisons

 [redacted]

~~CONFIDENTIAL~~

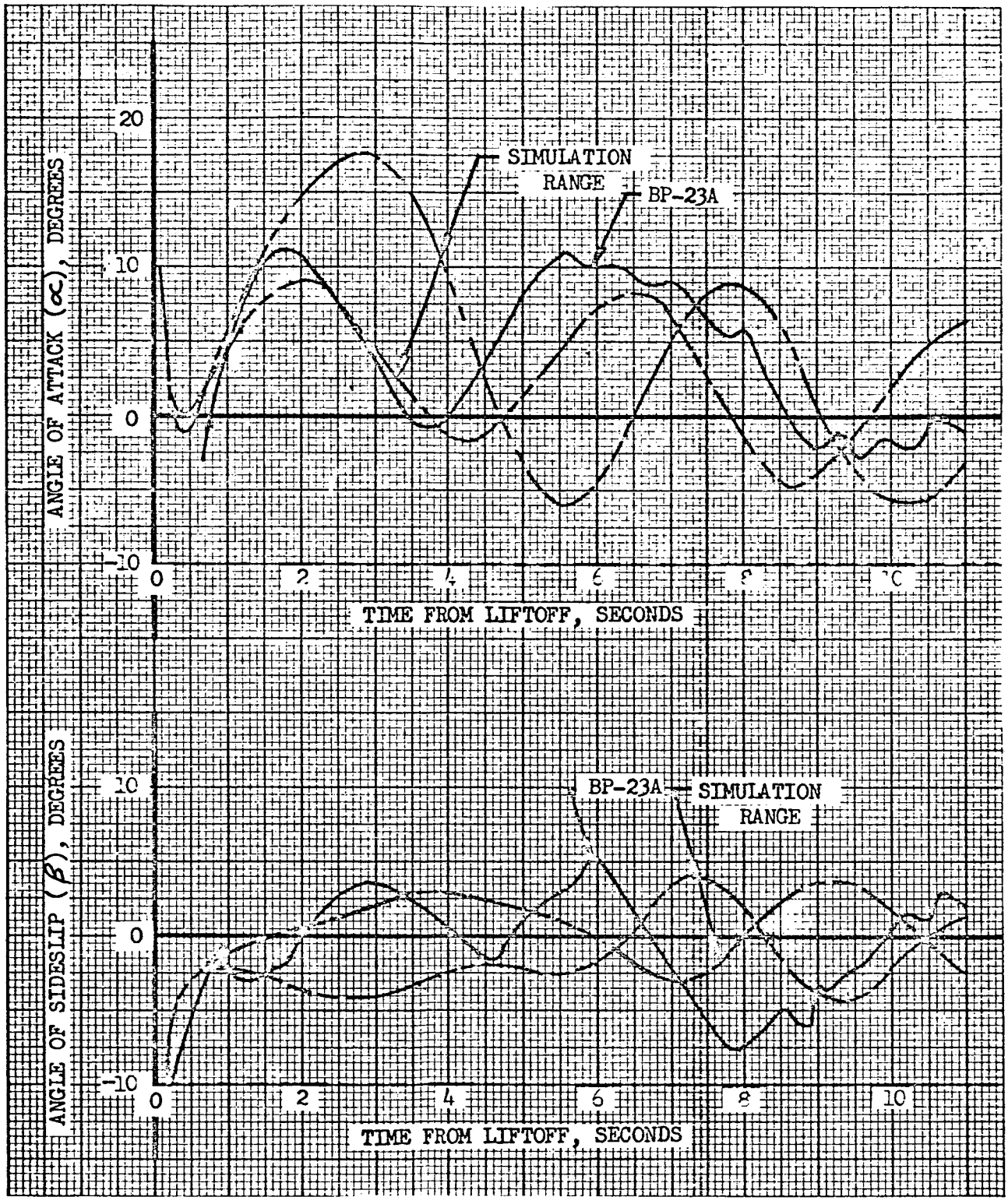

Figure 7.1-29 LEV Angles of Attack and Sideslip Time History Comparisons

~~CONFIDENTIAL~~

PERTURBATION FROM NOMINAL	THRUST VECTOR ALIGNMENT TOLERANCE			
	$+\Delta\epsilon_{XX}, \epsilon_{YZ_{NOM}}$ ΔP (Deg/sec)	$-\Delta\epsilon_{XX}, \epsilon_{YZ_{NOM}}$ ΔP (Deg/sec)	$\epsilon_{XX_{NOM}}, -\Delta\epsilon_{YZ}$ ΔP (Deg/sec)	$\epsilon_{XX_{NOM}}, +\Delta\epsilon_{YZ}$ ΔP (Deg/sec)
5% Thrust Increase	-0.4	0.2	-2	+2
+0.083 in. CG Y_A shift	+3	+2	-3	+3
+3 DEG/SEC Initial Yaw Rate	+0.6	+1	+2	+2
-3 DEG/SEC Initial Yaw Rate	-0.5	-0.5	-3	-3
Aerodynamic Data (BP-6)	negligible	negligible	negligible	negligible
Y_{REF} = -3 in, Z_{REF} = -3 in.	+35	+25	+50	+20
Y_{REF} = -3 in, Z_{REF} = +3 in.	+40	+25	+45	+35
Y_{REF} = +3 in, Z_{REF} = +3 in.	=35	-30	-20	-30
Y_{REF} = +3 in, Z_{REF} = -3 in.	=46	-30	-22	-50

Figure 7.1-30 Table of Averaged Effects on LEV Roll Rate Due to System Perturbations

[redacted]

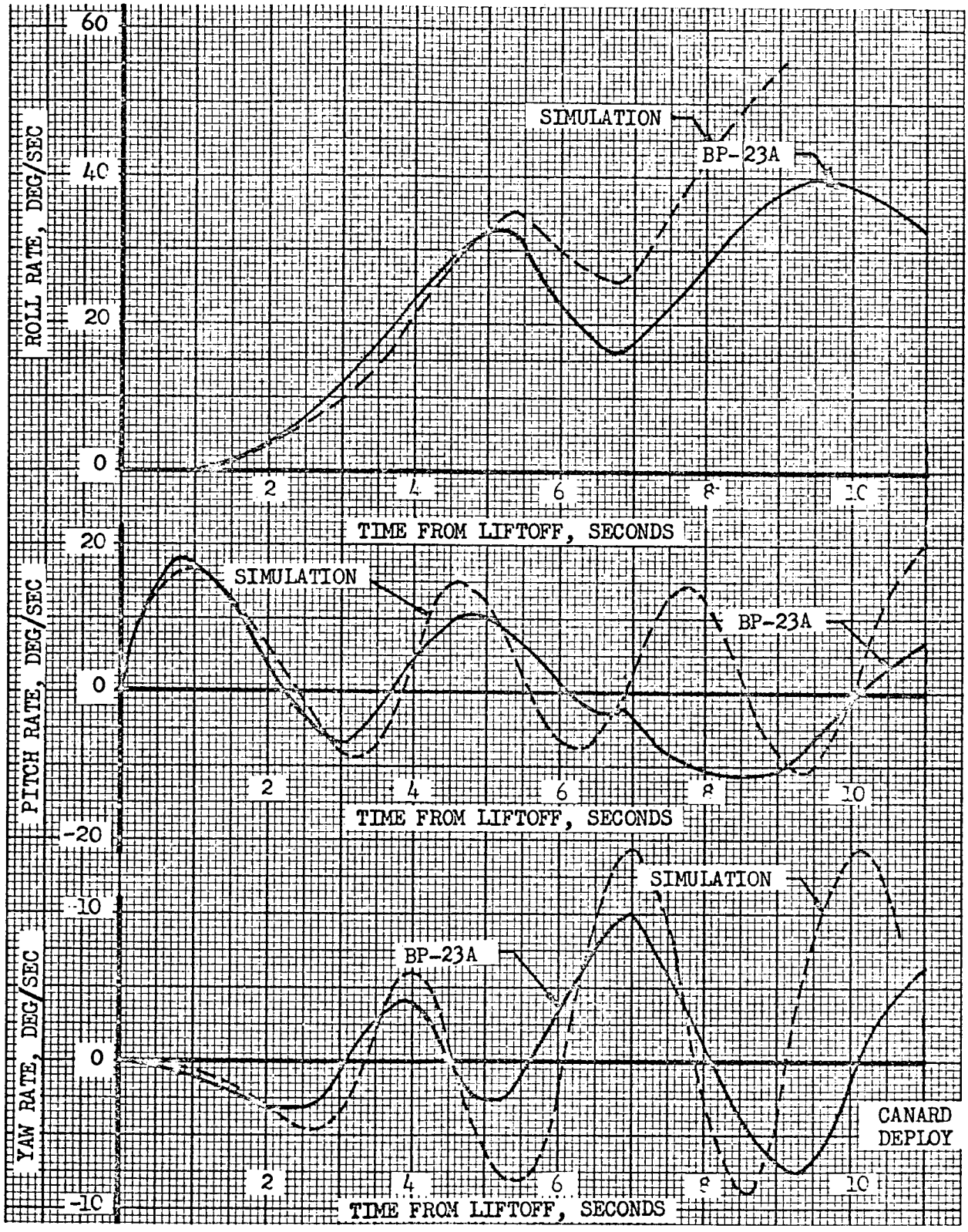

Figure 7.1-31 Effect of Perturbated Aerodynamics on LEV Body Rate Time History Comparisons

[redacted]

[redacted]

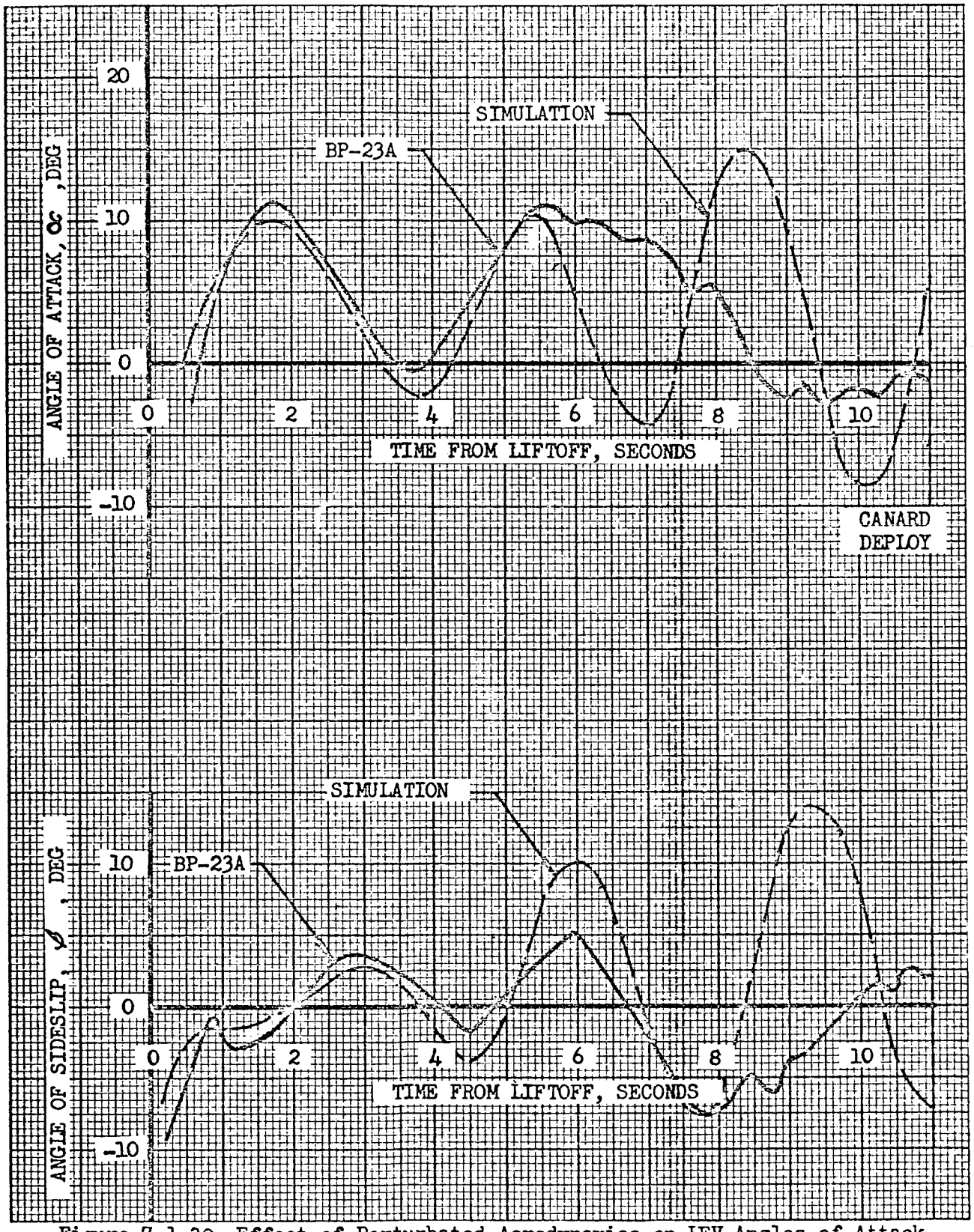

Figure 7.1-32 Effect of Perturbated Aerodynamics on LEV Angles of Attack and Sideslip Time History Comparisons

 [redacted]

[redacted]

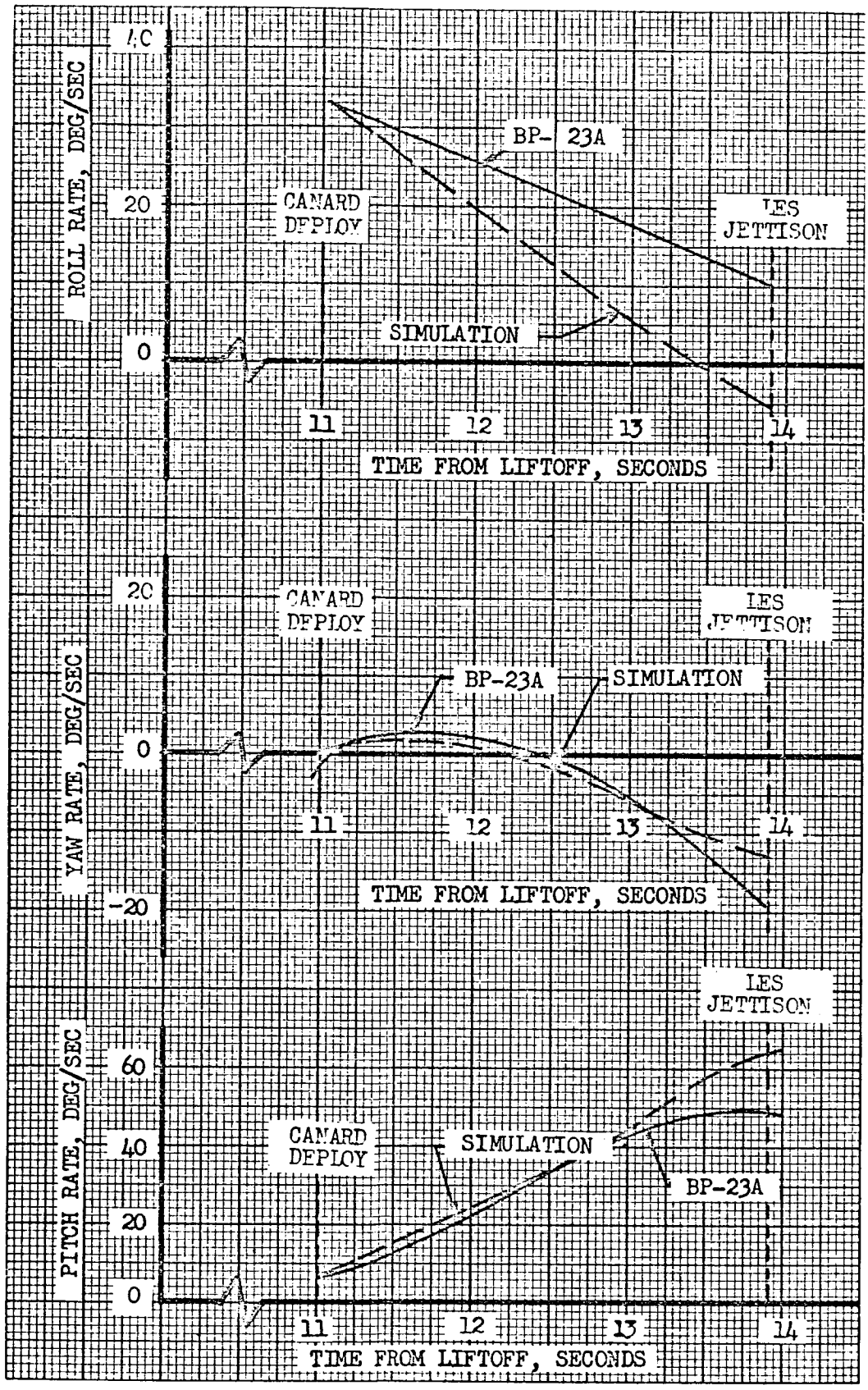

Figure 7.1-33 LEV with Canards Deployed Body Rate Time History Comparisons

[redacted]

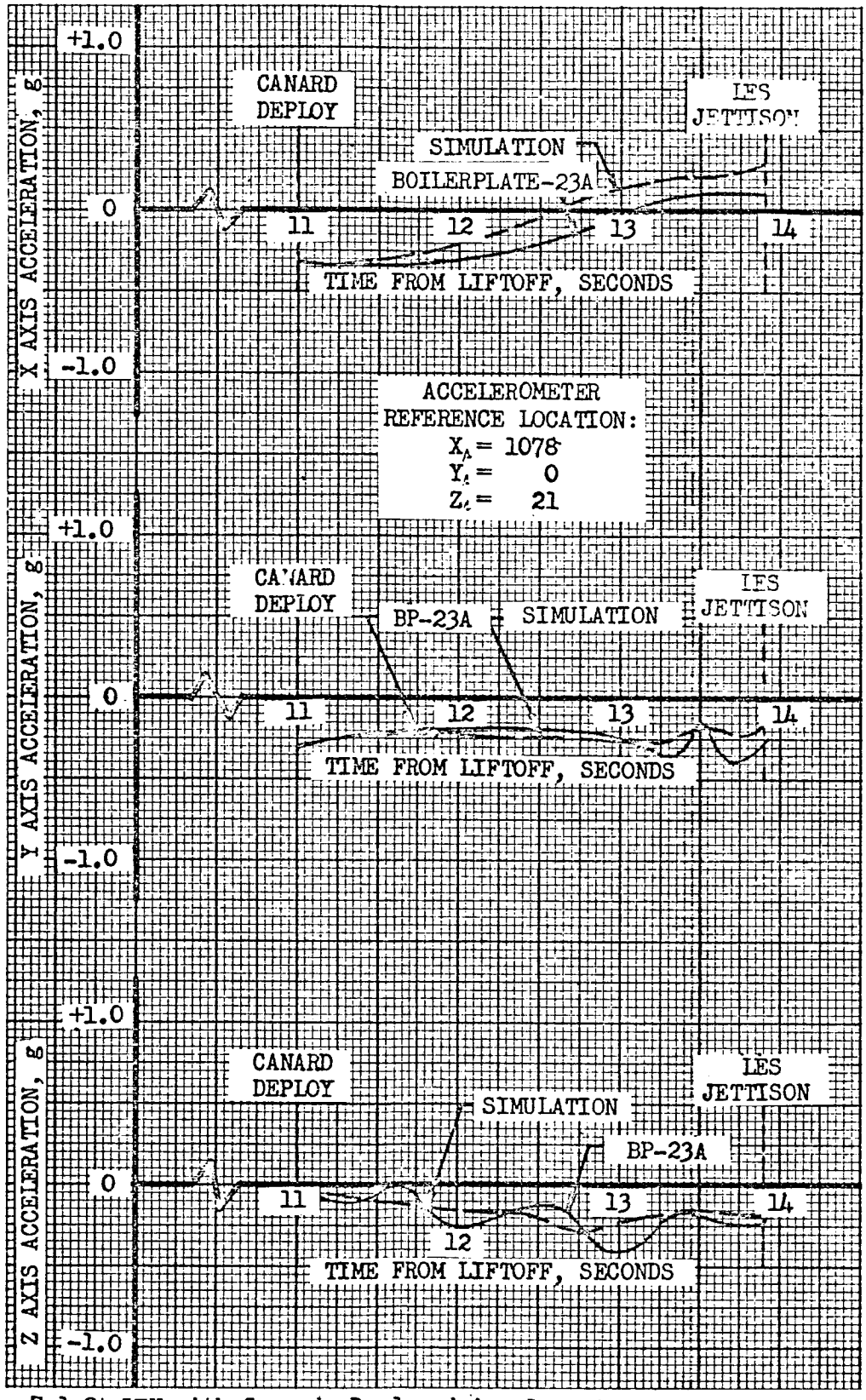

Figure 7.1-34 LEV with Canards Deployed Acceleration Time History Comparisons

[redacted]

[redacted]

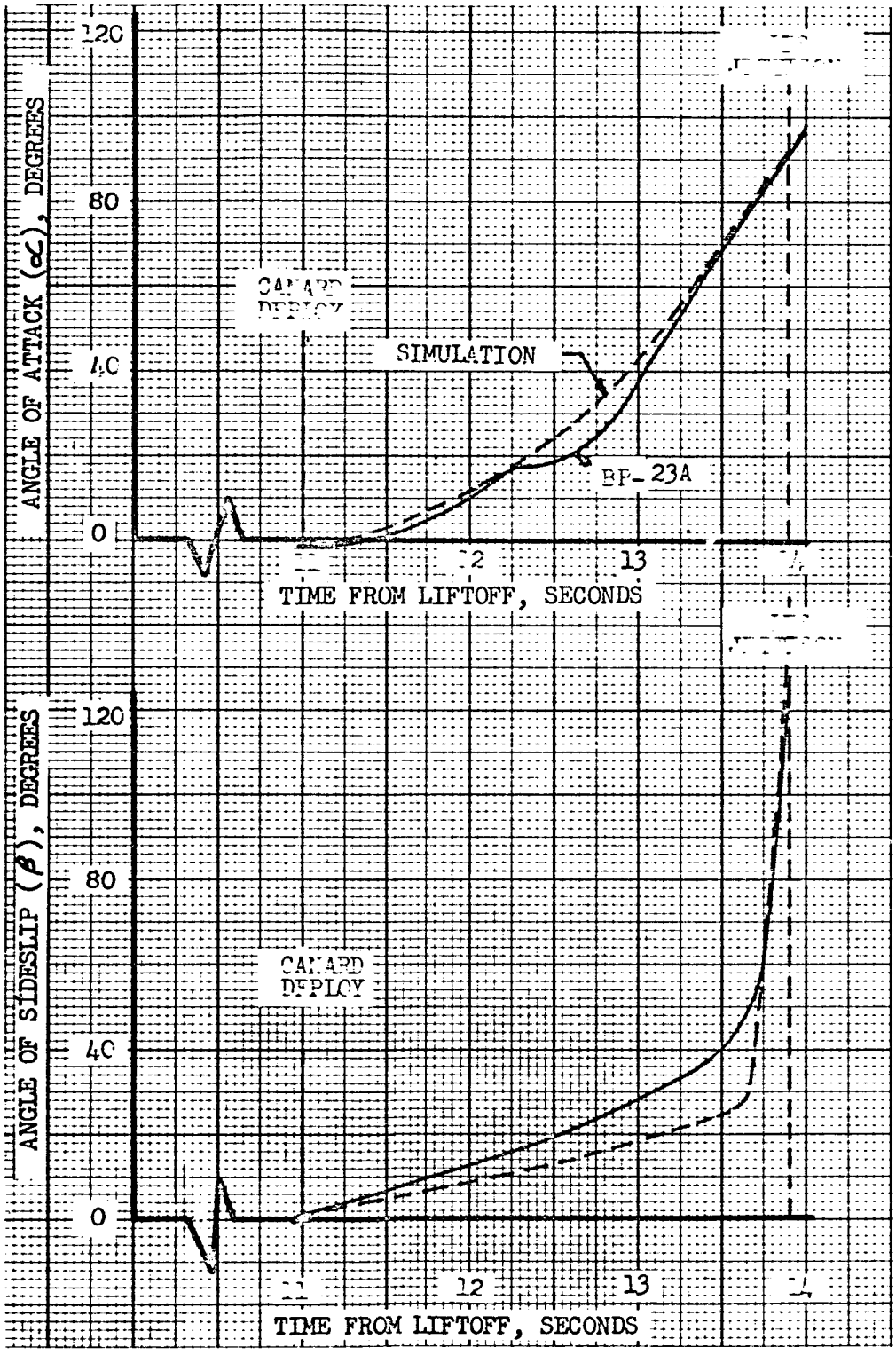

Figure 7.1-35 LEV with Canards Deployed Angles of Attack and Sideslip Time History Comparisons

[redacted]

[redacted]

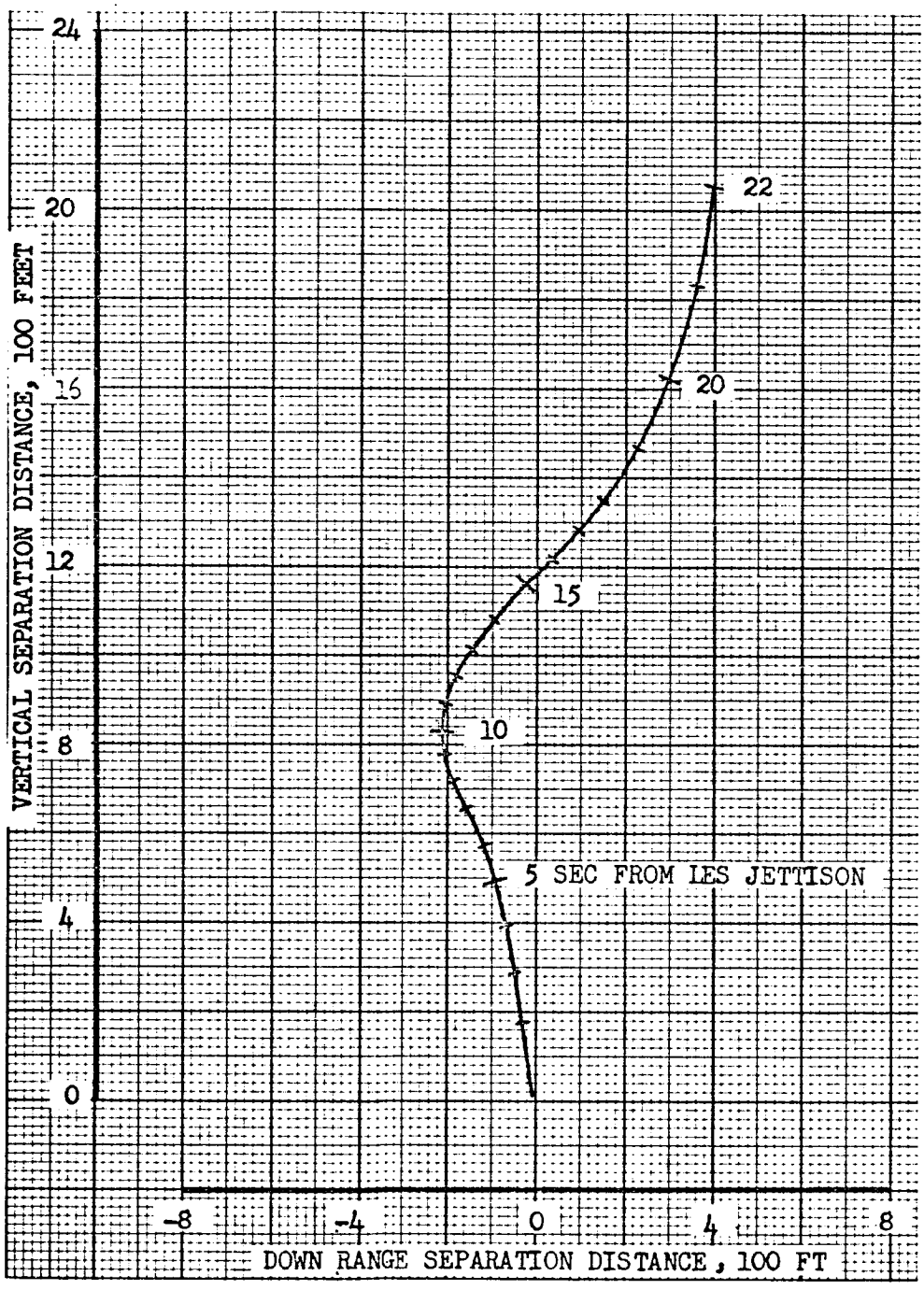

Figure 7.1-36 LES - CM Vertical and Downrange Separation

[redacted]

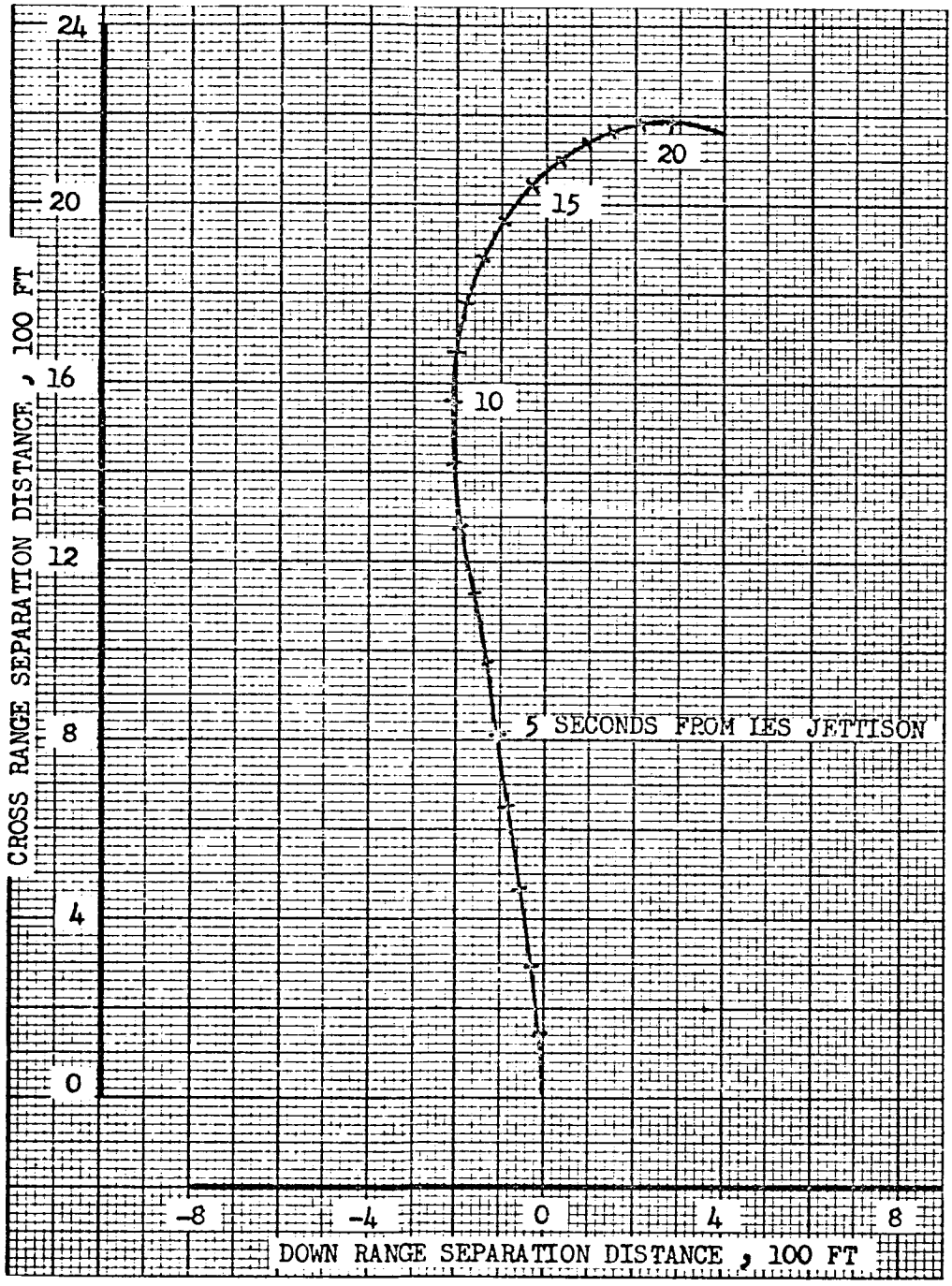

Figure 7.1-37 LES - CM Crossrange and Downrange Separation

[redacted]

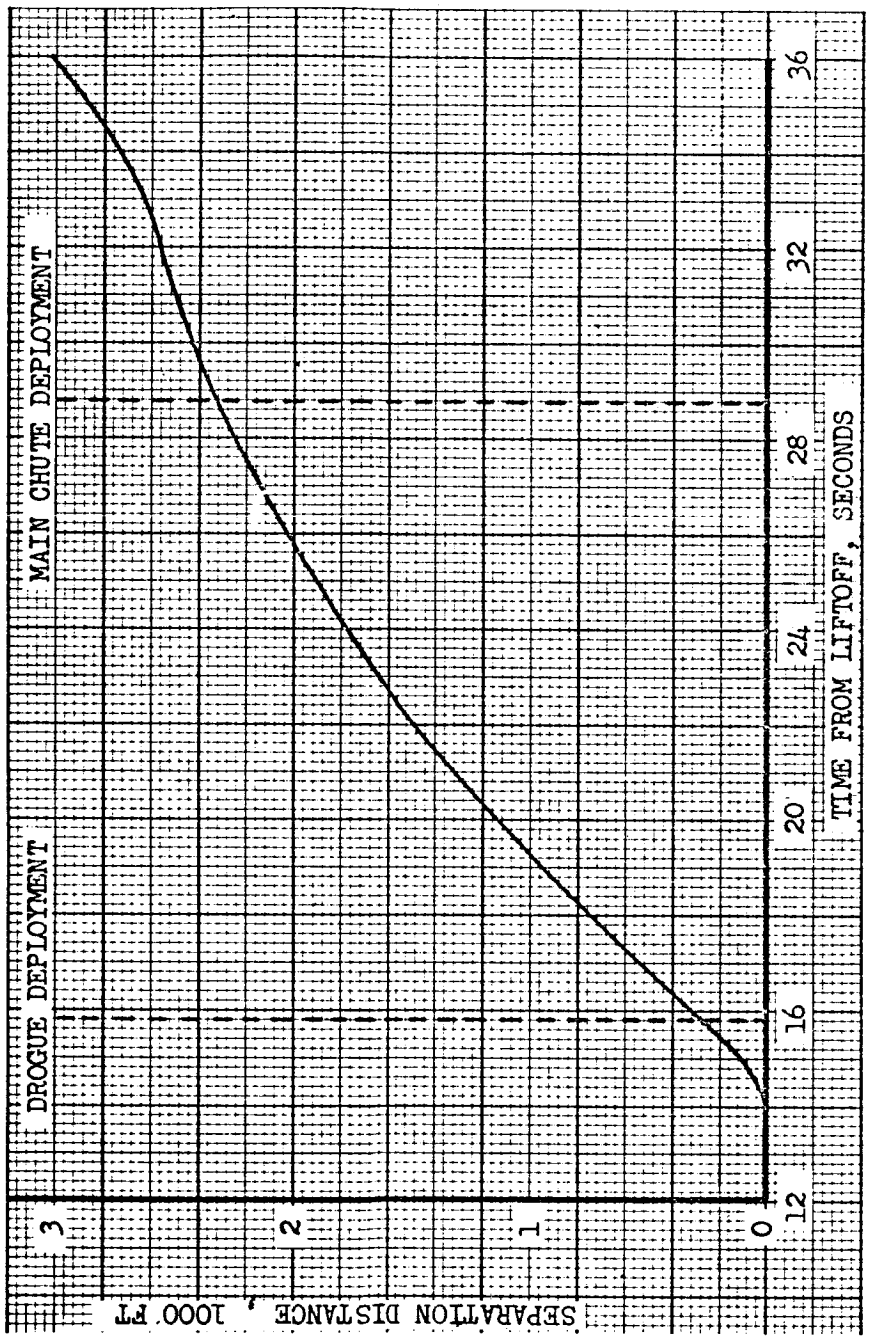

Figure 7.1-58 LES - CM Total Separation Distance Time History

[redacted]

~~CONFIDENTIAL~~

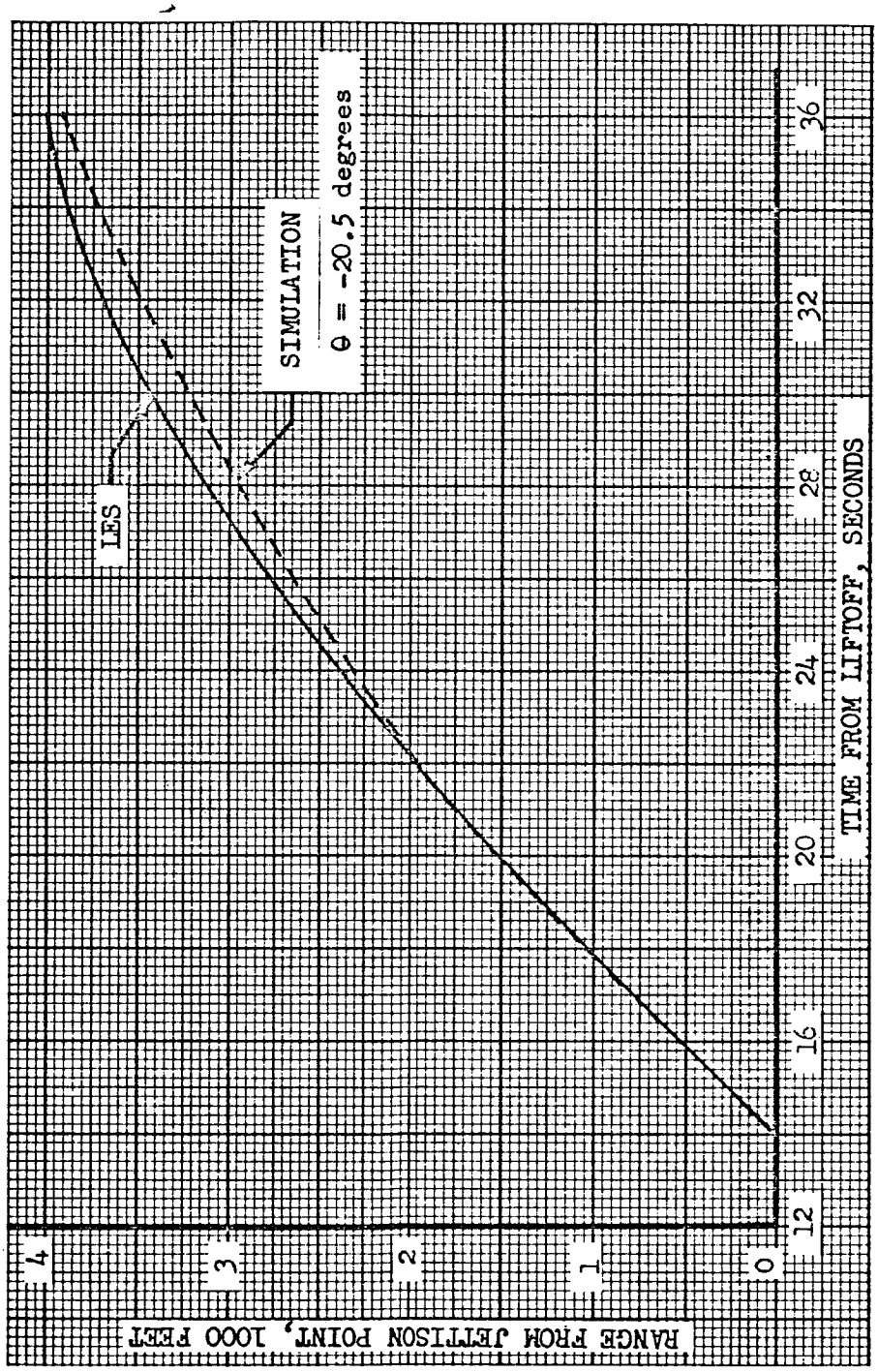

Figure 7.1-39 LES Range Time History Comparisons

~~CONFIDENTIAL~~

[redacted]

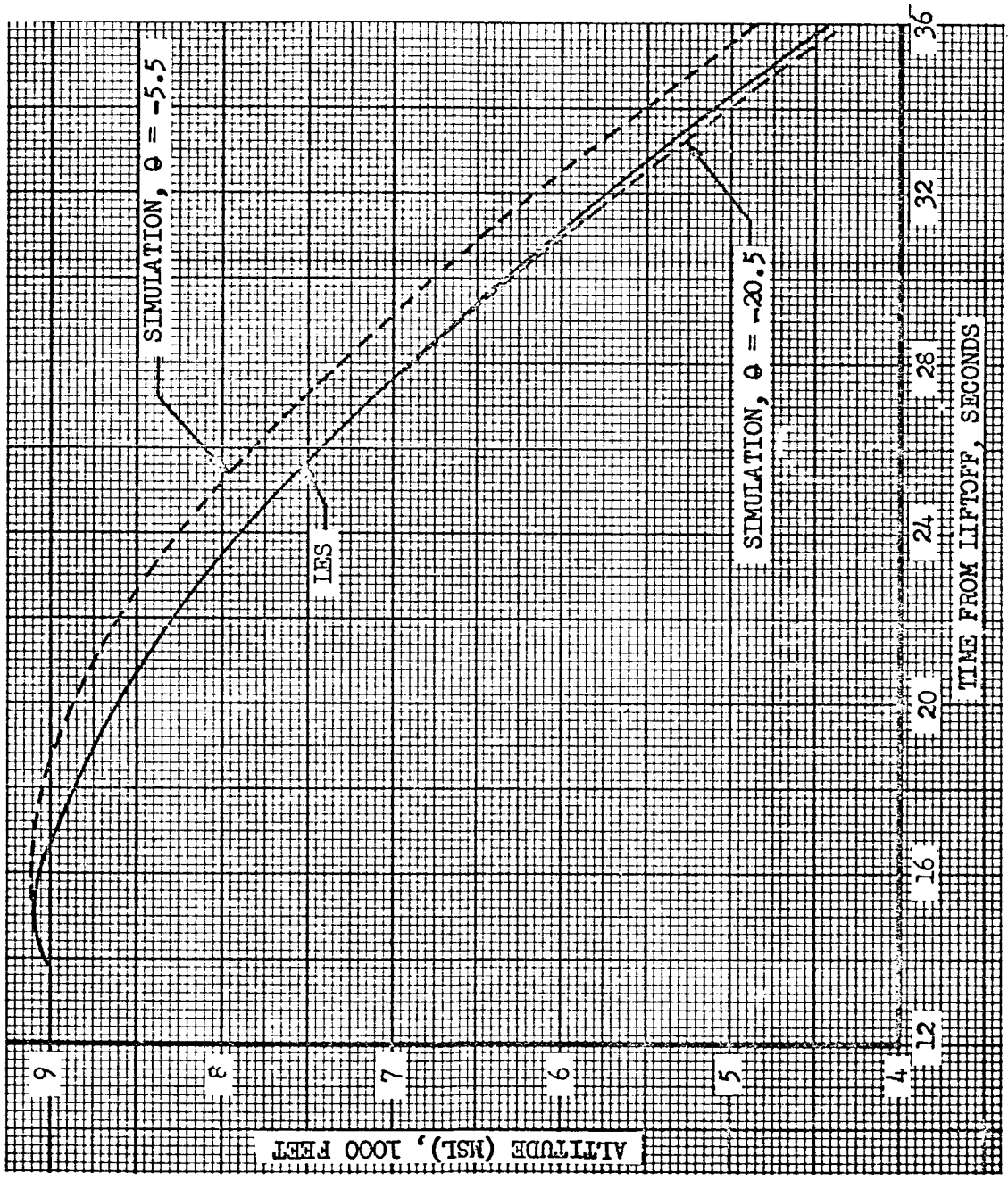

Figure 7.1-40 LES Altitude Time History Comparisons

[redacted]

[redacted]

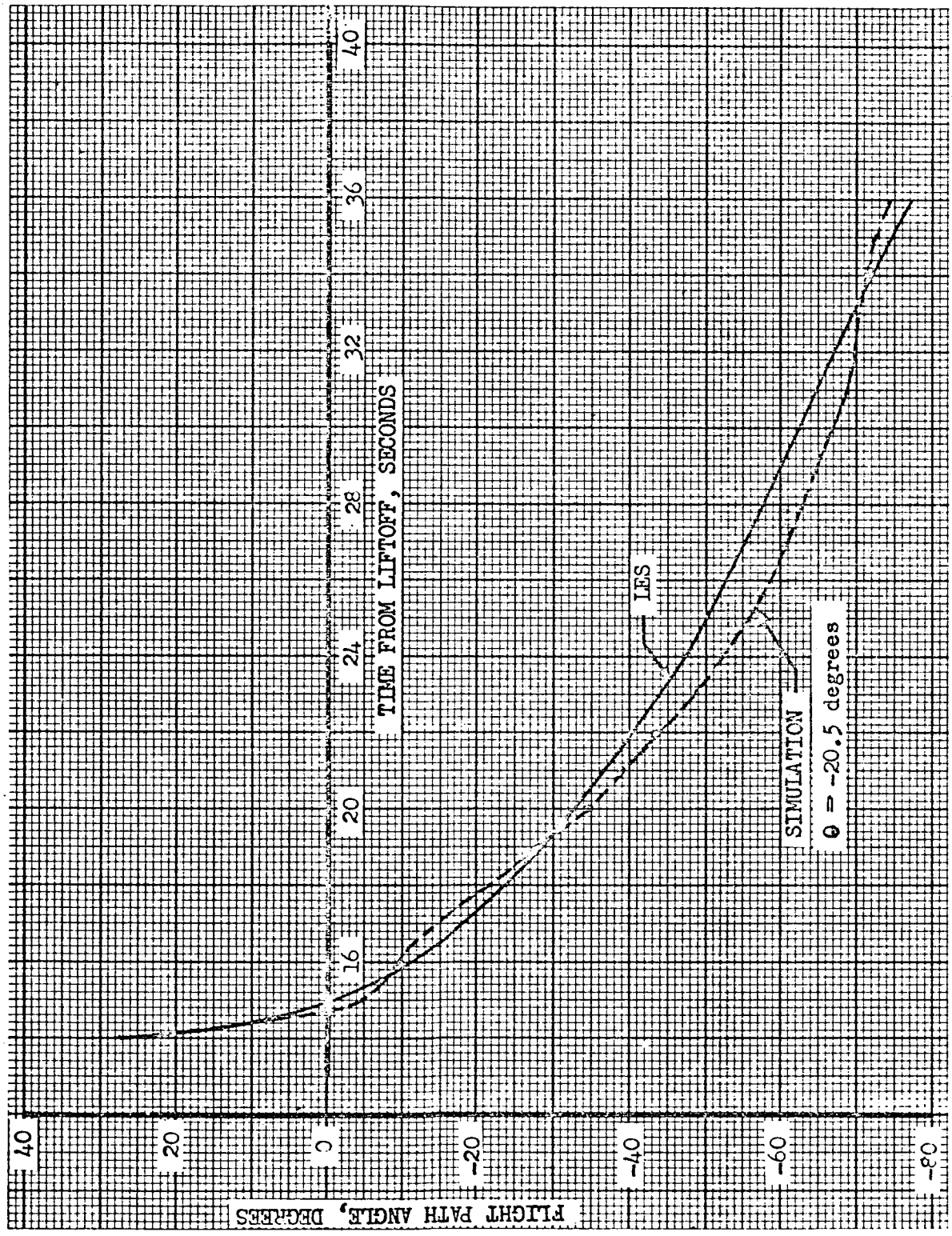

Figure 7.1-41 LES Flight Path Angle Time History Comparisons

[redacted]

[redacted]

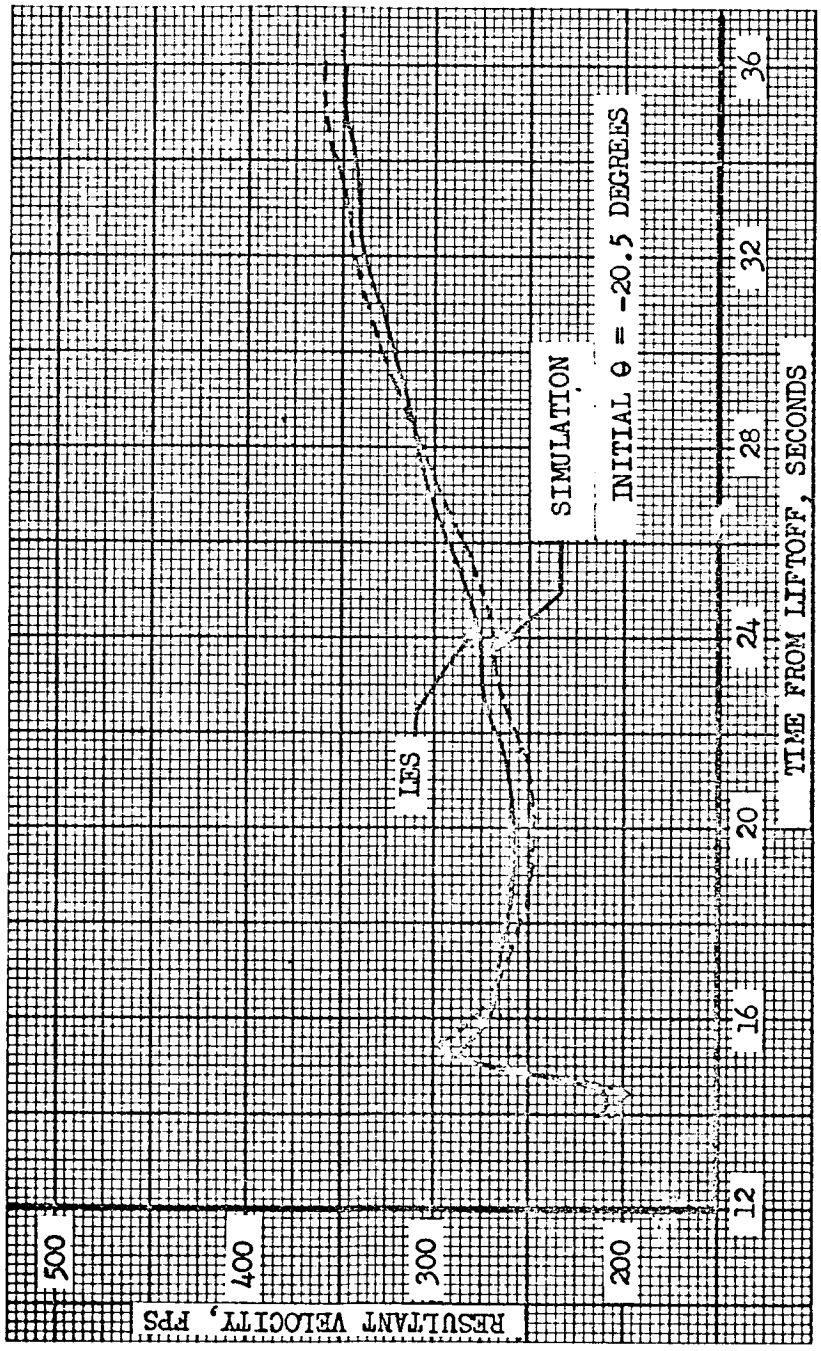

Figure 7.1-42 LES Resultant Velocity Time History Comparisons

[redacted]

CON[redacted]L

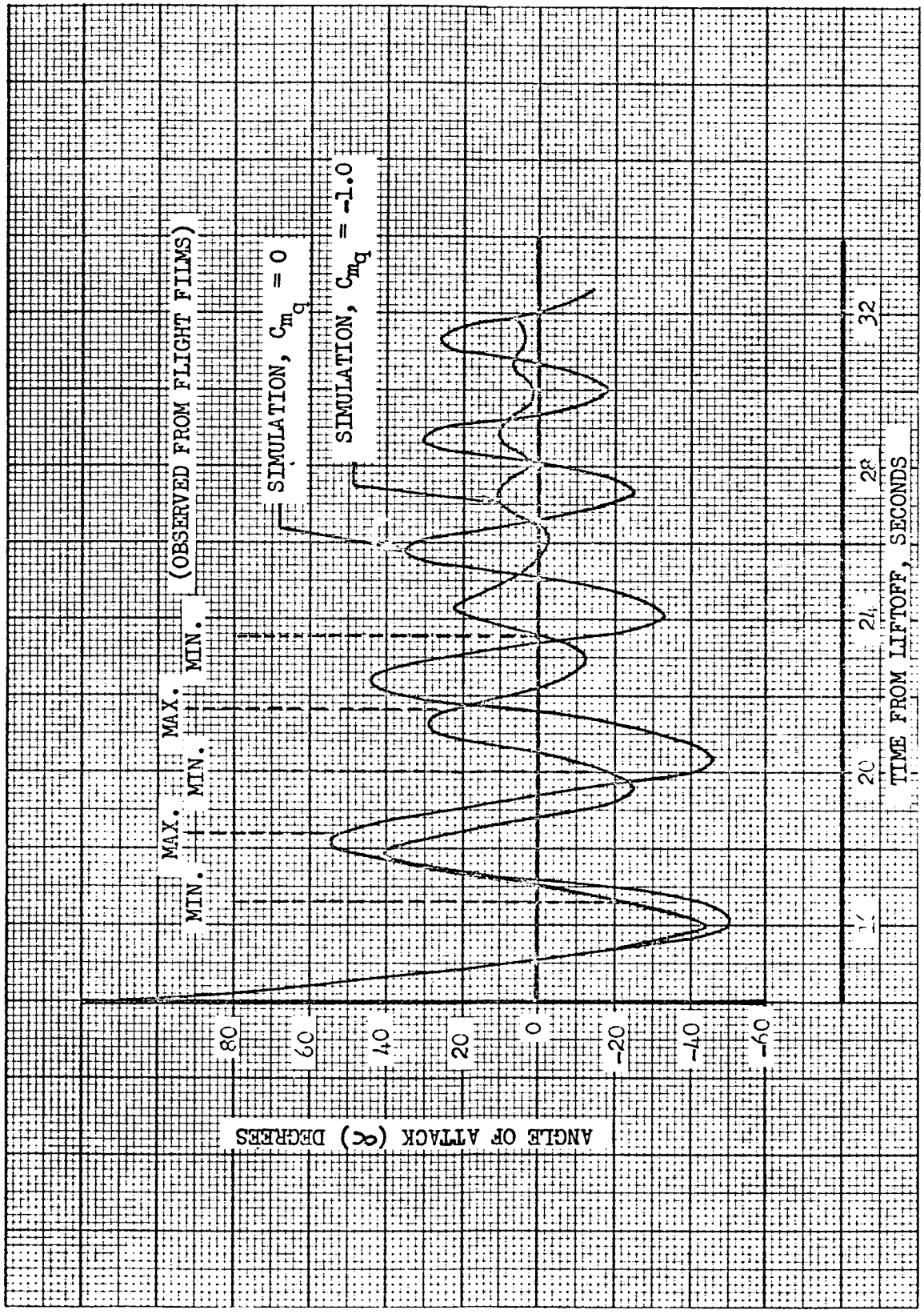

Figure 7.1-43 LES Pitch Plane Oscillations

[redacted]

[redacted]

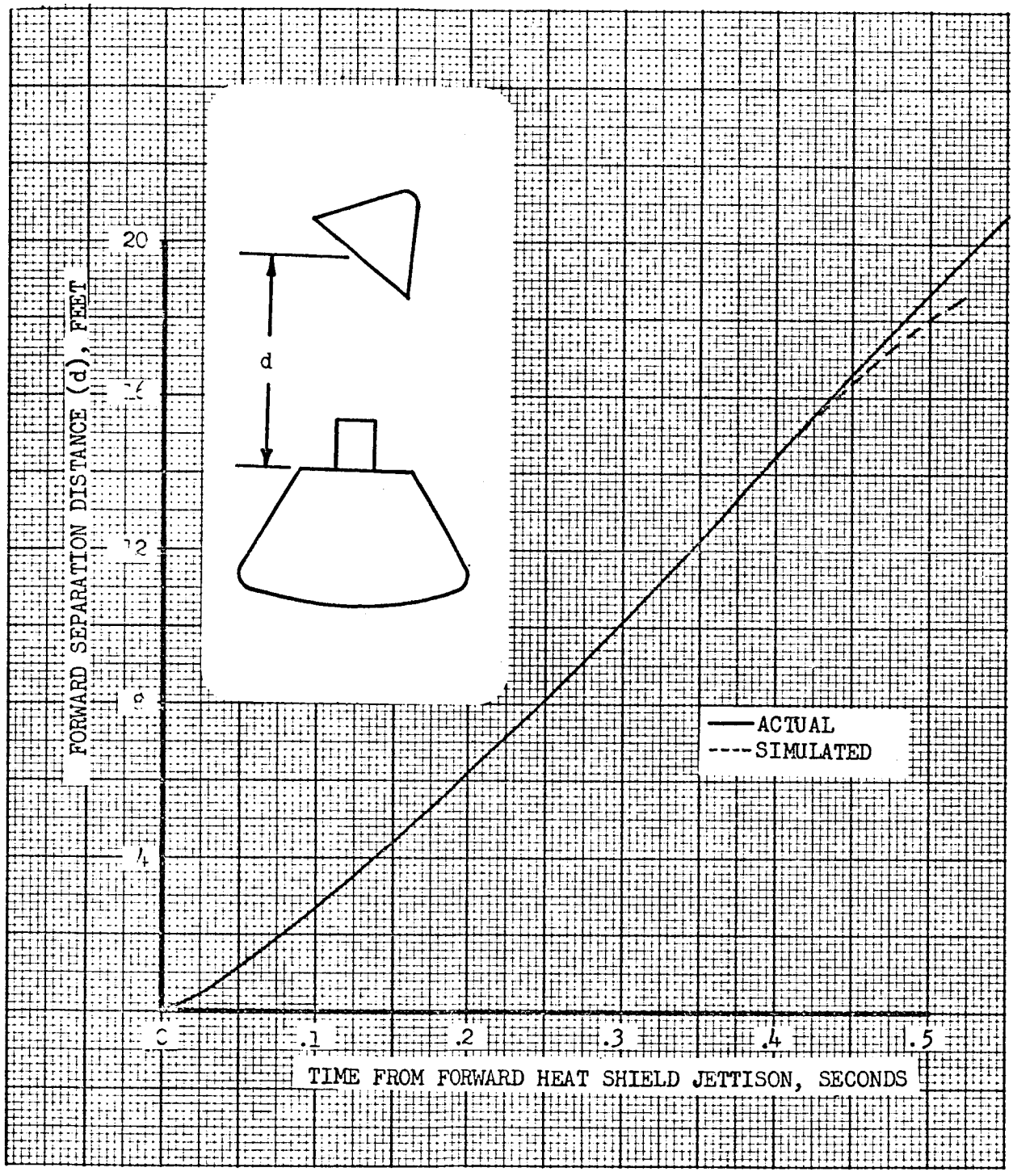

Figure 7.1-44 Forward Heat Shield Separation History

[redacted]

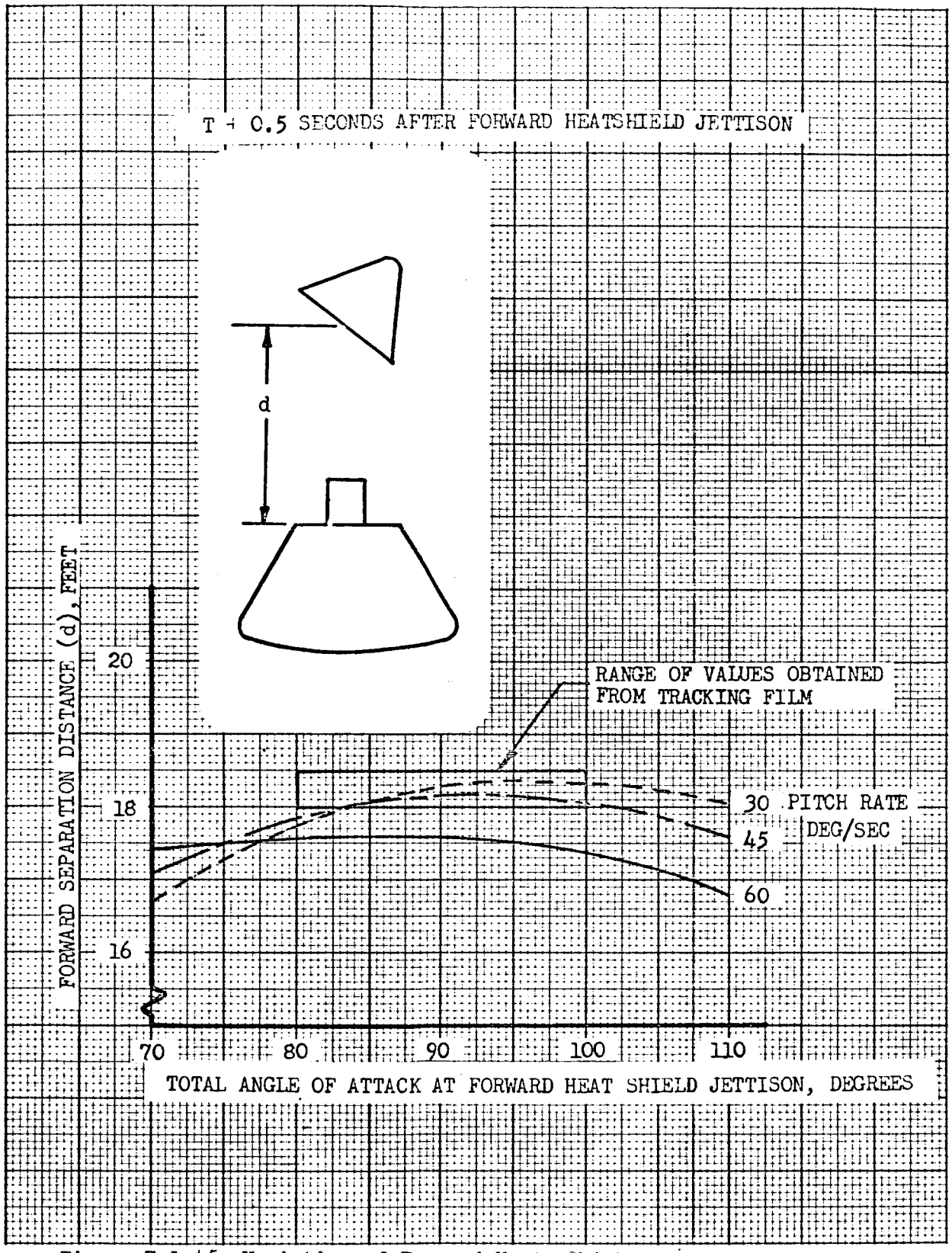

Figure 7.1-45 Variation of Forward Heat Shield Separation Distance with Initial Angle of Attack and Pitch Rate

[redacted]

CON~~FIDENTIAL~~.

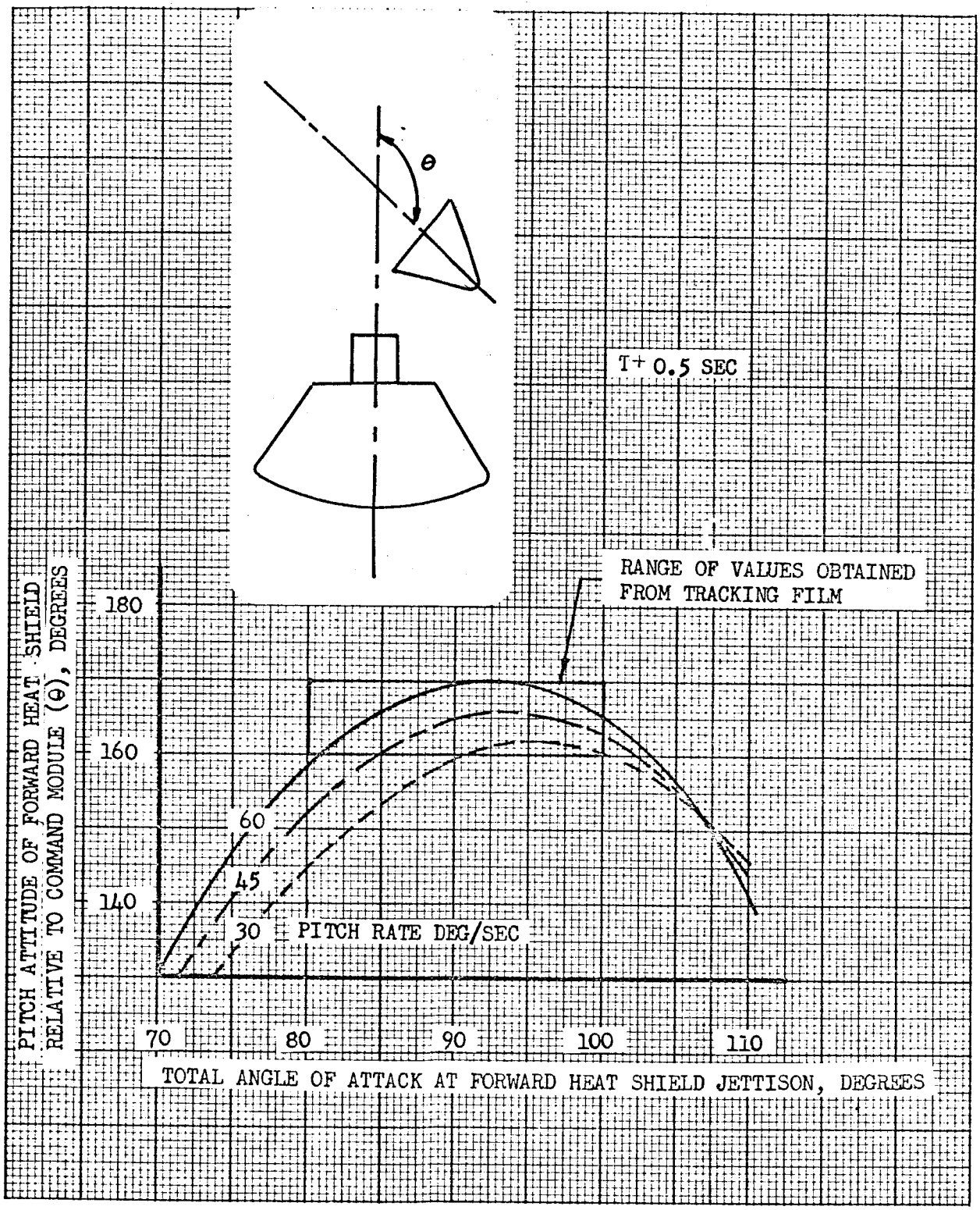

Figure 7.1-46 Variation of Forward Heat shield Relative Pitch Attitude with Initial Angle of Attack and Pitch Rate

[redacted]

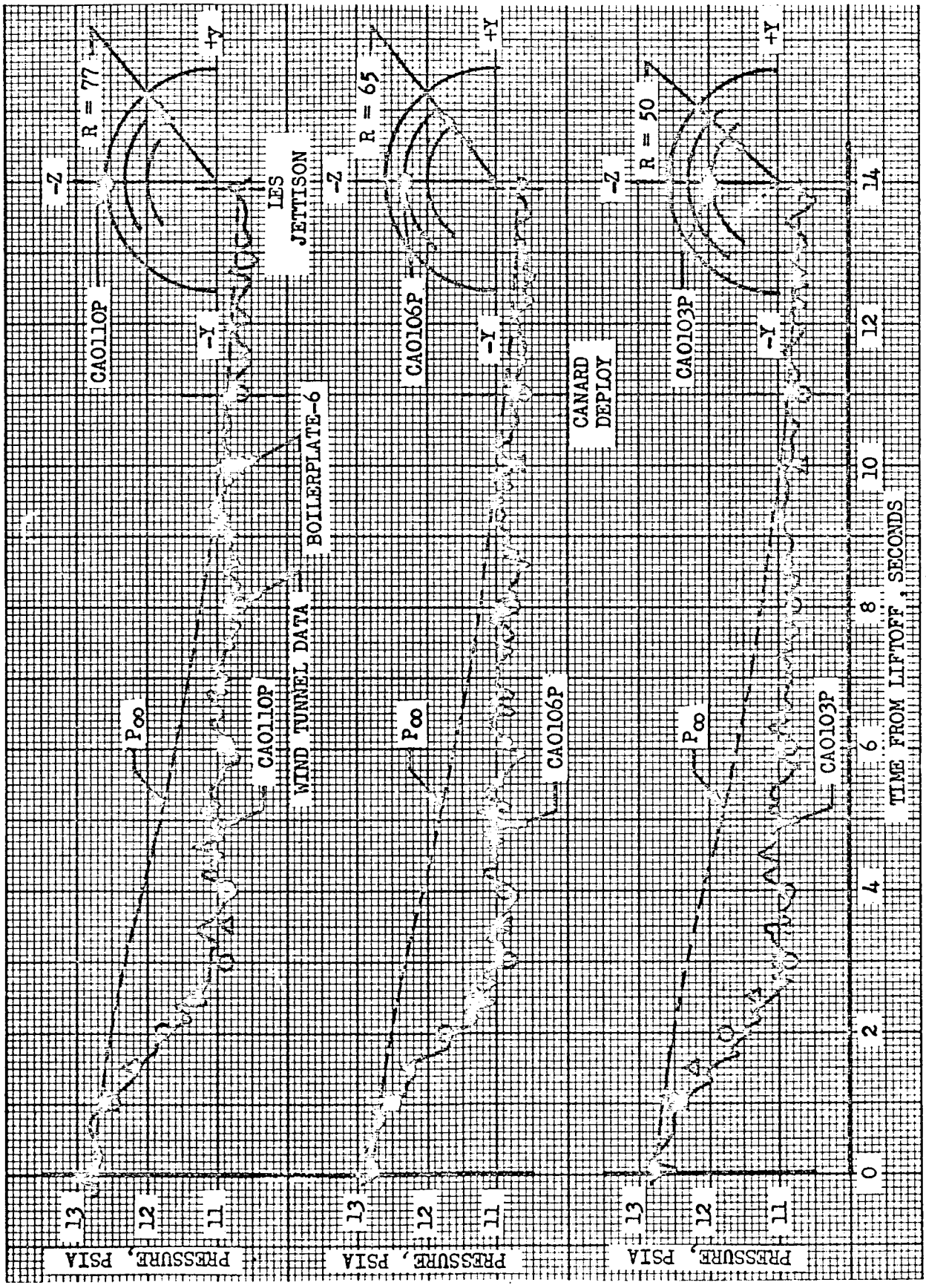

Figure 7.1-47 BP-23A Base Pressure Time Histories Compared to Wind Tunnel Data and BP-6 Flight Test Data

[redacted]

[redacted]

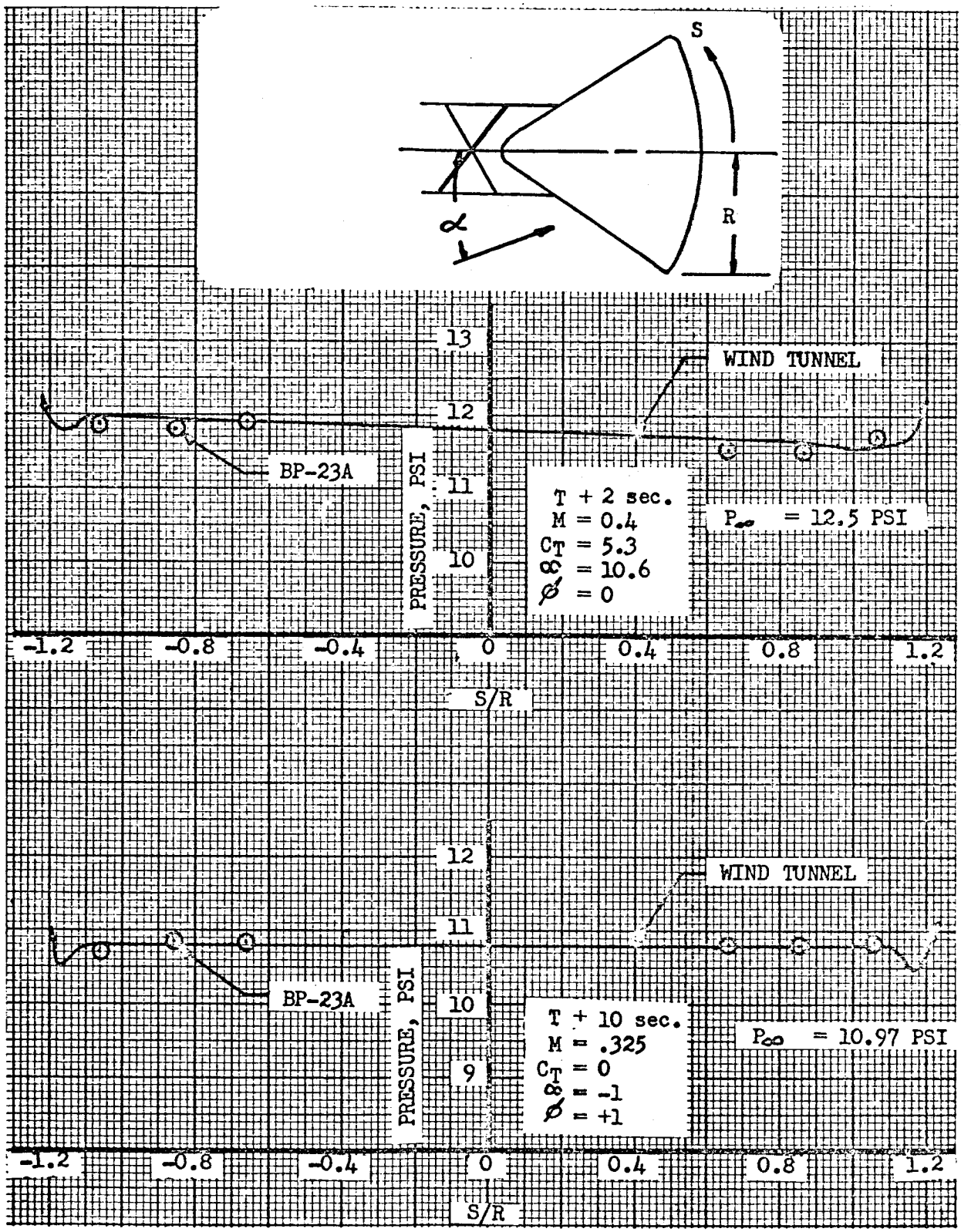

Figure 7.1-48 LEV Base Pressure Distribution During Abort

[redacted]

[redacted]

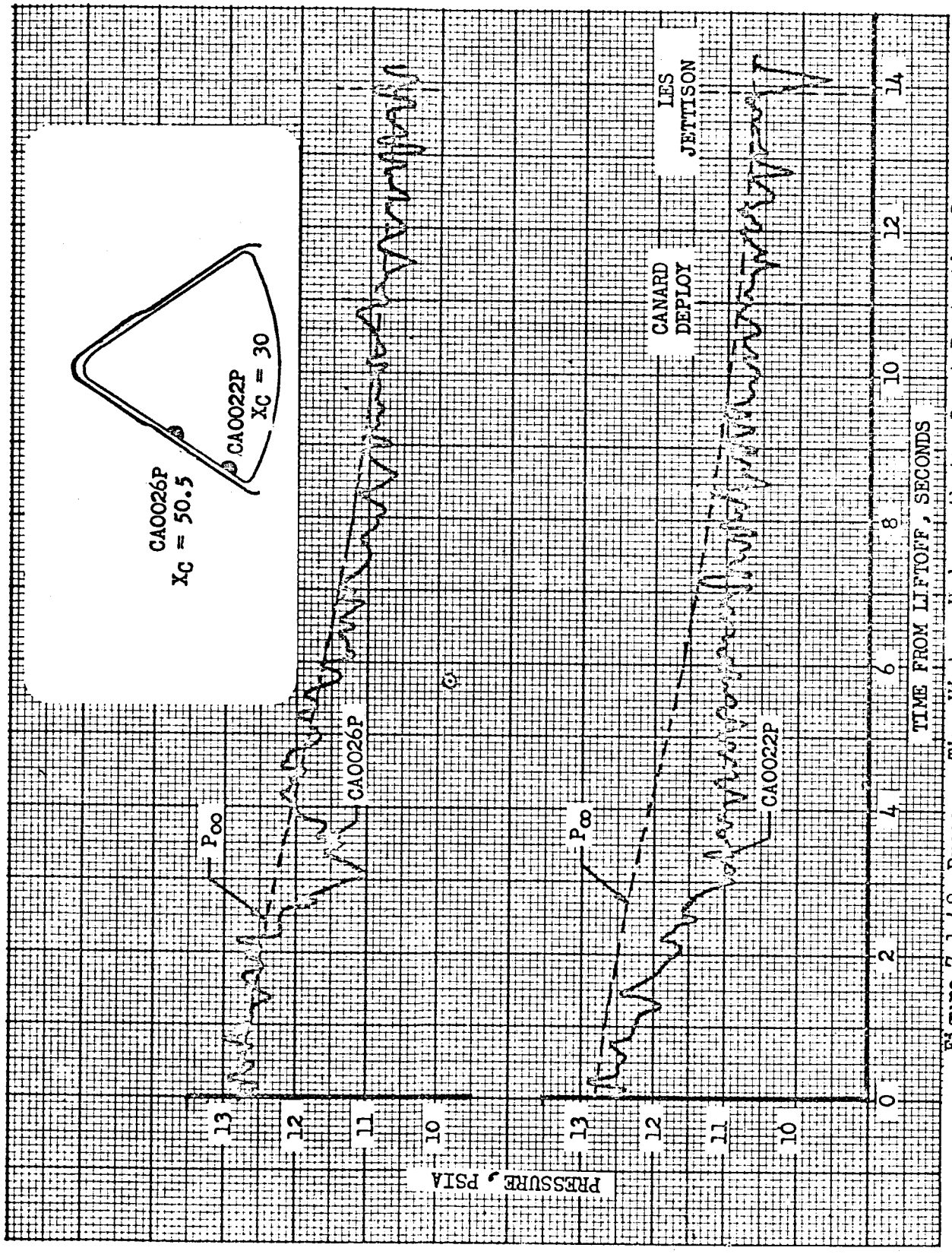

Figure 7.1-49 Pressure Time History Underneath the Boost Protective Cover

[redacted]

[redacted]

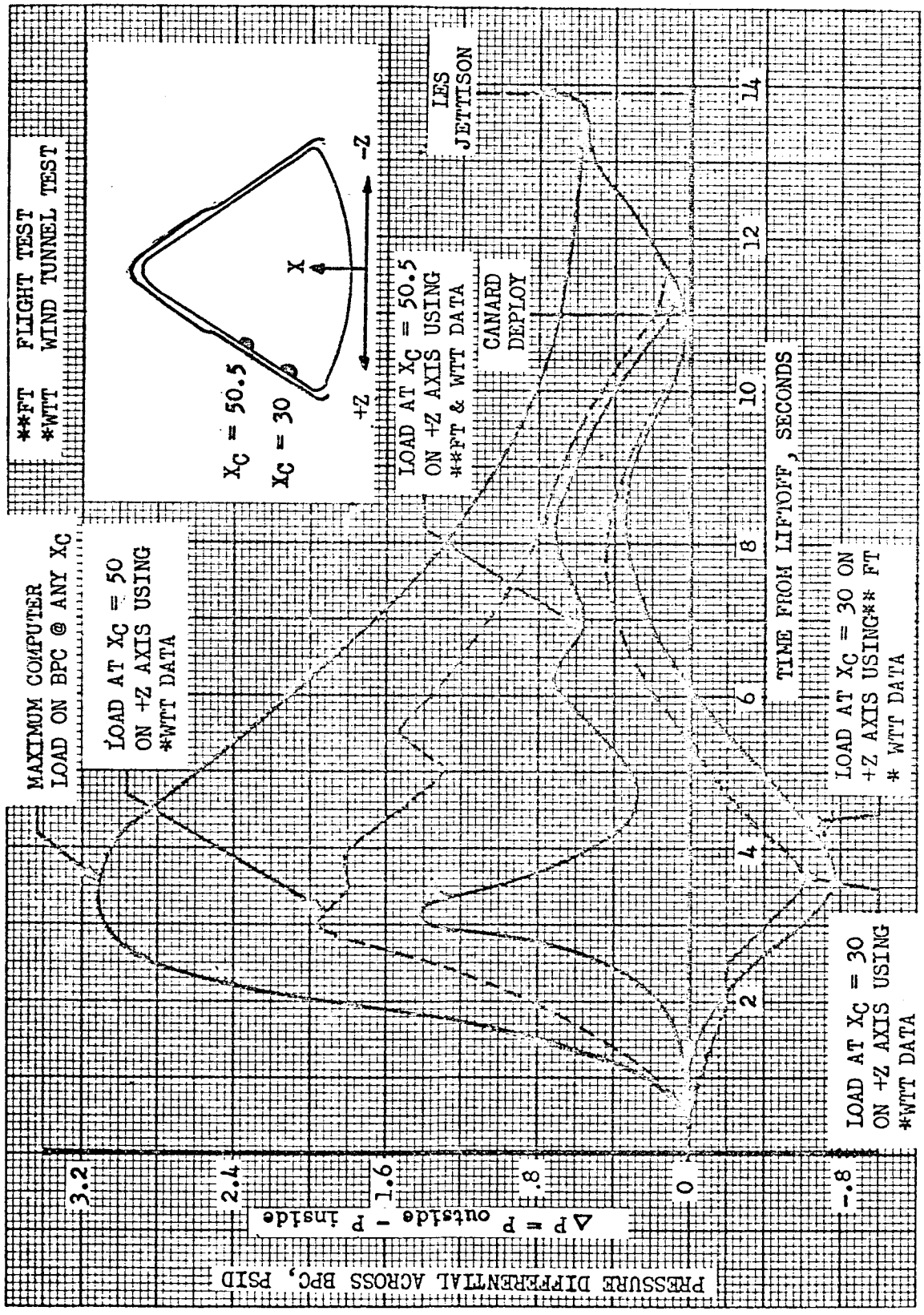

Figure 7.1-50 Pressure Differential Across the Boost Protective Cover

[redacted]

[redacted]

Time = T_1 (Start of picture sequence)

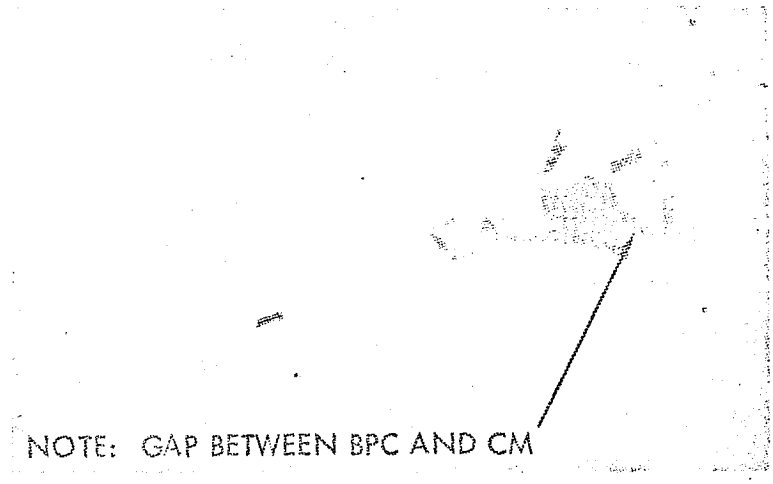

T_1 + 0.0167

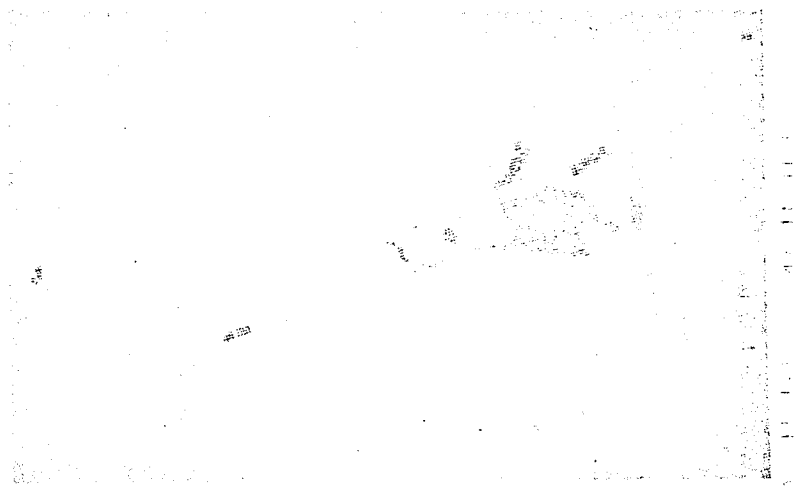

T_1 + 0.08334

Figure 7.1-51 Boost Protective Cover Pullaway

[redacted]

Form 158-E-38 New 4-62

[redacted]

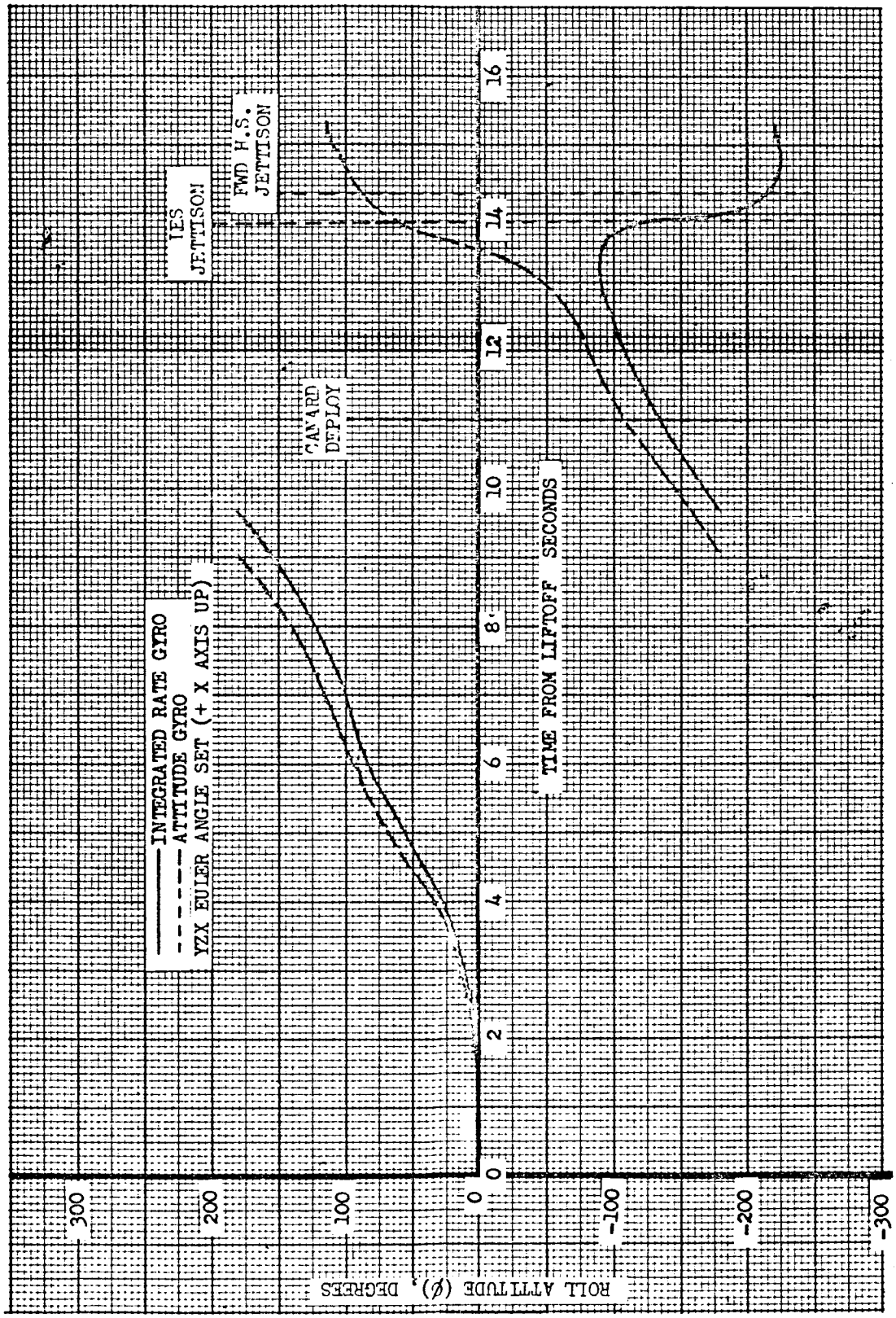

7.1-52 Comparison of Vehicle Roll Attitude Time History from Attitude and Integrated Rate Gyro Data

[redacted]

[redacted]

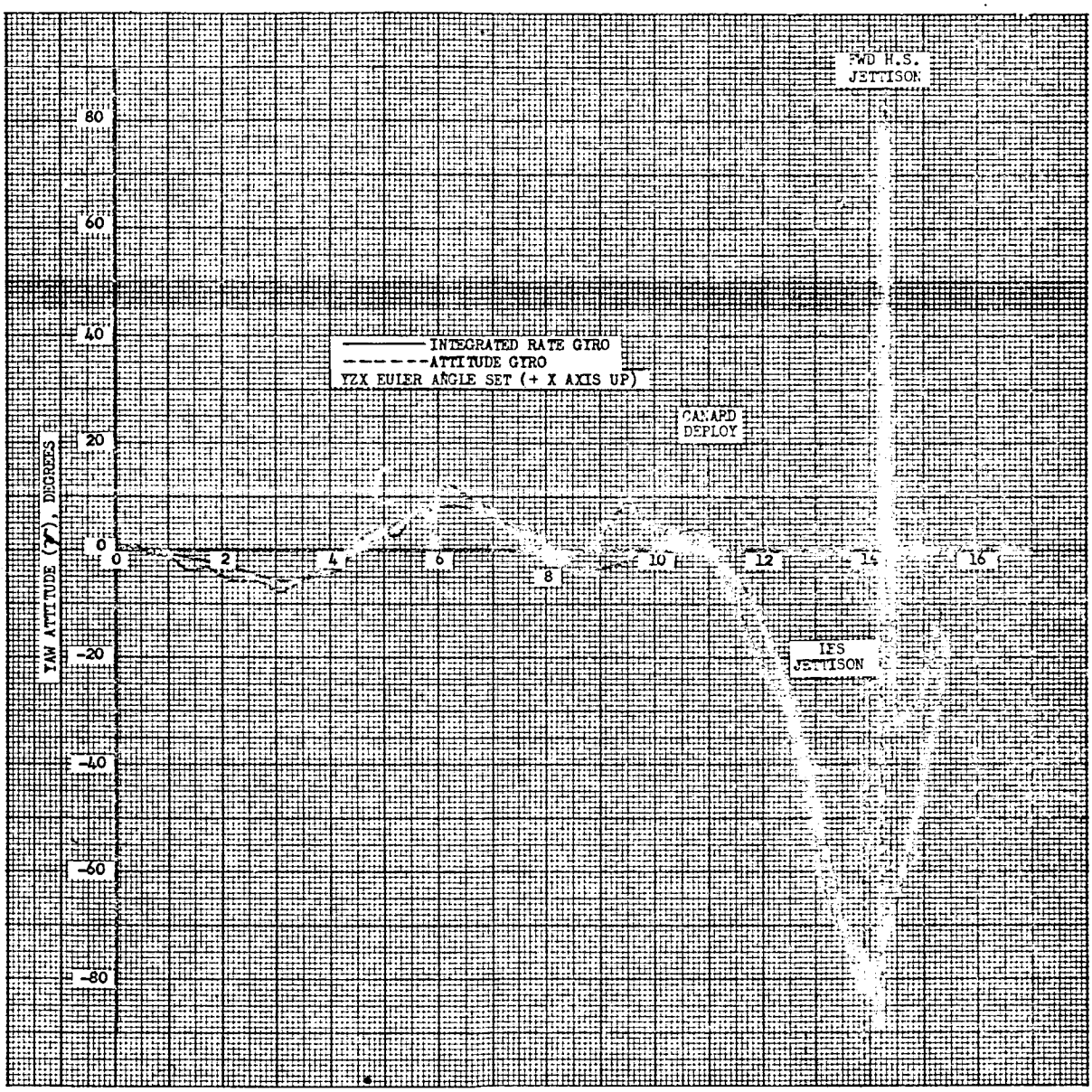

Figure 7.1-53 Comparison of Vehicle Yaw Attitude Time History from Attitude and Integrated Rate Gyro Data

[redacted]

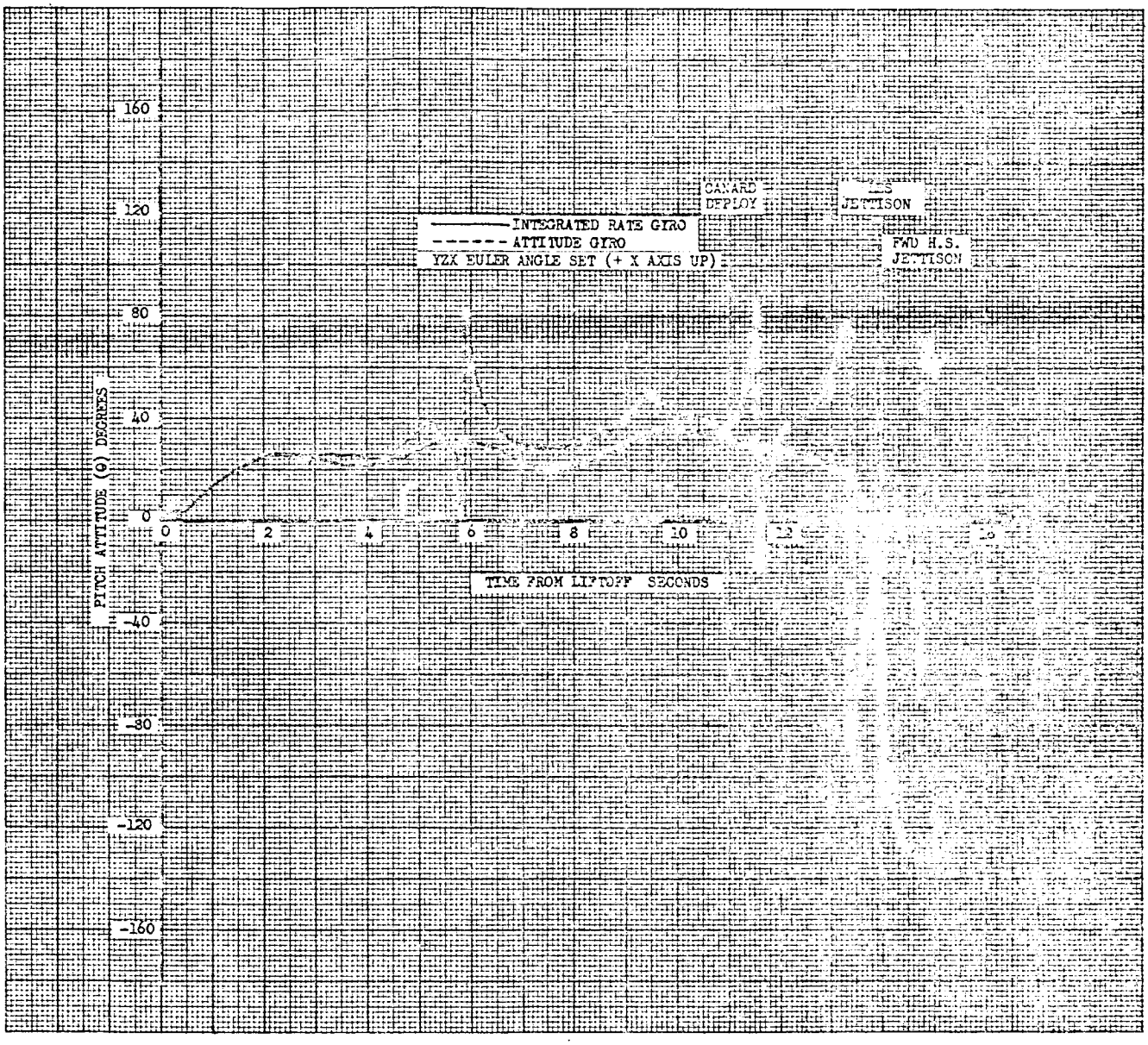

Figure 7.1-54 Comparison of Vehicle Pitch Attitude Time History from Attitude and Integrated Rate Gyro Data

[redacted]

[redacted]

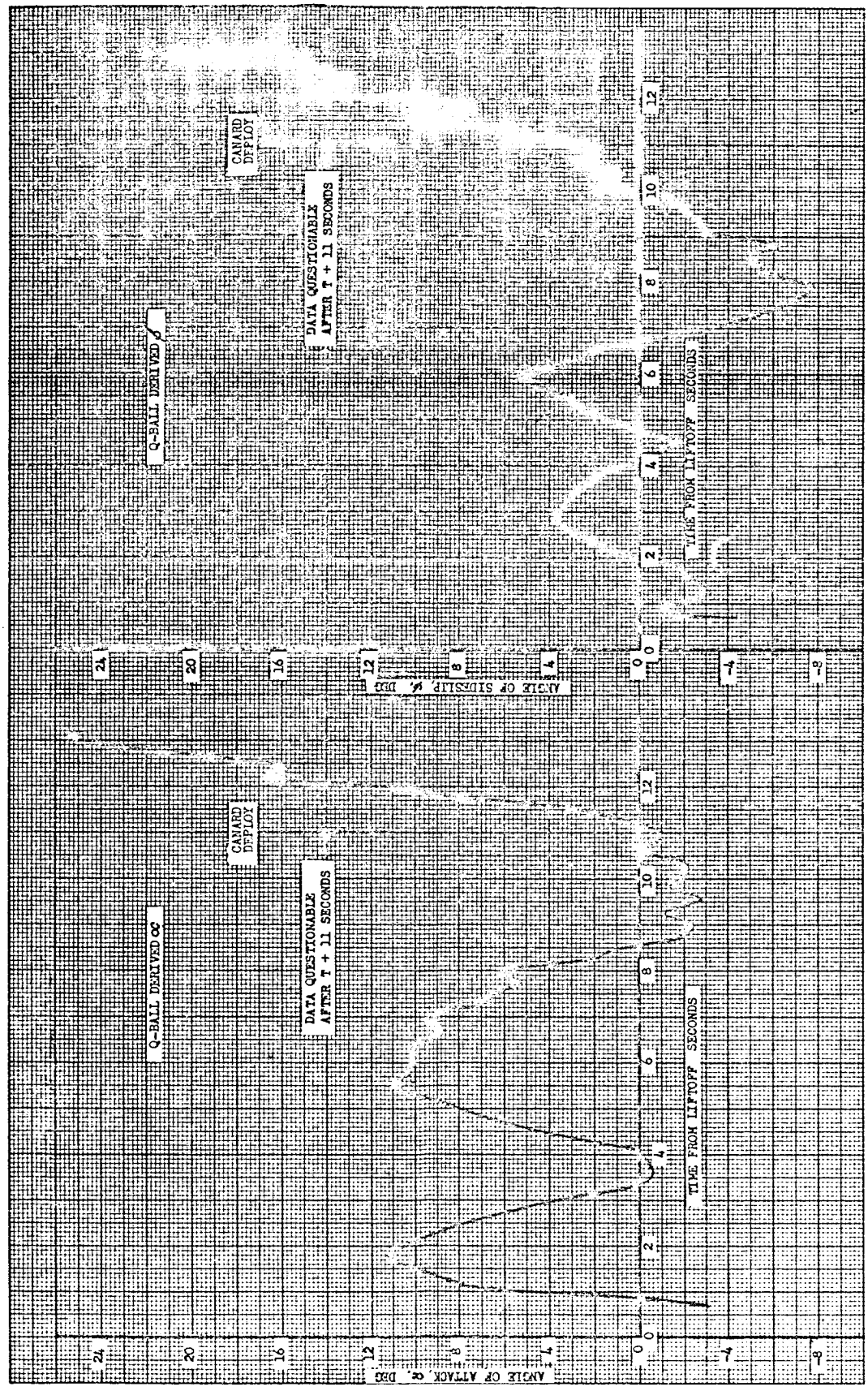

Figure 7.1-55 Q-Ball Derived Angles of Attack and Sideslip Time Histories

[redacted]

[redacted]

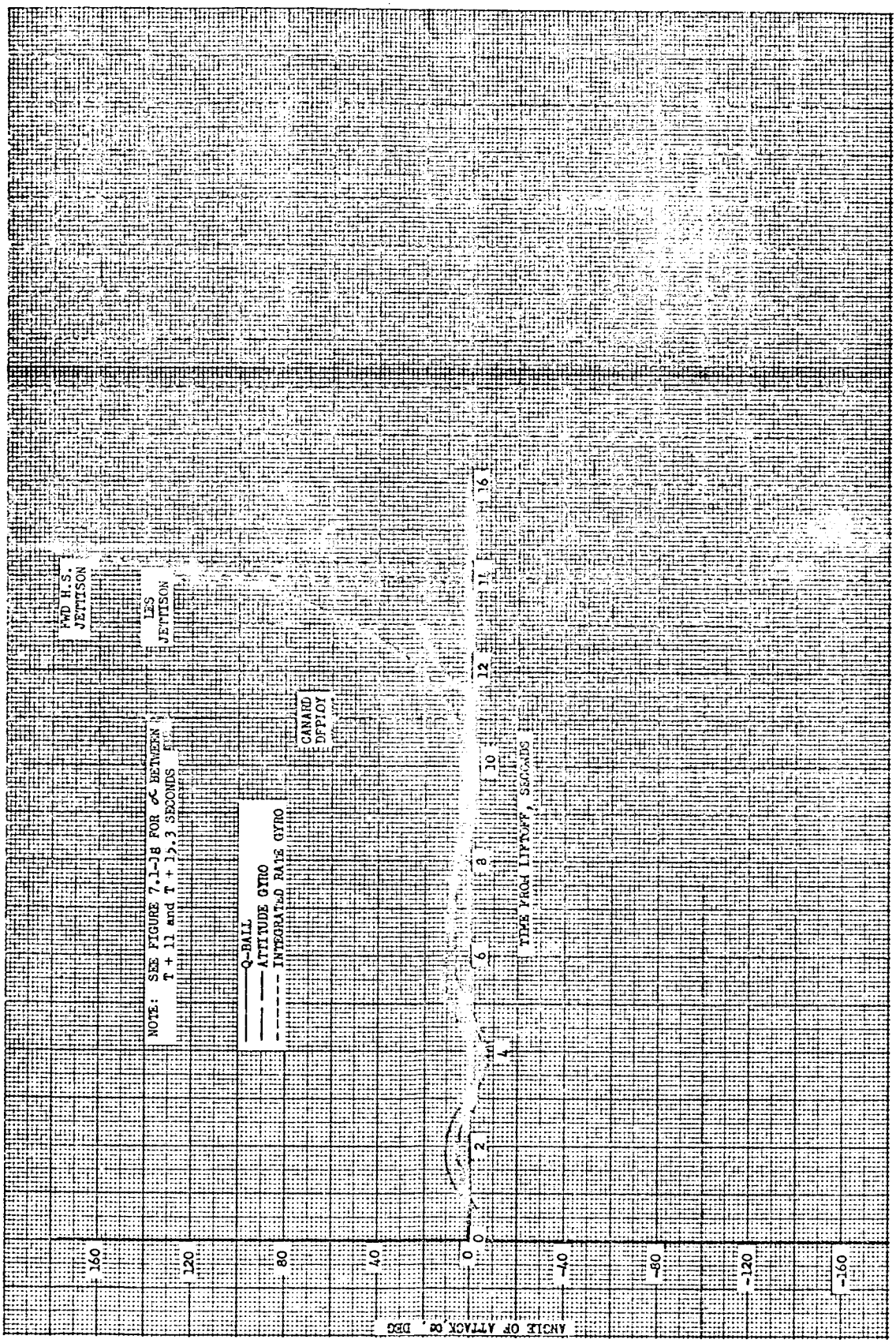

Figure 7.1-56 Comparison of Angle of Attack Time Histories from Q-Ball Attitude and Integrated Rate Gyro Data

[redacted]

[redacted]

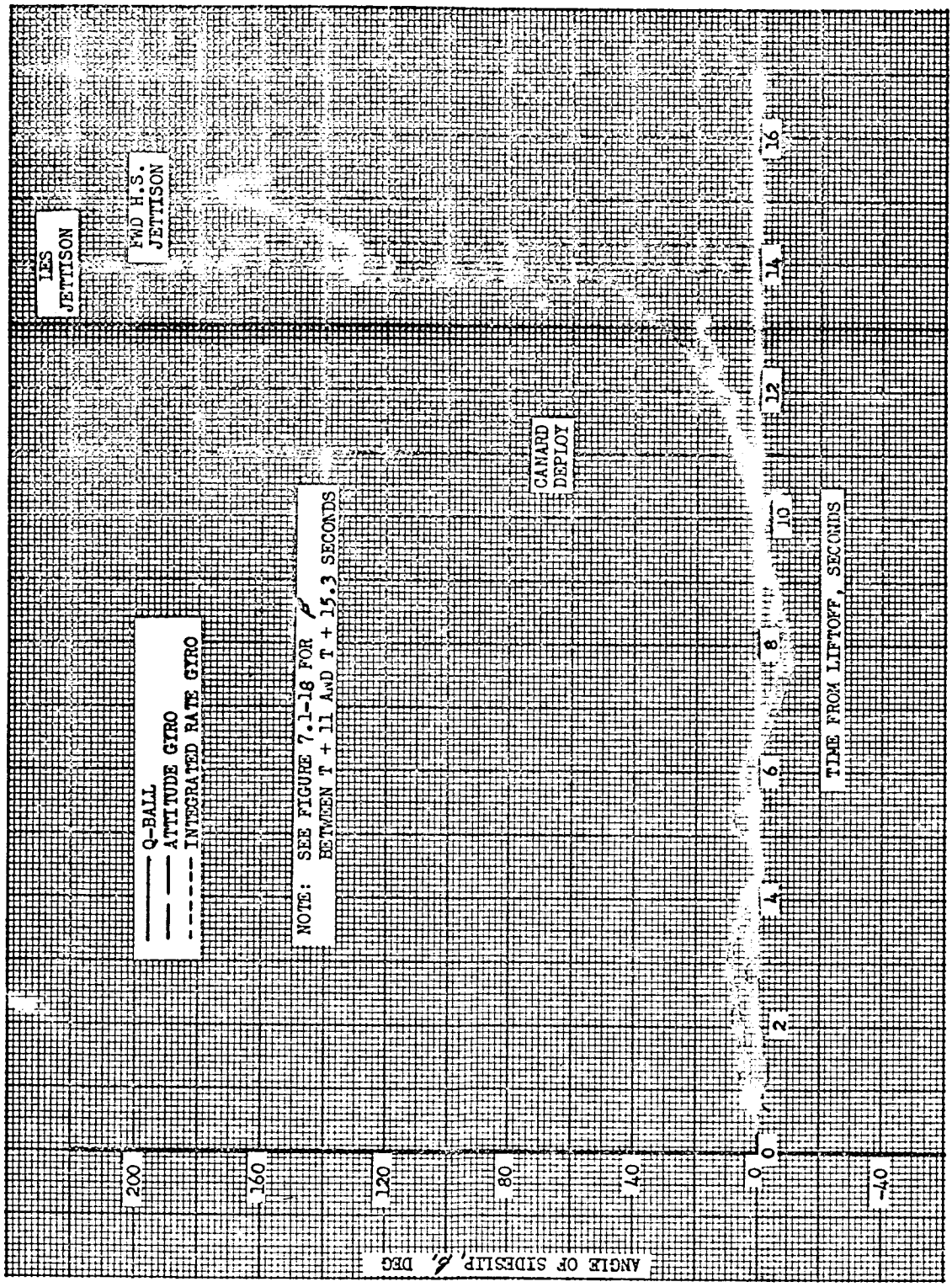

Figure 7.1-57 Comparison of Angle of Sideslip Time Histories from Q-Ball Attitude and Integrated Rate Gyro Data

[redacted]

[redacted]

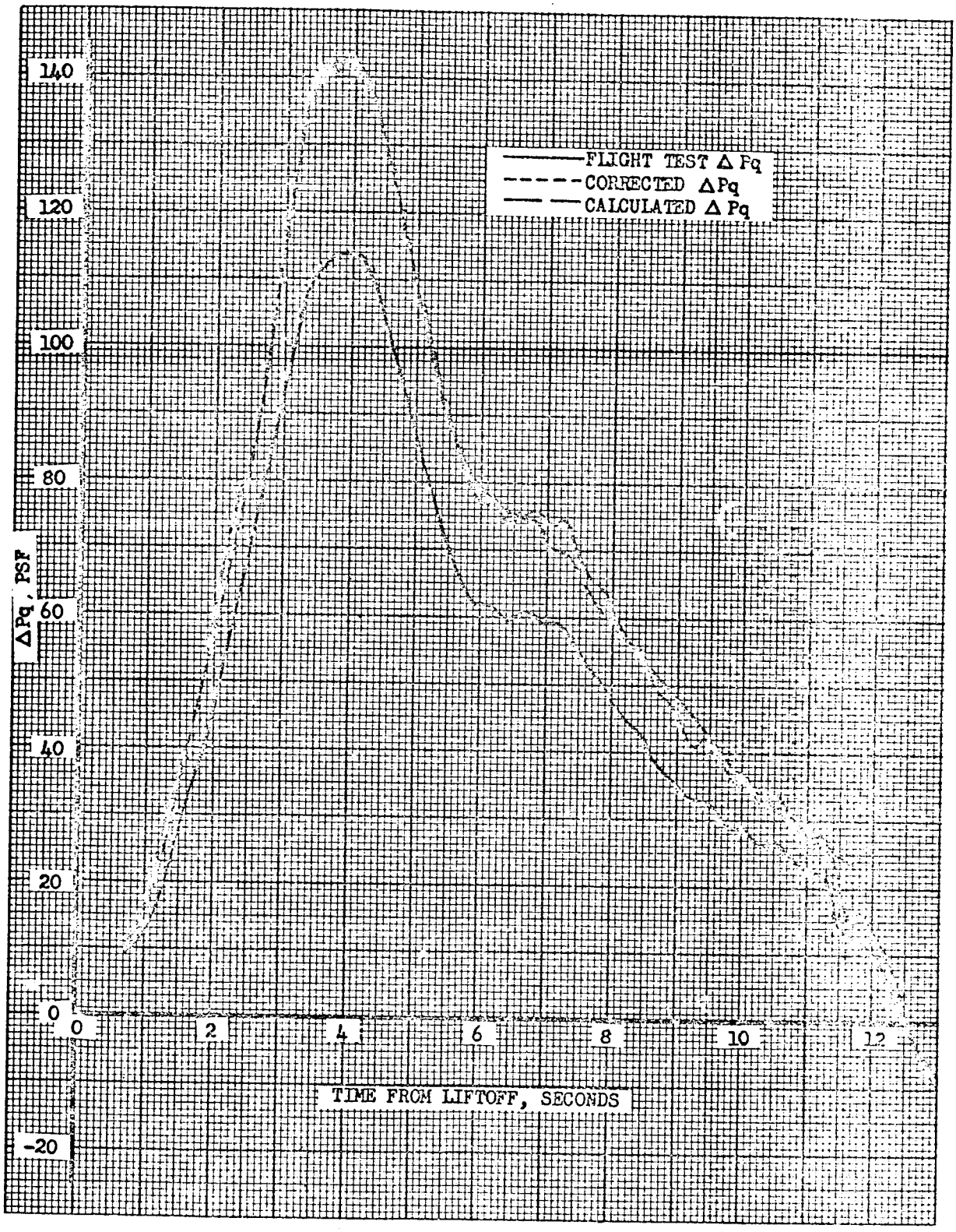

Figure 7.1-58 Comparison of Measured and Computed Δ Pq.

[redacted]

[redacted]

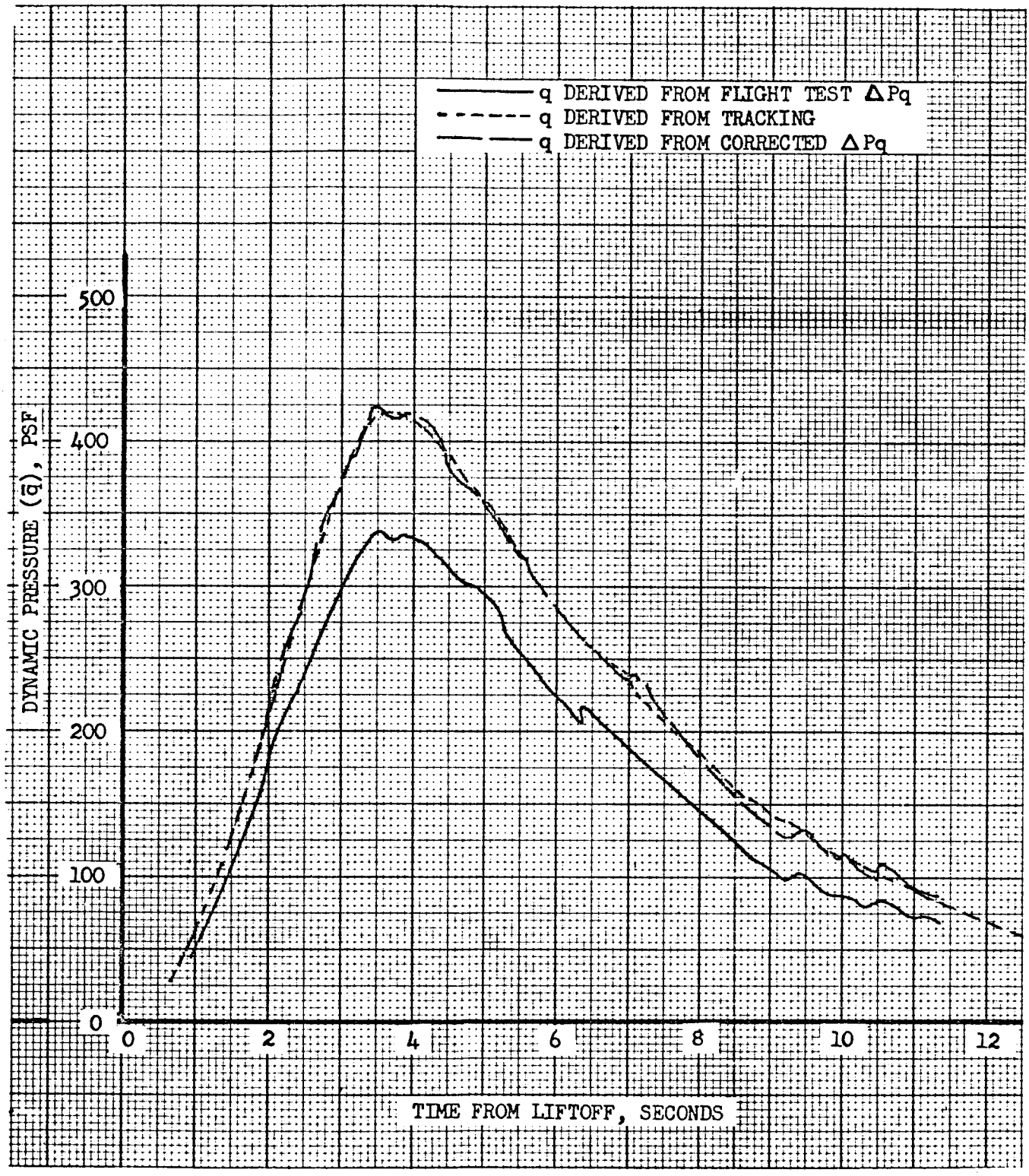

Figure 7.1-59 Comparison of Dynamic Pressure from Corrected and Uncorrected Q-Ball Data and Tracking Data

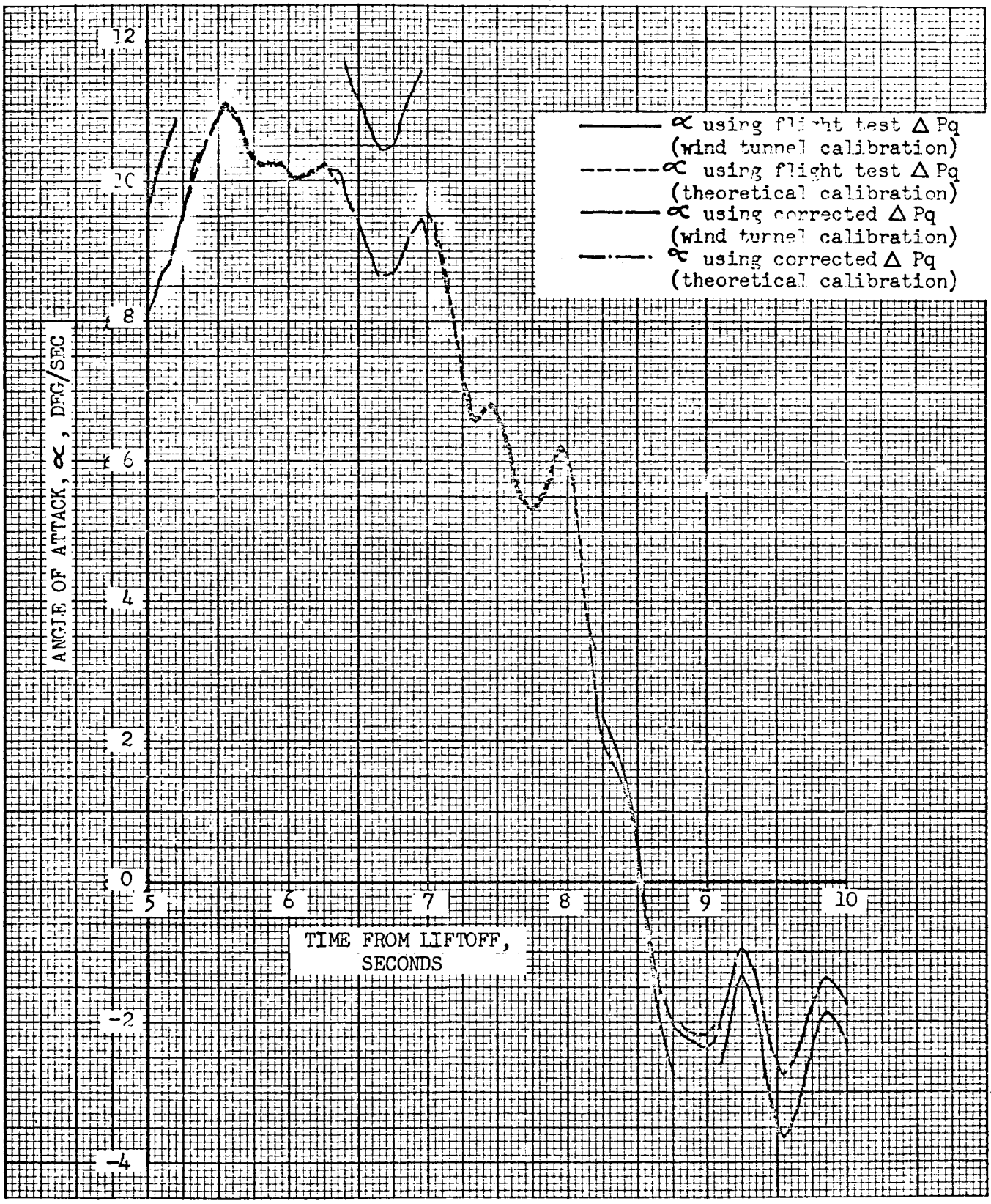

Figure 7.1-60 Effect of Q-Ball Bias on Q-Ball Derived Angles of Attack

[redacted]

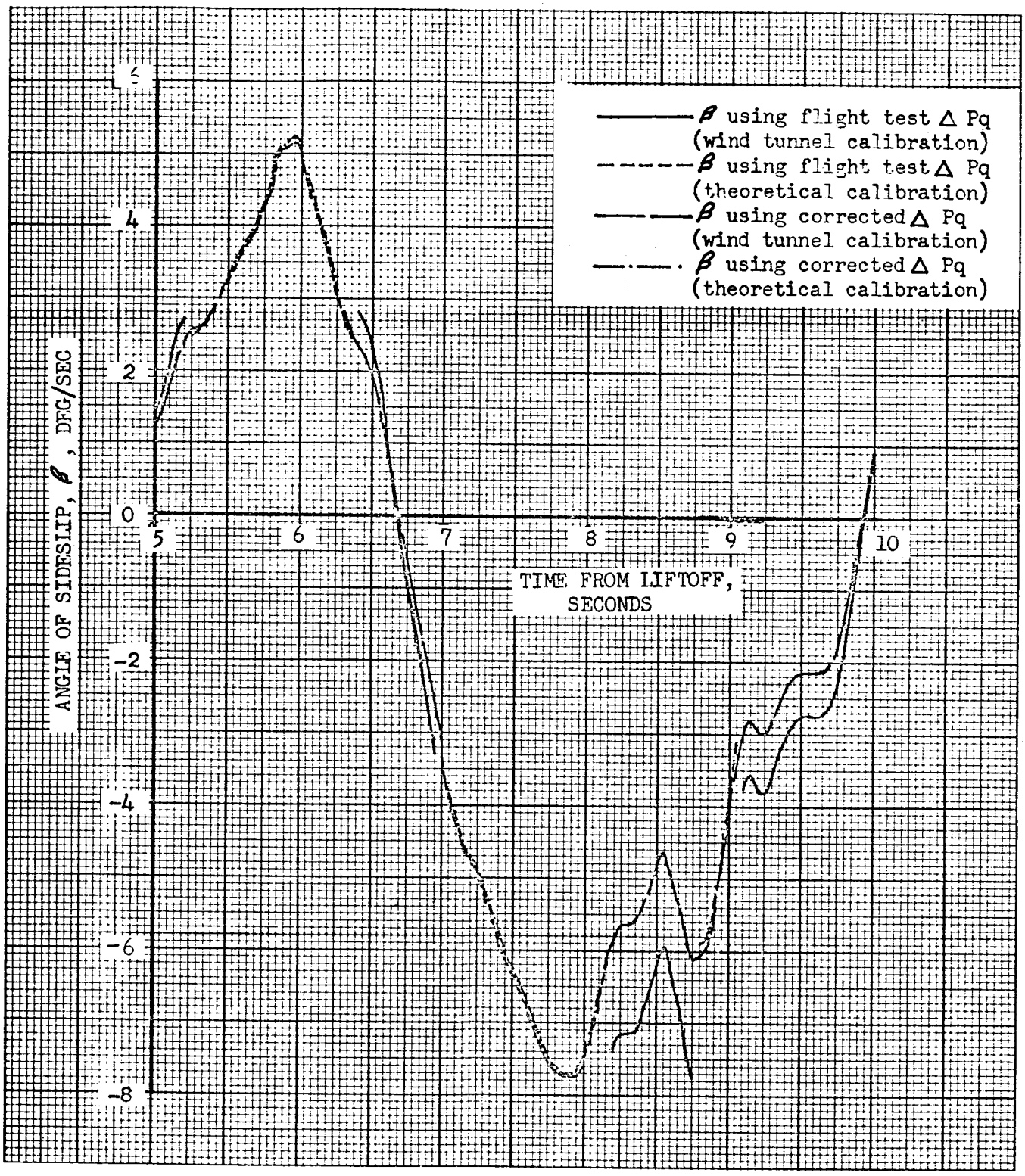

Figure 7.1-61 Effect of Q-Ball Bias on Q-Ball Derived Angles of Sideslip

[redacted]

[redacted]

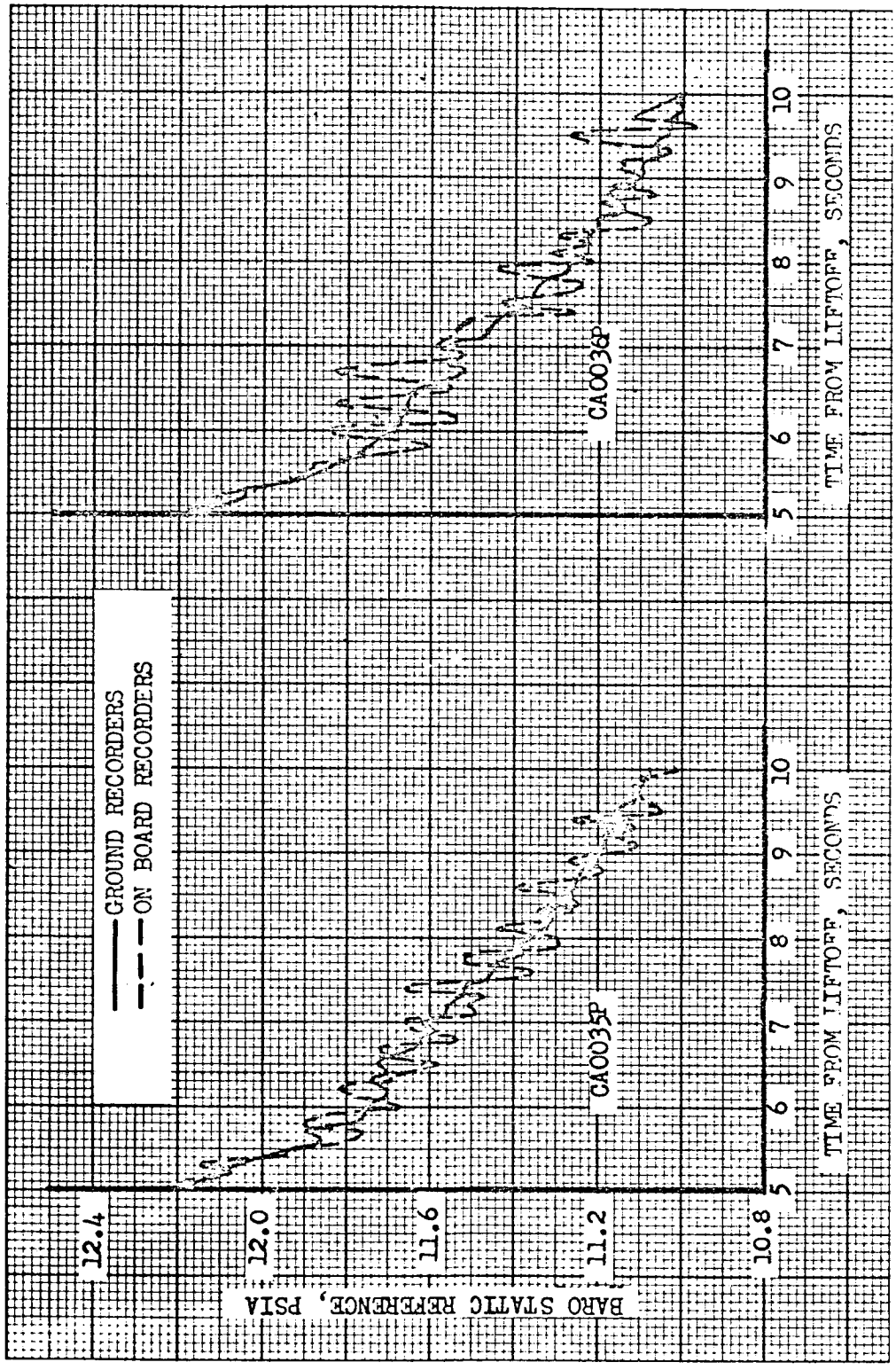

Figure 7.1-62 Comparison of Ground Recorded and Onboard Recorded Barostatic Pressures Data Sources

[redacted]

[redacted]

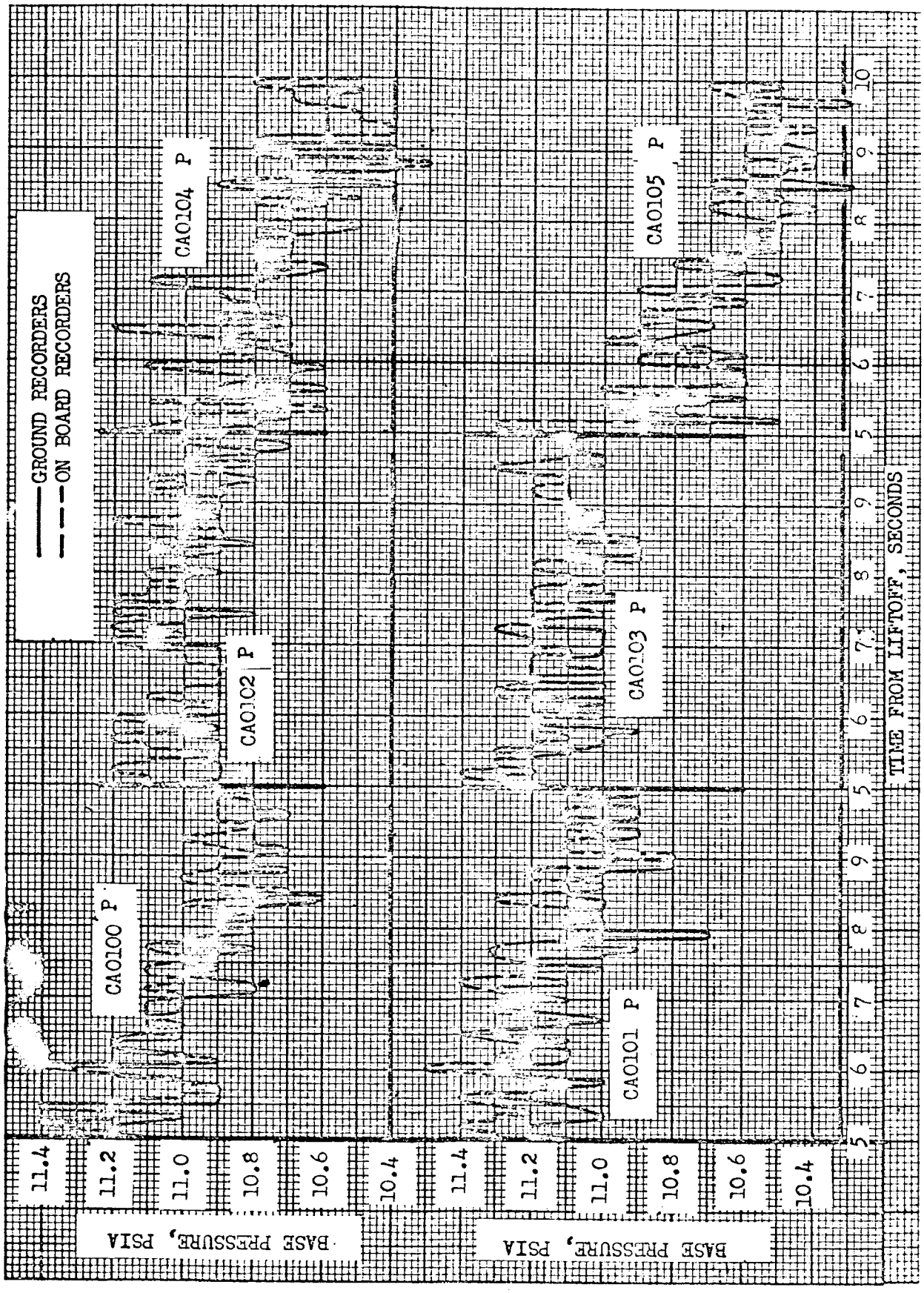

Figure 7.1-63 Comparison of Ground Recorded and Onboard Recorded Base Pressure Data Sources

[redacted]

[redacted]

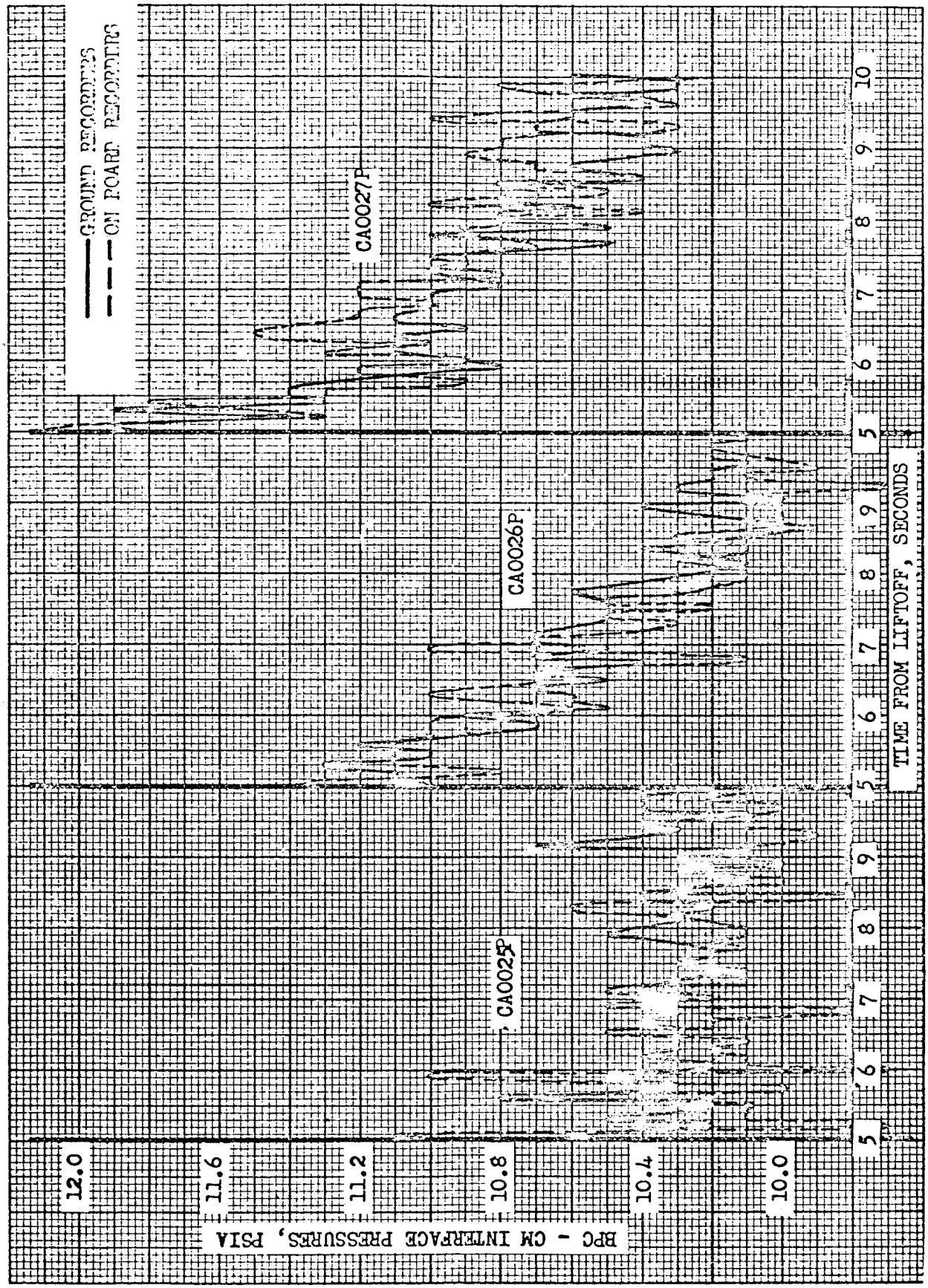

Figure 7.1-64 Comparison of Ground Recorded and Onboard Recorded Conical Surface Pressure Data Sources

[redacted]

[redacted]

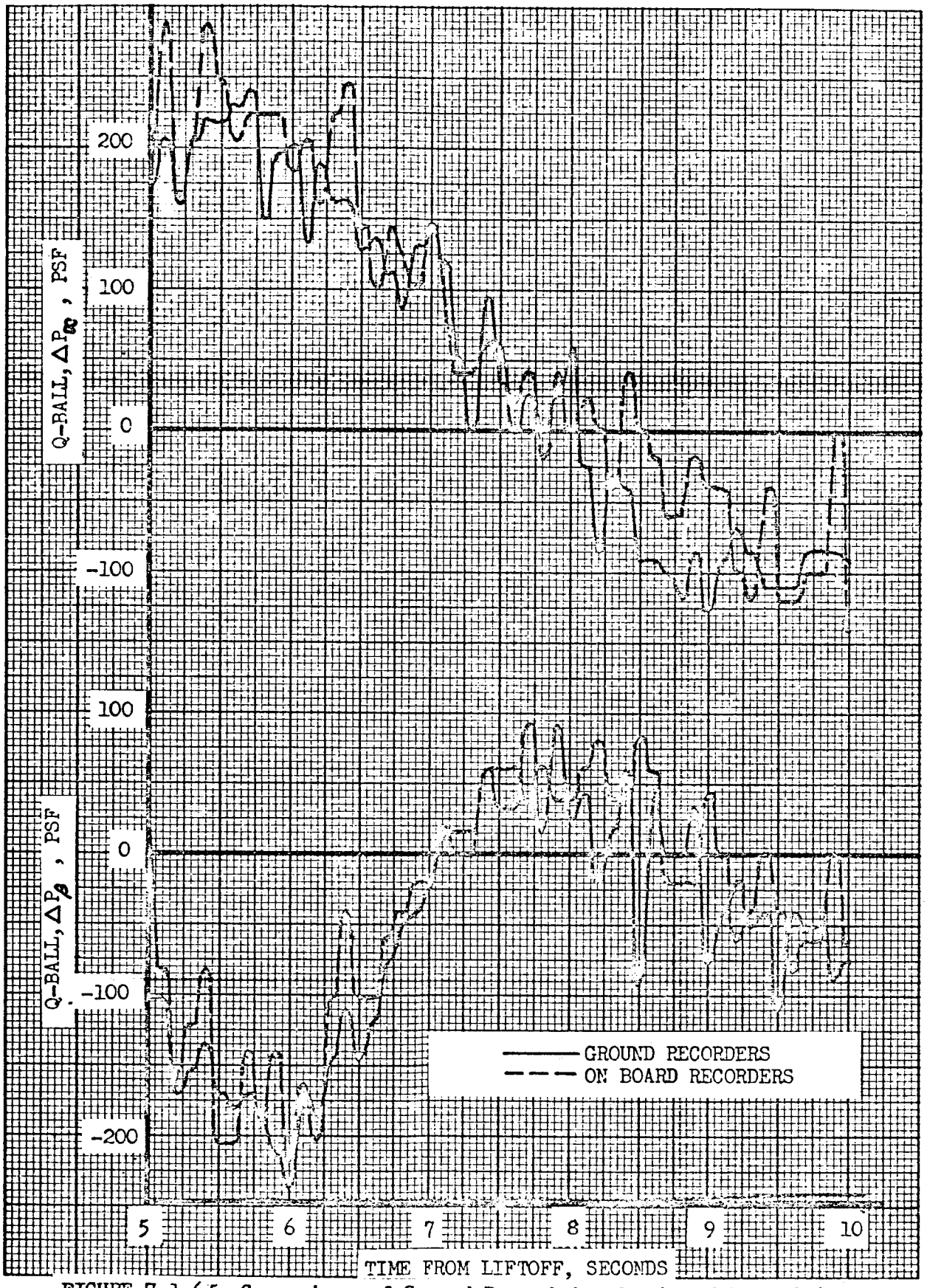

FIGURE 7.1-65 Comparison of Ground Recorded and Onboard Recorded Q-Ball Differential ΔP_β and ΔP_α Data Sources

[redacted]

[redacted]

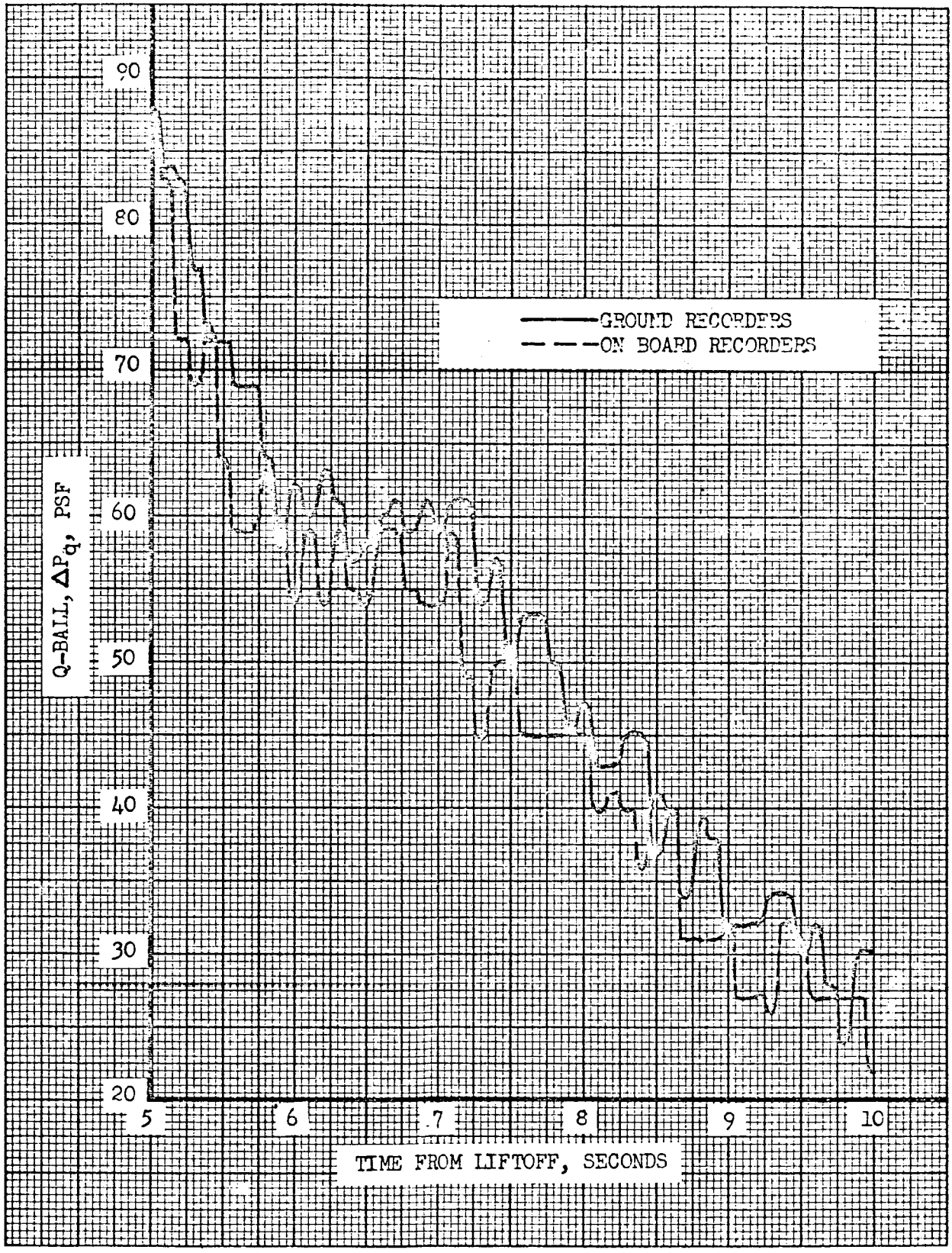

Figure 7.1-66 Comparison of Ground Recorded and Onboard Recorded Q-Ball Differential Δ Pq Data Sources

[redacted]

[redacted]

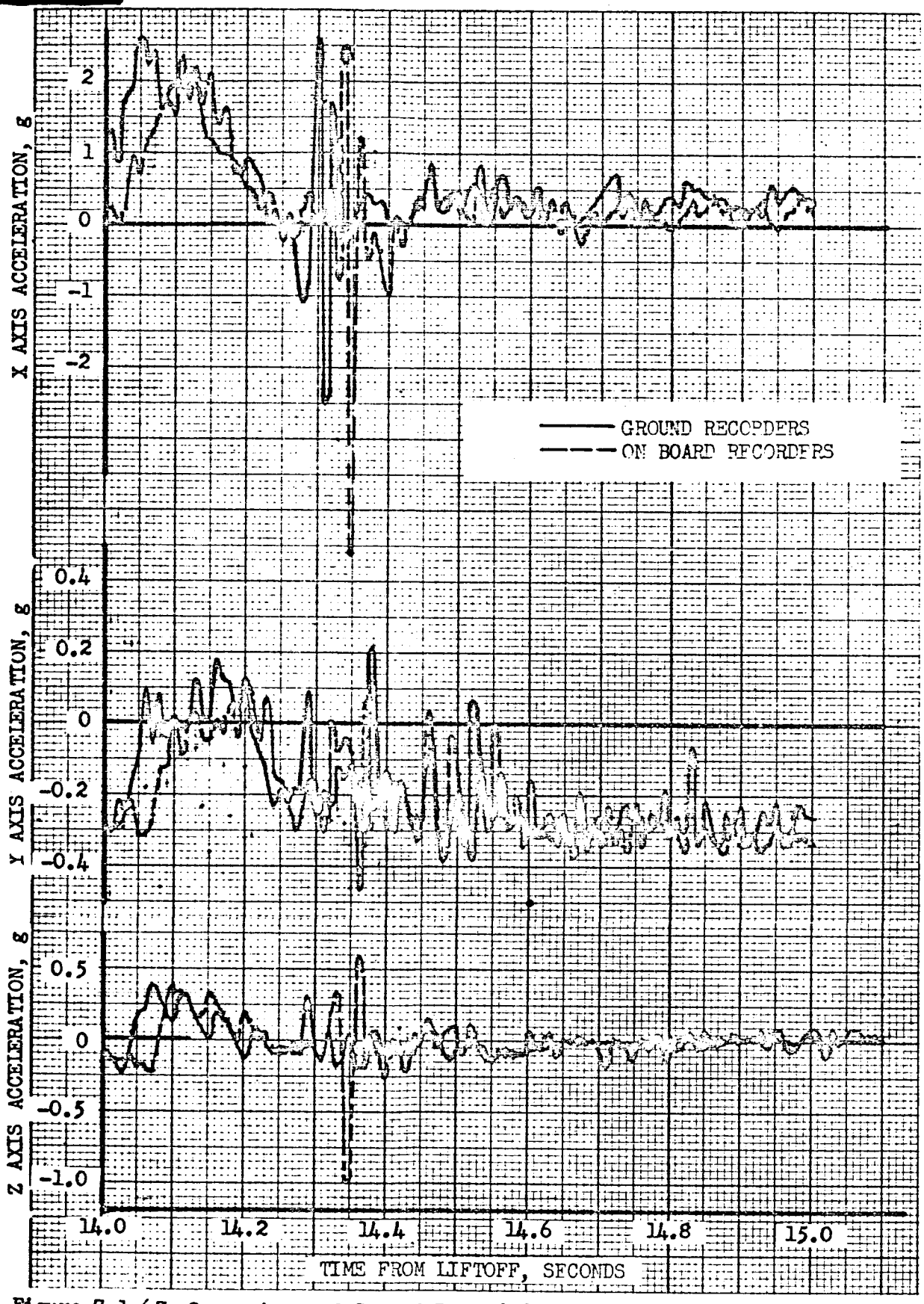

Figure 7.1-67 Comparison of Ground Recorded and Onboard X high, Y and Z Acceleration Data Sources

[redacted]

[redacted]

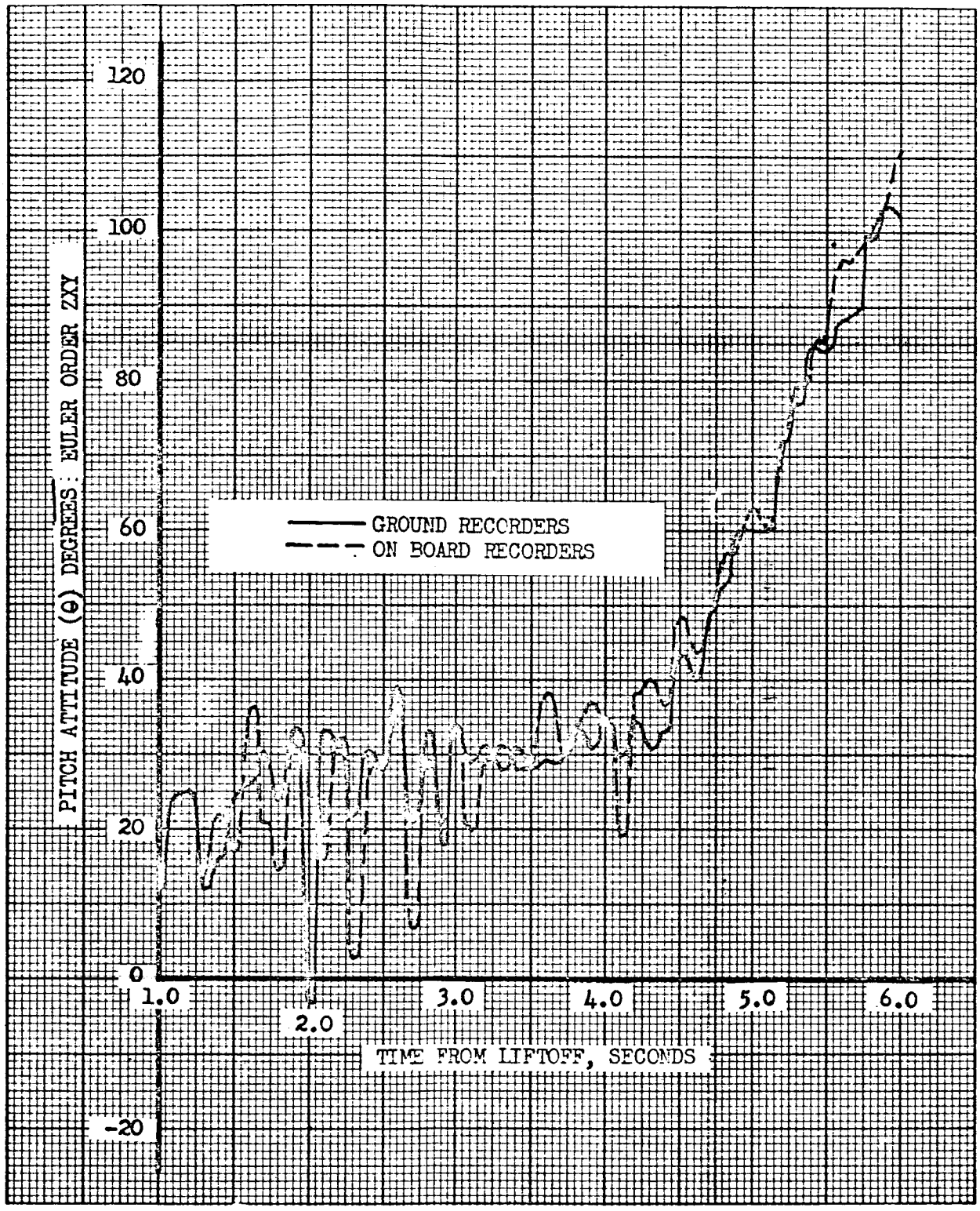

Figure 7.1-68 Comparison of Ground Recorded and Onboard Recorded Pitch Attitude Data Sources

[redacted]

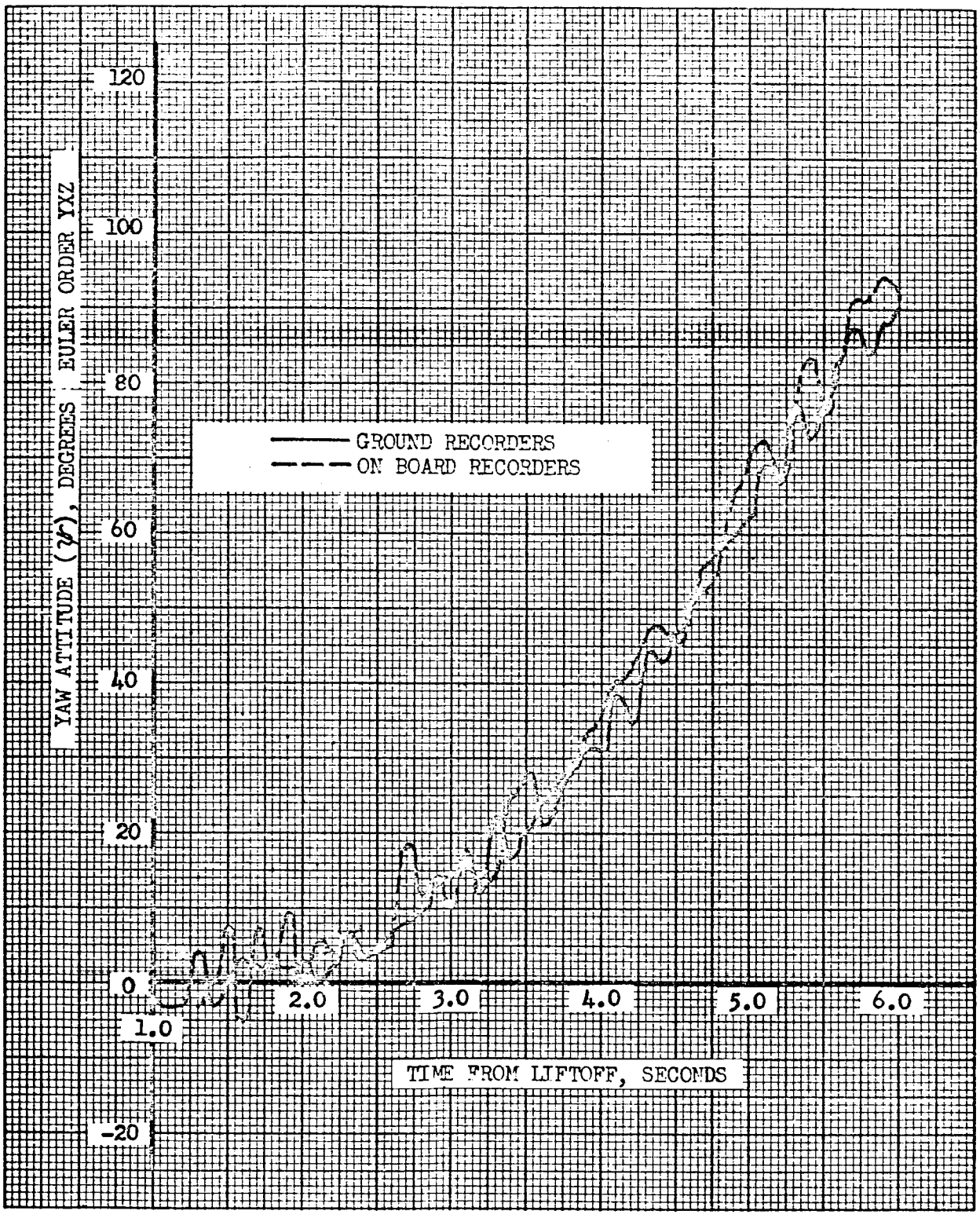

Figure 7.1-69 Comparison of Ground Recorded and Onboard Recorded Yaw Attitude Data Sources

[redacted]

[redacted]

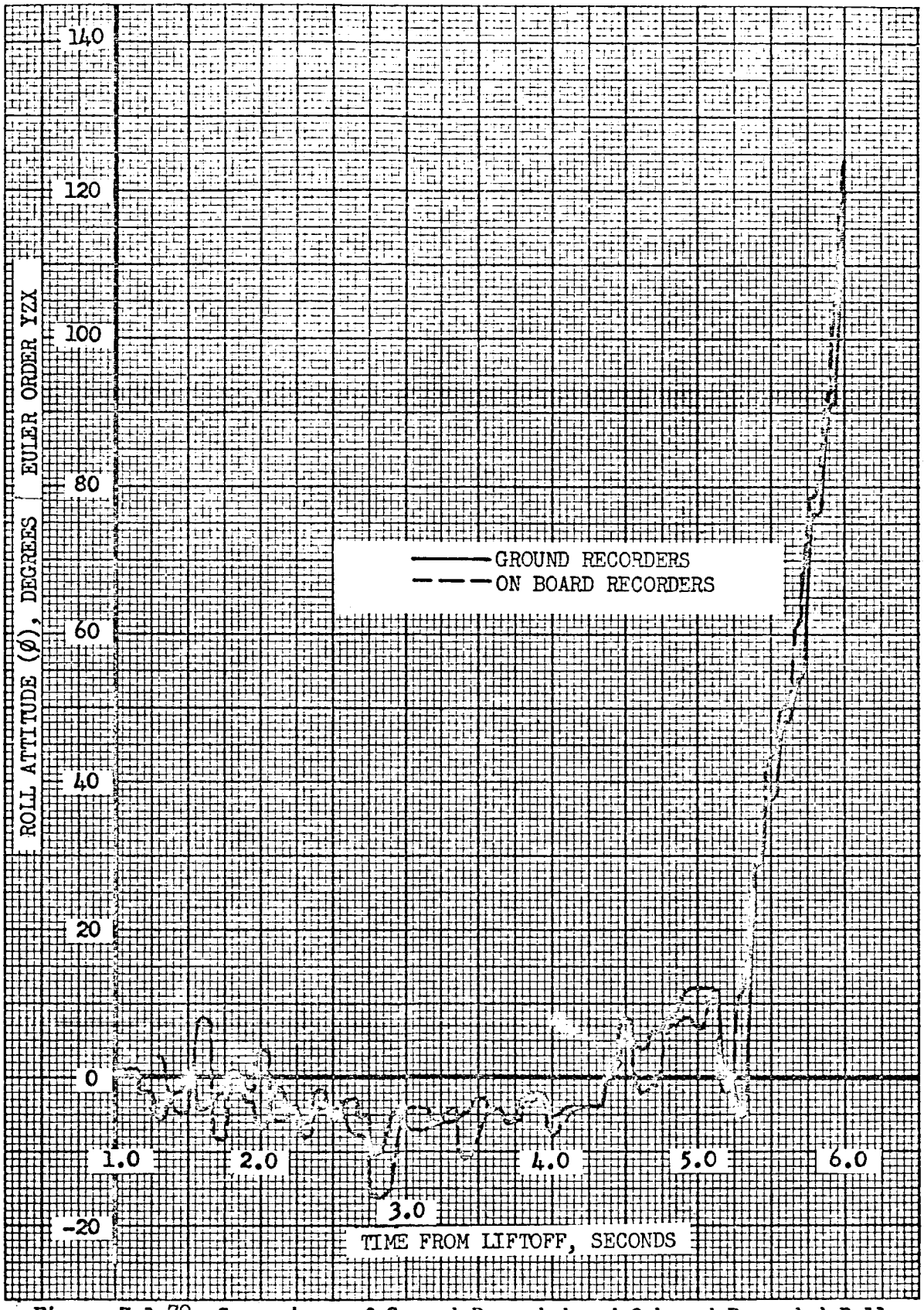

Figure 7.1-70 Comparison of Ground Recorded and Onboard Recorded Roll Attitude Data Sources

[redacted]

[redacted]

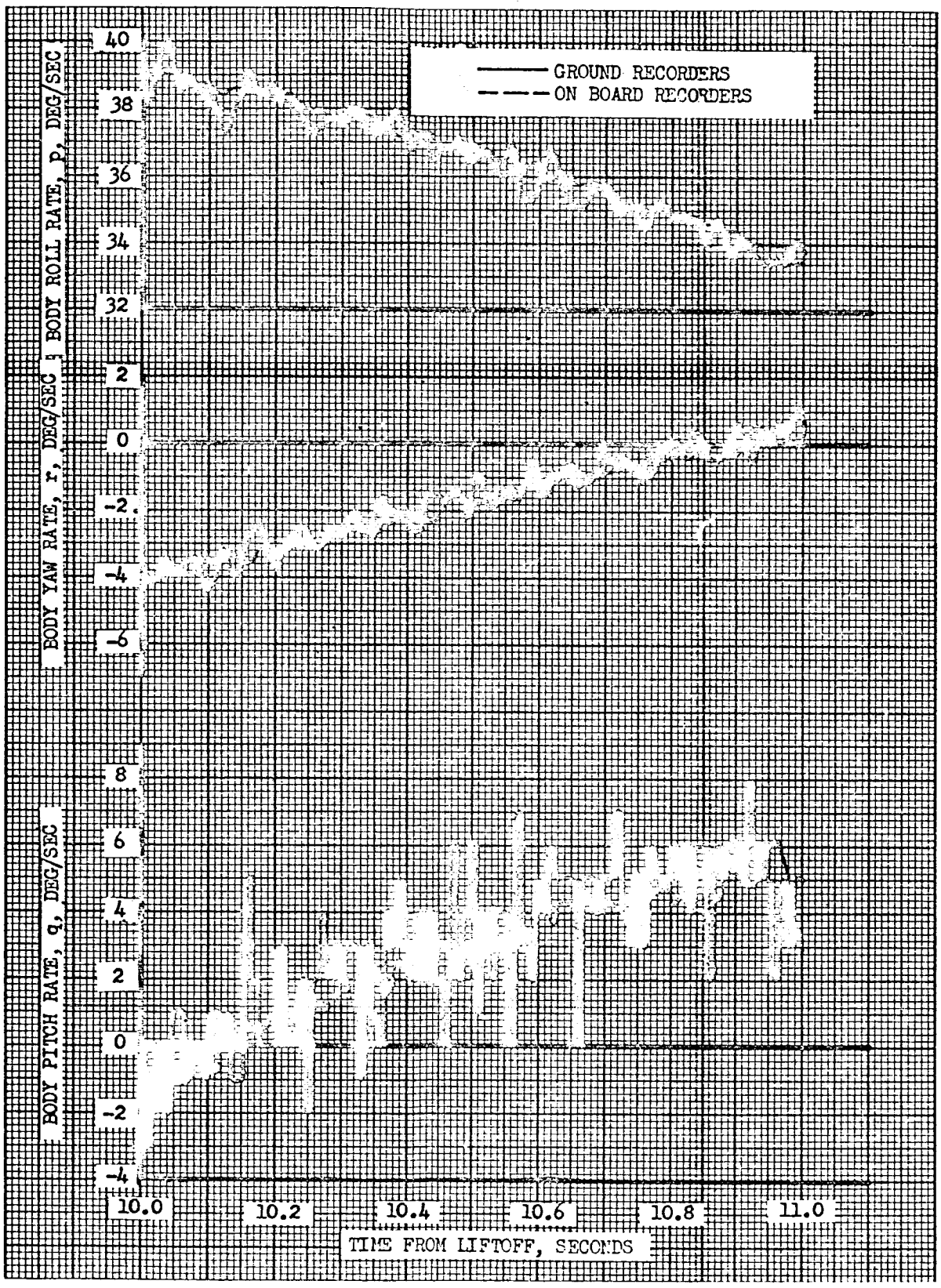

Figure 7.1-71 Comparison of Ground Recorded and Onboard Recorded Rate Gyro Data Sources

[redacted]

7.2 EARTH LANDING SUBSYSTEM

Summary

Utilizing the launch escape subsystem (LES), abort was initiated with the Boilerplate 23A test vehicle on the pad adapter. The ELS recovery sequence, starting at drogue deployment, occupied a period of approximately 97 seconds and culminated in a normal landing at an approximate elevation of 4,000 feet, msl.

All components of the earth landing subsystem functioned correctly, providing a normal descent and safe landing for the command module. Initial vehicle oscillations, including maximum rotation values, were sucessfully damped by both the drogue and the main parachutes.

Prior to the ELS sequence of events, the canard surfaces were deployed 10.9 seconds after abort initiation; then the tower was jettisoned 13.9 seconds after abort initiation, followed by the apex cover jettison 0.4 second later. Initiating the ELS sequence of events, the two drogue parachutes were deployed by mortar 2 seconds after tower jettison at an altitude of approximately 9,200 feet msl; then, at T + 28.6 seconds, the drogues were released at approximately 7,870 feet and the three pilot parachutes were deployed, extracting the three main parachutes from the parachute deck. In a normal manner the main parachutes opened to the reefed and disreefed conditions 8 seconds after line stretch. Figure 7.2-1 contains sequence photographs of significant events in the ELS recovery phase. Figure 7.2-2 shows the recovered command module and main parachutes after the safe landing.

Subsystem Description

The earth landing subsystem for Boilerplate 23A consisted of the ELS sequencer, two drogue parachutes, three pilot parachutes, three main parachutes, and associated hardware devices such as mortars, reefing-line cutters, and the drogue disconnect. The purpose of the earth landing subsystem was to orient the command module to the correct attitude for landing and to lower it safely to the ground. A configuration comparison with previous test vehicles and Block I spacecraft is given in section 5.0.

Earth Landing Subsystem Sequencer

The ELS sequencer for Boilerplate 23A consisted of an interim one-package configuration located on the inside wall of the egress tunnel, Figure 7.6-1. It contained baroswitches and time delay relays controlling

in sequence the functions of the parachute subsystem. It employed series/parallel redundant circuits to ensure reliability. The sequencer is illustrated in the block diagram of Figure 7.2-3. The integration with the other vehicle sequencers is illustrated in Figure 7.6-2.

In that the mission was a pad abort, the vehicle did not ascend to a sufficient altitude for either the high-altitude (33,100 feet) or the low-altitude (18,200 feet) baroswitch to open; therefore drogue deployment and subsequent drogue-release/pilot-parachute deployment were controlled by the time-delay relays of the LES and the ELS sequencers.

All functions of the ELS sequencers were performed satisfactorily.

Drogue Parachutes

The function of the drogue parachutes was to stabilize the command module in an aft-heat-shield-forward attitude and to decelerate the vehicle to a velocity low enough for safe deployment of the main parachutes.

The two drogue parachutes were 25-degree conical, FIST ribbon-type parachutes with a geometric porosity of 23 percent and a nominal diameter of 13.7 feet. The lower 180 inches of the drogue risers consisted of three strands of stainless-steel cable (9/32 inch diameter per strand). Each steel cable riser was dry-film lubricated and potted in dry foam for stowage in a mortar can. The dimensions of the drogue parachutes are given in Figure 7.2-4. The dual drogues were the Block I type flown with BP-22.

When deployed, the parachutes were reefed to 39 percent of the nominal diameter by two active reefing lines which each included two redundant reefing-line cutters. Following drogue deployment, the pryotechnic reefing-line cutters severed the active reefing lines 8 seconds after line stretch and enabled the drogue parachutes to inflate to 62 percent of their nominal diameter, where they were restricted from further inflation by a permanent reefing line.

The drogue parachutes were deployed by two separate mortars with firing current controlled by the 2-second timer in the ELS sequencer. The drogue parachutes were released from the command module by a pyrotechnic disconnect device activated by closing of the 14-second timer relay in the ELS sequencer and designed to cut through the single-point attach fitting. The drogue disconnect and the pilot parachute mortars were fired simultaneously.

[redacted]

Pilot Parachutes

The function of the three pilot parachutes was to deploy the main parachutes and facilitate the inflation of the main parachutes to the reefed diameter.

The pilot parachutes were of the ringslot type with a nominal diameter (D_o) of 7.2 feet; they were the Block I type flown with BP-22. Detached dimensions of the pilot parachutes are presented in Figure 7.2-4. The lower 108 inches of the pilot parachute risers consisted of one strand of stainless-steel cable 7/32 inch in diameter. The cable was dry-film lubricated and potted in foam for stowage in the mortar.

The pilot parachutes were deployed by three separate mortars with firing current controlled by a 14-second timer in the ELS sequencer.

Main Parachutes

The function of the three main parachutes was to decelerate the vehicle to a final descent velocity safe for landing.

The main parachutes were of the ringsail type with 75 percent of the fifth ring removed, and with a nominal diameter (D_o) of 83.5 feet; they were the Block I type flown with BP-22. Additional dimensions are given in Figure 7.2-4. The main parachutes were actively reefed to 9.5 percent of the nominal diameter for a designed time period of 8 seconds by two reefing lines with three reefing-line cutters per line. The reefing-line cutters were of interim design as flown with BP-22. Their failure in the BP-22 flight is discussed in section 7.7. A four-legged harness assembly attached the parachutes to the command module and suspended it at a hang angle of approximately 5 degrees from the vertical. The Block I type harness is two-legged and the suspension angle is 30 degrees. Another difference between these and the Block I parachutes was the use of a loose pack rather than a high-density bag pack.

Parachute Deck Assemblies

The parachute deck assemblies differed from the Block I spacecraft type in that the drogue mortar support ring and the pilot mortar support fitting were boilerplate hardware. This vehicle was rigged for the interim four-legged harness; hence Block I deck fittings were not used. There were also no recovery or location aids on the deck.

[redacted]

[redacted]

Sequence of Events

The recovery sequence proceeded as summarized below:

Event		Time Elapsed from Liftoff (Seconds) Actual	Predicted
LES sequence start		-0.2	-0.2
Liftoff		0.0	0.0
Canard deployment		10.9	11.0
Input from LES sequencer		13.7	14.0
Tower jettison		13.9	14.1
Apex cover jettison		14.3	14.4
Drogue parachutes deployment			
No. 1 and 2		15.8	16.0
Drogue parachutes disreef			
No. 1		23.9	24.0
No. 2		24.0	
Drogue parachutes release and pilot mortar fire		28.6	28.0
Pilot parachute inflation			
No. 1		29.5	
No. 2		29.5	
No. 3		29.6	
Main parachutes line stretch			
Actual times were computed from	No. 1	30.6	30.0
known increments and pilot para-	No. 2	30.6	
chute inflation times	No. 3	30.7	
Main parachutes disreef			
Actual times were computed from	No. 1	38.6	38.0
known 8 sec. time delay and line	No. 2	38.6	
stretch time	No. 3	38.7	
Main parachute full inflation			
No. 1		46.7	39.5
No. 2		46.7	
No. 3		48.2	
Landing		112.8	89.7

Flight Analysis

The earth landing subsystem functioned satisfactorily as determined by the correct sequence of events, altitude, dynamic pressures, descent velocities, parachute loads, vehicle oscillation damping, and the stabilized vehicle attitude.

[redacted]

[redacted]

The altitude, dynamic pressure, and flight path angle time histories for the ELS recovery sequence are presented in Figures 7.2-5, 7.2-6, and 7.2-7. These figures show satisfactory correlation between post-test analysis and actual flight data.

Tower jettison occurred at T + 13.9 seconds at an altitude of 9,000 feet; and the apex cover was jettisoned 0.4 second later. In sequence 1.9 seconds after tower jettison and at an altitude of 9,200 feet, the drogue parachutes were deployed. Command module angle of attack and dynamic pressure at drogue deployment were approximately 200 degrees and 34.0 psf. Deployment of the reefed drogue parachutes was normal and synchronous. The drogue parachutes disreefed at T + 23.9 and T + 24.0 seconds, respectively, and followed with a full normal inflation.

Command module oscillations throughout the drogue interval were primarily in the yaw plane, shifting to the pitch plane during the latter portion of the interval. The yaw motion resulted from the initial vehicle attitude (90 degrees yaw) and yaw rate (-20 degrees per second) at tower jettison.

The drogue loads were estimated from known dynamic pressure history and from empirically calculated drag area characteristics. Estimated total drogue loads were 3,470 pounds and 6,320 pounds, respectively, for reefed and disreefed conditions. These load estimates are consistent with telemetry acceleration data.

At T + 28.6 seconds, the drogue parachutes were released and the pilot parachute mortars were fired; altitude and dynamic pressure at this time were 7,870 feet and 39.5 psf. The pilot parachutes deployment and also their inflation was essentially synchronous.

The main parachutes, after extraction by the pilot parachutes, reached reefed inflation at essentially the same time. At approximately T + 38.5 seconds, 8 seconds after line stretch, the main parachutes disreefed and then fully inflated normally. A canopy skirt on the down-range side of one parachute delayed in coming out and resulted in an apparent but not significant real lag in the full inflation of the parachute.

The vehicle oscillations were essentially completely damped within 15 seconds after main parachute deployment. The command module stabilized as designed at an angle of approximately 5 degrees off the vertical.

Main-parachute loads were estimated from telemetry acceleration data. The estimated total main-parachute loads were approximately 30,000 pounds and 20,028 pounds, respectively, for reefed and disreefed conditions.

 [redacted]

Steady-state descent began at T + 44.0 seconds and approximately 5,940 feet. The terminal vertical velocity is shown in Figure 7.2-8.

Pendular oscillations of the test vehicle were negligible at landing. The vehicle landed at T + 112.8 seconds on a ground elevation of approximately 4,000 feet. Vertical and horizontal velocities at landing were approximately 28 feet per second and 14 feet per second, respectively. Surface winds were approximately 5 feet per second. The horizontal-velocity component in excess of the wind velocity is attributed to drift and glide of the parachutes.

Equipment Analysis

Earth Landing Subsystem Sequencer

The ELS sequencer functioned normally throughout the entire period of flight. Post-flight checkout of the sequencer verified that no malfunctions had occurred and that all time-delay circuits had operated within tolerances.

Drogue Parachutes

The drogue parachutes functioned normally. There was no apparent damage to the canopies, the suspension lines, or the risers. The drogues were satisfactorily disreefed by the reefing-line cutters. Two reefing-line rings, panels 9 and 13, were damaged during packing, but the deformation was not considered to have had any effect in this flight. The drogue parachutes were disconnected without difficulty by the pyrotechnic disconnect mechanism. The associated ordnance is discussed in detail in section 7.7. A post-flight photograph of the shear plate is given in Figure 7.2-9.

Pilot Parachutes

The pilot parachutes and their associated hardware functioned normally without failure or damage. There was however a kink, which resulted in flattening and a few wire separations, in one multistrand stainless-steel pilot-parachute riser; a post-flight photograph is given in Figure 7.2-10. There was similar kinking, with no wire separation, of a pilot-parachute riser in the Boilerplate 22 flight test; however, pull tests conducted on the riser at Northrop-Ventura indicated that no strength degradation resulted from the kink.

Main Parachutes

The main parachutes and their associated hardware functioned normally without failure or significant damage; they were disreefed satisfactorily by the type of reefing-line cutter used with the drogue parachutes, discussed above.

The main-parachute damage was as follows:

Parachute Number 1 (Serial Number 24)

Gore 68: One 2-inch tear (ground damage).
Minor ground damage to sails 1 through 12.
Both major and minor ground damage to the suspension lines.
Damage to top panel of the deployment bag.

Parachute Number 2 (Serial Number 25)

Gore 1: One 1/2-inch tear near cutter.
Minor ground damage to sails 1 through 12.
Both major and minor ground damage to the suspension lines.
Damage to top panel of deployment bag.

Parachute Number 3 (Serial Number 22)

Minor ground damage to sails 1 through 12.
Major and minor ground damage to the suspension lines.
Damage to top panel of deployment bag.

The parachute retention assembly released completely without difficulty and showed no evidence of damage. Figures 7.2-11 and 7.2-12 show the condition of the parachute deck after landing.

Conclusions

It is concluded that satisfactory performance of the earth landing subsystem, including the ELS sequencer, was demonstrated in this mission with the Boilerplate 23A test vehicle.

[redacted]

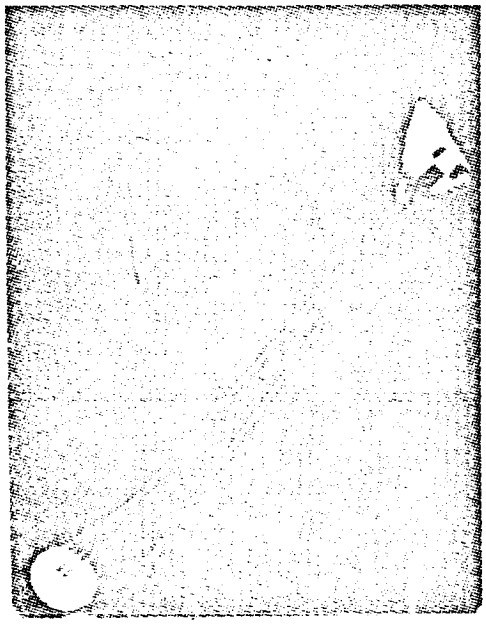

A. Drogue Parachute Lines Out; Clear Miss of Jettisoned Apex Coverand LES Tower

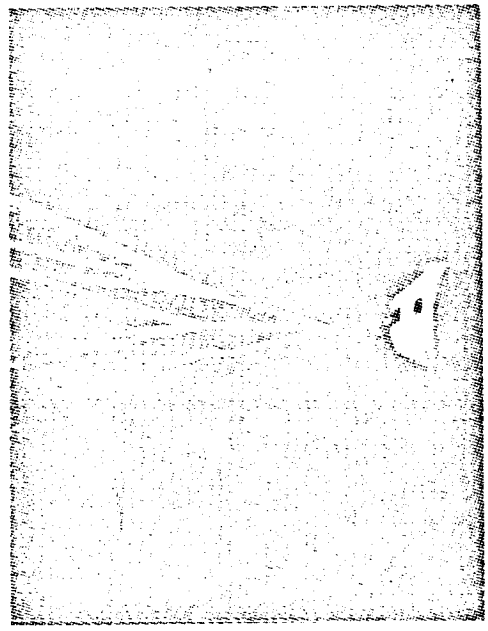

B. Drogue Parachutes in Reefed Condition

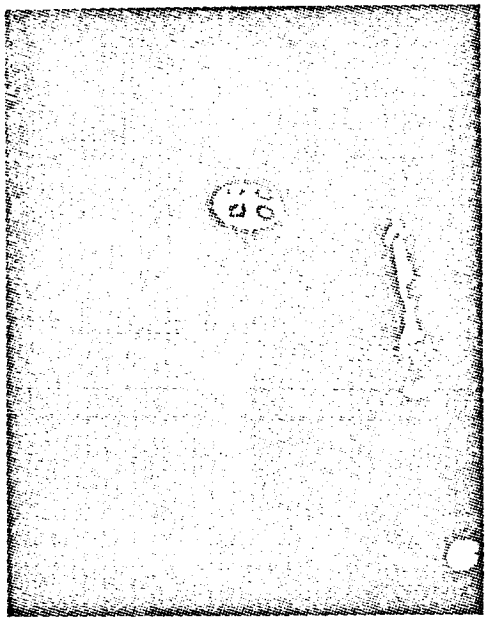

C. Drogue Parachutes in Disreefed Condition

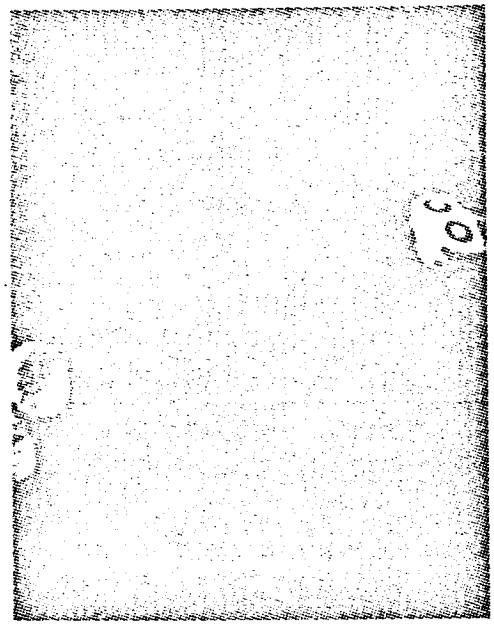

D. Command Module Safe on Main Parachutes Following Completion of Parachute Sequence

Figure 7.2-1. ELS Command Module Recovery

[redacted]

[redacted]

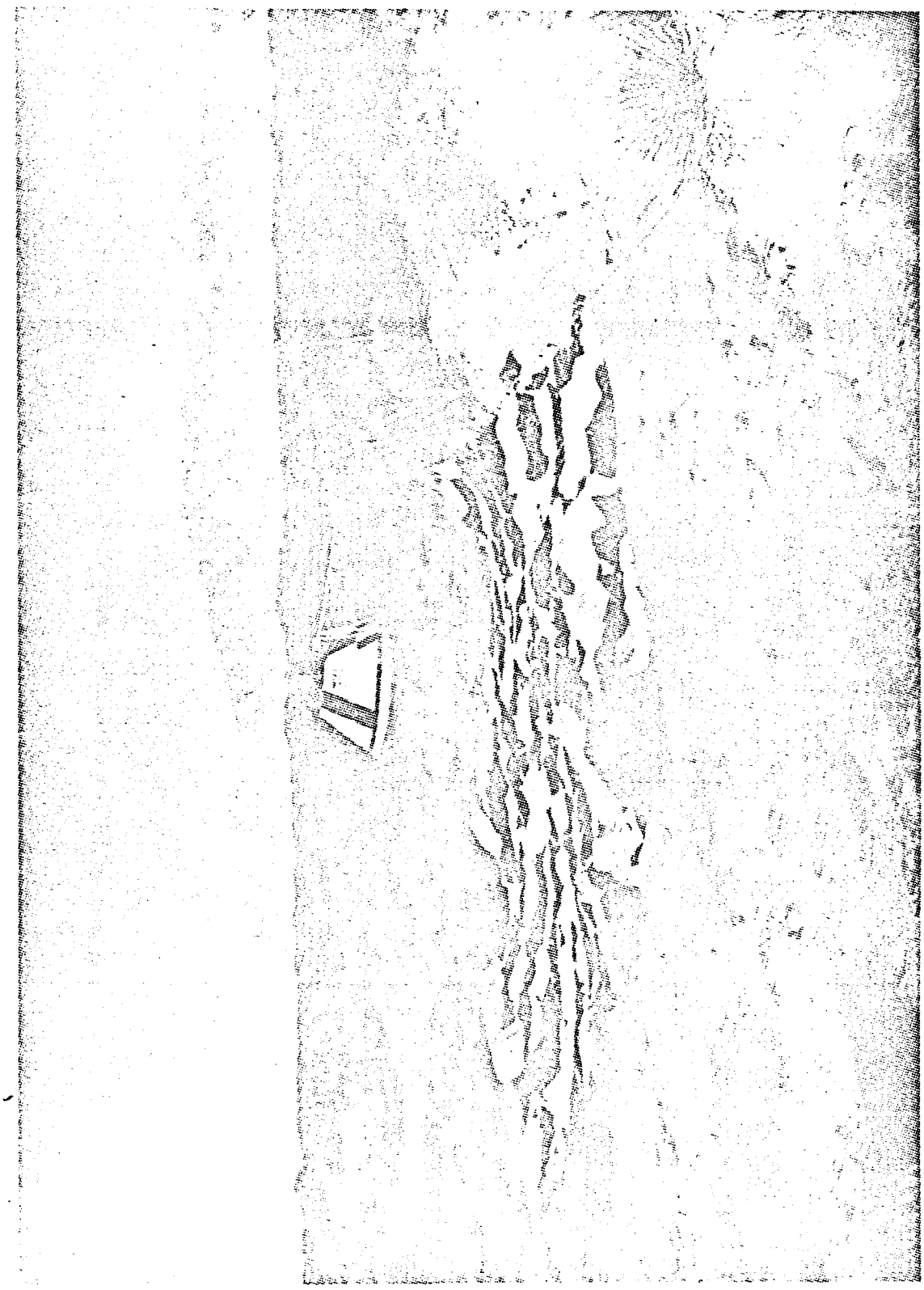

Figure 7.2-2. Recovered Command Module and Main Parachute on Ground

[redacted]

[redacted]

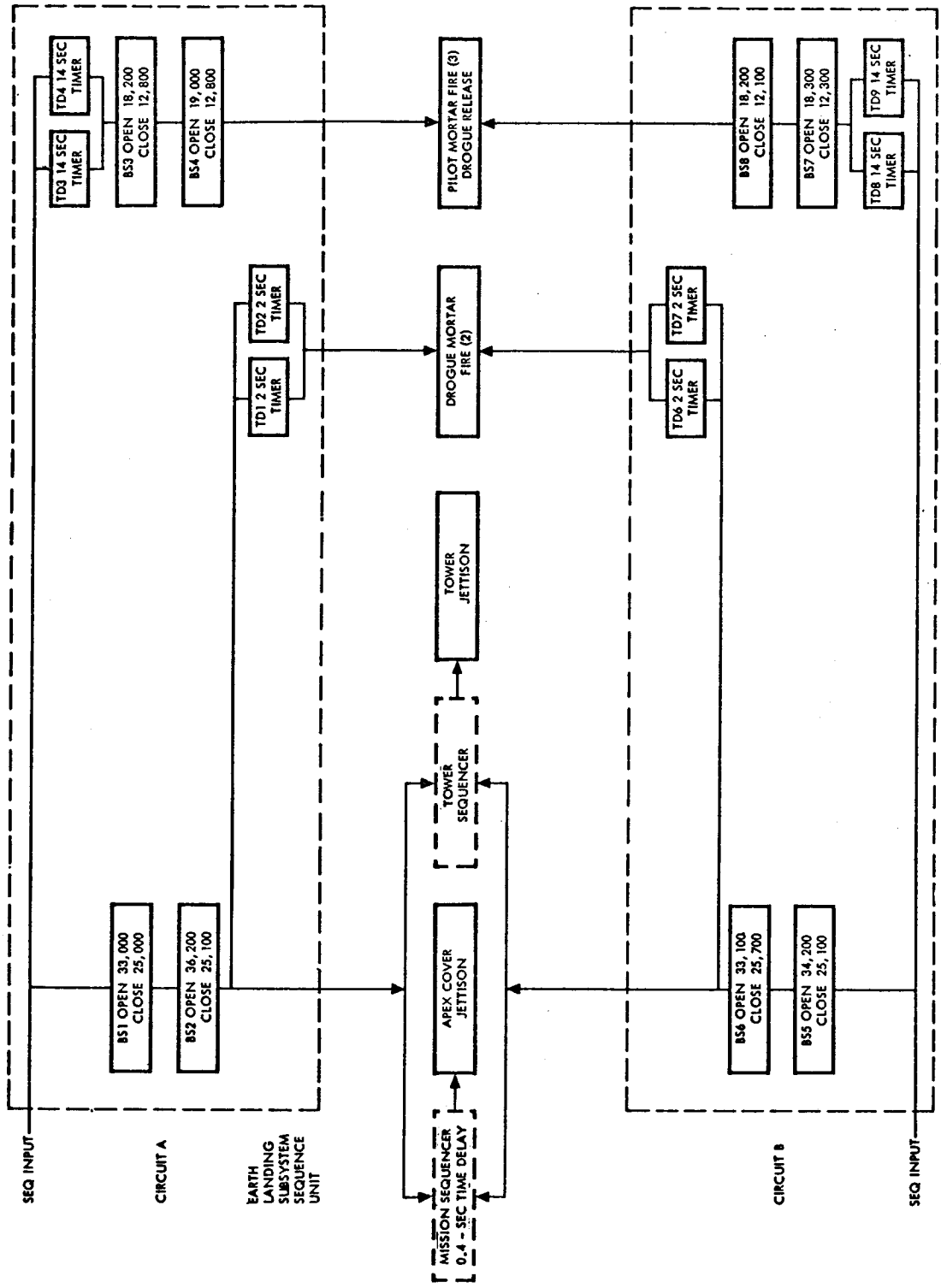

Figure 7.2-3. ELS Sequencer Block Diagram

[redacted]

[redacted]

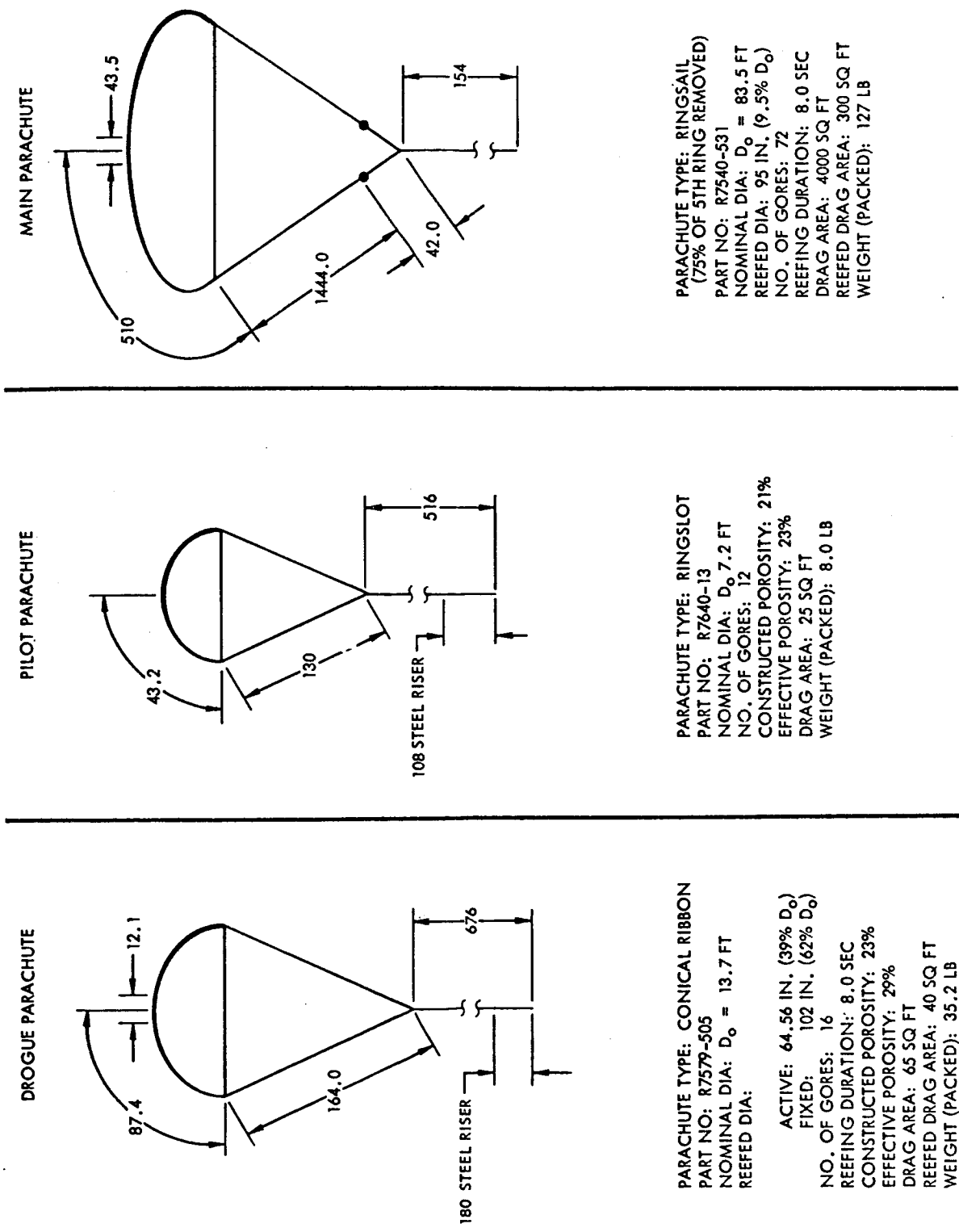

Figure 7.2-4. Boilerplate 23A Parachute Configuration

[redacted]

[redacted]

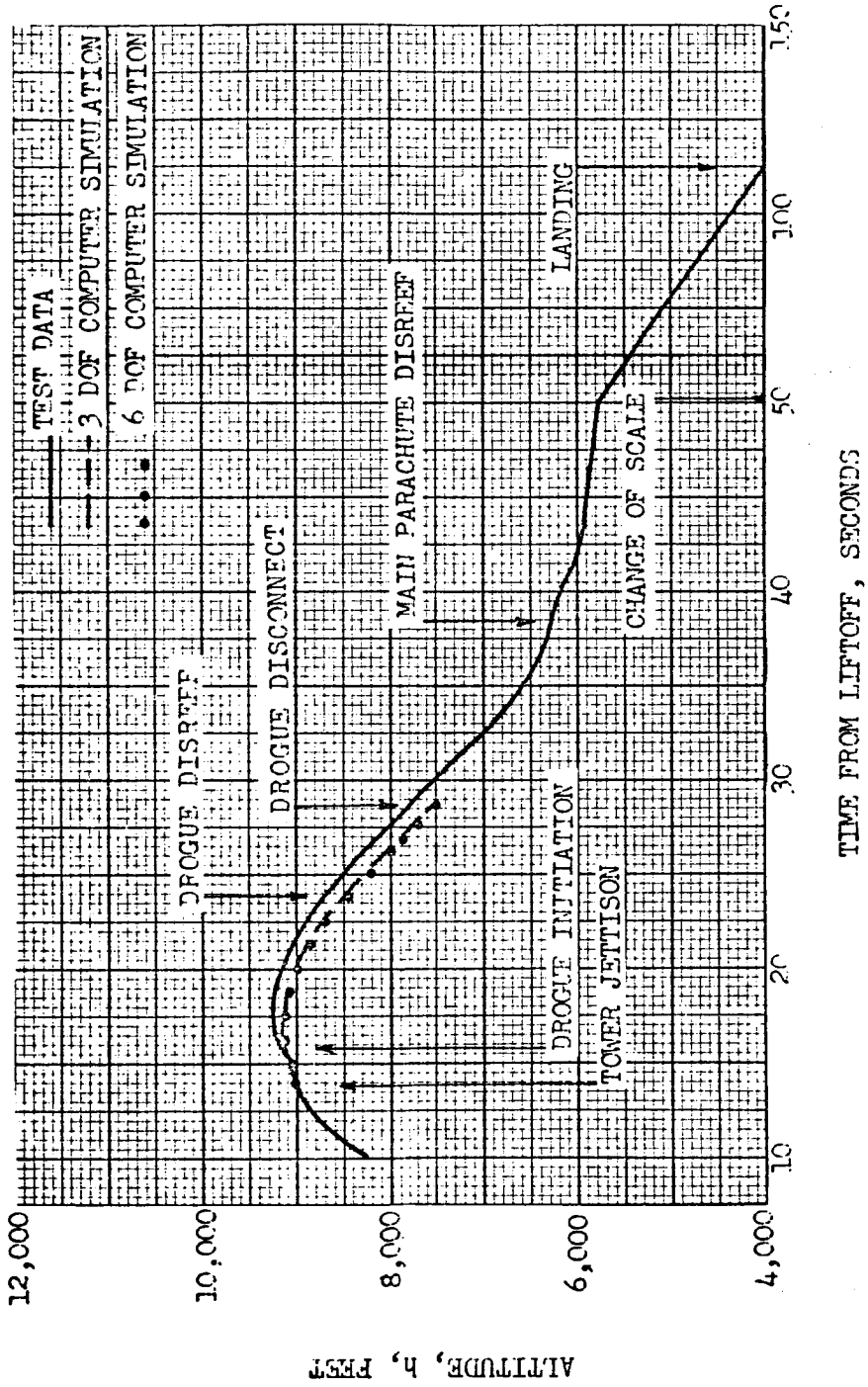

Figure 7.2-5. Command Module Altitude Time History

[redacted]

[redacted]

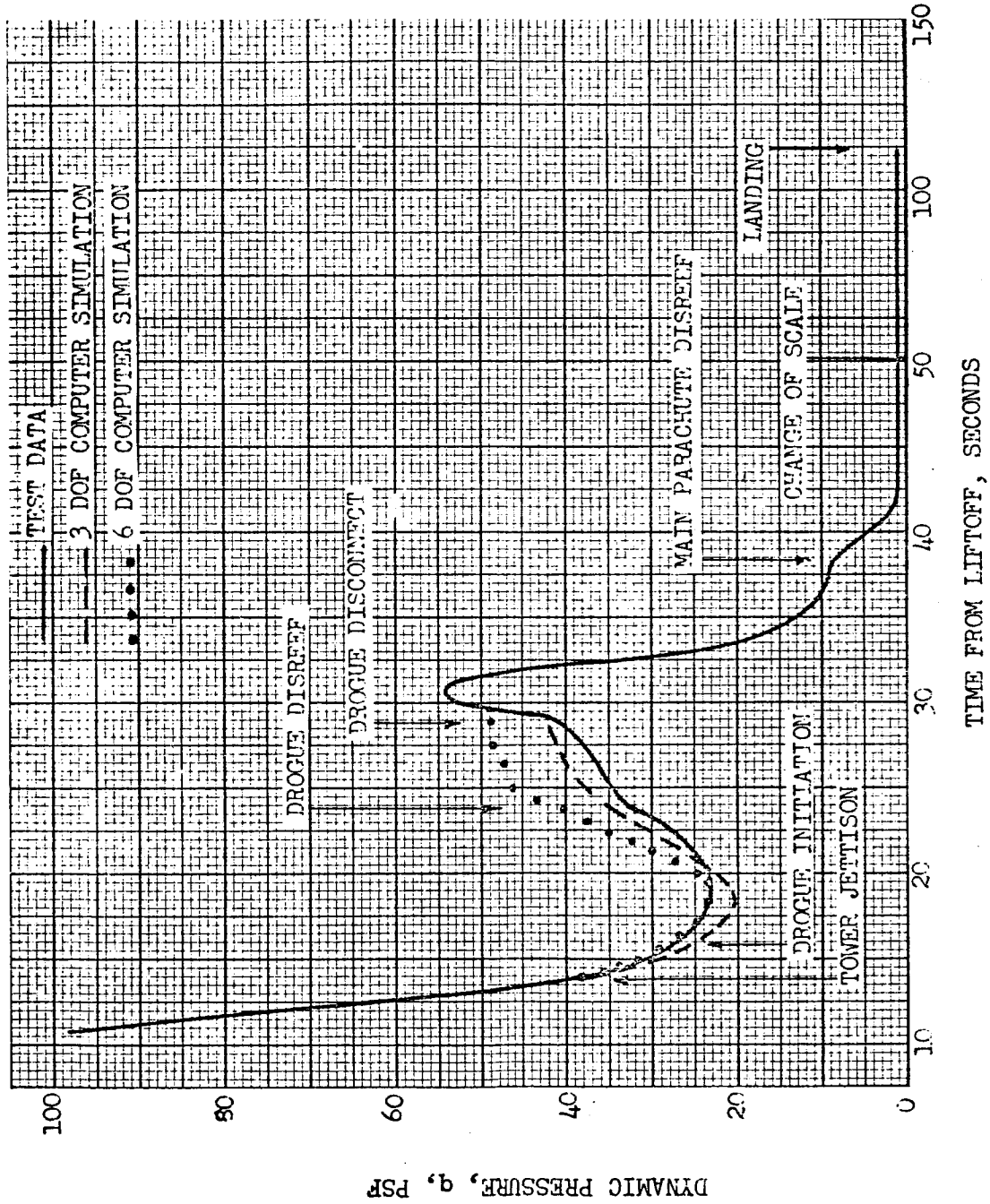

Figure 7.2-6. Command Module Dynamic Pressure Time History

[redacted]

[redacted]

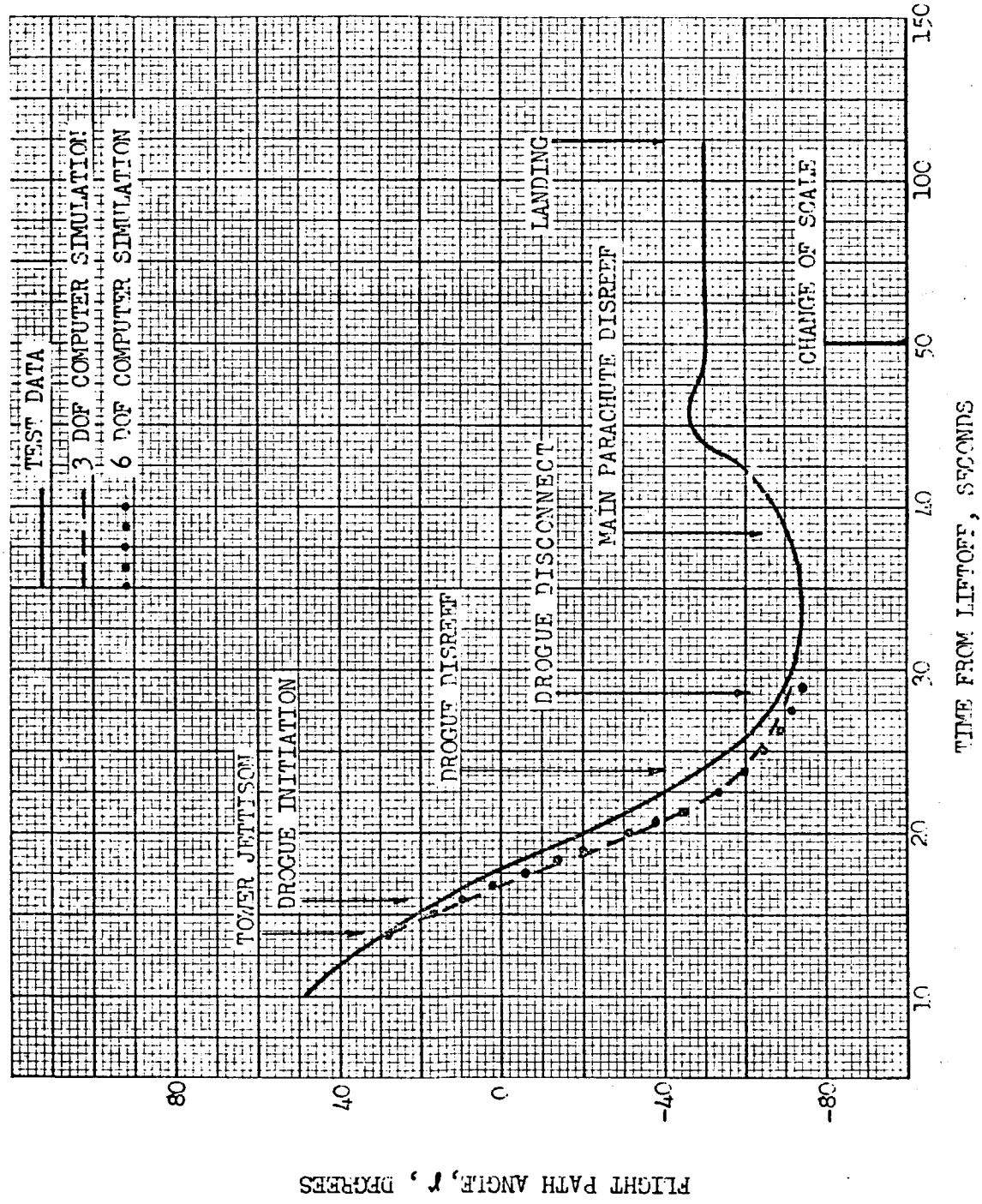

Figure 7.2-7. Command Module Flight Path Angle Time History

[redacted]

[redacted]

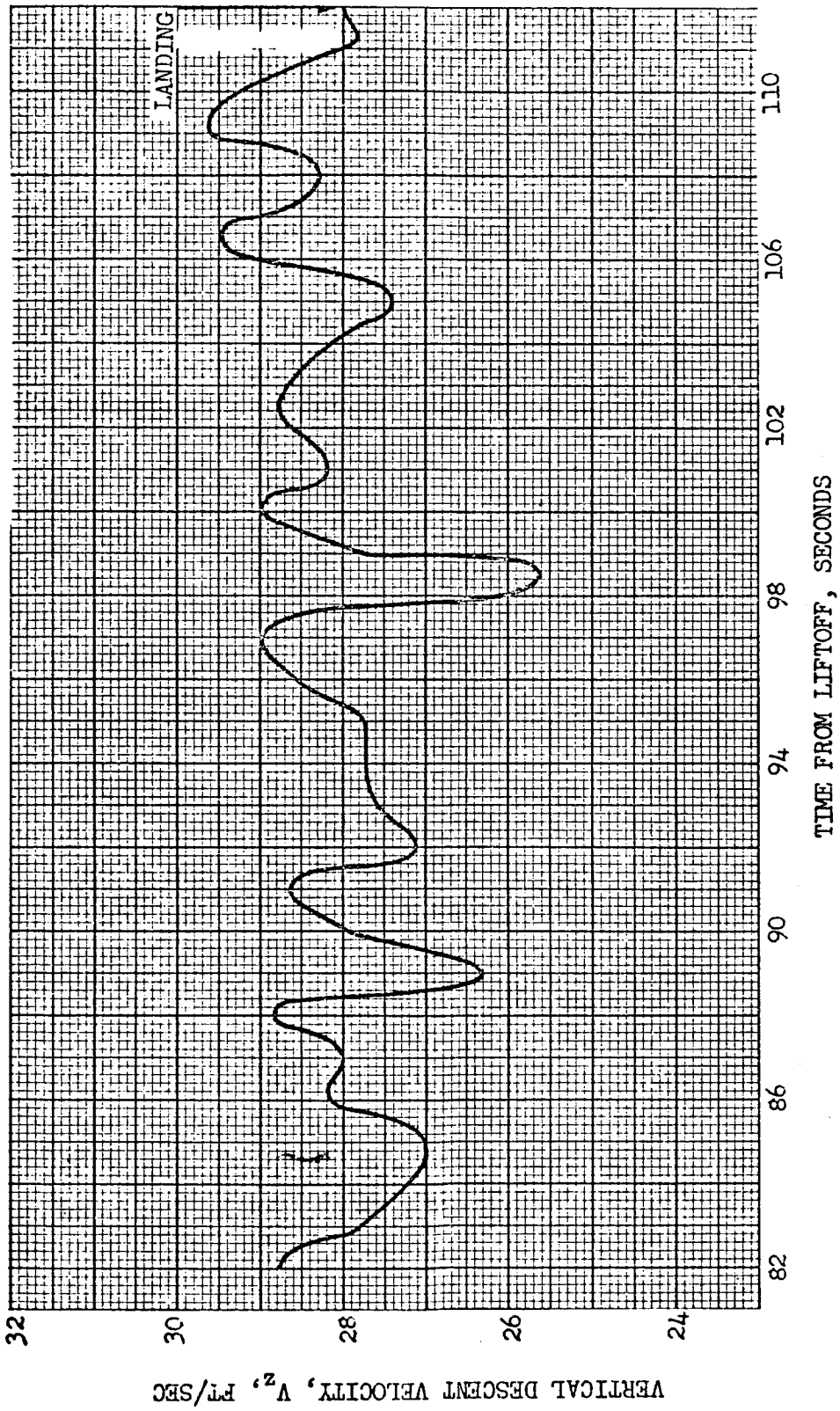

Figure 7.2-8. Command Module Final Descent Velocity Time History

[redacted]

[redacted]

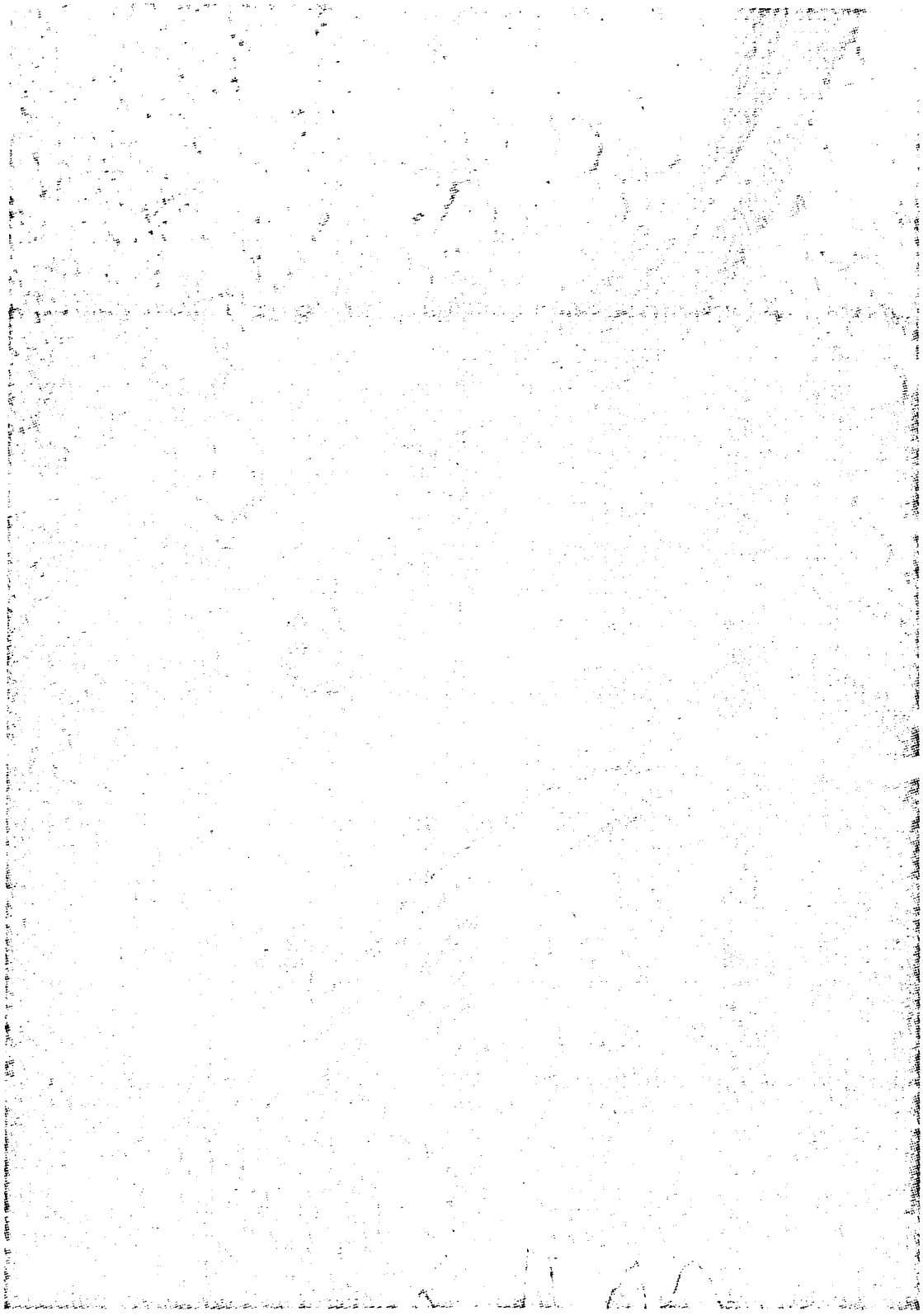

Figure 7.2-9. Drogue Disconnect, Single-Point Attachment Shear Plate, Mission PA-2

 [redacted]

[redacted]

Figure 7.2-10. Pilot Parachute Kinked Riser, Mission PA-2

[redacted]

[redacted]

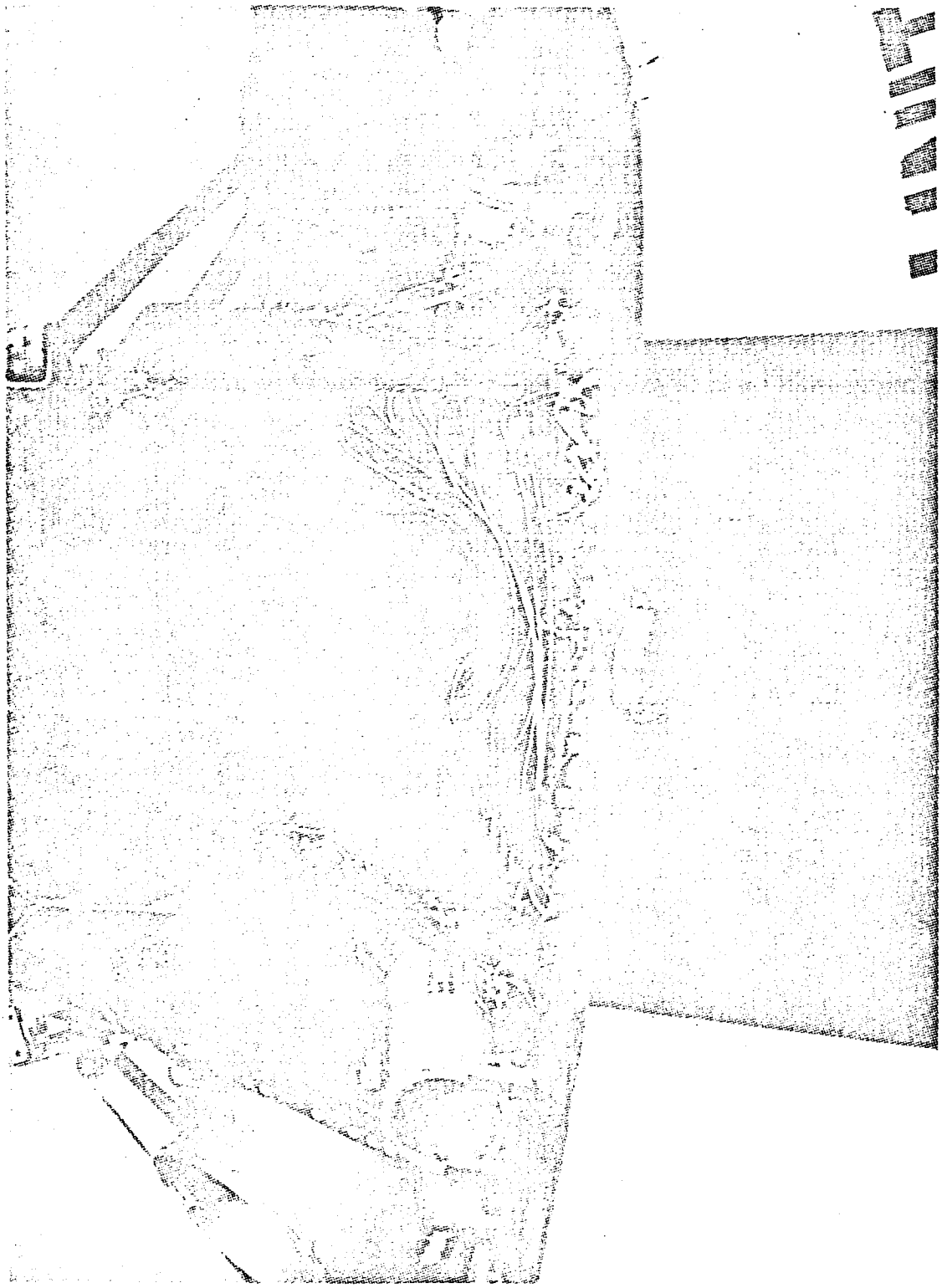

Figure 7.2-11. Mortars and Parachute Deck After Landing

[redacted]

[redacted]

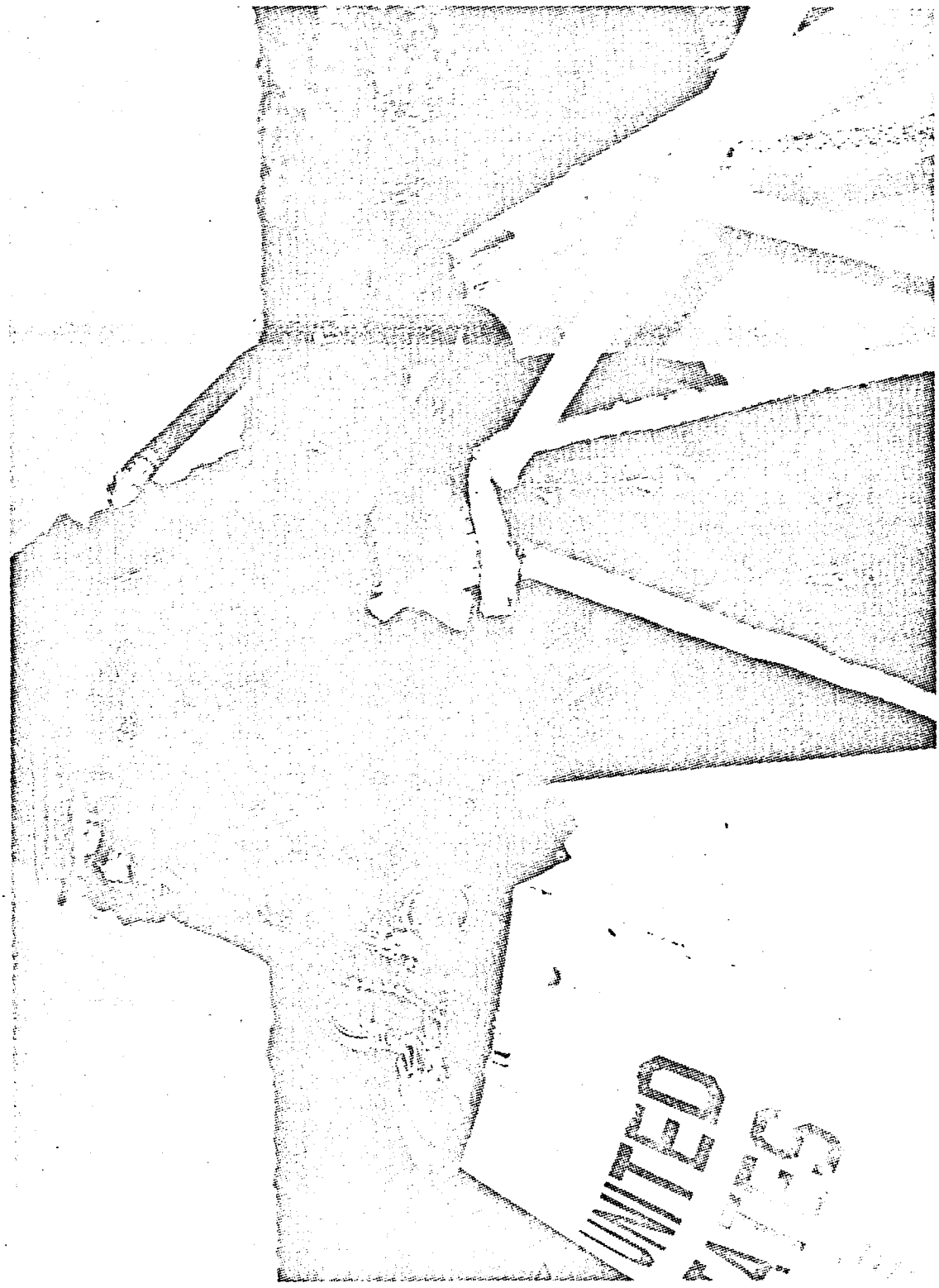

Figure 7.2-12. Harness and Parachute Deck After Landing

[redacted]

[redacted]

7.3 STRUCTURES

Summary

The Boilerplate 23A vehicle flight performance was structurally satisfactory. Analysis indicates that LES and canard design loads were not exceeded at any time during the flight. It was further determined that flight pressure data used in the analysis were in good agreement with computed pressures based on measured flight parameters.

The boost protective cover (BPC) broke up after vehicle turnaround and during the LES jettison. The soft BPC broke mostly into large pieces with vertical breaks generally occurring along the BPC splice joints. The horizontal break-line was approximately 6 inches below the BPC transition ring. The hard cover remained intact after tower separation; however, the motor exhaust burned and eroded the top 24 inches of the hard cover.

Examination of the LES revealed that the tower legs broke on impact. In-flight heating of the unprotected tower legs by LE motor exhaust had no evident structural effect.

No structural revisions are recommended for any succeeding boilerplate or the SC-002 flight on the basis of this test flight.

Subsystem Description

The Boilerplate 23A structure consisted of a spacecraft launch escape subsystem utilizing canard, boost protective cover, and a boilerplate command module. The general configuration description and comparison to other vehicles are given in section 5.0.

Launch Escape Tower

The launch escape tower was a welded tubular titanium-alloy structure in the shape of a truncated rectangular pyramid approximately 120 inches long and 46 by 50 inches at the base. A titanium skirt, mounted to the top of the tower, formed an attachment for the launch escape motor. The tower had provisions for attaching the boost protective cover to the lower tower section. The tower was attached to the command module by four explosive bolts (one at the base of each tower leg) which were detonated at the time of tower jettison.

[redacted]

[redacted]

Canard Subsystem

The canard subsystem consisted of two aerodynamic surfaces linked mechanically to a pyrotechnically actuated thruster which was energized after abort to deploy the aerodynamic surfaces to effect turnaround of the launch escape vehicle. The canard subsystem was attached to the structure at the forward end of the pitch control motor. Provisions for addition of ballast to the launch escape vehicle were incorporated into the canard structure.

Boost Protective Cover

The boost protective cover was fabricated in two main sections consisting of a forward hard section and an aft soft section. The hard section was fabricated of fiberglass face sheets and core sandwich. The soft section consisted of eight separate sections of cork bonded to glass cloth. Each of the eight sections was attached to one another and to the aft ring of the hard cover with bolts. The soft cover rested against the surface of the command module. The complete assembly was attached at hard points in the hard cover to the adjacent tower legs. The boost protective cover normally protects the command module from aerodynamic heating during the boost phase only and hence in sequence was jettisoned with the tower in the abort.

Ballast

Ballast of 697 pounds was added to the launch escape system to provide the desired center of gravity of X_A=1153 inches.

Command Module

The command module was a semi-monocoque aluminum structure which simulated the size, shape, weight, and center of gravity of the manned operational spacecraft. Its shape was approximately conical, with a height of 135 inches and a base diameter of 154 inches. The exterior surface was covered with cork to protect the aluminum structure from aerodynamic heating. The simulated aft heat shield was a sandwich honeycomb structure consisting of laminated fiberglass face sheets and aluminum core. Protuberances were added to the C/M surfaces to simulate Block I spacecraft external configuration.

Flight Loads

The principal test objectives for the Boilerplate 23A flight were to demonstrate LEV pad abort capability with a canard subsystem and a boost protective cover and to obtain performance and stability data for the LEV.

[redacted]

[redacted]

The amount of loads data and aerodynamic-pressure data obtained was limited. Twelve aerodynamic-pressure measurements were made on the CM base. The correlation between the measured pressures and the pressures computed from the measured flight parameters was very good in both the jet-on and jet-off flight ranges.

The measured time histories of dynamic pressure, angle of attack, and accelerations were less severe than the design pad-abort trajectory. It is concluded that the LES design loads for a pad abort were not exceeded.

The measured flight parameters at canard deployment were much less severe than the design conditions and it is concluded that the canard loads were much lower than design loads.

Canard Subsystem

The canard subsystem performed satisfactorily during the flight. The canard thruster deployed the canard panels to an open locked position. The canard effected rotation of the LEV in the horizontal plane approximately 90 degrees from the line of flight before jettison-motor ignition occurred. Positioning of the command module in a relatively aft-heat-shield-forward attitude in preparation for drogue parachute deployment was accomplished. The canard was almost completely destroyed on impact.

Launch Escape Tower

The launch escape tower performed satisfactorily. Test data from the flight indicate that the tower loads were not as severe as the design conditions.

Examination of the LES revealed that the tower legs broke on impact. Inflight heating of the unprotected tower legs by LE motor exhaust had no evident structural effect.

Boost Protective Cover

The boost protective cover remained intact on the command module all through launch escape motor burning with no evidence of failure. Ground-camera film coverage shows boost-cover breakup occurring at tower jettison.

The soft boost protective cover (BPC) broke up after vehicle turn-around and during the LES jettison. The soft BPC broke principally into large pieces with vertical breaks generally occurring along the BPC splice joints. The horizontal break-line was approximately 6 inches below the

[redacted]

[redacted]

BPC transition ring. The hard cover remained intact after tower separation and remained attached to the tower on LES landing; the LE motor exhaust, without structural effect, burned and eroded the top 24 inches of the hard cover.

Film-coverage analysis and postflight inspection indicate the boost protective cover performed as designed.

Command Module

The command module was instrumented to obtain base-pressure, conical-surface-pressure, static-pressure, internal-pressure, internal-temperature, and X, Y, and Z axial-acceleration data. Motion-picture coverage, from range cameras and from cameras on board the command module and the LES tower, supplied additional data. Still photographs also were taken of the structure after landing.

The command module exterior shows evidence of sooting, from the rocket motors, at the boost cover vent holes. Moderate scuffing of the scimitar antennas and the command module surface was caused by boost cover sliding.

The main heat shield shifted approximately 1/4 inch toward the -Z axis as a result of landing impact (Figure 7.3-1). The heat shield sustained major damage due to landing, but there was no buckling of the command module interior floor. Major damage to the heat shield was a crushing or break in the +Z to -Z axis (Figure 7.3-2).

There was no interior CM damage due to flight or landing impact.

Minor Malfunctions

Postflight inspection of the parachute system showed only minor ground damage. A steel riser cable of a pilot parachute was kinked, probably at deployment, approximately 24 inches from the riser clevis. There were no broken cable strands, and operation of the subsystem was not impaired in any way. The pistons of apex-cover thruster subsystem A (longerons 2 and 4) were slightly extruded into the piston rod cylinder holes. This extrusion was apparently caused by subsystem B actuating first or faster than subsystem A, thus allowing subsystem A to operate under a no-load condition.

[redacted]

[redacted]

Conclusions

The conclusion drawn from the review of the flight data is that the test vehicle flight performance was structurally satisfactory. The structural damage sustained by the vehicle was of a minor nature and was in no way detrimental to the support of all test objectives.

[redacted]

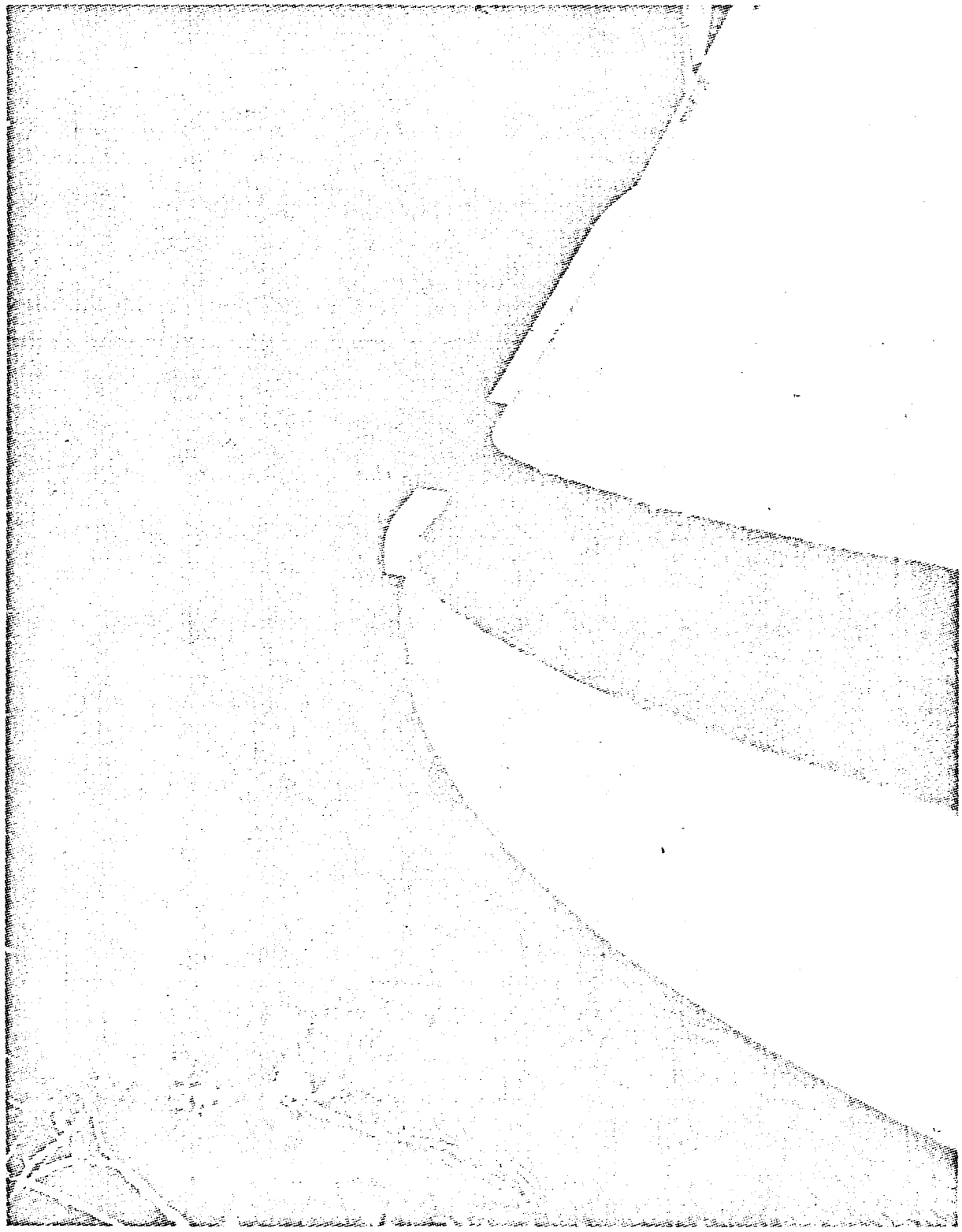

Figure 7.3-1. Main Heat Shield Shifted From Landing Impact, Mission PA-2

[redacted]

[redacted]

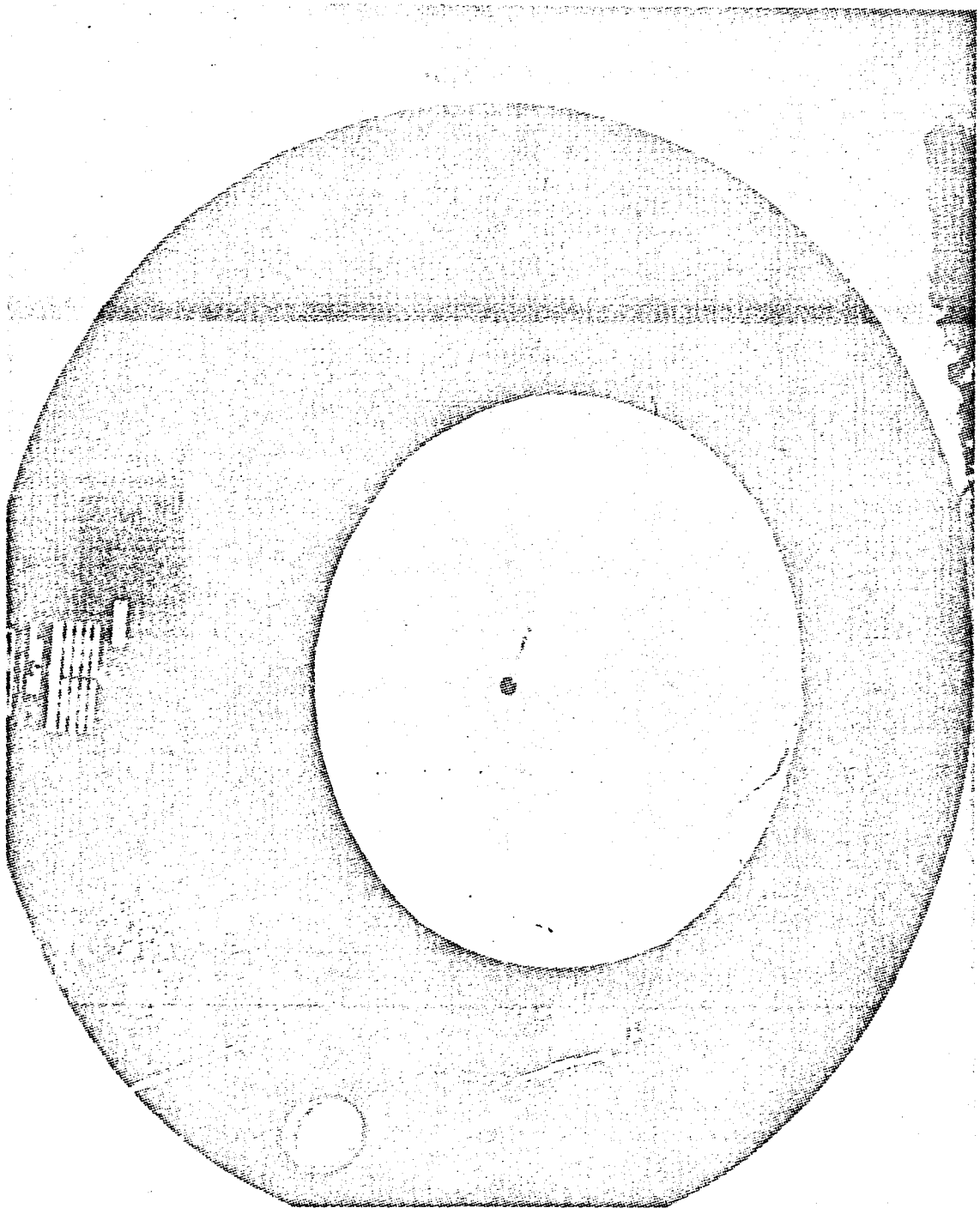

Figure 7.3-2. Main Heat Shield Cracked From Landing Impact

[redacted]

[redacted]

7.4 STRUCTURAL DYNAMICS

A detailed structural dynamics flight analysis was not made because fluctuating-pressure and low-range-acceleration instrumentation was not on board.

One possible analysis involved body bending modes from accelerometer data; however, the accelerometers installed for other purposes were of too high a range (±10 g) to provide reliable data. Body bending modes were determined from the Boilerplate 6 flight data; consequently, low-level accelerometer measurements were not required in this flight. Further, the tower leg vibration measurements were not included because the vibration transmission effect from the propulsion motors to the CM also was established in the Boilerplate 6 flight.

Acoustic analysis is not of significance in a low-q pad abort; hence, fluctuating-pressure instrumentation was not installed.

[redacted]

[redacted]

7.5 MASS CHARACTERISTICS

Launch Escape Vehicle

The launch escape vehicle consisted of the Boilerplate 23A command module and launch escape subsystem described in section 5.0. The actual mass characteristics, reference 10, are summarized in Figure 7.5-1, which includes weight and balance data on the sequence of events from abort initiation to command module landing.

A total of 3,800 pounds of ballast was included in the Boilerplate 23A command module, and was distributed to provide the required balance; an additional ballast of 1,000 pounds was added to the Boilerplate 23 command module to obtain the total. The launch escape subsystem of Boilerplate 23A required 697 pounds of ballast to attain the required balance. The total weight of the Boilerplate 23A test vehicle at launch was 19,092 pounds.

Comparison of Test Vehicles with Block I Spacecraft

In Figure 7.5-2, parts A and B, a weight and balance comparison is given of mission PA-2 test vehicle with the PA-1 test vehicle and the Block I vehicle, references 3 and 11. The difference between the BP-23A CM weight and the Block I CM weight results in part from the omission of RCS propellant from BP-23A; the Block I weight at landing does not include RCS propellant in that it is normally jettisoned as indicated in Figure 7.5-2. An additional difference, apparent at launch and within tolerance, results from normal field deviation.

Flight Data

The flight weight and balance data are given in Figure 7.5-3 for the launch escape vehicle abort phase. The two phases in the launch escape subsystem jettison, with the complete and with the partial hard boost protective cover, are given in Figure 7.5-4.

The weight data were determined from the known weight of propellant onboard, flight motor chamber pressure data, scale-motor burning rate data with samples of actual propellant, and motor burning rate correlations. These correlations were developed from scale-motor test and from full-scale motor test-stand data.

The flight weight and balance data were used in the flight simulations included in section 7.1.

	Weight, Pounds	Center of Gravity, Inches			Moment of Inertia, Slug-Feet^2		
		X_A*	Y_A	Z_A	I_{XX}	I_{YY}	I_{ZZ}
LES	8,202	1301.2	-0.4	1.2	555	21,212	21,205
CM	10,891	1042.2	0.1	5.2	6,145	5,470	5,190
LEV at time of launch (abort)	19,092	1153.5	-0.1	3.5	6,719	94,428	93,470
LEV at launch-escape motor burnout	15,913	1125.0	-0.1	4.0	6,642	76,377	75,423
LES at LE motor burnout	5,022	1304.5	-0.3	0.6	495	19,861	19,206
LES at jettison-motor burnout (without soft boost cover)	4,487	1318.6	-0.2	0.9	223	14,346	13,693
CM prior to drogue parachute deployment (after apex-cover jettison)	10,485	1039.9	0.1	5.3	6,075	5,111	4,831
CM after drogue-parachute deployment (including pilot and main parachutes)	10,434	1039.7	0.1	5.5	6,064	5,069	4,797
CM at landing	10,009	1037.6	0.1	5.4	6,010	4,804	4,510

*See Figure 5.1-1 for definition of X_A

Figure 7.5-1. Table of Mass Characteristics, Mission PA-2

[redacted]

Vehicle Condition	Weight, Pounds		
	PA-1	PA-2	Block I Control
Test vehicle at launch (LEV)	15,822	19,092	19,200
LEV at launch escape motor burnout	12,619	15,913	16,010
LES at jettison motor burnout	3,753	4,817	4,810
CM prior to drogue parachute deployment (after apex-cover jettison; 180 pounds of RCS oxidizer jettison with Block I)	8,659	10,485	10,406
CM after drogue parachute deployment	8,631	10,434	10,350
CM at landing (90 pounds of RCS fuel jettison while on main parachutes with Block I)	8,231*	10,099*	9,841

*No RCS propellant included in mission.

A. Vehicle Weights

Vehicle Condition	Center-of-Gravity Location, Inches		
	PA-1	PA-2	Block I
LEV at time of launch (abort)			
X_A axis	1152.8	1153.5	1153.5
Y_A axis	+0.33	-0.1	0.1
Z_A axis	+4.29	3.5	3.0
LEV at launch escape motor burnout			
X_A axis	1124.35	1125.0	1125.0
Y_A axis	+0.41	0	0.1
Z_A axis	+5.38	4.0	3.6

B. Centers of Gravity

Figure 7.5-2. Table of Weights and Centers of Gravity, Comparing Apollo Mission PA-2 Test Vehicle With PA-1 Test Vehicle and Block I Spacecraft

[redacted]

Time Sec	Weight Pounds	Center of Gravity, Inches			Moment of Inertia, Slug-Feet^2					
		X_A	Y_A	Z_A	I_{XX}	I_{YY}	I_{ZZ}	I_{XY}	I_{XZ}	I_{YZ}
0.0	19092.0	1153.5	-0.1	3.5	6718.8	94428.0	93470.3	12.7	-748.1	56.4
0.5	18713.1	1150.5	-0.1	3.6	6713.7	92485.0	91527.8	13.4	-722.4	56.3
1.0	18323.1	1147.4	-0.1	3.6	6707.5	90518.0	89561.2	14.0	-696.1	56.3
1.5	17903.1	1144.0	-0.1	3.7	6699.4	88310.5	87354.3	14.7	-666.3	56.3
2.0	17513.1	1140.6	-0.1	3.7	6690.6	86172.5	85216.8	15.4	-637.3	56.3
2.5	17133.1	1137.1	-0.1	3.8	6681.0	84001.8	83046.6	16.1	-607.7	56.3
3.0	16783.1	1133.8	-0.1	3.8	6671.1	81921.0	80966.3	16.7	-579.1	56.3
3.5	16483.1	1130.9	-0.1	3.9	6661.9	80071.5	79117.3	17.3	-553.6	56.3
4.0	16318.1	1129.2	-0.1	3.9	6656.5	79027.0	78073.0	17.6	-539.1	56.3
4.5	16193.1	1127.9	-0.1	3.9	6652.3	78222.4	77268.5	17.8	-528.0	56.3
5.0	16123.1	1127.2	-0.1	3.9	6649.9	77766.7	76813.0	18.0	-521.6	56.3
5.5	16063.1	1126.6	-0.1	3.9	6647.7	77373.1	76419.5	18.1	-516.2	56.3
6.0	16023.1	1126.1	-0.1	4.0	6646.3	77109.1	76155.6	18.2	-512.5	56.3
6.5	15983.1	1125.7	-0.1	4.0	6644.9	76843.9	75890.4	18.3	-508.8	56.3
7.0	15963.1	1125.5	-0.1	4.0	6644.2	76710.8	75757.3	18.3	-506.9	56.3
7.5	15943.1	1125.3	-0.1	4.0	6643.5	76577.4	75624.0	18.3	-505.1	56.3
8.0	15933.1	1125.2	-0.1	4.0	6643.1	76510.6	75557.2	18.4	-504.2	56.3
9.0	15913.1	1125.0	-0.1	4.0	6642.4	76376.8	75423.4	18.4	-502.3	56.3

Figure 7.5-3. Table of Weight and Balance Data for Launch Escape Vehicle Abort Phase. Mission PA-2

		Center of Gravity, Inches			Moment of Inertia, Slug-Feet^2					
Time, Sec*	Weight, Pounds	X_A	Y_A	Z_A	I_{XX}	I_{YY}	I_{ZZ}	I_{XY}	I_{XZ}	I_{YZ}
With Complete Boost Protective Cover										
0.0	5021.7	1304.5	-0.3	0.6	494.7	19,861.1	19,206.2	9.8	213.1	0.1
Without Soft Boost Protective Cover										
0.2	4670.0	1322.1	-0.2	1.0	228.5	14,660.4	14,007.4	-23.4	110.8	-0.5
0.4	4637.1	1321.5	-0.2	0.9	227.6	14,605.8	13,952.8	-23.3	109.7	-0.5
0.6	4600.6	1320.8	-0.2	0.9	226.4	14,544.3	13,891.3	-23.2	108.4	-0.5
0.8	4564.1	1320.1	-0.2	0.9	225.3	14,481.8	13,828.8	-23.1	107.1	-0.5
1.0	4530.1	1319.5	-0.2	0.9	224.1	14,422.6	13,769.7	-23.0	105.9	-0.5
1.2	4498.1	1318.8	-0.2	0.9	223.0	14,366.1	13,713.2	-23.0	104.7	-0.5
1.4	4486.9	1318.6	-0.2	0.9	222.6	14,346.1	13,693.3	-22.9	104.3	-0.5

*Time from jettison motor ignition

Figure 7.5-4. Table of Weight and Balance for Launch Escape Subsystem Jettison Phase, Mission PA-2

[redacted]

7.6 LAUNCH ESCAPE SEQUENCER SUBSYSTEM

Summary

The launch escape sequencer subsystem functioned satisfactorily and demonstrated its ability to control a pad-abort sequence. All events were initiated within the specified time limits. All components functioned correctly.

Subsystem Description

The launch escape sequencer subsystem consisted of a mission sequencer, two tower sequencers, and an inactive abort backup timer. The sequencer locations are given in Figure 7.6-1, and the subsystem configuration is described in section 5.0. The two logic batteries in the electrical power subsystem (EPS) provided power for the logic network, and the two EPS pyro batteries were used to fire onboard pyrotechnic devices. The purpose of the sequencer subsystem was to automatically control and sequence the application of electrical power to the pyrotechnic devices which fired the launch escape motors, deployed the canard, and jettisoned the launch escape tower and the apex cover; it also armed the earth landing sequence controller which is discussed in sections 5.0 and 7.2. The sequencer subsystem included redundancy so that premature operation of any logic component, or failure of a component to operate, would not cause mission failure.

Figure 7.6-2 is a simplified schematic diagram of subsystem A. Subsystem B was identical.

The launch escape sequencer subsystem for Boilerplate 23A was similar to that used for Boilerplate 22 (reference 8). The functions performed by the Boilerplate 23A launch escape sequencer subsystem will be performed by a master events sequence control (MESC) in the spacecraft vehicles.

The tower sequencers were similar to those used on Boilerplate 23 (reference 7).

Subsystem Performance

Figure 7.6-3 is a functional diagram which illustrates the events sequence and gives the actual times for the mission.

The abort was initiated and the sequencer was started at T - 0.2 second. The four 11.0-second (± 5%) timers timed out in 11.2 seconds, deploying the canard and activating the 3-second time-delay relays K14 and K16. The four 3-second (± 5%) timers timed out between 2.8 and 2.9 seconds and armed the earth landing subsystem sequencer at T + 13.8 seconds at an altitude of

9,100 feet. At this point the high-altitude baroswitches were closed (the specified lower limit for contact opening is 36,000 ± 2,000 feet); the arming signal therefore initiated tower separation and tower jettison and activated the 0.4-second time-delay relays K24 and K26. The apex cover was jettisoned when the time-delay relays, K24 and K26, timed out 0.4 second later, completing the function of the launch escape sequencer subsystem. All components of the subsystem functioned correctly.

[redacted]

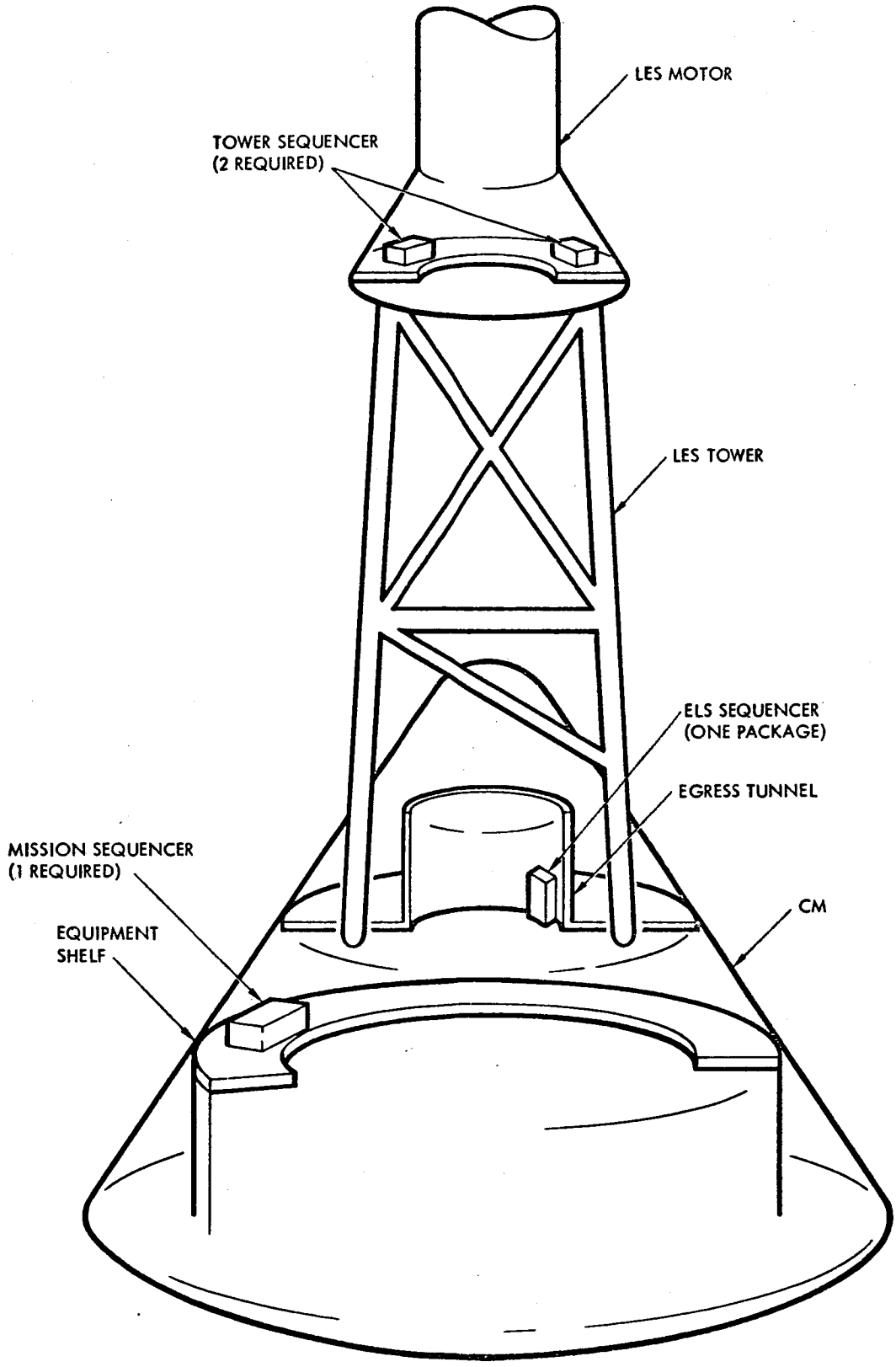

Figure 7.6-1. Boilerplate 23A Sequencer Subsystem Locations

[redacted]

[redacted]

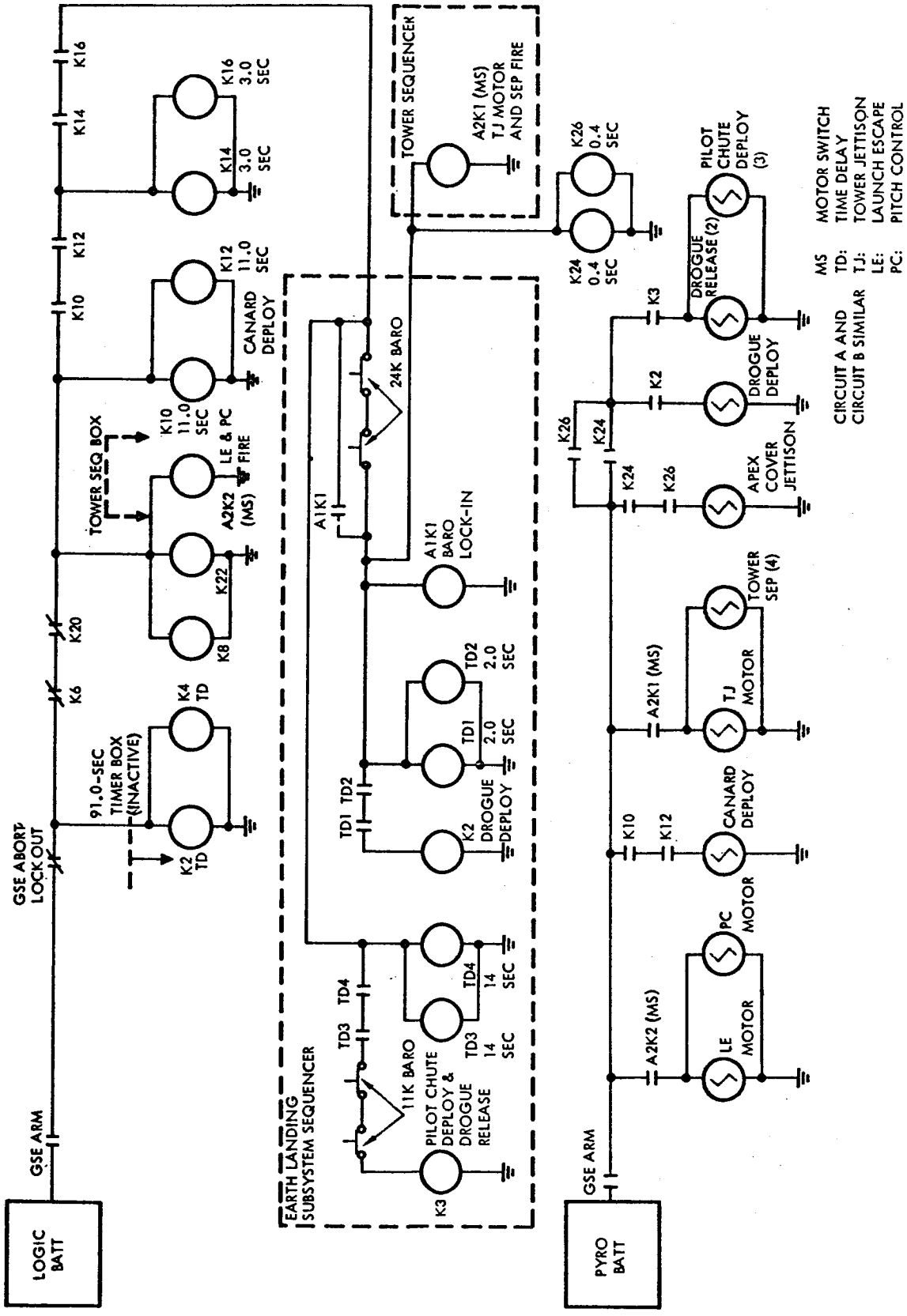

Figure 7.6-2. LES Sequencer Schematic

[redacted]

[redacted]

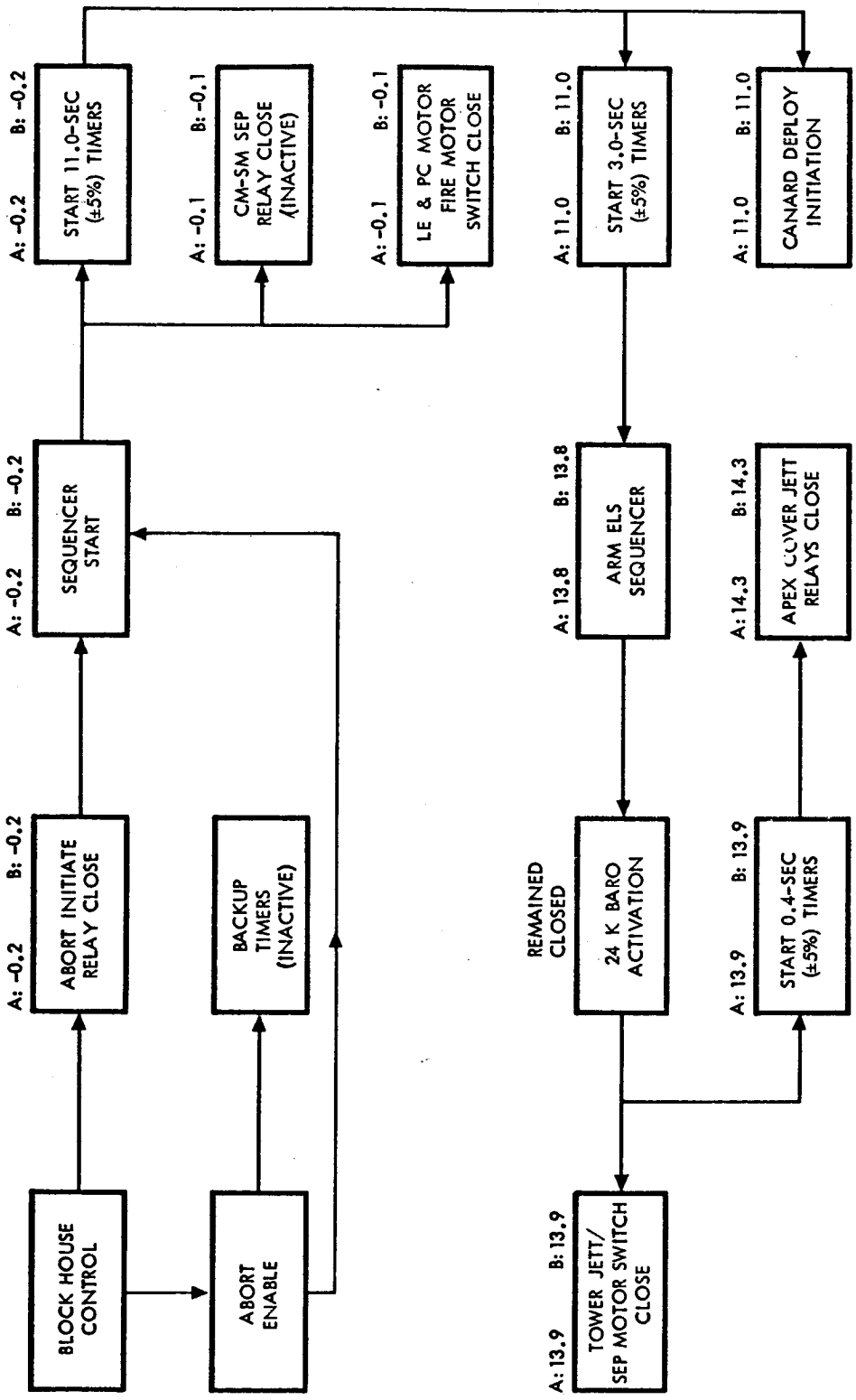

NUMBERS INDICATE TIME (SECONDS) OF EVENT OCCURRENCE

Figure 7.6-3. LES Sequencer Events

[redacted]

[redacted]

7.7 ORDNANCE EQUIPMENT

Summary

Ordnance devices were used in Boilerplate 23A to perform the following functions:

Launch escape and pitch control motor ignition
Canard deployment
Launch escape tower separation
Tower jettison motor ignition
Apex cover jettison
Drogue parachute deployment
Drogue parachute disreef
Drogue parachute release
Pilot parachute deployment
Main parachute disreef

All functions were performed satisfactorily. All devices were recovered and examined; only one irregularity was found, involving superficial damage to one pair of apex thruster pistons in an interim design.

Subsystem Description

The part, lot, and serial numbers of the various devices are listed in Figure 7.7-1.

Launch Escape and Pitch Control Motor Igniters

Two redundant Type I cartridges, with integral Apollo standard initiators, were used to ignite each of the launch escape and pitch control motors. This type of cartridge is currently undergoing qualification testing and is scheduled for use in all Apollo spacecraft.

Tower Jettison Motor Igniters

Two redundant Type II cartridges were used to ignite the tower jettison motor. The Type II cartridge is of Apollo spacecraft type and differs from the Type I cartridge differs from the Type I cartridge only in the thread size.

[redacted]

Single-Mode Explosive Bolts

Launch-escape-tower separation was achieved by means of four single-mode explosive bolts. Their description is given in reference 7, section 7.8, One bolt was installed at the foot of each leg. The bolts used for Boilerplate 23A were the improved type used for Boilerplate 22, which were different in two respects from those used successfully for other flight tests. To increase the separation safety margin, weight of the charge was increased from 2.25 grams to 2.85 grams, and body thickness around the charge cavity was increased. Use of the single-mode bolt is an interim measure. Dual-mode bolts will be used when their development is complete and they become available.

Canard Deployment Subsystem

The subsystem description is given in reference 7, section 7.8. The canard panels were deployed by the force developed by two redundant Type VII pressure cartridges, each of which was capable of deploying both panels. The pressure cartridges were activated by Apollo standard initiators. This was the third flight test of the Block I type subsystem; the first two tests were conducted successfully with Boilerplates 22 and 23.

Drogue Parachute Release Subsystem

The two drogue parachutes were released from the command module by cutting a tension member in the disconnect assembly. The subsystem is described in reference 8, section 7.8. Two linear shaped charges were used, one charge being clamped to each side of the titanium tension member. Two Apollo standard detonators were used in a redundant configuration. The configuration used for Boilerplate 23A was the same as that used for Boilerplate 22 and is scheduled for use on all Block I spacecraft. The concept for Block II spacecraft is entirely different. The proposed design for those spacecraft is a guillotine cable-cutting device.

Parachute Deployment Mortars

Individual mortars were used to deploy the two drogue and the three pilot parachutes. They are described in reference 7, section 7. The drogue parachute mortars used Type I pressure cartridges, and the pilot parachute mortars used Type II pressure cartridges. Each mortar used two cartridges; successful firing of both cartridges was necessary to ensure satisfactory parachute pack ejection velocity. They therefore were fired into a common breech and plenum chamber so that a cartridge which failed to fire on electrical command would be fired sympathetically by the other cartridge. The same type was used successfully on Boilerplates 3, 6, 12, 19, 22, and 23 and also are scheduled for use on the other Apollo flight vehicles.

[redacted]

Parachute Reefing-Line Cutters

The drogue and main parachutes were disreefed by 8-second time-delay reefing-line cutters. They are described in reference 8, section 7.8. This type of cutter incorporates a powder train which is ignited by a percussion initiator actuated at parachute line stretch by a lanyard. To provide redundant operation, two cutters were used for each drogue parachute active reefing line, and three cutters were used for each main parachute reefing line. The same type of cutter was used for the flight test of Boilerplate 22, in which one redundant cutter on each of the drogues failed to fire. These failures were attributed partly to the high dynamic loads imposed on the drogue parachutes during the test. Low dynamic loads were predicted for the Boilerplate 23A flight; it was therefore considered safe to use identical, unmodified cutters. The cutters will be redesigned before the next flight use.

Apex-Cover Thruster Subsystem

This was the second flight test in which the apex cover was jettisoned independently of the launch escape subsystem. Apex-cover jettison first was used in the Boilerplate 22 flight. Two redundant subsystems with two thrusters in each were used. Either subsystem was independently capable of jettisoning the apex cover. The thruster subsystem differed from spacecraft design in that the tension ties securing the apex cover to the command module were not located in the thrusters, and the pressure cartridges were of Type III instead of Type VI.

Apollo Standard Detonators and Initiators

The Apollo standard detonator, which contains an integral standard initiator with a no-fire rating of 1-watt/1-ampere for 5 minutes, contains two bridgewire circuits. The A-B bridgewire is connected into the firing circuitry while the C-D bridgewire is left open and isolated. These devices are similar to those used for Boilerplate 23 and are described in reference 7, section 7.8.

Standard initiators were used in all Boilerplate 23A pyrotechnic devices except reefing-line cutters and explosive bolts. The total number of standard initiators used was 22.

Two standard detonators were used to fire the linear shaped charges in the drogue disconnect subsystem.

The standard initiator and the standard detonator, which are undergoing qualification testing, are scheduled for use in all Apollo spacecraft. They have been used successfully in Boilerplates 3, 6, 12, 13, 15, 19, 22, and 23.

 [redacted]

[redacted]

Pressure Cartridges

The Type I, II, and VII pressure cartridges used in the parachute mortars and the canard actuator were similar to those used for previous boilerplate flights and scheduled for use in all Apollo spacecraft. Each cartridge contained 28 pellets in 4 tiers of 7 each. They are described in detail in reference 7, section 7.8.

Type III cartridges were used in the apex-cover thruster subsystem. This type also contains 28 pellets in 4 tiers of 7 each. This was the only scheduled flight test of the Type III cartridge. Type VI cartridges are scheduled for use in all Apollo spacecraft.

Subsystem Performance

All pyrotechnic devices performed satisfactorily. The interim-type apex-cover thruster subsystem functioned satisfactorily; but postflight inspection indicated thruster piston damage, discussed below.

Thruster subsystem A fired first and successfully jettisoned the apex cover. When subsystem B fired 0.1 second later the two pistons were unloaded, and were driven into their stops with sufficient force to damage the pistons. However, the damage was superficial and caused no subsystem malfunction. This anomaly cannot occur on the spacecraft-type thruster subsystems in that their pistons are attached to the apex cover, and all four pistons will be withdrawn from their cylinders and jettisoned with the cover when the first subsystem fires.

Pyro battery B voltage was low for approximately 0.5 second following subsystem B thruster firing, and investigation revealed that the fusistor in the apex-cover thruster initiator circuit had opened. It is therefore apparent that an electrical short circuit existed for a period immediately following subsystem B thruster actuation. Postflight examination of the initiator failed to disclose the source of this short circuit. The initiator will be disassembled and examined further in an effort to disclose the cause of the over-current. This short circuit is discussed also in sections 7.6 and 7.9.

[redacted]

Subsystem	Cartridge			Initiator		
	Part No.	Serial No.	Lot No.	Part No.	Serial No.	Lot No.
Canard	V15-590220	AAD2233	06362	ME453-0009	9659	18
	V15-590220	AAD2234	06362	ME453-0009	9727	18
Launch Escape						
Launch escape motor	ME453-0014-0081	1097	1	ME453-0009	4549	11
	ME453-0014-0081	1223	2		4739	9
Pitch control motor	ME453-0014-0081	1233	2		4868	9
	ME453-0014-0081	1248	2		4685	9
Tower jettison motor	ME453-0014-0082	0006	AAA		11576	23
	ME453-0014-0082	0009	AAA		11579	23
Tower Separation						
Explosive bolt	ME111-0001-0016	0061	ACM	S01-2-314	0055-0061	ACF
		0062	ACM		0066-0064	ACF
		0064	ACM		0118-0117	ACF
		0043	ACM		0149-0150	ACF
Drogue Mortar	ME453-0005-0041	5287	5	ME453-0009	8613	16
		5288	5		8612	16
		5293	5		8603	16
		5298	5		8633	16
Pilot Mortar	ME453-0005-0042	5279	4	ME453-0009	8905	16
		5312	4		8964	16
		5313	4		8744	16

Figure 7.7-1. Table of BP-23A Ordnance Devices (Sheet 1 of 2)

[redacted]

Subsystem	Cartridge			Initiator		
	Part No.	Serial No.	Lot No.	Part No.	Serial No.	Lot No.
Pilot Mortar (cont)	ME453-0005-0042	5316 5324 5326	4 4 4	ME453-0009	8961 8957 8605	16 16 16
Drogue Disconnect Cutter assembly	V16-576260-21 V16-576260-31	0026 0082	2 2	None	-- --	-- --
Detonator	ME453-0021-0004	0049 0075	ABC ABC	ME453-0009	13453 13541	28 28
Apex Cover Jettison	ME453-0005T0023	0930 0931	1A 1A	ME453-0009	2498 2433	4 4

Figure 7.7-1. Table of BP-23A Ordnance Devices (Sheet 2 of 2)

7.8 LAUNCH ESCAPE PROPULSION SUBSYSTEM

Summary

The launch escape propulsion subsystem used was of the Block I spacecraft type. The three propulsion motors functioned properly, producing thrust within acceptable limits. Tables summarizing significant characteristics and performance of the motors are presented in Figures 7.8-1 and 7.8-2. Definitions of terms used are given in Figure 7.8-3.

The Boilerplate 23A launch escape propulsion subsystem was of the configuration to be used in the manned spacecraft flights and included the launch escape (LE) motor, the pitch control (PC) motor, and the tower jettison (TJ) motor. Each motor consisted of a steel case and a case-bonded ammonium-perchlorate/polysulfide propellant grain. Hot-wire igniter cartridges were used to initiate boron/potassium-nitrate pellets which, in the LE and TJ motors, ignited a solid-propellant Pyrogen igniter, which in turn ignited the main propellant grain. Because of its small size, the PC motor did not need a Pyrogen igniter.

The LE motor provided the thrust to lift the command module from the launch pad. It had four nozzles canted 35 degrees from the motor center line. The carbon throat inserts of the nozzles in the XZ plane were sized with different throat diameters to produce a nominal thrust-vector offset of 2 degrees 45 minutes. This offset was necessary to direct the thrust vector of the LE motor near the center of gravity of the launch escape vehicle. The PC motor provided the initial pitching moment intended to direct the command module downrange out of the path of the launch vehicle. The TJ motor, firing through two nozzles canted 30 degrees from the motor center line in the XZ plane, was then used to separate the LE subsystem from the command module. Nozzle throat diameters were sized to provide a nominal 3.8-degree thrust-vector offset to divert the LE subsystem from the path of the command module.

The LE subsystem also included the tower between the LE motor and the command module, the interstage between the LE and TJ motors (which is considered part of the TJ motor), the canard subsystem, the ballast enclosure and ballast, and the nose cone and Q-ball. The tower, canard, and Q-ball are discussed in other sections of this report.

Preflight History

Launch Escape Motor

The launch escape motor S/N ED35A (ME467-0003-1000) was cast and manufactured on December 12, 1964, and delivered to WSMR in March 1965.

The only difference between this motor and the motor used for Boilerplate 22 is that the latter was field-equipped with thermocouples to measure the propellant grain temperature as well as the case temperature.

Pitch Control Motor

The pitch control motor S/N 61AA (ME467-0005-0007) was cast on September 29, 1964, and delivered to WSMR in March 1965. This motor was identical to the motor used on Boilerplate 22.

Tower Jettison Motor

The tower jettison motor (ME467-0004-1003) was identical to the motor used on Boilerplate 22. This motor was originally cast and manufactured as configuration ME467-0004-0007 on September 20, 1963, and delivered to WSMR in January 1964, as a spare motor for Boilerplate 12. In September 1964, the motor was retrofitted with a qualification-type Pyrogen (stronger pellet basket) and a set of 3.8-degree nozzles. With this retrofit, the motor was redesignated as ME467-0004-1000. In December 1964, the motor was returned to Thiokol for interstage retrofit and permanent storage. The motor, originally the Boilerplate 12 spare, now designated as ME467-0004-1001 because of the interstage retrofit, was redelivered to WSMR in March 1965, to support the Boilerplate 23A LE subsystem buildup, although according to schedule requirements the Boilerplate 23A motor was not due at WSMR until May 1965.

Prior to the launch escape subsystems buildup in April 1965, the Boilerplate 12 spare motor was reworked in the field to an ME467-0004-1003 configuration by the addition of the nozzle plug cork insulation (Figure 7.8-4). This insulation was necessary, as determined by the Boilerplate 22 thermal analysis, to protect the styrofoam nozzle plugs from aerodynamic heating.

Surveillance Tests

Specified ballistic and physical property tests were performed by Lockheed and Thiokol with satisfactory results prior to NAA's final acceptance of the three LES solid motors for the Boilerplate 23A flight test. Scale-motor propellant and propellant specimens used in the tests were taken from the production propellant batches of the LE, PC, and TJ motors. The burning-rate data obtained from the aged-scale-motor firings were compared with the original batch-check scale-motor results and, by correlations, compared to full-scale motor burning rate. Standard-shape (JANAF dogbone) propellant specimens were used to check for propellant physical properties.

[redacted]

Letters from Thiokol and Lockheed in April and May 1965, respectively, stated that the surveillance tests showed no significant difference in propellant characteristics due to aging, and that the three motors were completely acceptable for flight test. The Lockheed letter also stated concurrence on the flight readiness of the launch escape motor on the basis of field inspection of the propellant grain on March 12 and 13, 1965.

Propellant Grain Temperature

The Boilerplate 23A launch escape motor was not instrumented to measure propellant grain temperature. An approximate grain temperature value of 80±5 degrees was estimated from the official WSMR ambient-temperature record over the 12-hour period prior to launch. It is recognized that accurate grain temperature is essential for the evaluation of motor performance; therefore thermocouples will be installed on the SC-002 and SC-009 launch escape motors, and they are planned for installation on two additional launch escape motors at ETR.

Performance

Launch Escape Motor

The performance of the launch escape motor was well within specification requirements. A comparison of the major performance parameters, actual and predicted, is given in Figure 7.8-2.

The amount of propellant consumed was calculated using the telemetry chamber-pressure data. The results indicate the telemetry data require a 2-percent decrease to establish a balance between the calculated and the actual propellant consumed, determined by preflight weights. A comparison of the telemetry pressure data (decreased by the above-mentioned 2 percent) and the predicted chamber pressure, covering the complete burning time, is given in Figure 7.8-5 (the corrected telemetry data are plotted as the actual pressure). The propellant grain temperature used was estimated at 80 F as previously discussed. The predicted pressure is less than the corrected telemetry data, on average, by 0.4 percent (Figure 7.8-2). Without data correction, the deviation would be only 2.4 percent.

The launch escape motor thrust calculated from the corresponding chamber-pressure values of Figure 7.8-5 are given in Figure 7.8-6. Based on thrust from Figure 7.8-6, a flight simulation was made as discussed in Section 7.1. The results of the simulation confirm that the LE motor performance was satisfactory. If the thrust were evaluated from the uncorrected telemetry chamber pressure data rather than the above generally accepted method, the simulated flight trajectory would agree, in this particular case, with the tracking data to within 1 percent.

Pitch Control Motor

The performance of the pitch control motor was very close to that predicted. The actual and predicted major performance parameters are compared in Figure 7.8-2. Two chamber pressure-time curves, comparing the actual (corrected telemetry) with the predicted values, are given in Figure 7.8-7. The telemetry data were decreased 2 percent as above to adjust the calculated propellant consumption to the actual. In general, the predicted values were slightly higher than the actual values. Based on calculations with the chamber-pressure values of Figure 7.8-7, the PC motor thrust values are given in Figure 7.8-8.

Tower Jettison Motor

No instrumentation was provided on this motor. Analysis of the tracking data indicates that the tower jettison motor performed satisfactorily. The predicted thrust-time history based on the results of batch-check and full-scale motor firings is shown in Figure 7.8-9. The propellant used in this motor came from the same propellant batch as one developmental motor (AD-25), two qualification test motors (AQ II-2 and AQ I-3), and two boilerplate test motors (BP-12 and BP-23).

Conclusions

Analysis of the flight-test performance of the Boilerplate 23A launch escape subsystem solid rocket motors indicates that all motors ignited as programmed and that the launch escape and pitch control motors performed well within their design limits. Optical tracking data indicate that the tower jettison motor also performed satisfactorily.

Characteristic	Launch Escape Motor (S/N ED-35A)	Pitch Control Motor (S/N 61AA)	Tower Jettison Motor (ME467-0004-1003)
Nozzles			
No. of nozzles	4	1	2
Type of nozzles	Conical	Conical	Scarfed Conical
Cant angle, degrees	35.0	0	30.0
Divergent half-angle, degrees	17.5	—	10.0
Throat area, sq in.			
No. 1	18.55	1.223	10.184
No. 2	21.23	—	8.767
No. 3	24.43	—	—
No. 4	21.24	—	—
Nozzle exit area, sq in.			
No. 1	198.32	2.076	—
No. 2	198.40	—	—
No. 3	198.25	—	—
No. 4	198.35	—	—
Ignition system			
Type	Pyrogen	Pellet Basket	Pyrogen
Initiator type	Hotwire	Hotwire	Hotwire
No. of initiators	2	2	2
Weight			
Propellant, lb	3146	8.89	203.55
Hardware and liner, lb	1594	40.18	320.88
Total, lb	4740	49.07	524.43
Dimensions			
Chamber case diameter, in.	26.00	10.51	26.0
Overall length, in.	185.57	22.00	55.64

Figure 7.8-1. Table of Boilerplate 23A LES Motor Characteristics

Performance at P_a = 12.68 psia and 80 F / Parameter	Launch Escape Motor				Pitch Control Motor			
	Predicted	Actual	Δ, %	Spec.	Predicted	Actual	Δ, %	Spec.
Burning Time, t_b, sec	3.2	3.25	+1.6		0.60	0.60	0	0.50 - 0.70
Action Time, t_a, sec	6.2	6.25	+0.8		0.97	0.93	-4.0	
Total Time, t_t, sec	8.9	9.0	+1.1		1.29	1.25	-3.0	
Max. Chamber Press., P_{max}, psia	1500	1510	+0.7	2218 (max)	1738	1730	-0.5	2670 (max)
Av. Press. Over Burning Time, $\overline{P}_b$, psia	1310	1315	+0.4		—	—		
Max. Thrust, F_{max}, lb	155,000	156,200	+0.8	200,000 (max)	2900	2890	-0.3	6000 (max)
Av. Thrust Over Burning Time, $\overline{F}_b$, lb	139,000	140,200	+0.9		—	—		
Total Impulse, I_t, lb-sec	559,800	555,500	-0.8	515,000 (min)	1758	1727	-1.7	1750±3%

Figure 7.8-2. Table of Boilerplate 23A Launch Escape Motor and Pitch Control Motor Performance

[redacted]

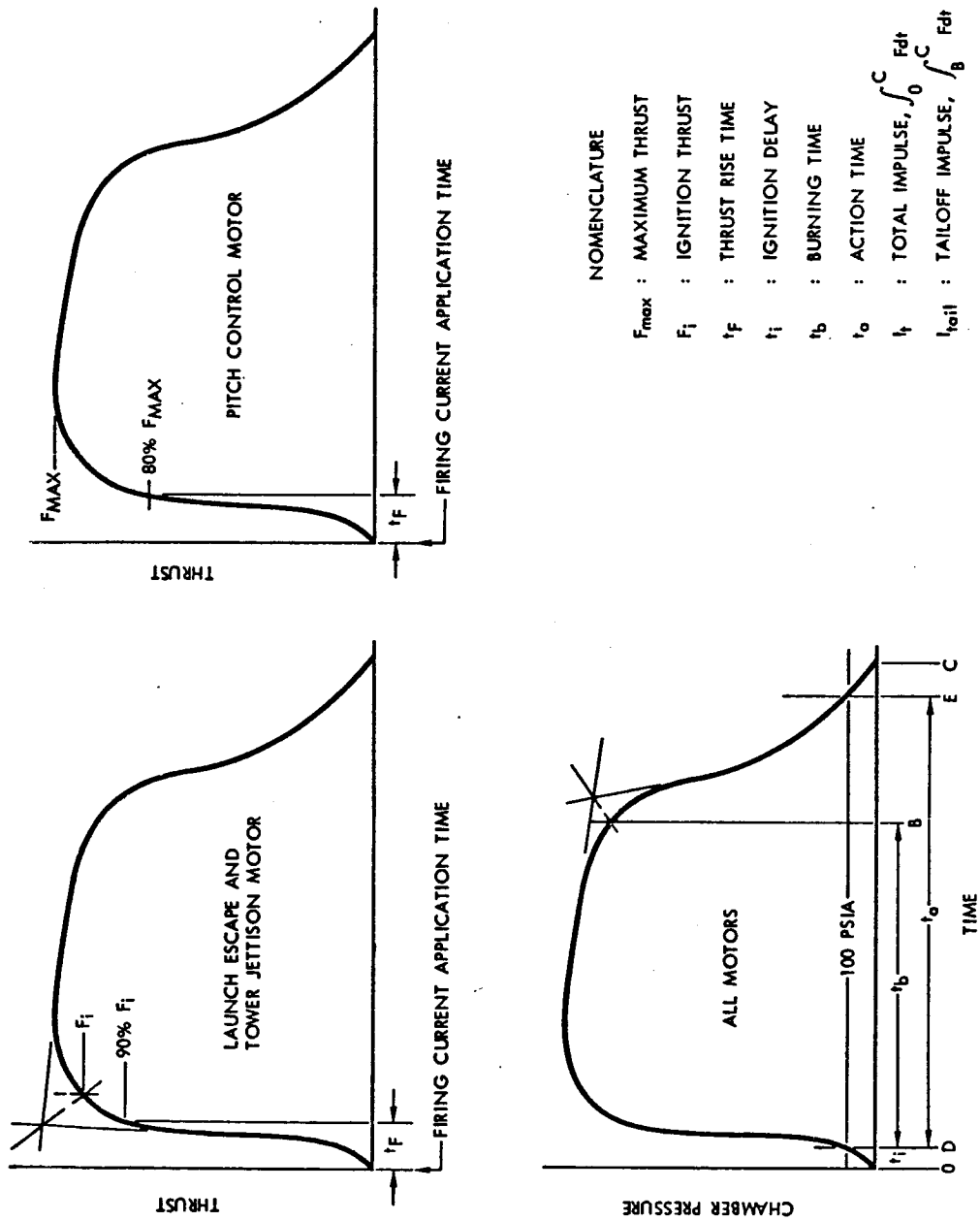

NOMENCLATURE

F_{max} : MAXIMUM THRUST

F_i : IGNITION THRUST

t_F : THRUST RISE TIME

t_i : IGNITION DELAY

t_b : BURNING TIME

t_o : ACTION TIME

I_t : TOTAL IMPULSE, $\int_0^C F dt$

I_{tail} : TAILOFF IMPULSE, $\int_B^C F dt$

Figure 7.8-3. BP-23A Ballistic Definitions

[redacted]

[redacted]

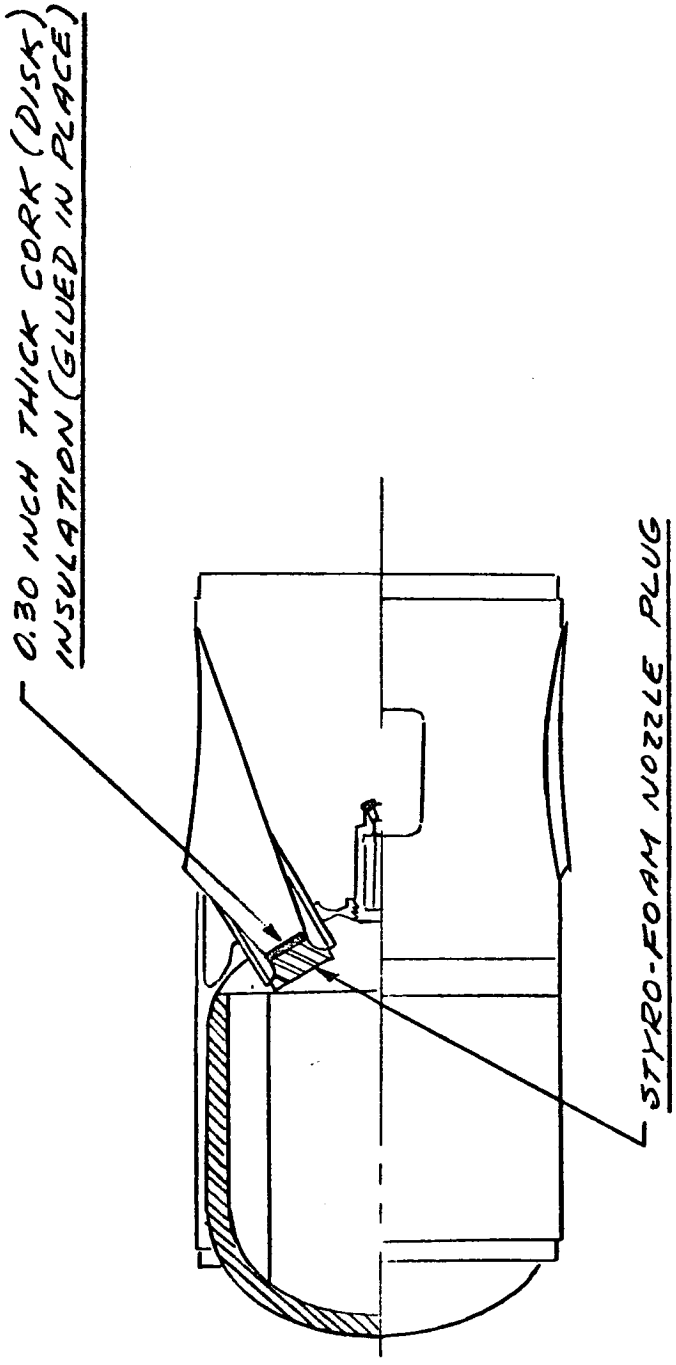

Figure 7.8-4. BP-23A Tower Jettison Motor With Nozzle Plug Insulation

[redacted]

~~CONFIDENTIAL~~

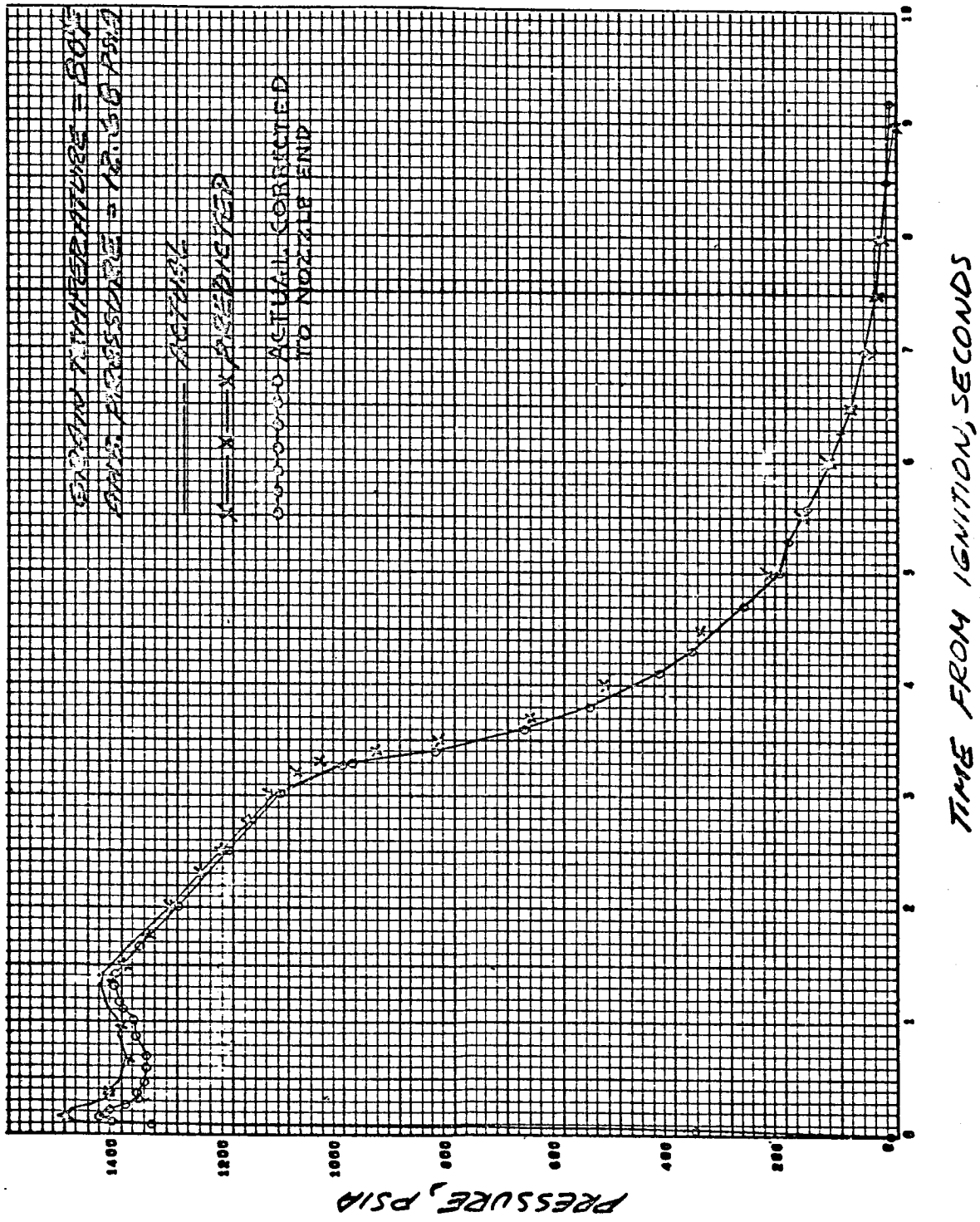

Figure 7.8-5. Launch Escape Motor Pressure-Time History

~~CONFIDENTIAL~~

[redacted]

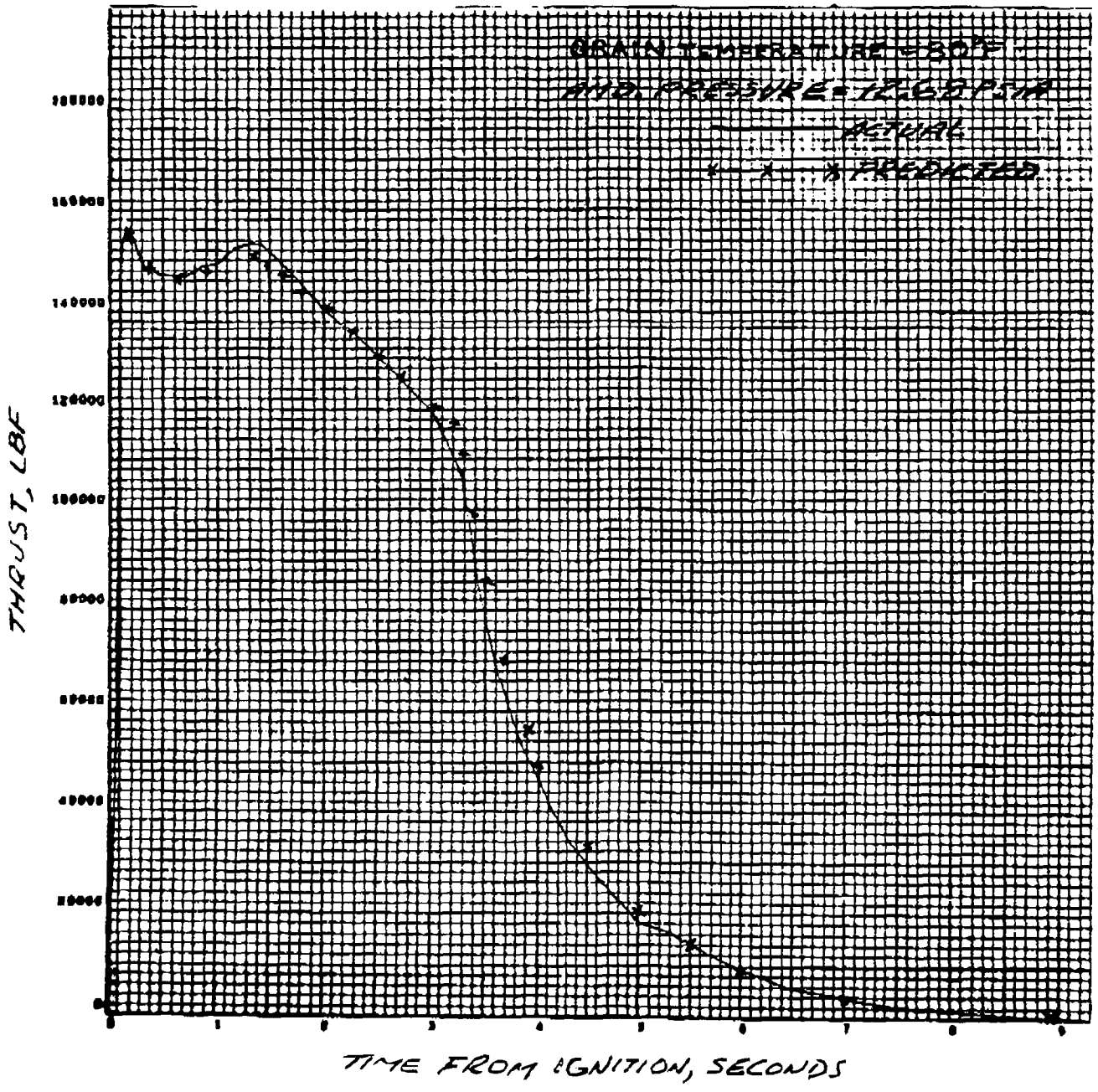

Figure 7.8-6. Launch Escape Motor Thrust-Time History

[redacted]

JSC LIBRARY FAX:2814852327 OCT 14 2005 9:08 P.04

[redacted]

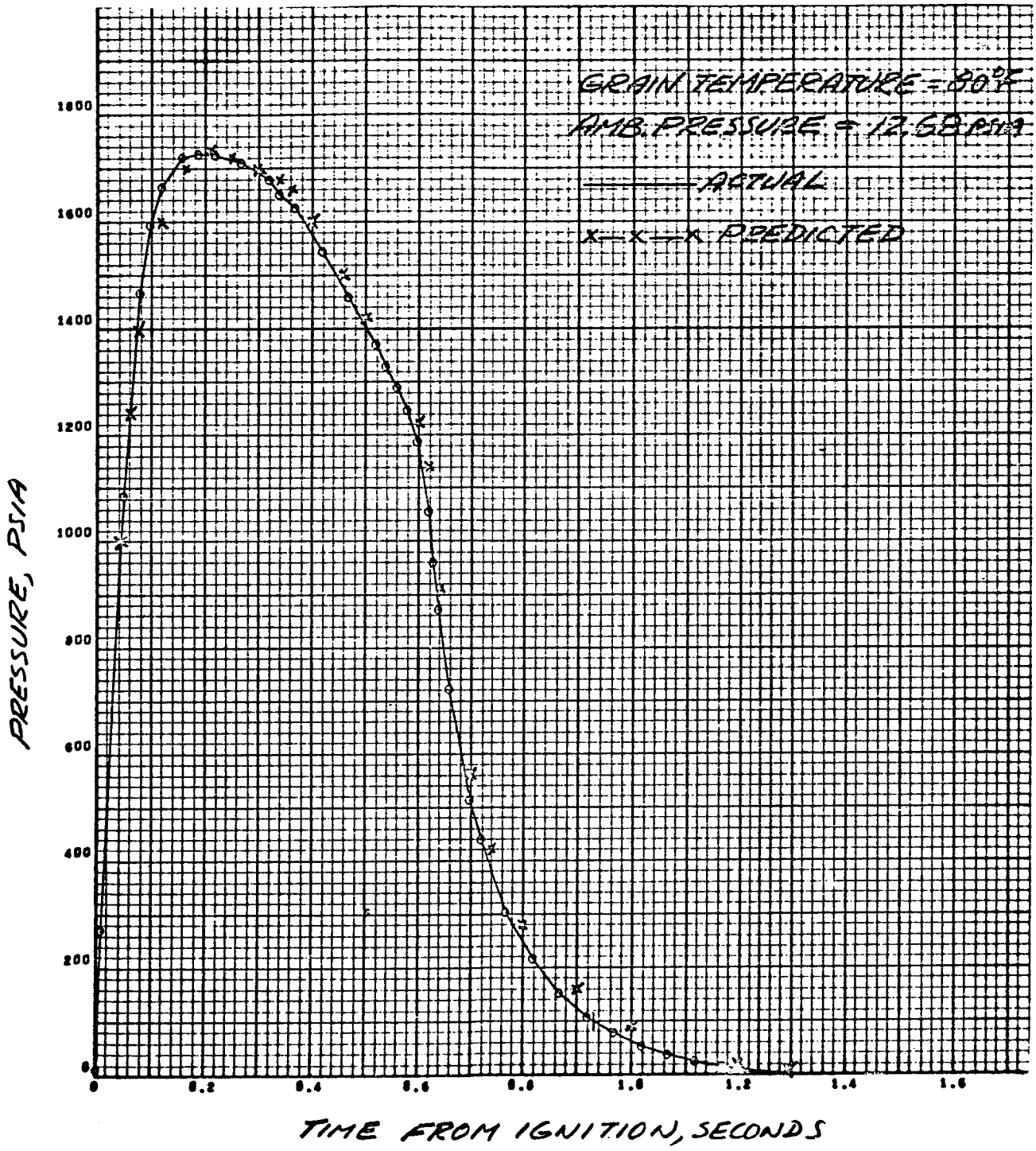

Figure 7.8-7. Pitch Control Motor Pressure-Time History

[redacted]

[redacted]

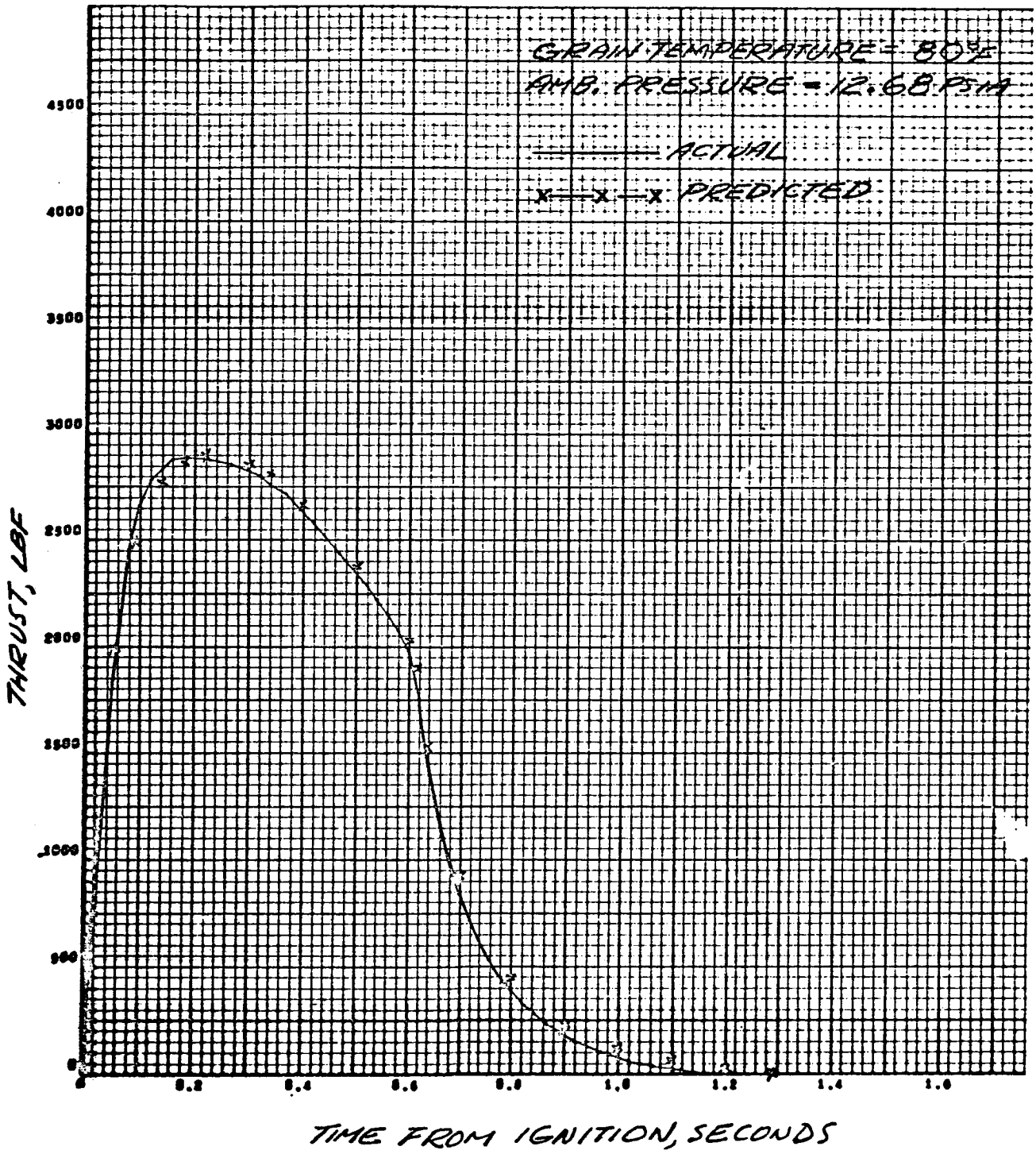

Figure 7.8-8. Pitch Control Motor Thrust-Time History

[redacted]

[redacted]

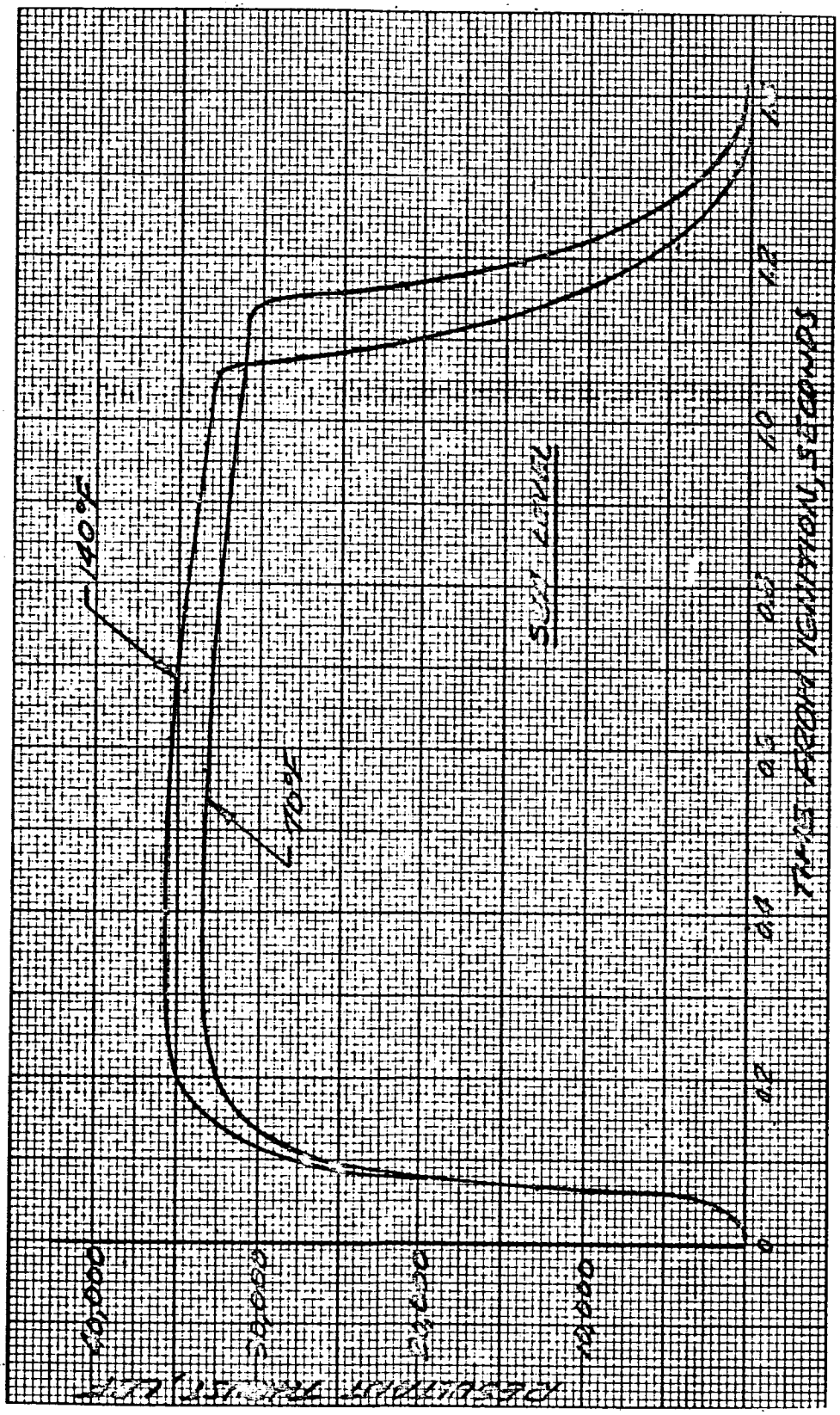

Figure 7.8-9. Tower Jettison Motor Predicted Thrust-Time History

[redacted]

[redacted]

7.9 ELECTRICAL POWER SUBSYSTEM

Summary

The electrical power subsystem performed satisfactorily during the flight of Boilerplate 23A. The main bus voltages remained constant at approximately 30 volts. The logic bus voltages varied from 32.5 to 31.5 volts. The pyro bus voltages remained above 36 volts throughout the flight except for pyrotechnic firing transients and except for a voltage decrease on bus B to approximately 30 volts for a period of 0.4 second during which a short circuit existed in the apex-cover thruster subsystem B.

The pyro batteries for this mission were of the new MAR 4249 type. The flight and postflight tests of the new batteries were entirely successful.

Subsystem Description

The electrical power subsystem supplied d-c power to the instrumentation and communications subsystems (telemetry equipment, transducers, and the tape recorder), to the earth landing subsystem sequencers, to the launch escape subsystem sequencers, and to the pyrotechnic devices on the spacecraft. The electrical power source consisted of five silver-zinc batteries. The subsystem is described in reference 7, section 4.2.6. The subsystem differed from the Boilerplate 23 configuration only in the substitution of two new-type pyro batteries for the four batteries used before.

The main battery, type MAP 4095 (20 cells, 120 ampere-hours at 12-ampere discharge rate), supplied power to the main A and B buses and in turn to the instrumentation and communications equipment. The logic power was supplied to the sequencer subsystem by two type MAR 4090 batteries (18 cells, 6 ampere-hours at 1-ampere discharge rate). Both these types were flown on previous boilerplate vehicles and are not the type which will be flown in spacecraft vehicles.

The two new-type pyrotechnic batteries, type MAR 4249 (20 cells, 5 ampere-hours at 10-ampere discharge rate), supplied power to fire the onboard pyrotechnic devices. This was the first flight test of the battery; however, it is not the type which will be flown in spacecraft vehicles.

Preflight Battery Preparation

The MAP 4095 and MAP 4090 batteries were activated and charged in conformity with the procedures adopted for Boilerplate 15 and Boilerplate 23 (references 6 and 7).

[redacted]

[redacted]

The MAR 4249 batteries were activated and charged in conformity with the procedures outlined in OCP-A-1102-BP-23A. These batteries required a deep discharge prior to charging.

During the preparation of the MAP 4095 batteries, a considerable amount of cell destruction occurred. The cause of the destruction was found to be folding of the nylon separators between plates of opposite polarity. This folding permitted short-circuiting between plates and consequent cell destruction. Close monitoring of the flight and spare batteries was initiated, and several defective cells were discovered and replaced. The manufacturer was made aware of this quality-control problem, which should not recur.

Flight Performance

The main bus voltages remained at approximately 30 volts throughout the flight. Total current demand prior to liftoff was approximately 14 amperes, and decreased to 12 amperes at liftoff and 11 amperes at tower jettison (T + 13.9 seconds).

At liftoff, both logic batteries read 32.5 volts. The voltage level of both batteries dropped to 31.5 volts when the ELS sequence was initiated (T + 13.8 seconds) and remained constant at that level throughout the remainder of the flight.

The pyro battery voltages remained above 36 volts except for pyrotechnic firing transients and, in the case of battery B, a decrease to approximately 30 volts for a period of 0.4 second immediately following firing of apex-cover thruster subsystem B (T + 14.3 seconds). This 0.4-second transient was attributed to a short circuit in the initiator circuit. The voltage was restored to the normal level when the load was removed by the opening of the protective fuse in ELS sequencer B.

Postflight Tests

The results of the postflight tests performed on the MAR 4249 batteries are:

Load	Serial No. 25		Serial No. 26	
	Volts	Amperes	Volts	Amperes
No load	37.1	---	37.1	---
1.50 ohms	30.1	20.1	30.3	20.2

[redacted]

Load	Serial No. 25		Serial No. 26	
	Volts	Amperes	Volts	Amperes
1.00 ohm	27.8	27.8	28.1	28.1
0.75 ohm	26.1	34.8	26.6	35.5
0.50 ohm	23.6	47.2	24.1	48.2

Conclusions

All five batteries gave satisfactory performance. The results of the postflight test indicate superior performance, full charge, and no degradation of the MAR 4249 pyro batteries as compared with the minimum performance of the MAR 4090 batteries used for previous missions. The MAR 4249 bus B battery additionally withstood the 0.4-second short circuit in the apex cover jettison subsystem discussed in section 7.7.

The battery bus voltages from the onboard tape recorder did not include the low-voltage spikes that were found in the telemetry data when no events were occurring. These low-voltage spikes were attributed to noise.

[redacted]

7.10 INSTRUMENTATION SUBSYSTEM

Summary

The instrumentation subsystem performed satisfactorily throughout the flight and, within the specified application limits, provided good data. The rate and attitude gyros and the Q-ball were especially limited and provided useful data only for a portion of the flight as discussed herein. A minor loss of onboard commutated data for the period T + 0 to T + 1.3 seconds involved a short-duration problem in the DPDM circuit of the 90 x 10 commutator. In that the corresponding data were received by the ground station, the PAM circuit of the 90 x 10 commutator was not affected by the problem.

An analysis of the flight data indicates the maximum inaccuracy due to instrumentation calibrations, airborne telemetry, and ground station playback was ±5 percent.

The description and the performance of the altitude-indicator special instrumentation are given in section 7.16.

Subsystem Description

The vehicle development flight instrumentation was NASA-furnished R&D instrumentation and, with the exceptions noted herein, of the types used previously on boilerplate flight vehicles. This instrumentation will be replaced with NAA-designed instrumentation for the Block I spacecraft. The principal difference between BP-23A instrumentation and that used on BP-23 was the deletion of heat-flux, strain, canard-displacement, and fluctuating-pressure measurements. Further, the number of static-pressure measurements was reduced approximately 50 percent, and only three temperature measurements were required. The altitude indicator measurements were new and required the use of two continuous telemetry channels.

The instrumentation block diagram is presented in Figure 7.10-1. An itemization of the measurements and sensor locations is presented in reference 2. The two onboard camera locations are given in Figure 7.10-2. A detailed description of the instrumentation equipment and operation is included in the Boilerplate 23 Instrumentation Manual, reference 12.

The instrumentation subsystem included one differential PDM (90 x 10 commutator) and one PAM/FM/FM telemetry subsystem, a 14-track onboard tape recorder, and the required transducers and associated signal-conditioning equipment. The subsystem is similar to the one used in BP-23 but did not include a low-level signal commutator subsystem (90 x 1.25). All data were transmitted by the air link and were routed also to the onboard tape recorder to provide, normally, a backup data source. The onboard tape

 [redacted]

data, however, because of some noise on the ground station tape, were selected as the primary data source for the final telemetry data package. Selected ground station data were used as a basis for flight dynamics analysis discussed in section 7.1.

Subsystem Performance

The R&D instrumentation subsystem performed satisfactorily and provided good data within the application limits discussed herein.

One minor exception involved the onboard commutated data loss, for the period T + 0 to T + 1.3 seconds, which resulted from a short-duration problem in the DPDM circuit of the 90 x 10 commutator. In that the PAM circuit of the 90 x 10 commutator was not affected, no corresponding loss in ground station data was encountered.

Instrumentation Application Limits

Because of their application limits, the Q-ball and the attitude gyros recorded usable data only for part of the flight. The LES tower camera normally is limited by sooting, although in this flight almost its entire roll of film was run before the lens was covered with soot.

Q-Ball

The Q-ball is a nose-mounted dynamic pressure (q) and air-flow direction sensor; it measures the vehicle dynamic pressure, the angle of attack (pitch), and the angle of sideslip (yaw) through three differential-pressure sensors on the vehicle spherical nose surface. The interim design used in the flight boilerplates is to be replaced with units from MSFC for Block I spacecraft.

Inherently, the Q-ball has limits of ±40 degrees in the angle of attack. An additional limit exists with dynamic pressures less than 100 psf, where the data are inaccurate because of limited low-range resolution. While not of consequence for this flight, the maximum q values are limited to 1250 psf.

The Q-ball flight data were acceptable for the period of T + 1.4 to T + 11 seconds, approximately. The performance of the Q-ball, and the required calibration corrections to wind-tunnel data, are discussed in detail in section 7.1.

Attitude Gyroscopes

Three separate attitude gyros of a two-degrees-of-freedom gimbal configuration were mounted in the command module to indicate roll, yaw and

pitch attitudes of the vehicle. These gyros were similar to those previously flown in boilerplate vehicles, with the exception of those in Boilerplate 22; the latter consisted of two separate gyros (also a free gyro type) requiring the use of inner gimbal rotation to obtain three-axis data, and included additional to the BP-23 gyros a servo-driven gimbal to prevent gimbal lock.

The roll-attitude gyro measures ±175 degrees of roll; however, it loses reference with ±85 degrees of pitch or yaw. Hence, reliable data were provided only for the first 13 seconds. Qualitative data were obtained for the period after T + 33 seconds.

The pitch and yaw attitude gyros were limited by design to ±85 degrees of roll; consequently, their data were of value only for the first 5.7 seconds of flight. Failure of the pitch gyro microswitch which caused a false indication of a caged condition, discussed in section 6.0, did not affect the attitude-gyro performance.

The rate gyros in the three-axis package were limited in design to a maximum rate of ±60 degrees per second. This rate was exceeded by the pitch rate and yaw rate gyros during T + 25 to T + 35 and T + 15 to T + 35 seconds of flight, respectively. The roll-rate gyro, however, provided usable data for the entire flight.

Onboard Cameras

Both the LES tower camera and the CM camera operated satisfactorily with a programmed start at T + 2 seconds. Color and quality of footage were excellent. Unexpectedly, almost the entire roll of film (550 feet) in the tower camera was run before the lens was sooted from the LES motor plume. In previous flights, sooting of this camera lens seriously limited the amount of usable film.

Conclusions

The principal source of difficulty involved application of the gyroscopes. Additional testing, by NASA or by NAA if directed, is required in preflight simulations with the gyros for the SC-002 flight to increase the amount of useful data obtainable through better application of the gyroscopes.

The tests should be performed on a three-axis table and should determine the best initial gyro axis orientation to obtain reliable data during each specific vehicle maneuver predicted for the flight. The tests should determine also whether one or two additional gyros should be installed to measure any particular vehicle maneuvers not covered by the gyros now on board.

[redacted]

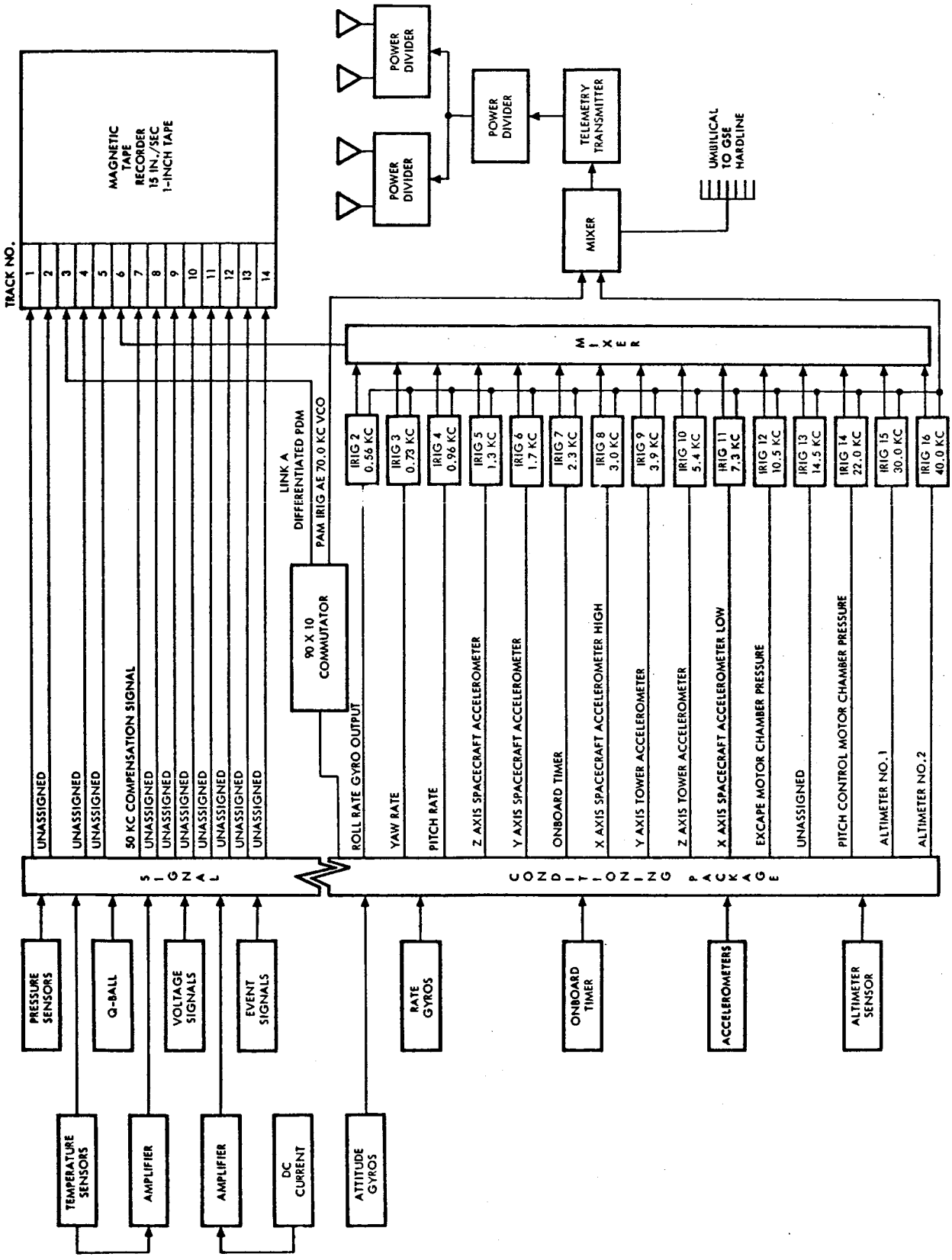

Figure 7.10-1. Boilerplate 23A Instrumentation Diagram

[redacted]

[redacted]

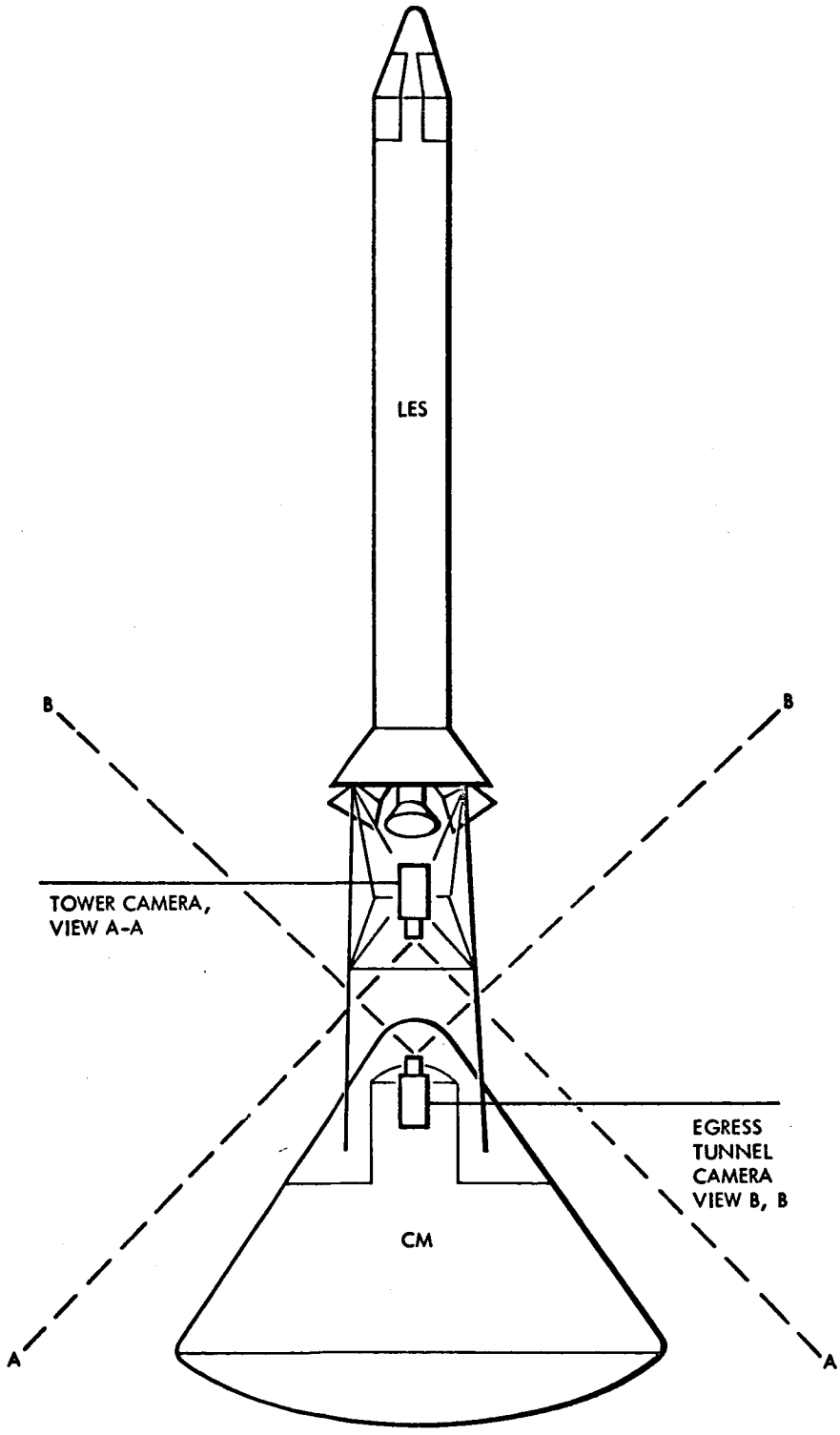

Figure 7.10-2. Boilerplate 23A Onboard Camera Locations

[redacted]

7.11 COMMUNICATIONS SUBSYSTEM

Summary

All elements of the communications subsystem performed satisfactorily. Radio-frequency links of good quality were provided during countdown and flight. The onboard tape recorder data, however, were of better quality than the data from the ground station tape, a few sections of which contained noise.

Subsystem Description

The communications subsystem for Boilerplate 23A consisted of one NASA-supplied VHF PAM/FM/FM unit, with associated antenna subsystem for the transmission of instrumentation data (Figure 7.10-1). The equipment, similar to that used on previous boilerplate flights, was not typical of the equipment which will be used on the spacecraft vehicles.

Telemetry Subsystem

The telemetry data acquisition subsystem consisted of the modulator and RF packages (containing the necessary voltage-controlled oscillators, mixers, and calibrator) that were required to multiplex the continuous signals and transmit the composite signal to the supporting ground stations. The transmitter output thus included the one commutated and the 14 continuous subcarrier channels in standard IRIG configuration; output power was 10 watts at a carrier frequency of 247.3 megacycles.

Telemetry Antennas

The transmitter output was fed to four cavity-type VHF antennas via three two-way reactive power dividers.

Telemetry Transmitter Performance

The telemetry transmitter performed satisfactorily and provided data of good quality. Temperatures of the exciter and the power amplifier remained well within limits. Adequate circuit margin was provided, and continuous VHF coverage was evidenced by range reports on received signal levels.

7.12 ELECTROMAGNETIC COMPATIBILITY

The data from the Boilerplate 23A telemetry system and the onboard recorder were examined for electromagnetic interference anomalies which might have caused a subsystem malfunction or which might have degraded the data. The period from T - 4 seconds to command module landing was covered.

There is no evidence of significant electromagnetic interference. The overall appearance of the data is clean, and the noise level is within the allowable limit of ±3 percent.

[redacted]

7.13 DATA COVERAGE AND AVAILABILITY

Summary

Overall coverage of the mission was satisfactory. The optical tracking, photographic, and meteorological data were good. Locations of the range telemetry, meteorological, and camera stations are given in Figures 7.13-1 and 7.13-2.

Delivery of most data on the Boilerplate 23A mission was more timely than has been the case with other missions conducted at WSMR.

Photographic Coverage

Photographic coverage of the mission was good. All events were recorded in sufficient detail to satisfy postflight analytical requirements. All reproductions were of good quality.

Tracking Telescopes

Seven 16-mm copies of films from tracking telescopes were received 2 days after the flight.

Cinetheodolite

Five 16-mm copies of films from cinetheodolites were received 2 days after the flight.

Clock Cameras

Five 16-mm copies of films from high-speed fixed cameras were received 2 days after the flight.

Onboard Cameras

Copies of the films from the two onboard cameras were received 16 days after the flight.

Still Photography

Preflight and postflight still photographic coverage was good. Duplicator copies were requested; however, only one copy of postflight pictures was received at Downey, approximately 27 days after the flight. Previously, NAA letters of transmittal have aided in tracing misdirected

[redacted]

or misdelivered photographic documentation. Apparently no such letter was issued to cover transmittal of Boilerplate 23A photographs, and the problem of tracing the elusive package was therefore compounded.

Tracking Data

All tracking data were acquired by optical equipment. Radar tracking was not available because for the low-altitude abort the C-band transponder was not installed in the vehicle. A magnetic tape containing position data was received 8 days after the flight, but within 2 days it was found that the data were referenced to the wrong launch pad. These data were corrected and released as preliminary data. Final corrected tape data were received from WSMR 21 days after the flight. All data were edited and smoothed at Downey before release.

Attitude Data

A magnetic tape containing pitch and yaw optical attitude data was received 28 days after the flight. While it is considered correct, these data have not been designated as final. No roll data have been received; because of field difficulties, these data are not expected until 6 months after the flight.

Meteorological Data

A deck of IBM cards containing meteorological data was received 7 days after the flight. The data were satisfactory.

Telemetry Data

Magnetic tapes from three stations were received 14 hours after the flight and a tape from a fourth station was received 7 days after the flight. The tape from station J-56, included in the first three tapes, was used to provide quick-look data but was found to be noisy.

A copy of the magnetic tape from the onboard recorder was received 2 days after the flight. The data on this tape were cleaner than the data from the J-56 tape; consequently the onboard recorder tape was selected as the prime source of data.

Conclusions

Data coverage and quality were good. Delivery was more timely than in the past.

[redacted]

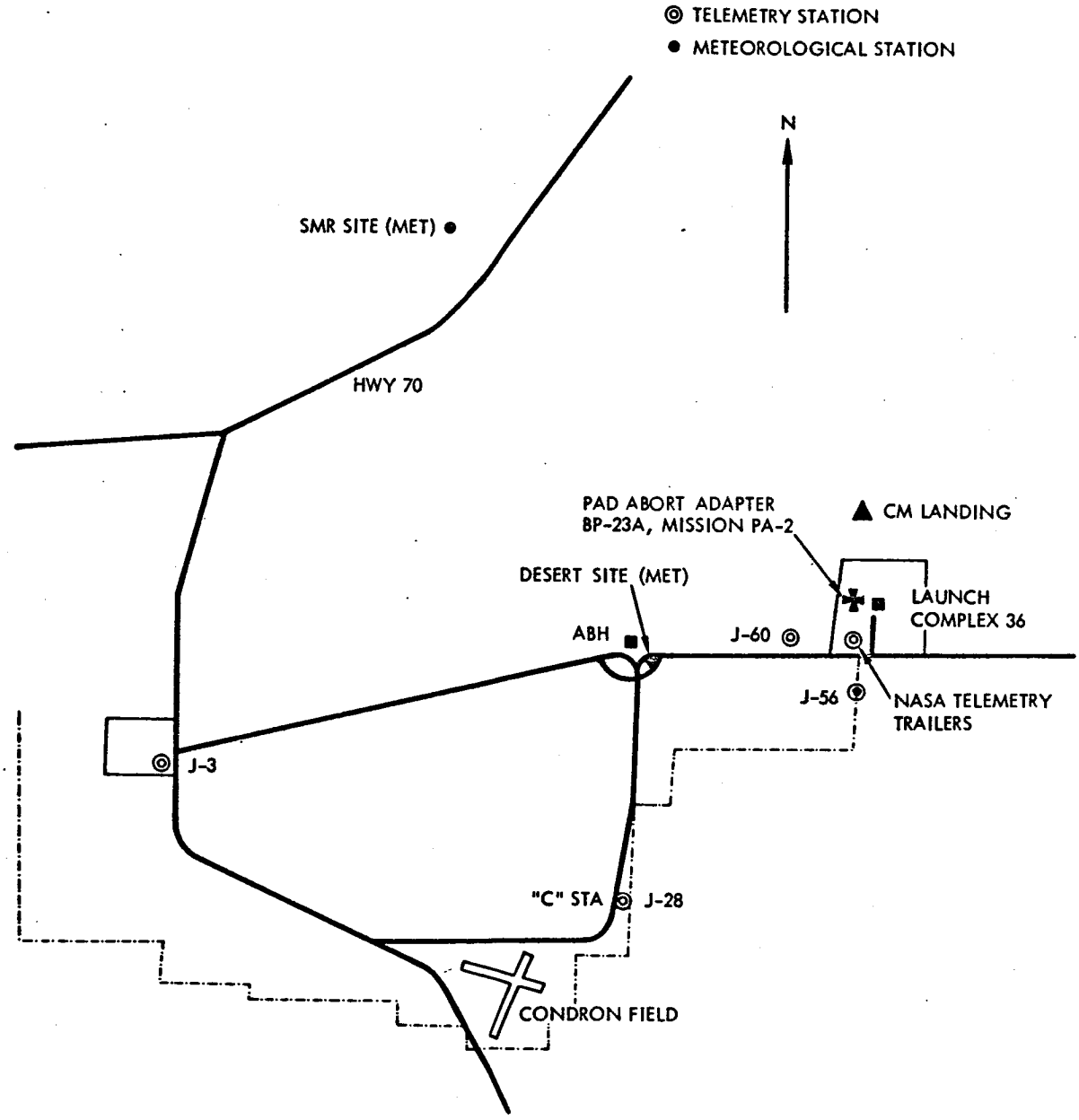

Figure 7.13-1. Telemetry and Meteorological Station Locations for Mission PA-2

~~CONFIDENTIAL~~

[redacted]

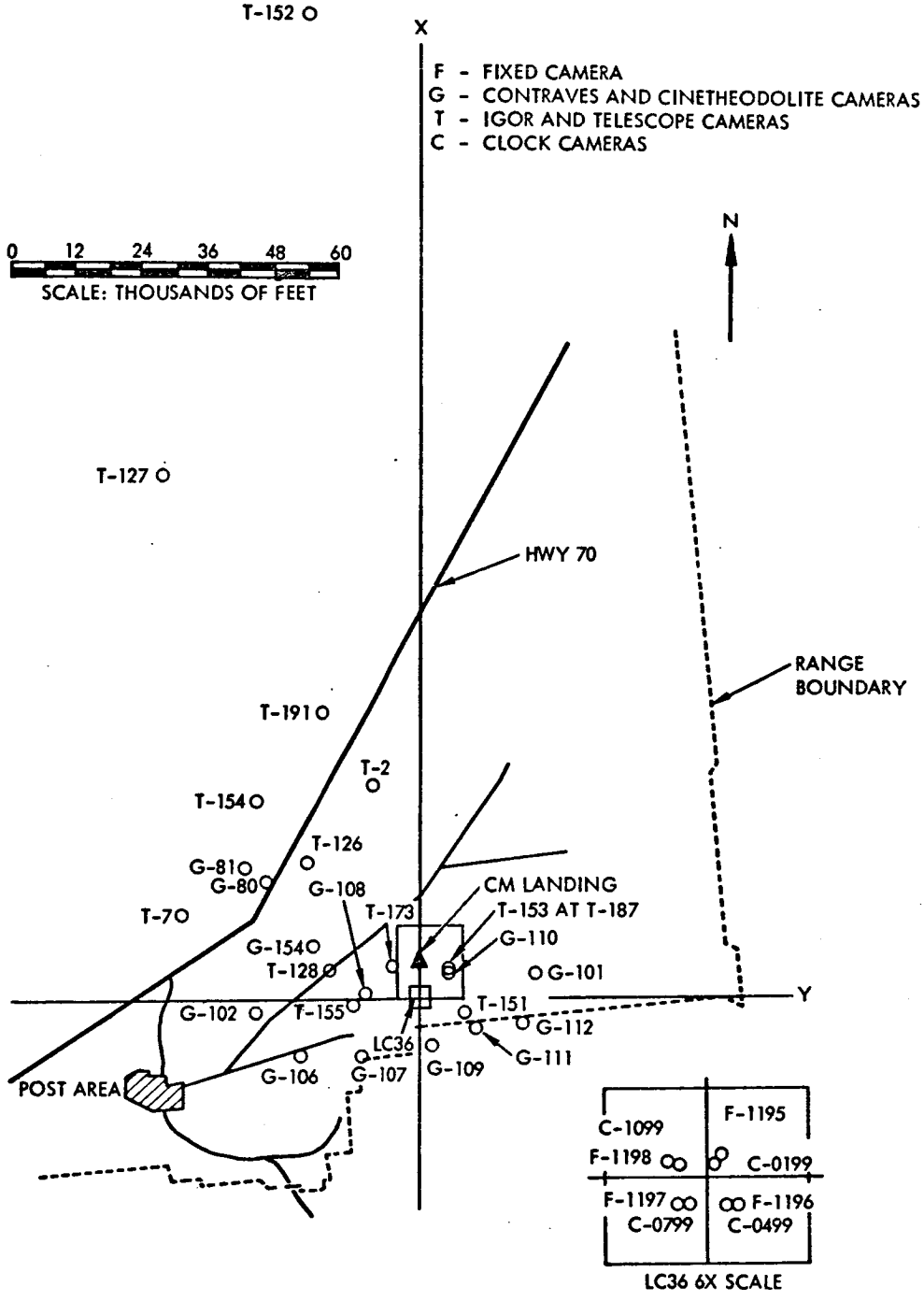

Figure 7.13-2. Camera Locations for Mission PA-2

[redacted]

[redacted]

7.14 GROUND SUPPORT EQUIPMENT

Summary

Eighty items of ground support equipment (GSE) were used for the checkout, launch, and recovery of Boilerplate 23A at WSMR. Of these items, seventy-seven performed satisfactorily. Thirty-nine are to be used with spacecraft operations.

The three items which did not give satisfactory performance were the H14-142 LES Socket, the H14-074-101 Spacecraft Sling, and the H14-9015 Weight and Balance Set.

The H14-142 could not be used and a piece of special equipment was fabricated as a substitute for use with Boilerplate 23A. A new piece of equipment will be designed for spacecraft operations.

The H14-074-101 and the H14-9015 were difficult to use, but are not considered to require redesign. Consideration is being given to changes in the operating procedures to decrease the difficulties encountered in using these pieces of equipment.

Introduction

The ground support equipment used to support Boilerplate 23A operations is discussed herein under the following categories:

(a) Equipment which did not perform satisfactorily;

(b) Equipment not used;

(c) Equipment modified or fabricated at WSMR which performed satisfactorily;
Equipment modified at WSMR from BP-22 configuration to meet BP-23A requirements;
Equipment modified at WSMR from BP-23 configuration to meet BP-23A requirements;
Equipment modified at WSMR from BP-6 configuration to meet BP-23A requirements;
Special Test Equipment (STE) designed and fabricated at WSMR under test preparation sheet (TPS) authorization;

(d) Equipment which performed satisfactorily without modification

[redacted]

Equipment Which Did Not Perform Satisfactorily

H14-074-101 Spacecraft Sling

This sling is used for erection and stacking of the LES on the CM.

This sling is very difficult to install and remove when the launch escape subsystem is stacked on the command module. The installation or removal procedure requires a man to hoist himself with the H14-093 boatswain's chair to secure part of the sling. Methods for decreasing the difficulty are under consideration.

H14-9015 Weight and Balance Set

This set is used to hold the CM during weight and balance operations.

The operation of positioning the command module on the three jacks of the weight and balance set was very difficult to perform. If the spherical seats of the load cells were not exactly in line with the CM jack pads, they tended to rotate and let the CM slip off the load cells and jacks; methods for reducing the difficulty of this alignment procedure are under consideration.

H14-142 LES Socket

This socket is used with a standard wrench for installation of the single-mode explosive bolts.

This socket could not be used because of difficulty in holding the socket in mesh with the bolt; therefore an STE wrench was fabricated at WSMR per TPS 22-GSE-59. A wrench of new design will be available for spacecraft flights.

Equipment Not Used

H14-018 Escape Tower Support

This unit is used to support the launch escape tower for mating with the launch escape motor.

It was not necessary to use this unit, as its function was performed adequately by the tower sling.

[redacted]

[redacted]

H14-044 Parachute Handling Sling

This sling facilitates the handling of the main parachute while packed inside its deployment bag.

The sling was not used, as the parachutes were handled manually.

H14-096 LES Ballast Pickup Hook

This hook is used to hoist and position the LES ballast plates for installation on the LES ballast support frame.

The hook was not used, as the ballast plates were handled manually.

C14-112 C-Band Radar Checkout Unit

This unit verifies proper operation of the transponders by checking power output receiver sensitivity, bandwidth, frequency, pulse jitter, crystal current, and interrogation.

The C-band equipment was not included in this low-altitude flight.

Equipment Modified or Fabricated at WSMR Which Performed Satisfactorily

Equipment which was modified at WSMR from BP-22 configuration to meet BP-23A requirements, and which performed satisfactorily, included:

A14-003-101 Pyrotechnic Initiators Substitute Set

This set substitutes for the pyrotechnic initiators during spacecraft subsystems checkout.

The set was modified to add capability for checkout of the BP-23A apex thrusters. The change was accomplished by EO 295645.

C14-019 Test Conductor Group

This console is used to centralize the monitoring and control of subsystem functions exercised during prelaunch preparations and countdown.

The unit was modified in order to make it compatible with the BP-23A gyro and telemetering equipment. In addition, a pad-abort initiator switch was added. Changes were accomplished under MCR-A 825 by EO 211576, 211577, 211579, and 356155.

[redacted]

C14-135 Signal Conditioner

This unit is used to provide current amplification and isolation for low-level signals originating in the spacecraft.

Modifications include addition of an abort-initiate relay for pad-abort firing. Changes were accomplished under MCR-A 825 by EO 280029, 211566, and 356931.

C14-457 Blockhouse Junction Box

This unit is used to interconnect cabling from the barricaded structure to the C14-019 test conductor console.

Modifications included the routing of the gyro case monitor (yaw) function to the C14-019 console. Changes were accomplished by EO 356756.

C14-552 Electrical Terminal Distributor

This unit provides connection points for the associated cable set which connects to the GSE, the CM, and the launch escape tower.

This unit was rewired to the BP-23A configuration by EO 211562, 211653, and 211565.

Equipment which was modified at WSMR from BP-23 configuration to meet BP-23A requirements, and which performed satisfactorily, included:

C14-108-31 Electrical Cable Set

This set of cables is used to connect the spacecraft and associated GSE electrically for subsystem tests and launch operations.

This cable set was modified by the addition of one cable and other minor changes. Changes were accomplished by modification list drawing G16-880121.

Equipment which was modified at WSMR from BP-6 configuration to meet BP-23A requirements, and which performed satisfactorily, included:

A14-013 Pad Abort Adapter

This unit is used to support the command module and launch escape subsystem for the abort tests.

The unit was modified to add a larger bracket for support of additional umbilical lanyards. The change was accomplished by EO 294767, 294768, 294769, 356154, and 294763.

C14-171 Pad Junction Box

This unit is used to distribute stimuli and responses to and from the boilerplate vehicle.

The unit was rewired to the BP-23A configuration by EO 294751, 294752, 294753, 294754, 294755, 294756, 294757, 294758, 294759, 294760, 294761, 294762, 356151, and 356152.

Special test equipment designed and fabricated at WSMR which performed satisfactorily, included:

TPS 23A-GSE-13 Tower Lifting Eyes

These lifting eyes were fabricated to provide a means of attachment to the launch escape tower for hoisting.

TPS 23A-GSE-34 Cable Set

This cable set was required to provide apex-thruster firing signals to the squib simulators.

TPS 22A-GSE-59 LES Explosive Bolt Wrench

This wrench, which was also used on Boilerplate 22, was fabricated as a substitute for the H14-142 socket, which would not hold the single-mode explosive bolt satisfactorily during the torquing operation.

Equipment Which Performed Satisfactorily Without Modification

The equipment itemized below performed satisfactorily without modification. The equipment description is included on the following page or in reference 7, section 7.16.

[redacted]

A14-007 LES Optical Alignment Set

A14-010 Command Module Cover

A14-026-101 Cap and Plug Set

A14-036-301 Ground Air Circulating Unit

A14-046 Auxiliary Crane Control (Hydroset)

A14-047 Box Level

A14-128 Parachute Subsystem Installation Kit

A14-134 10-Ton Crane Control (Hydroset)

A14-183 LES Canard Actuator Tool Set

This tool set consists of two special-purpose tools for assembling or disassembling the actuator thruster cylinder and reservoir tube, and disengaging the cylinder collet from the piston rod during manual checkout operations.

C14-002-0002 Baroswitch Test Unit

C14-020 Data Recording Group

C14-029-101 Launch Escape Subsystem - BME

C14-031 Tape Recorder Checkout Unit

C14-032-101 Antenna Checkout Group

C14-051-101 Pyrotechnic BME

C14-108-11 Electrical Cable Set

C14-126 ELS Sequencer - BME

C14-137 Q-Ball Test Fixture

C14-172 Pad Junction Box

C14-174 Telemetry Kit

This kit augments the GFP telemetry equipment and trailer furnished by NASA.

[redacted]

[redacted]

C14-458 Static EMI Checkout Device

This device provides an indication of excess current induced into the pyrotechnic subsystem initiator circuits during static EMI tests.

C14-461 EMI Test Breakout Box Set

This box set provides the test points that enable given circuits to be monitored at specific points for electromagnetic interference.

H14-011 Launch Escape Alignment Stand

H14-016 LES Weight and Balance Fixture

H14-017 Weight and Balance Fixture

H14-021 GSE Handling Cart

H14-029 Structural Skirt Sling

H14-040 Electronic Weighing Kit (3,000-Pound Capacity)

H14-041 Electronic Weighing Kit (30,000-Pound Capacity)

H14-043-101 Jettison Motor Sling

H14-052 Jettison Motor Support

H14-055 Launch Escape Motor Support

H14-057-101 Forward Compartment Heat Shield Sling

H14-083-101 LES Transport Cradle

H14-084-101 Roll-Over Adapter

H14-085-201 LES and LE Motor Horizontal Handling Sling

This sling reduces handling time in weight and balance operations by facilitating alignment of the LES and launch escape motors with different centers of gravity.

H14-086 Boilerplate Tubular Support-Base Assembly

[redacted]

H14-090-301 Recovery Area Access Stand

This stand provides access to the recovery area (parachute deck) of the CM while it rests on its support base or on its support and dolly, vertical alignment fixture, or ground adapter.

H14-093 Boatswain's Chair

H14-094 Jettison Motor, Pitch Control Motor, and Nosecone Sling

This sling facilitates handling during assembly for weight and balance operations prior to complete LES buildup.

H14-097 LES Buildup Access Stand

H14-099 Pitch Control Motor - LES Wrench

H14-101 Access Platform (3 feet to 10 feet)

H14-125 Umbilical Disconnect Spanner Wrench

H14-139 Forward Compartment Heat Shield Retention Bolt Guide

H14-045 Shipping Container Sling

H14-156 LE Tower Horizontal Handling Sling

H14-161 LES Motor Propellant Grain Inspection Set

H14-9001 CM Test Vehicle Sling Set

H14-9006-101 Weight and Balance Sling Set

H14-9014 Test Vehicle Adapter Sling Assembly

This sling is used for hoisting and positioning the ground adapter into transporters and fixtures for acceptance and preflight tests.

H14-9056-101 Heat Shield Sling

H14-9076 General Purpose Dolly

S14-015-101 Electrical Battery Charger

S14-055 R&D Instrumentation Cooling System Servicing Unit

[redacted]

S14-078 LES Rocket Motor Pressure Leak-Test Cart

S14-090 Mobile Pressure Test Unit

This unit checks the pressure leak rate in the CM heat shield separation subsystem and regulates the applied pressure used to check out and calibrate the pressure transducers on the launch escape motor and pitch control motor chambers.

S14-091 Battery Conditioner

This unit provides circuitry for detusking (removing high initial voltage from) the spacecraft batteries prior to installation in the spacecraft. This unit also provides a dummy load used to calibrate battery charging unit S14-015.

GFP-A-015 Maintenance and Storage Trailer

This trailer is a general utility vehicle which provides facilities for repair and maintenance of equipment and provides storage space for tools and equipment.

GFP-A-028 Optical Alignment Set

This equipment is used to establish precise vertical planes within an accuracy of 6 seconds of arc and leveling within an accuracy of 2 seconds of arc.

GFP-A-066 Telemetry Trailer No. 1

This trailer is used to receive and process telemetry data during vehicle flight.

GFP-C-176 Apollo Instrumentation Test Console

GFP-C-419 Instrumentation Tape Recorder - TM Trailer

This tape recorder is used to record telemetry data.

GFP-H-100 Access Platform (13 feet to 20 feet)

This unit is a variable-height platform used to gain access to the vehicle in the range of 13 to 20 feet.

[redacted]

GFP-H-101 Access Platform (3 feet to 10 feet)

This unit is a variable-height platform used to gain access to the vehicle in the range of 3 to 10 feet.

GFP-H-203 Command Module Transportation and Positioning Trailer

This trailer positions, transports, and transfers the CM to different checkout stations.

Conclusions

Except for the problems discussed herein, the ground support equipment used for the mission performed satisfactorily. With respect to the exceptions, the H14-142 LES socket, which was not usable, no longer is a problem in that a newly designed wrench will eliminate it as a requirement for spacecraft operations; consideration is being given to improved field procedures to decrease the difficulty in the use of the H14-074 and the H14-9015.

The following items of GSE, all of which are scheduled for use with Apollo spacecraft vehicles, are now considered to have demonstrated suitability for their proposed use.

A14-007	LES Optical Alignment Set
A14-026-101	Cap and Plug Set
A14-036-301	Ground Air Circulating Unit
A14-046	Auxiliary Crane Control
A14-047	Box Level
A14-128	Parachute System Installation Kit
A14-134	10-Ton Auxiliary Crane Control
A14-183	LES Canard Actuator Tool Set
C14-051-101	Pyrotechnic BME
C14-137	Q-Ball Test Fixture (Analyzer)
C14-458	Static EMI Checkout Device

[redacted]

[redacted]

H14-011	LE Alignment Stand
H14-016	LES Weight and Balance Fixture
H14-017	Weight and Balance Fixture
H14-018	Escape Tower Support
H14-021	GSE Handling Cart
H14-029	Structural Skirt Sling
H14-043	Jettison Motor Sling
H14-044	Parachute Handling Sling
H14-052	Narrow Base Positioning Trailer
H14-054	Jettison Motor Support
H14-055	LE Motor Support
H14-074	Spacecraft Sling
H14-083-101	LES Transport Cradle
H14-084-101	Roll-Over Adapter
H14-085-201	LES and LE Motor Horizontal Handling Sling
H14-093	Boatswain Chair
H14-094	Jettison Motor, Pitch Control Motor, and Nosecone Sling
H14-096	LES Ballast Pickup Hook
H14-097	LES Buildup Access Stand
H14-099	LES Pitch Control Motor Wrench
H14-145	Shipping Container Sling
H14-156	Launch Escape Tower Horizontal Handling Sling
H14-161	LES Motor Propellant Grain Inspection Set

[redacted]

H14-9015	Weight and Balance Set
S14-078	LES Rocket Motors Pressure Leak Test Cart
S14-091	Battery Conditioner
GFP-H-101	Access Platform (3 feet to 10 feet)
GFP-H-203	CM Transportation and Positioning Trailer

7.15 WINDOW SAMPLE ANALYSIS

Sample Description and Installation

Four window-glass samples (aluminosilicate glass, Corning Code 1723) were located on the command module in areas near the Apollo spacecraft side and rendezvous windows, Figure 7.15-1. The window samples, each 4 x 5 inches, were mounted flush to the vehicle surface and under the soft boost cover as in the previous boilerplate vehicle test, reference 8.

Analysis Results

The recovered window samples were analyzed at the WSMR test site by means of visual inspection, visual comparison tests, and light-transmission tests.

The results of the visual inspection of the recovered window samples by NASA and NAA observers indicated that no soot was deposited on the window samples. The samples appeared clean except for a slick film detected on samples A, B, and D. The underside of the boost protective cover also felt slick. In that it was possible for the boost cover to have contacted the window samples, the cover could have been the source of the film.

The visual comparison was made by viewing a lantern-slide projection of the Florida coast alternately through a recovered glass sample and a clean glass sample when both were mounted side by side in a special jig. The astronaut observer stated that visibility through the recovered samples had not been impaired to the point where horizon scan or ground orientation would have been difficult during an abort. It was also stated that visibility had not been reduced sufficiently to affect observations to any significant degree during visual rendezvous and docking maneuvers.

Light-transmission tests were performed as in reference 8 with the recovered glass samples and a clean glass sample. Each of the four recovered glass samples exhibited 5 percent greater loss than the reference sample in the transmission tests.

Conclusions

The window samples recovered after this flight were not sooted, and they did not show any significant decrease in visibility.

These results, however, do not eliminate sooting completely as a possible problem in all flights. In this flight, during tower jettison and boost cover breakup, the vehicle pitch and yaw maneuvers placed the command module out of the motor plume and eliminated the possibility of

[redacted]

sooting. Sooting could not have been severe, in any case, in that the LE motor was essentially spent, with the motor plume barely reaching to the CM soft boost cover.

[redacted]

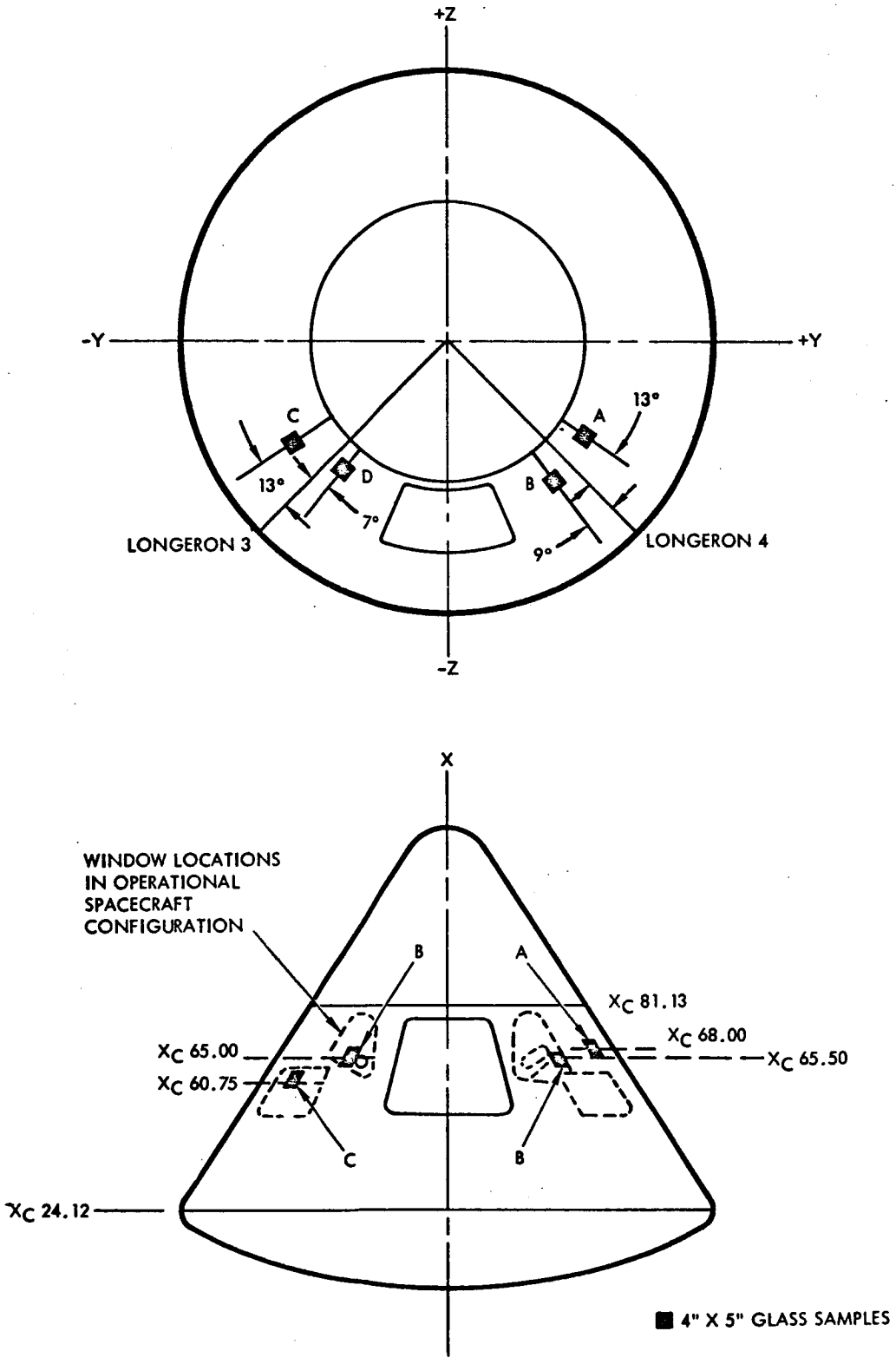

Figure 7.15-1. Window Sample Locations for Mission PA-2

[redacted]

7.16 ALTITUDE INDICATOR TEST

An altimeter employing a high-sensitivity pressure transducer will be provided on spacecraft. The altitude indications will inform the astronaut when to deploy the main parachutes in the event of a critical condition associated principally with an abnormal launch in a low-altitude abort.

To obtain data on measurement accuracy and porting locations for the spacecraft installation, two transducers were installed as shown in Figure 7.16-1. For the No. 1 transducer a new pressure port was located on the parachute deck (near the spacecraft barostatic reference port location), and for the No. 2 transducer use was made of the existing top ELS baroswitch tee port.

Off-the-shelf but qualifiable pressure transducers of the strain-gage type were field-calibrated and installed. Calibration data at temperatures covering the expected flight temperature range of the CM interior (10 to 15 degrees F change from initial temperature) were obtained. As normally would be found with self-contained reference-pressure transducers (one pressure port sealed) no appreciable calibration change resulted with the small temperature range involved. During periods when aerodynamic effects were negligible, flight data confirmed satisfactory calibration of the transducers and measurement accuracy of the subsystem.

Figure 7.16-2 presents the pressure history from the two taps. The selected telemetry pressure data presented have been machine-smoothed to eliminate scatter from the measuring subsystem and have been biased to ambient conditions at the pad. The onboard data had a scatterband of approximately 0.15 psi before smoothing, and the telemetry data had somewhat less (reference Figure 7.1-62). After apex-cover jettison the pressure pickup located on the parachute deck generally read about 0.15 psi below ambient and the pickup located on the egress tunnel read about 0.25 psi below flight ambient pressures.

Since altitude is a linear function of the flight ambient pressure P_∞, and $P_\infty = P_L - C_p q$, where P_L is the measured pressure, C_p is the pressure coefficient, and q is the dynamic pressure, a location on the vehicle for an altimeter should be chosen such that $C_p = 0$. P_L then equals P_∞ and local pressure can be converted directly to altitude. However, if $C_p \neq 0$, as with BP-23A, then q must be measured before an altitude can be calculated. If q and C_p can be considered constant (the q range during drogue descent is narrowly limited during a pad-abort mission) then the measured pressure will be different by a constant amount, and the altimeter can be calibrated accordingly.

[redacted]

Non-dimensional pressure coefficients for the two pressure tap locations are presented in Figure 7.16-3. The pressure coefficient measured at the spacecraft baro-reference pressure pickup location is shown to be approximately -0.65 ± 0.25. The C_p measured on the side of the egress tunnel was approximately -1.10 ± 0.30. This indicates that the parachute deck is a better location for the altimeter than the side of the egress tunnel. The large variations in C_p shown on the curves are due to low flight dynamic pressure. For example, a 0.1-psi change in measured pressure with a dynamic pressure of only 0.2 psi will give a 0.5 change in pressure coefficient.

In Figure 7.16-4, computed altitude based on the measured local pressure is compared with the true altitude from T + 14 to T + 29 seconds. Comparison of the curves shows that the pressure tap located at the baro-static reference pressure location resulted in altitude indications approximately 250 to 300 feet above true altitude. Altitude indicated from the pressure tap located on the egress tunnel is approximately 500 feet above the true altitude. It should be noted, however, that the altitude shift is approximately constant in both cases for the time span shown and the associated altitude of 9200 to 7800 feet msl. This indicates that a bias technique can validly be used to compensate for the base pressure effect in the calibration of the spacecraft altitude indicator.

Prior to apex-cover jettison, venting of the parachute compartment also would cause some error. As indicated in Figure 7.16-2 by the close agreement in the data of CE0035P, CE0036P, and CA0027P, the error was negligible in this flight. In that the only period of interest is after apex-cover jettison and through drogue descent, T + 14 to T + 28.6 seconds, the error is not of consequence. Additional details are included in Section 7.1.

~~CONFIDENTIAL~~

[redacted]

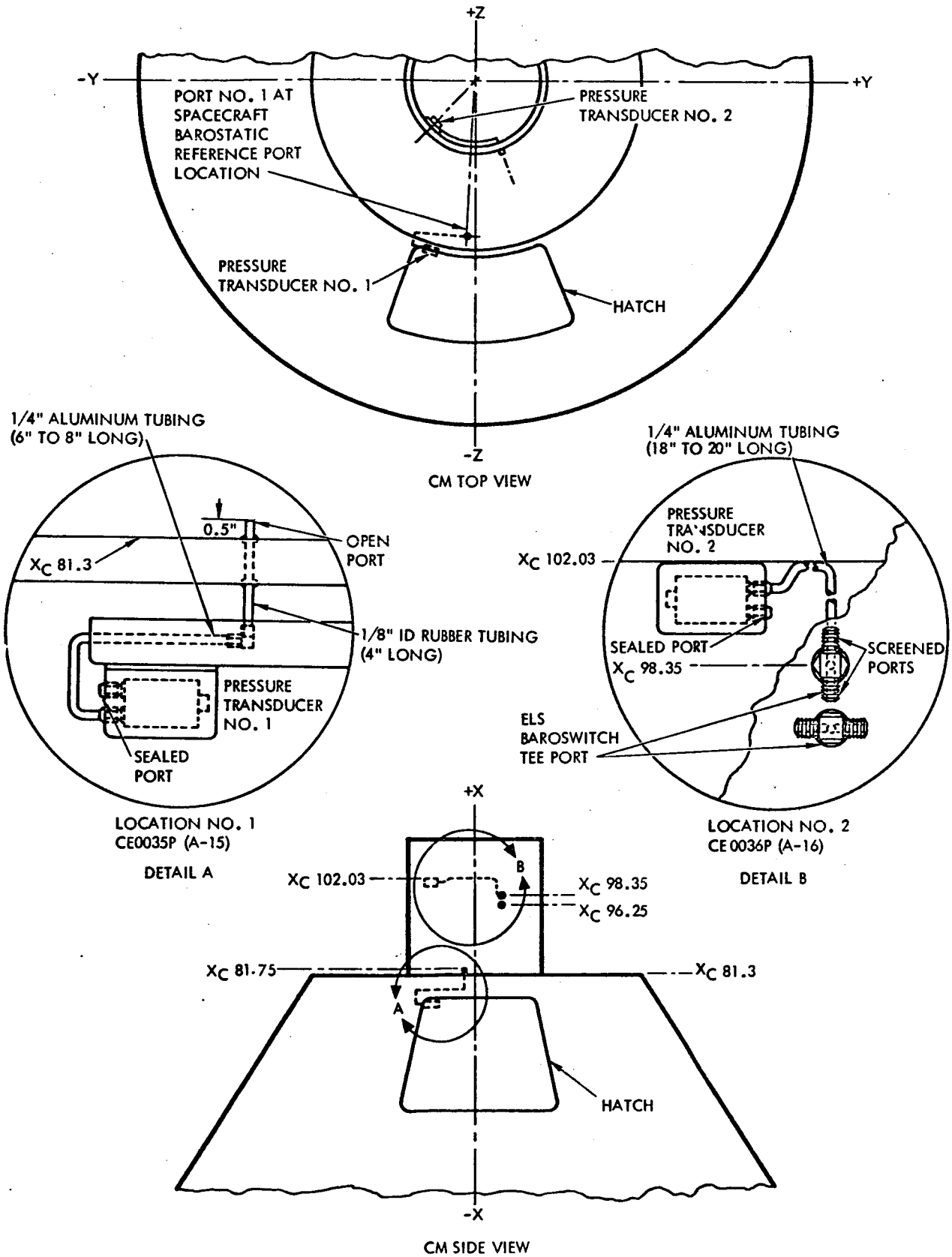

Figure 7.16-1. Locations of Transducers and Pressure Ports, Altitude Indicator Test, Mission PA-2

[redacted]

[redacted]

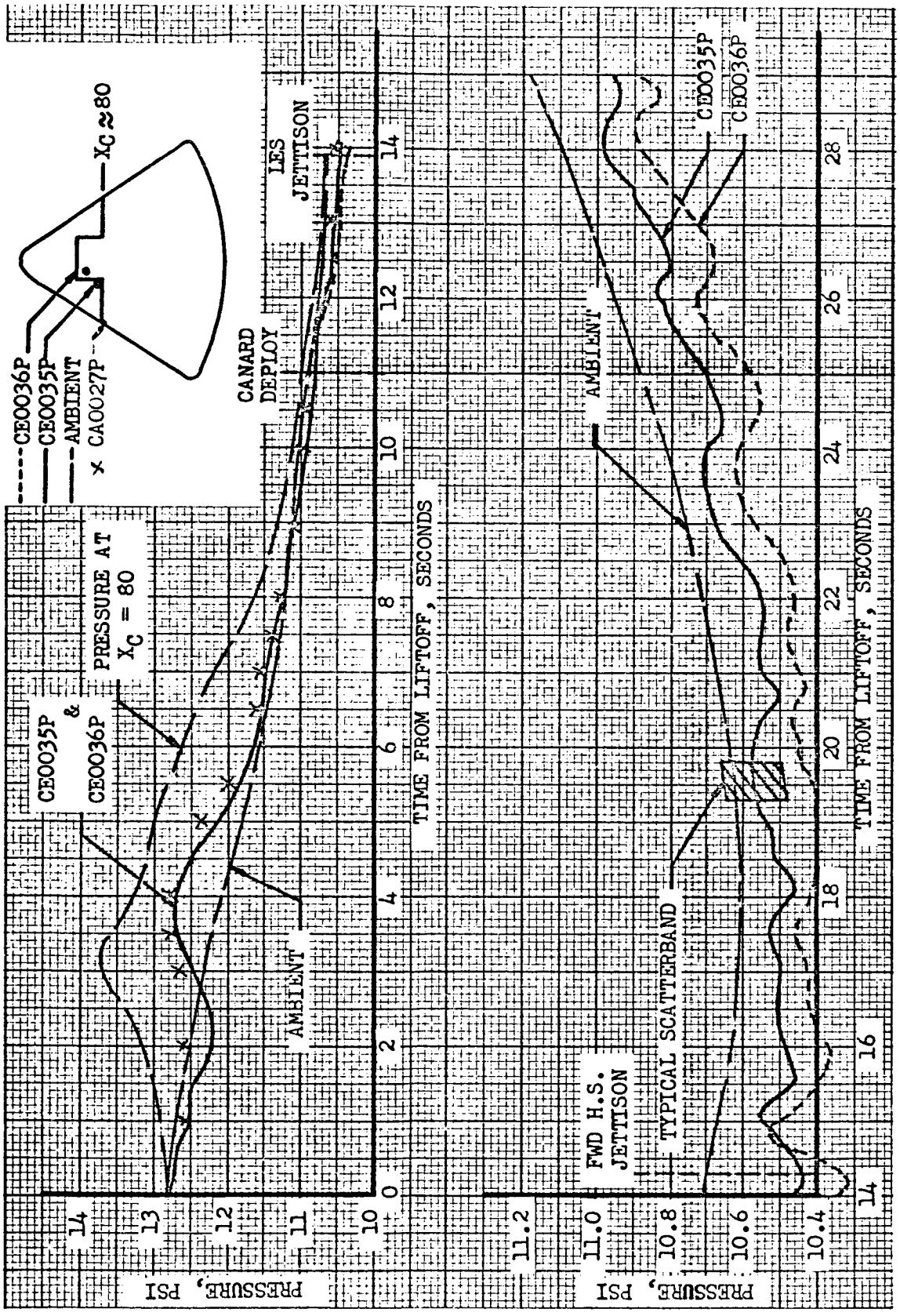

Figure 7.16.2 Smoothed Baro-Reference Pressure Time History

[redacted]

[redacted]

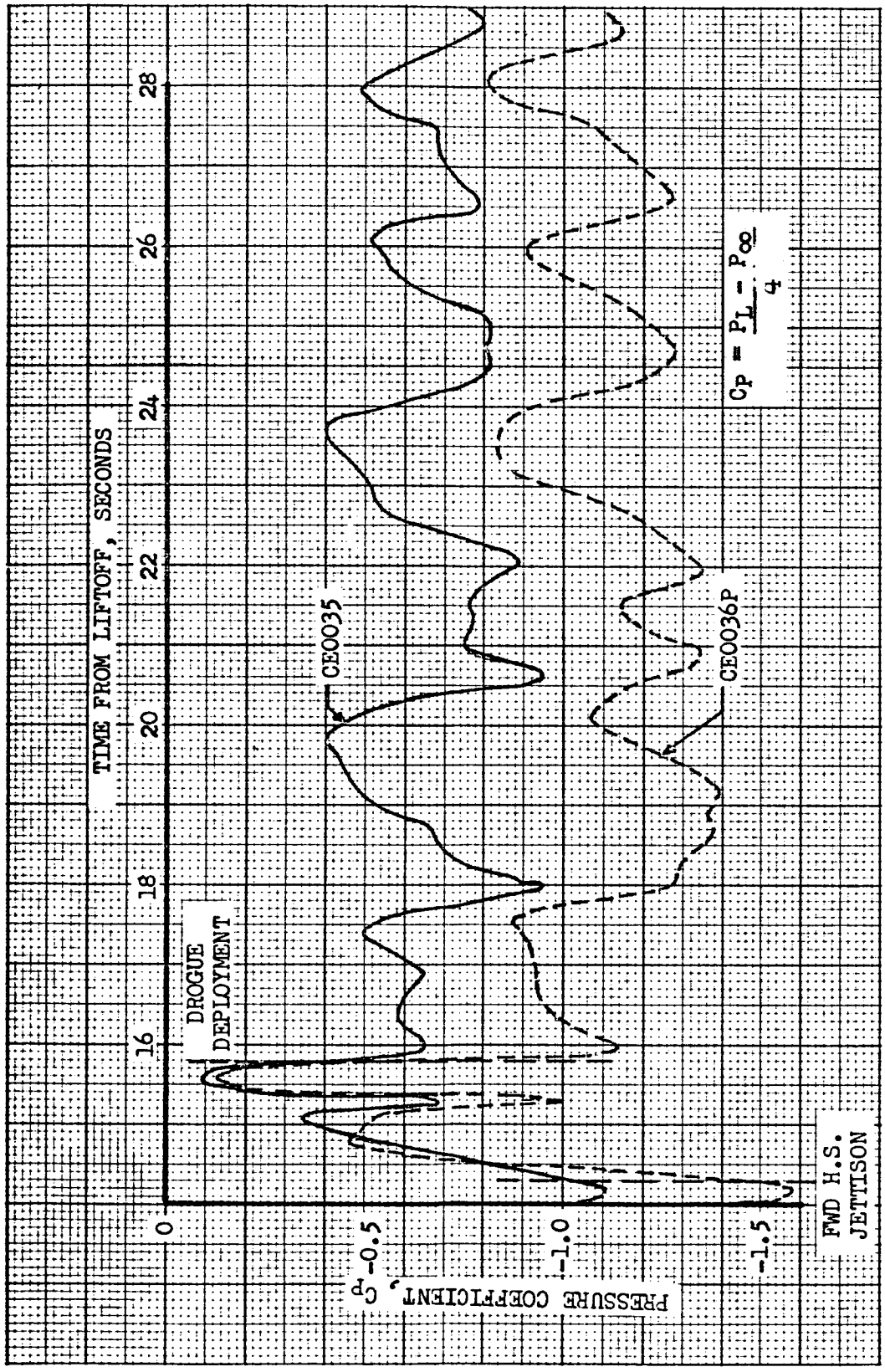

Figure 7.16.3 Command Module Base Pressure Coefficient During Drogue Descent

[redacted]

[redacted]

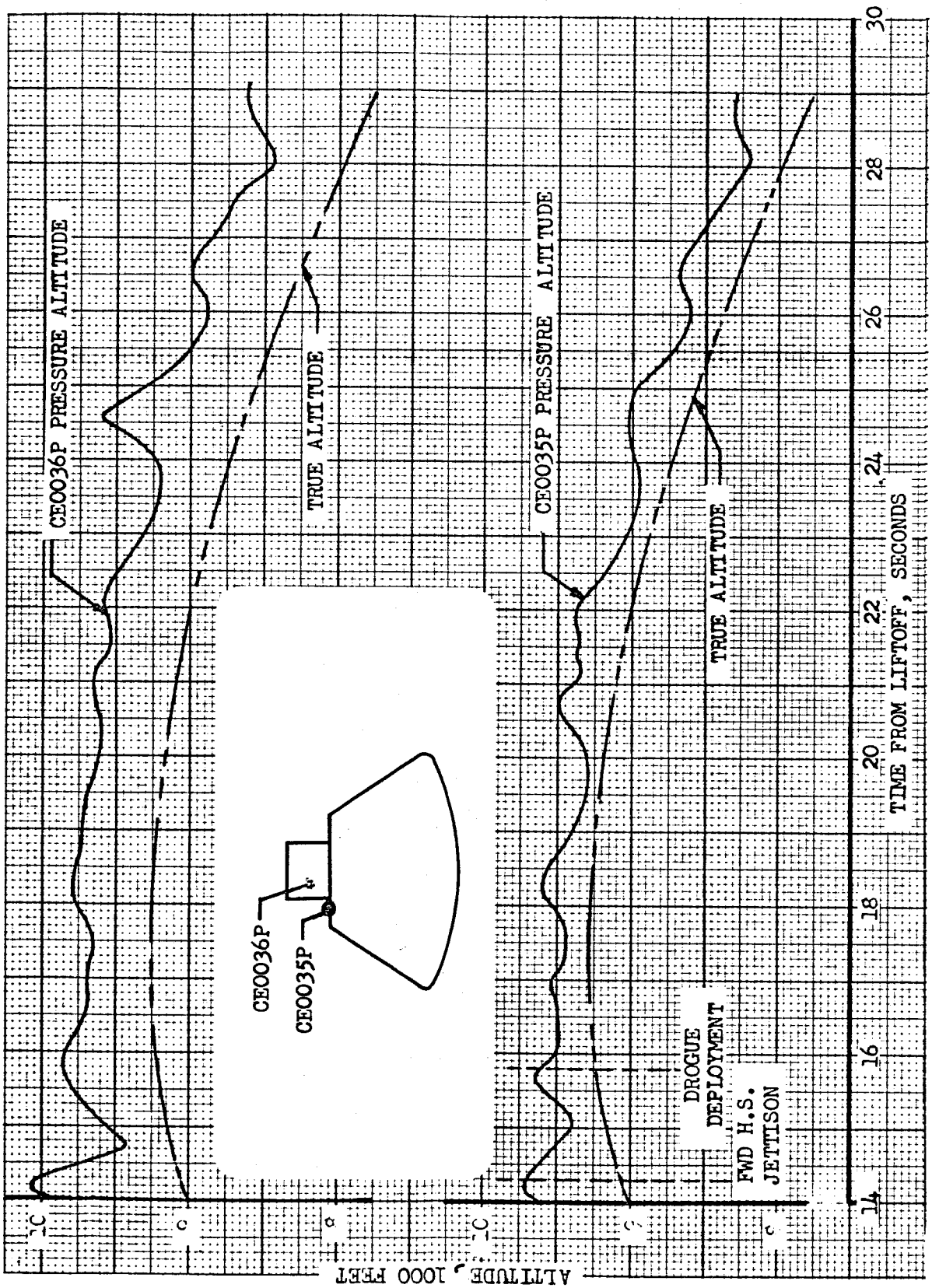

Figure 7.16.4 Command Module Altitude Indicated by the Baro-Reference Pressure

[redacted]

8.0 SUMMARY OF MALFUNCTIONS AND DEVIATIONS

No significant malfunctions or deviations were encountered in the flight, and none was found in postflight inspections. Minor malfunctions and deviations are discussed below.

A moderate LEV roll rate resulted in a vehicle turnaround essentially in the horizontal rather than in the vertical plane. No detrimental effect was noted (reference section 7.1).

One pair of apex-cover thruster pistons was damaged because of a difference in firing time between the two thruster pairs. The thrusters, of interim design, nevertheless performed satisfactorily. Spacecraft thrusters will be designed with inherent safeguards against such damage (reference section 7.7).

A squib of the subsystem B apex-cover thruster subsystem short-circuited and caused a 4-volt pyro and logic voltage drop for 0.4 second, with no detrimental effect (reference section 7.9).

A postflight inspection revealed a pilot-parachute multistrand stainless-steel-cable riser kink which probably occurred on deployment. No effect on performance was noted, and a postflight test on a similar kink in the previous flight indicated that no loss in strength ensued (reference section 7.2).

A short-duration problem in the instrumentation 90 x 10 commutator DPDM circuit resulted in a loss of the first 1.3 seconds of commutated data in the onboard tape recorder. The problem did not affect the PAM circuit of the 90 x 10 commutator; consequently these data were obtained through RF telemetry (reference section 7.10).

Although no instrumentation malfunction was involved, loss or degradation of data resulted because of the application limits of instrumentation, particularly the rate and attitude gyros and the Q-ball (reference sections 7.1, 7.10, and 7.16).

Except for these minor malfunctions and deviations, the Boilerplate 23A subsystems performed satisfactorily.

9.0 PREFLIGHT HISTORY

The following are significant events which occurred during Boilerplate 23A operations at WSMR Launch Complex 36.

Date	Event
Dec. 10, 1964 May 1, 1965	Refurbishment of BP-23 to meet BP-23A requirements
April 22, 1965	Assembly and leveling of the H14-016 LES weight and balance fixture completed per OCP-A-3037
April 23, 1965	LES horizontal weight and balance procedure completed per OCP-A-3038
May 1, 1965	BP-23A Development Engineering Inspection (DEI)
May 3, 1965 May 11, 1965	Top deck buildup per OCP-A-3027
May 13, 1965	CM horizontal weight and balance procedure completed per OCP-A-3035
May 14, 1965	CM vertical weight and balance procedure completed per OCP-A-3036
May 20, 1965 May 28, 1965	Pad buildup
May 21, 1965	LES thrust-vector alignment completed per OCP-A-3039
May 25, 1965	OCP-A-3039 rerun because of an alignment equation error
June 1, 1965	CM mated to A14-013 pad adapter per OCP-A-3020

Date	Event
June 2, 1965	LES-to-CM mating and thrust-vector alignment completed per OCP-A-3015
June 2, 1965	Functional verification of facility GSE completed per OCP-A-9030
June 10, 1965 June 14, 1965	Integrated combined system tests performed per OCP-A-0507
June 16, 1965 June 21, 1965	Soft boost cover installed
June 23, 1965	Simulated countdown completed per OCP-A-0010
June 25, 1965	Installation of altitude sensing subsystem completed
June 25, 1965	FRR held at PSDF auditorium
June 28, 1965	Countdown started per OCP-A-0010
June 29, 1965	Countdown completed with successful launch at 06:00 MST

10.0 PROGRAM SUMMARY

Spacecraft No. and Flight Date	Configuration	Mission and Performance
Boilerplate 6 November 7, 1963 Mission PA-1	Command module with prototype launch escape subsystem.	Pad abort test. This mission successfully demonstrated the capability of the prototype launch escape and earth landing subsystems to perform their intended functions during a pad abort. The actual trajectory was within the pad abort envelope and all trajectory parameters followed the predicted trends. All primary objectives were accomplished. All subsystems functioned satisfactorily.
Boilerplate 12 May 13, 1964 Mission A-001	Command module, service module, and prototype launch escape subsystem. Little Joe II launch vehicle.	Transonic abort test. This mission successfully demonstrated the capability of the launch escape and earth landing subsystems during an abort in the transonic region. The loss of one main parachute provided a bonus test condition by proving the capability of the earth landing subsystem to lower the command module to a noncatastrophic landing on only two parachutes.
Boilerplate 13 May 28, 1964 Mission A-101	Command module, service module, insert, and adapter; prototype launch escape subsystem.	To determine launch and exit parameters and to demonstrate the normal mode of launch escape subsystem jettison. This was

[redacted]

Spacecraft No. and Flight Date	Configuration	Mission and Performance
Boilerplate 13 (Cont)	Saturn I launch vehicle (SA-6).	the first orbital spacecraft (nonrecoverable) and the first to be launched by a Saturn launch vehicle. The objectives were accomplished. All subsystems functioned satisfactorily.
Boilerplate 15 September 18, 1964 Mission A-102	Command module, service module, insert, adapter; prototype launch escape subsystem. Saturn I launch vehicle (SA-7).	To determine launch and exit parameters and to demonstrate the alternate mode of launch escape subsystem jettison by use of the launch escape and pitch control motors. This was the second orbital spacecraft (nonrecoverable). The objectives were accomplished. All subsystems functioned satisfactorily.
Boilerplate 23 December 8, 1964 Mission A-002	Command module, service module, and prototype launch escape subsystem with canard. Little Joe II launch vehicle with attitude control subsystem.	High-dynamic-pressure abort test. This mission successfully demonstrated the capability of the launch escape and earth landing subsystems to perform their design functions during an abort at dynamic pressures higher than will be encountered on Saturn flights. Dual drogue parachutes, canard, and boost protective cover were tested for the first time. All subsystems functioned satisfactorily. Test objectives were accomplished with only two minor discrepancies.

[redacted]

Spacecraft No. and Flight Date	Configuration	Mission and Performance
Boilerplate 16 February 16, 1965 Mission A-103	Command module, service module, insert, adapter; prototype launch escape subsystem. Saturn I launch vehicle (SA-9) with redesigned unpressurized IU. Pegasus I micrometeoroid satellite.	Launch vehicle qualification test and first Pegasus micrometeoroid experiment. LES carried to provide correct aerodynamic conditions. All systems functioned satisfactorily. Pegasus satellite was placed in planned orbit.
Boilerplate 22 May 19, 1965 Mission A-003	Command module, service module, and prototype launch escape subsystem. Little Joe II launch vehicle.	High-altitude abort test. The High-altitude aspect of the mission was not accomplished. The launch escape vehicle successfully aborted from a catastrophic launch vehicle failure at low altitude. All systems functioned satisfactorily.
Boilerplate 26 May 25, 1965 Mission A-104	Command module, service module with one dummy RCS engine quad with two of the four nozzles instrumented with six thermocouples each, insert, adapter; prototype launch escape subsystem. Saturn I launch vehicle (SA-8). Pegasus II micrometeoroid satellite.	Launch vehicle qualification test and second Pegasus micrometeoroid experiment. LES carried to provide correct aerodynamic conditions. All systems functioned satisfactorily. Pegasus satellite was placed in planned orbit. Aerodynamic heating data were obtained from nine of the twelve thermocouples.

Spacecraft No. and Flight Date	Configuration	Mission and Performance
Boilerplate 23A June 29, 1965 Mission PA-2	Command module with prototype launch escape subsystem. The vehicle configuration included, additional to the configuration of the first pad abort vehicle (BP-6): Block I control weight, a canard subsystem, a boost protective cover, and an apex-cover jettison subsystem.	Pad abort test. This mission successfully demonstrated the capability of the launch escape and earth landing subsystems to perform their intended functions in a pad abort.

11.0 REFERENCES

Reference	Identification	Title and Date
1	NASA Program Apollo Working Paper No. 1176	Program Apollo Flight Mission Directive, Apollo Mission PA-2 (BP-23A). June 9, 1965
2	NAA Report SID 63-574	Apollo Measurement Requirements, Boilerplate 23A. April 1, 1965
3	NAA Report SID 63-1416-1	Project Apollo Flight-Test Report, Boilerplate 6. December 4, 1963
4	NAA Report SID 63-1416-2	Project Apollo Flight-Test Report, Boilerplate 12. July, 1964
5	NAA Report SID 63-1416-3	Project Apollo Flight-Test Report, Boilerplate 13. August, 1964
6	NAA Report SID 63-1416-4	Project Apollo Flight-Test Report, Boilerplate 15. November, 1964
7	NAA Report SID 63-1416-5	Project Apollo Flight-Test Report, Boilerplate 23. February, 1965
8	NAA Report SID 63-1416-6	Project Apollo Flight-Test Report, Boilerplate 22. August, 1965
9	NAA Report SID 65-29-1A	Vehicle Test Plan, Apollo Mission PA-2, Boilerplate 23A. March 19, 1965
10	NAA Report SID 63-143-17W	Actual Weight and Balance Report, Boilerplate 23A. LES and CM for Pad Abort. June 14, 1965
11	NAA Report SID 64-1700	Mass Properties Data - Block I Control Weights for Apollo Spacecraft. October 16, 1964

[redacted]

Reference	Identification	Title and Date
12	NASA Program Apollo Manned Spacecraft Center Publication	Apollo Instrumentation Manual for Apollo Mission A-002. October 31, 1964
13	NAA Report SID 64-174, Rev B	Aerodynamic Data Manual for Project Apollo. July 1, 1965
14	NAA Report SID 63-1464	Data Report for the Wind Tunnel Test of the Apollo Launch Escape Vehicle Jet Effects Model (FSJ-1) in the Langley Research Center 16-Foot Transonic Tunnel (Series III). December, 1963